



HAL
open science

Vieillissement thermique et radiochimique de matrices EPDM pures et chargées d'ATH: mise au point de relations structure/propriétés

Amin Shabani

► To cite this version:

Amin Shabani. Vieillissement thermique et radiochimique de matrices EPDM pures et chargées d'ATH: mise au point de relations structure/propriétés. Autre. Ecole nationale supérieure d'arts et métiers - ENSAM, 2013. Français. NNT: 2013ENAM0015 . pastel-00941289

HAL Id: pastel-00941289

<https://pastel.hal.science/pastel-00941289>

Submitted on 3 Feb 2014

HAL is a multi-disciplinary open access archive for the deposit and dissemination of scientific research documents, whether they are published or not. The documents may come from teaching and research institutions in France or abroad, or from public or private research centers.

L'archive ouverte pluridisciplinaire **HAL**, est destinée au dépôt et à la diffusion de documents scientifiques de niveau recherche, publiés ou non, émanant des établissements d'enseignement et de recherche français ou étrangers, des laboratoires publics ou privés.

École doctorale n° 432 : Science des Métiers de l'Ingénieur

Doctorat ParisTech

T H È S E

pour obtenir le grade de docteur délivré par

l'École Nationale Supérieure d'Arts et Métiers

Spécialité " Mécanique-Matériaux "

présentée et soutenue publiquement par

Amin SHABANI

le 27 mai 2013

**Thermal and Radiochemical Aging of neat and ATH filled EPDM:
Establishment of Structure/Property Relationships**

Directeur de thèse : **Xavier COLIN**

Jury

Mme. Isabelle ROYAUD, Professeur, Institut Jean Lamour, Université de Lorraine
Mme. Florence DELOR-JESTIN, Maître de conférences, HDR, LPMM, ENSCCF
M. Gregory B. MCKENNA, Professeur, Department of Chemical Engineering, Texas Tech University
M. Xavier COLIN, Professeur, PIMM, ENSAM Paris
M. Grégory MARQUE, Docteur, EDF R&D
M. Fahmi ZAÏRI, Maître de conférences, HDR, Laboratoire de Mécanique de Lille, Université Lille1
M. Yannick GOUTILLE, Docteur, NEXANS NRC

Président
Rapporteur
Rapporteur
Examineur
Examineur
Examineur
Invité

**T
H
È
S
E**

To my parents

Remerciements

Ce travail, réalisé au sein du laboratoire PIMM, fait partie du projet NPP proposé par EDF R&D. Je remercie tous les partenaires académiques et industriels (ENSAM, EDF, Nexans, CNRS) pour le soutien qu'ils m'ont apporté pendant la réalisation de ces travaux.

Tout d'abord, je voudrais remercier le professeur Gregory B. McKenna et le docteur Florence Délor-Jestin pour avoir accepté de rapporter ce manuscrit, ainsi que le professeur Isabelle Royaud qui m'a fait l'honneur de présider mon jury de thèse. Je tiens également à remercier le docteur Fahmi Zaïri et le docteur Yannick Goutille d'avoir accepté de faire partie de ce jury de thèse.

Je tiens à remercier le professeur Xavier Colin, le directeur de cette thèse, pour son encadrement et son engagement. Sa créativité et son implication dans la recherche reste, pour moi, un exemple à suivre. Je remercie également le docteur Carole Monchy-Leroy et le docteur Grégory Marque pour m'avoir accueilli au sein du département MMC d'EDF R&D et participé à mon encadrement.

Je souhaite ensuite remercier le docteur Cédrique Lorthioir du CNRS de Thiais pour la réalisation des essais de RMN, et le docteur Pascal Halary de la société Nebaltec pour sa collaboration scientifique.

Pour finir, je tiens à adresser mes remerciements à mes collègues de bureau : Wissam, Yahya, Magali, Virginie, Mathieu, Severine et Nidhal pour leur bonne humeur. Je ne saurais oublier Bardia, Nada, Sophie, Alex, Mouna et tous les autres doctorants et post-doctorants, et aussi les membres du PIMM : Paulo, Alain, Anne, Gaëlle, ..., avec qui j'ai passé des bons moments.

Table of contents

General introduction	1
1 Literature Review	7
1.1 Rubber elasticity	12
1.1.1 Generalities	12
1.1.2 Tridimensional network	12
1.1.3 Elastic properties	14
1.1.4 Properties at break	17
1.2 Crosslinking by peroxides	19
1.2.1 Introduction	19
1.2.2 Initiation by DCP	20
1.2.3 Ethylene-Propylene Copolymers (EPR)	22
1.2.4 Ethylene Propylene Diene Terpolymers (EPDM)	24
1.3 Fillers	29
1.3.1 Criteria for choosing fillers	29
1.3.2 Fire retardant filler	31
1.3.3 Matrix/filler interactions	33
1.3.4 Swelling of filled elastomers	36
1.4 Aging of polymers	38
1.4.1 Methods for life-time prediction	38
1.4.2 Aging at molecular scale	42
1.4.3 Macromolecular scale	57
1.4.4 Macroscopic scale	63
2 Materials & Experimental Techniques	81
2.1 Raw materials	85
2.1.1 Elastomer	85
2.1.2 Crosslinking agent	85
2.1.3 Filler	86
2.2 Samples	86

2.2.1	Neat samples.....	86
2.2.2	Filled samples.....	87
2.3	Aging conditions	88
2.3.1	Thermal aging.....	88
2.3.2	Radiochemical aging	88
2.4	Characterization methods	89
2.4.1	Molecular scale.....	89
2.4.2	Macromolecular scale.....	95
2.4.3	Macroscopic scale – Tensile testing	99
3	Initial Characterization	103
3.1	Characterization of raw materials.....	108
3.1.1	Linear EPDM	108
3.1.2	Fillers.....	118
3.2	Kinetic analysis of EPDM crosslinking by DCP.....	125
3.2.1	Molecular scale.....	125
3.2.2	Macromolecular scale.....	138
3.2.3	Final network structure.....	150
3.2.4	Tensile testing – Large deformation.....	151
3.3	Effect of fillers on initial properties	154
3.3.1	Molecular scale.....	154
3.3.2	At macromolecular scale	155
3.3.3	Macroscopic scale-Tensile testing.....	163
4	Aging of EPDM & Composites Molecular and Macromolecular Aspects.....	169
4.1	Molecular aspects of thermal aging of EPDM	173
4.1.1	Thermogravimetric analysis	173
4.1.2	FTIR spectrophotometry	177
4.1.3	Thermal oxidation of thick plates.....	190
4.2	EPDM network under irradiation	197
4.2.1	Formation of oxidation products	198

4.2.2	Hydroperoxide titration by DSC	200
4.3	Macromolecular structure evolution of EDPM network	205
4.3.1	EPDM network under thermal stress.....	205
4.3.2	EPDM network under irradiation	211
4.4	Discussion of swelling behavior throughout oxidative aging	216
5	Mechanical Aspects.....	221
5.1	Effect of thermal aging on mechanical properties.....	226
5.1.1	Changes in Young's modulus.....	226
5.1.2	Discussion	230
5.1.3	Ultimate properties	236
5.2	Effect of radiochemical aging on mechanical properties	244
5.2.1	Neat EPDM Young's modulus.....	244
5.2.2	Macromolecular changes.....	245
5.2.3	Fillers effect.....	247
5.3	Macroscopic scale	250
5.3.1	Ultimate properties of Neat EPDM network	250
5.3.2	Fillers effect.....	253
	Conclusion.....	254
	Reference.....	256
	Conclusions and Prospects	257
	Conclusions et Perspectives	263

General introduction

The life-time of any installation is endangered by the aging of materials used in its construction. Polymers, as one of the developing and upcoming materials, are increasingly used in various industrial applications due to their vast range of properties. For instance, elastomers are widely used in cable industry due to their flexibility, insulation properties and high limits of deformation. Elastomer insulations and sheaths of electrical cables used in reactor building of a nuclear power plant are highly exposed to ionizing irradiations and relatively high temperatures, which both considerably accelerate the aging process. These elastomers are mostly PVC, or PE and its copolymers and terpolymers. One of widely used PE terpolymers is EPDM, which should be crosslinked in order to reach an acceptable level of mechanical properties. However, pure elastomer network does not possess high mechanical properties and consequently reinforcement is considered by adding fillers into the polymer matrix. One of frequently used fillers is Aluminum trihydrate (ATH), which shows fire retardancy at high loadings.

Several studies have been brought out on crosslinking and aging of neat and filled EPDM matrices, whether on chemical or on mechanical aspects of these phenomena. This study is aimed to bring some answers to the current questions in this field and tentatively establish lacking relationships between the material's structure (at different scales) and its mechanical behavior. Therefore, the main axes of research will be the followings:

- I. Crosslinking EPDM with peroxide: Creation of EPDM network throughout crosslinking, and the structure of final network before exposure to usage criteria, is of key importance to understand the oxidation processes. For instance, the presence of residual double bonds, which have not been consumed during the processing operation, sensitizes EPDM matrices to oxidation [1].
- II. Effect of fillers on network structure: Pristine ATH establishes relatively weak physical interactions with polymer chains. In order to ameliorate filler/polymer matrix interactions, ATH particles are chemically treated and hydrocarbon molecules are grafted into their surface. These surface treatment molecules are expected to create chemical bonds with the polymer chains throughout the crosslinking step and thus, replace the initial physical interactions [2].
- III. Aging of neat EPDM matrix: The modification of the elastomer structure at the molecular scale under thermo- or radio-oxidation has direct consequences at the macromolecular scale and subsequently, on the mechanical properties (in particular on elastic and fracture properties). In this study, we try to establish the correlation between these different scales

properties. Furthermore, the effects of exposure temperature and irradiation dose rate will be carefully investigated.

- IV. Effect of fillers on aging: Fillers are initially introduced for reinforcement purposes, but do they also have an impact on the material during aging? If yes, what are these impacts and how do they affect the aging mechanism. Furthermore, how does the presence of the chemical surface treatment affect these phenomena?

This manuscript will be divided into five main chapters. The first chapter is devoted to a brief literature review on the different aspects under study, going from rubber elasticity to aging of filled EPDM matrices. The second and third chapters are dedicated to introduce the materials under study, the experimental techniques and initial characterization of samples. In chapter four, we will see how the exposure under different sources of stress (thermal and radiochemical solicitations) can affect the structure of materials at molecular scale through chemical primary acts. We will also define the effect of these changes on the properties at macromolecular scale. The monitoring of these latter, and also their consequences at macroscopic scale and on mechanical properties, will be the subject of the fifth chapter. Finally, conclusions to this study will be drawn and the future prospects will be recommended.

Introduction générale (in French language)

La durée de vie de toute installation peut être réduite par le vieillissement des matériaux qui sont utilisés dans sa construction. Les polymères, qui sont l'une des familles de matériaux en voie de développement et à venir, sont de plus en plus utilisés dans les applications industrielles en raison de leur large éventail de propriétés. En particulier, les élastomères sont largement utilisés dans l'industrie des câbles en raison de leur flexibilité, leurs propriétés d'isolation et leurs limites de déformation élevées. Les isolants et les gaines élastomère des câbles électriques utilisés dans le bâtiment réacteur d'une centrale nucléaire sont fortement exposés aux irradiations ionisantes et aux hautes températures, ce qui accélèrent considérablement le processus de vieillissement. Ces élastomères sont pour la plupart en PVC et PE, et ses copolymères et terpolymères comme l'EPR, ou l'EPDM qui contient des insaturations. La raison de la présence de ces insaturations est que la gomme initiale doit être réticulée avant utilisation pour avoir un niveau de propriétés mécaniques acceptables pour l'application visée. Néanmoins, le réseau élastomère pur ne possède pas des propriétés mécaniques élevées et, par conséquent, il est nécessaire de le renforcer en ajoutant des charges dans la matrice polymère. Une de ces charges fréquemment utilisée dans les câbles est le trihydrate d'aluminium (ATH) qui présente des propriétés ignifugeant à des concentrations élevées.

Plusieurs études ont été menées sur la réticulation et le vieillissement des matrices EPDM pures et chargées, que ce soit sur la chimie ou sur les aspects mécaniques de ces phénomènes. Cette étude a pour objectif d'apporter un certain nombre de réponses aux questions actuelles dans ce domaine et d'essayer d'établir des relations manquantes entre la structure de ces matériaux (à différentes échelles) et leur comportement mécanique. Par conséquent, les principaux axes de recherche seront les suivants:

- I. La réticulation de l'EPDM par les peroxydes: La connaissance de l'évolution de la structure de la matrice EPDM tout au long de sa réticulation pendant l'opération de mise en œuvre, mais aussi de son état initial avant l'exposition aux sollicitations extérieures, est d'une importance clé pour pouvoir être capable de comprendre les processus d'oxydation par la suite. Par exemple, la présence de doubles liaisons résiduelles, qui n'ont pas été totalement consommées pendant l'opération de mise en œuvre, sensibilise des matrices EPDM à l'oxydation [1].
- II. L'effet des charges sur la structure du réseau au niveau de l'interphase: L'ATH vierge établit de faibles interactions physiques avec les chaînes de polymère. Afin d'améliorer les interactions charge/matrice polymère, la surface des particules ATH subit un traitement chimique, qui consiste à greffer des molécules hydrocarbonées sur leur surface. Ces molécules de traitement de surface créent des liaisons chimiques avec les chaînes de polymère pendant l'étape de réticulation, et remplacent ainsi les interactions physiques initiales[2].
- III. Le vieillissement de la matrice EPDM pure: L'évolution de la structure moléculaire de l'élastomère sous l'effet de la thermo- ou de la radio-oxydation a des conséquences directes à

l'échelle macromoléculaire et, par la suite, sur les propriétés mécaniques (en particulier sur les propriétés élastiques et à la rupture). Dans cette étude, nous essaierons d'établir le lien entre les propriétés à ces différentes échelles. En outre, les effets de la température d'exposition et de la dose d'irradiation seront soigneusement analysés.

- IV. L'effet des charges sur le vieillissement: Les charges sont d'abord introduites à des fins de renforcement, mais ont-elles aussi un impact sur le matériau au cours du vieillissement? Si oui, lequel? Et comment? Par ailleurs, comment la présence du traitement chimique sur la surface des charges influe-t-il sur ces phénomènes?

Ce manuscrit se divisera en cinq grandes parties. Le premier chapitre est consacré à une synthèse des études de la littérature menées sur les différents aspects de l'étude, depuis l'élasticité caoutchoutique jusqu'au vieillissement des matrices EPDM chargées. Les deuxième et troisième chapitres sont consacrés à l'introduction des matériaux de l'étude, des techniques expérimentales et de la caractérisation initiale des échantillons. Dans le quatrième chapitre, nous verrons comment l'exposition à différentes sollicitations extérieures (thermiques et radiochimiques) peut affecter la structure des matériaux à l'échelle moléculaire sous l'action d'actes chimiques élémentaires. Nous définirons ainsi l'impact de ces modifications sur les propriétés à l'échelle macromoléculaire. Le suivi de ces dernières, mais aussi les conséquences de ces modifications à l'échelle macroscopique et sur les propriétés mécaniques, seront également étudiées dans le cinquième chapitre. Suite à l'ensemble de ces travaux, des conclusions seront éditées à partir de ces résultats et les perspectives à cette étude seront dressées.

References

1. Rivaton, A., S. Cambon, and J.-L. Gardette, *Radiochemical ageing of EPDM elastomers. 3. Mechanism of radiooxidation*. Nuclear Instruments and Methods in Physics Research Section B: Beam Interactions with Materials and Atoms, 2005. **227**(3): p. 357-368.
2. Planes, E., *Influence des charges sur l'évolution des propriétés mécaniques des EPDM chargés lors de leur vieillissement par irradiation*. 2008.

CHAPTER I

1 Literature Review

Extended abstract (in French language)

L'étude et le contrôle de la durée de vie des matériaux polymères est un enjeu important pour le monde de la recherche industrielle. Pour mesurer les modifications apportées aux isolants et gaines des câbles en polymère pendant leur utilisation, le secteur de l'électricité a choisi les propriétés mécaniques comme critère de fin de vie. Les élastomères, qui font l'objet de cette étude, présentent un type particulier et unique de comportement mécanique, qui est connu sous le nom d'*élasticité caoutchoutique*. Par ordre chronologique, ce chapitre commence par une introduction sur les caoutchoucs et leur élasticité, qui est de nature entropique.

Un élastomère, dans son état brut, n'est pas utilisable pour une application industrielle. Pour atteindre des propriétés à la rupture intéressantes, il doit passer par une étape de réticulation. Ainsi, la réticulation des élastomères, en particulier la réticulation des EPDM par le peroxyde de dicumyle, fait l'objet d'une attention particulière dans cette étude.

Une fois que l'état réticulé du matériau, qui constitue l'état initial du matériau avant vieillissement, a été bien compris, le vieillissement, qui est l'objectif principal de cette étude, est examiné. Pour ce faire, les modifications induites par le vieillissement sont étudiées à trois échelles successives : moléculaire, macromoléculaire, et macroscopique. À l'échelle moléculaire, les réactions chimiques en présence d'oxygène conduisent à la formation de produits d'oxydation. Certaines de ces réactions chimiques induisent des coupures de chaînes ou créent de nouveaux nœuds de réticulation, et ainsi modifient structure du réseau à l'échelle macromoléculaire. Cette seconde échelle est aussi le lien de raccordement entre les échelles moléculaires et l'échelle macroscopiques, où se produisent les modifications des propriétés mécaniques.

Les élastomères sont généralement renforcés par l'introduction de charges dans la matrice polymère pour former un *composite*. Les trois principaux avantages d'utilisation des charges sont:

- i. L'amélioration des propriétés mécaniques
- ii. L'obtention de propriétés spécifiques (e.g. retardateur de flamme)
- iii. La réduction du coût

Ainsi, dans chaque section de ce chapitre, le rôle de charges est clarifié et leurs effets sur le comportement physico-chimique et mécanique initial et à long terme des matrices élastomères sont introduits.

Les principaux résultats de la littérature présentés dans ce chapitre peuvent être résumés en quelques points:

L'utilisation croissante des matériaux polymères dans l'industrie nécessite une connaissance globale de ce type de matériaux et de leur comportement à différentes échelles, ainsi que le lien entre ces échelles. Dans le cas de l'EPDM, qui est le principal matériau de cette étude, il a fait l'objet de plusieurs études depuis plusieurs années. Bien que moins développé que le PE, le PP et l'EPR, il présente plusieurs complications liées à la présence d'un termonomère insaturé. Les modifications des propriétés pendant le vieillissement et la durée de vie de l'EPDM dépendent fortement de l'état initial du caoutchouc après réticulation. En effet, la présence d'insaturations résiduelles dans le mécanisme de vieillissement à l'échelle moléculaire peut conduire à des altérations du comportement de l'EPDM aux échelles macromoléculaire et macroscopique. Pour le moment, l'absence d'une étude approfondie, qui concatènerait ces trois aspects généraux, se fait sentir.

En outre, l'effet omniprésent des charges sur chaque aspect de l'étude semble avoir été mis au second plan. Présentes avant la réticulation de la matrice, les charges réactives sont capables de participer aux réactions de cuisson du caoutchouc, et ainsi de modifier le mécanisme de formation de réseau, ainsi que la structure du réseau au niveau de l'interphase charge/matrice polymère. Par ailleurs, la dégradation de l'interphase est un facteur supplémentaire à considérer lors de l'étude des modifications des propriétés mécaniques pendant le vieillissement. En effet, la perte des interactions physiques à l'interface réduit le rôle de renfort des particules de charge. Cette perte d'interaction peut être améliorée par la création des liaisons chimiques covalentes entre des chaînes de polymère et les particules de charge.

Dans ce travail, nous allons essayer de garder une vision multi-échelle des différentes étapes expérimentales, depuis l'état de pré-réticulé jusqu'à l'état vieilli des matériaux. Sur la base de ce qui a été revisité dans cette étude bibliographique, les principaux axes de recherche seront:

- La réticulation de l'EPDM par le peroxyde, la composition et la structure du réseau tridimensionnel et ses propriétés mécaniques,
- L'effet des charges et de leur réactivité chimique sur la réticulation de la matrice EPDM ces propriétés à différentes échelles structurales,
- Le vieillissement de la matrice EPDM sous sollicitations thermiques et radiochimiques et son impact sur les propriétés mécaniques,
- L'effet des charges sur le processus de vieillissement.

Dans les chapitres qui suivent, on tentera de garder un équilibre entre les aspects chimiques, physico-chimiques et mécaniques du vieillissement de la matrice EPDM grâce à des investigations aux échelles moléculaire, macromoléculaire et macroscopique.

Introduction

Studying and controlling the life-time of polymeric materials has been an important issue for industrial research world. The electricity industry, in order to measure the modifications brought to polymeric cables during usage, has chosen mechanical properties as the criteria for life-time prediction. Elastomers, which are the issue of this study, have a special and unique type of mechanical behavior that is known as *rubber elasticity*. In a chronologic order, this chapter will begin by an introduction to rubbers and their elasticity, which is known to be of entropic nature. The so-called entropic elasticity is the modeling basis for this type of behavior.

An elastomer at its raw state is not satisfactorily efficient enough and, in order to attain interesting ultimate properties, it has to go through a crosslinking step. Thereupon, the crosslinking of elastomers and the crosslinking of ethylene propylene diene monomer by dicumyl peroxide, in particular, will be the subsequent topic of this study.

Once the crosslinked state of materials is well understood, the oxidative aging, which is the main aim of this study, will be reviewed. To do so, the modifications induced by aging will be introduced at three consecutive scales: molecular, macromolecular and macroscopic. At molecular scale chemical reactions take place in the presence of oxygen, leading to formation of oxidation products. Some of these chemical reactions induce chain scissions or create new crosslinks, and thus modify the macromolecular structure of the polymer. Consequently, the physicochemical and mechanical properties of the material are modified as well. This second scale is as well the connecting link between the molecular and the macroscopic scales, wherein occur the modifications in mechanical properties.

Elastomers are generally reinforced by the introduction of fillers into polymer matrix to form a *composite*. The three main advantages of using fillers are:

- iv. Improving of mechanical properties
- v. Obtaining specific properties (e.g. fire retardancy)
- vi. Reducing the final cost

Hence, in each section of this chapter, the role of fillers will be clarified, and their effects on the initial and long-term physicochemical and mechanical properties of elastomers will be introduced.

1.1 Rubber elasticity

1.1.1 Generalities

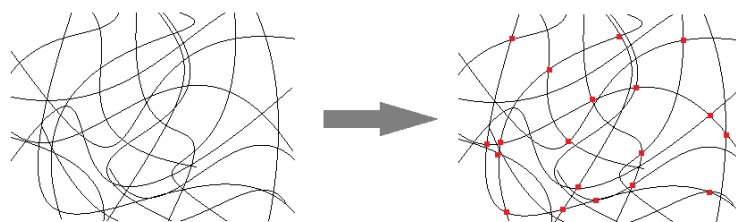
A polymer chain is made up of the repetition of monomer units which are chemically bonded. In an amorphous state, chains are randomly oriented and form *random coils*. In a polymer, all the chains do not have the same length (or number of monomers) and cover a range of size, but for every polymer, a critical length exist after which entanglements happen between macromolecular chains. Below the critical length, the polymer behaves like a viscous liquid. After entanglements formation, the movement of chains is hindered. By increasing the chain length, the movement of the chains becomes more and more difficult up to a critical point after which the increase in molecular mass becomes insignificant. At this critical mass, a characteristic property of polymers can be defined known as molecular mass between entanglements, which is the average value of inter entanglements molecular mass.

Polymers, based on their chemical structure and molecular mass, can show various mechanical behaviors. An elastomer is a type of polymer that presents a viscoelastic behavior showing relatively low elastic properties. But this type of material, and only this type, shows a unique mechanical behavior which is the ability to endure very high deformation yields (up to 1000%) under an imposed force, and deformation recoverability after force removal. In an elastomer, the polymer chains must have a high degree of flexibility and deformability to undergo large deformations [1].

As mentioned above, an elastomer shows a recoverability which is not complete. In order to obtain a total recoverability, chemical bonds are artificially formed between macromolecular chains. The formation event of inter-chain chemical bonds is called *crosslinking* and the resulting chemical bonds are known as crosslinks. The formation of crosslinks creates a tridimensional network of macromolecular chains jointed together, which is often referred to as *rubber*.

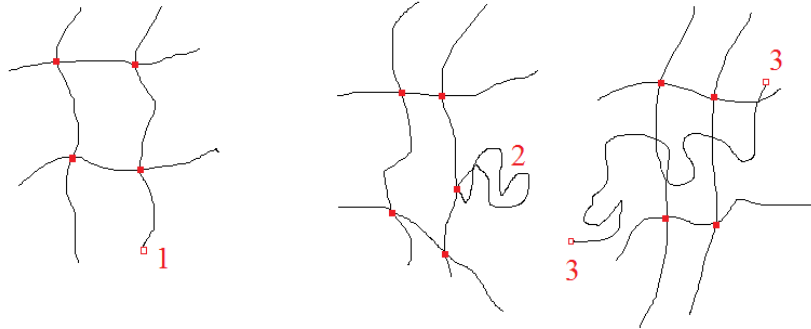
1.1.2 Tridimensional network

Total recoverability of an elastomer is obtained after network formation which is called *crosslinking* (*or curing*) where the chemical bonds are formed between macromolecular chains (Scheme 1-1).



Scheme 1-1: Formation of crosslinks

Tridimensional crosslinked network consist of sub-chains delimited between two crosslinks. A sub-chain which takes part in elastic properties of the network is called *elastically active*. In an ideal network, all chains are elastically active. As an example of (quasi-)ideal networks, one can refer to thermoset polymers, which are made up of multi-functional ($f > 2$) monomers such as epoxy/diamine or polyester/styrene. On the contrary, networks formed from crosslinking of linear chains, in this case elastomers, always contain flaws. The most frequent defects that keep the network far from ideality are chain loops, dangling chains, and free chains (Scheme 1-2).



Scheme 1-2: Real elastomer network defects, 1) dangling chain 2) closed loop 3) free chain

After total curing, the network is often characterized by the average mass of sub-chains between two junctions (M_c) and the functionality of crosslinks (f), which is the average number of chains ending into (or going out from) a crosslink. In an ideal network, every chain ends in two distinct crosslinks and is elastically active meaning that no dangling chain can exist, neither a closed loop nor a trapped entanglement, nor a free macromolecule. Such a network is determined by the concentration of elastically active sub-chains (ν) or by the concentration of crosslinks (x), where these two are connected by the following equation (1-1):

$$\nu = \frac{f}{2}x \quad 1-1$$

If the average concentration of effective chains is expressed in mol.g^{-1} , then the average mass of chains between crosslinks M_C (g.mol^{-1}) would be:

$$M_C = \frac{1}{\nu_t} \quad 1-2$$

A non-ideal network, on the contrary, contains flaws that complicate the calculation of crosslink density. Assuming that the number of dangling chains b is largely higher than other defects, and therefore neglecting them, then the total number of sub-chains ν_t will be $\nu + b$.

$$\nu_t = \nu + b \quad 1-3$$

If the number average mass of macromolecular chains is M_n , then number of dangling chains is equal to $2/M_n$. By regrouping this information we have:

$$\nu = \nu_t - b = \frac{1}{M_c} - \frac{2}{M_n} \quad 1-4$$

Equation 1-4 shows how the parameters of network are connected, but the crosslink density of the network needs to be determined theoretically or measured experimentally. Methods permitting the measurement of crosslink density are based on the theory of rubber elasticity. The most well-known methods are based on measurements of swelling ratio, Young's modulus or glass transition temperature (T_g).

1.1.3 Elastic properties

Gough [2] realized that by stretching a rubber, it warms up and frees some heat, and absorbs energy when it retracts. Years after, scientists tried to explain this phenomenon, with mostly incorrect explanations until the breakthrough works of Meyer et al. [3], where they explained that, once extended under stress, an elastomer tends to retract in order to gain back higher entropy.

The entropic origin of rubber elasticity can be shown by a thermo-elastic experiment in which an elastomeric network is deformed by force f to the length L . An increase in temperature at a constant force f results in a decrease of the length L . This is explained by the entropic origin of rubber elasticity where, at the repose state of the material at temperature T , the elastomer is at its maximum entropy. An imposed force decreases this latter due to the rearrangement and, consequently, the alignment of the chains. Hence, by increasing the temperature, the network tends to retrieve its original state resulting to shrinkage. Meyer and Ferri [4] have shown the temperature dependence of rubber elasticity by using the explained test on a slightly crosslinked rubber (Figure 1-1).

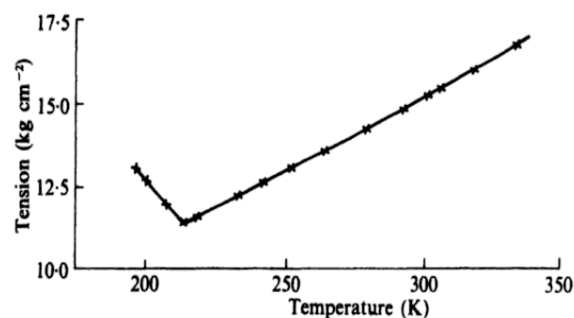


Figure 1-1: Demonstration of entropic origin of rubber elasticity^[4]

Entropic elasticity can be represented as well by an increasing in temperature when exerting an abrupt deformation in adiabatic situation. This phenomenon was first introduced by Gough and Joule [5] and presented later by Treloar (Figure 1-2) [6]:

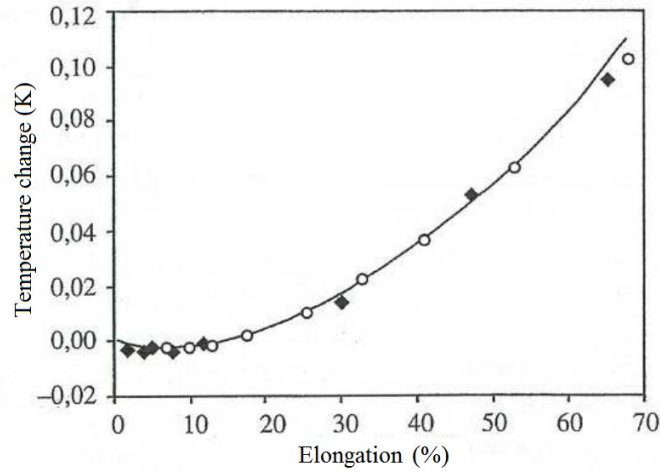


Figure 1-2: Response of an elastomer to abrupt deformation vs. ΔT [6]

The refractive force in an elastomer sample is due to the elastic energy stored in elastically active chains under deformation. The configuration of chains does not affect the interaction between neighboring chains and their free energy[7]. This means that the stored elastic energy can be obtained by the summation of the elementary energies of individual chains. Guth and Mark [8] presented the concept of an isolated polymer chain and deduced an equation to calculate the refractive force (F_R) for an imposed end-to-end displacement (L):

$$F_R = \left(\frac{3kTL}{nq^2}\right)\left(\frac{1-\cos\theta}{1+\cos\theta}\right) \quad 1-5$$

where k is the Boltzmann's constant, T the absolute temperature, θ the bond angle, n the number of segments and q their length.

After the theory of Guth and Mark, several authors tried to reconsider the rubber elasticity [9-11] and the outcome for the value of the retractive force of an ideal network. These pioneering works led to the theory of Flory [10]:

$$f = \frac{vkT}{l_0}(\Lambda - \Lambda^{-2}) \quad 1-6$$

with f the deformation work (dF/dl), l_0 the initial length of the sample, ν the number of chains per volume unit and Λ the macroscopic deformation. By dividing Equation 1-6 by initial cross-section and considering that $v_0 = s_0 l_0$, we have:

$$\frac{f}{s_0} = \frac{\nu kT}{V_0} (\Lambda - \Lambda^{-2}) = \frac{\rho RT}{M_c} (\Lambda - \Lambda^{-2}) = C_1 (\Lambda - \Lambda^{-2}) \quad 1-7$$

where R is the perfect gas constant and M_c the molecular mass of elastically active chains. ($\nu k = nR$ with n the mole number of chains).

Although this theory is largely used, it is important to emphasize that this result is for an ideal rubber network. In order to apply Equation 1-7, the polymer should satisfy some criteria [12]:

- i. In the experimental conditions the polymer must be stable, i.e. no degradation or post-crosslinking must happen and no effect of trapped entanglements or crystallization must occur during measurements,
- ii. The chains must be dynamically flexible which happens at temperatures higher than T_g and melting point T_m ,
- iii. The chains must be long enough so that the statistical calculations could be applicable,
- iv. The chains length distribution must follow a Gaussian distribution, i.e. for a chain with a fix end, the probability to find the other free end in a defined volume element, follows Gaussian statistics.

The theory of Flory is helpful to understand the mechanical behavior of elastomers at low strains where the behavior of polymer can be considered purely elastic. Moving towards higher strains, the deviation from ideal network's behavior appears and the Flory theory does not fit the experimental data. Mooney and Rivlin [13, 14] has considered the deviation from experimental results by introducing a new constant into the theory (C_2):

$$\sigma = 2 \left(\Lambda - \frac{1}{\Lambda^2} \right) \left(C_1 + \frac{C_2}{\Lambda} \right) \quad 1-8$$

where C_1 is the elastic parameter of rubber and C_2 is the term of deviation from the ideal network, and Λ the macroscopic deformation. The term C_2 is considered to be related to physical interactions and entanglements between chains which hinder the mobility of the chains [7]. Any factor capable to decrease inter-chain interactions and leading to the behavior of an ideal network decreases C_2 (e.g. higher crosslink density or higher crosslink functionality).

A polymer based on its physical state can behave differently to an imposed strain. This behavior as well as dependence on temperature and deformation rate is shown in Figure 1-3. As mentioned

previously, an elastomer shows relatively low resistance to deformation, which can be seen in Figure 1-3a for a non-crosslinked elastomer. Different behaviors of polymers are shown in the same Figure.

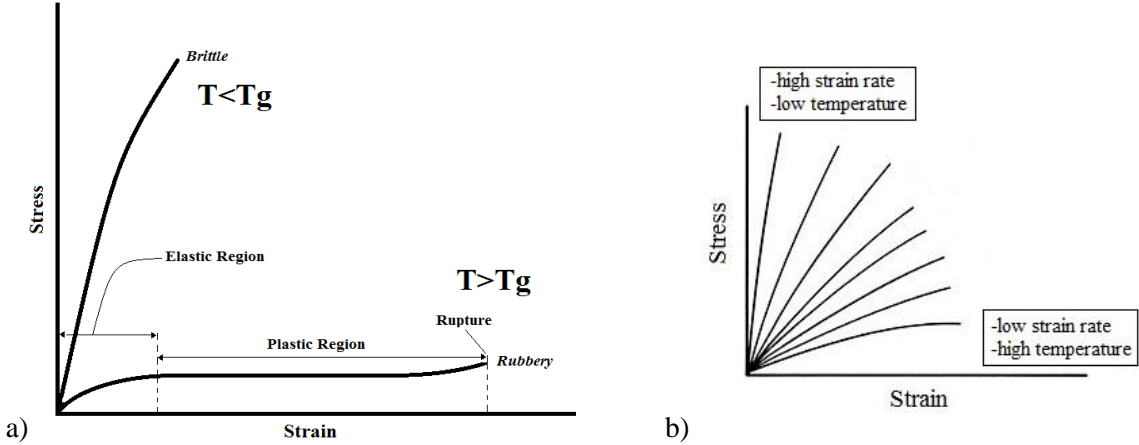
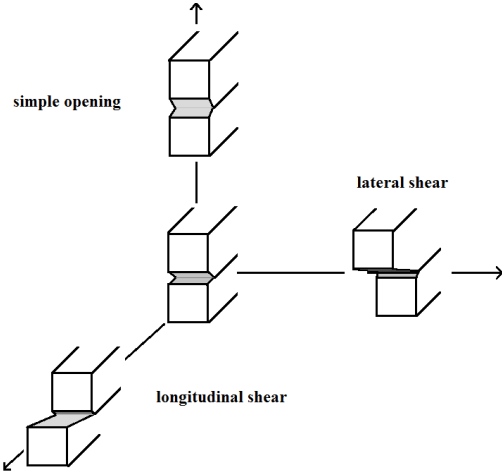


Figure 1-3: a) Different tensile mechanical behaviors of polymers. b) Dependence of tensile properties on the temperature and deformation rate.

An elastomer, below its glass transition temperature behaves as a brittle material and, by passing through this temperature, it shows a rubbery behavior which is the state for usage. For a very low deformation, the response is linear with the applied force and deviates from this linearity as the deformation increases. Through the elastic region of low deformation, the mechanical properties are functions of temperature and strain rate. These two latter operate in opposite ways, i.e. a rise in temperature is equivalent to a decrease in strain rate and vice versa (Figure 1-3b).

1.1.4 Properties at break

Depending on the mode of force application to a pre-cracked elastomer sample, three stress types can be exerted to open the sample, defined along the three principle axes (Scheme 1-3):



Scheme 1-3: Types of force application to open a pre-cracked elastomer sample

Supposing that the fracture of elastomers is due to the rupture of the chemical bonds in polymer chains under stress, the total break energy should be equal to the sum of the elementary energies of all bonds dissociated during fracture. This hypothesis was negated by Bueche who found that this calculated value is higher than the experimental ones by three orders of magnitude. Thus, he deduced that break is originated by a high local stress exerted on a limited number of chains and is gradually shifted to neighboring chains until the complete failure of the sample [15].

A perfect network does not exist and every material has irregularities and flaws such as cracks and voids. Practically, these defects are the initiating source of break. Short chains of a network show limited extensibility and can break sooner under large stress [16]. The energy balance, during a time interval dt , for a crack of length a in a plate of thickness l is (Equation 1-9):

$$\dot{U}_{ex} = \dot{U}_e + \dot{U}_c + \dot{U}_d + l\sigma_s \dot{a} \quad 1-9$$

with U_{ex} the energy brought to the system, U_e , U_c , U_d respectively the elastic, kinetic and viscous dissipated energies. σ_s is the necessary surface energy for creating a new surface (void). In the case of pure elastic rupture, all energies are zero except for elastic energy and crack creation. Thus, the energy restitution rate W would be:

$$W = \frac{1}{B} \left(\frac{dU_{ex}}{dt} - \frac{dU_e}{dt} \right) \quad 1-10$$

W depicts the available energy for crack propagation.

The elongation at break, as well as the tensile strength, depends on temperature. The tensile strength decreases while the sample is heated towards T_g and decreases vastly for temperatures well above T_g . However, the evolution of the elongation at break is different and more complex. Through glassy domain, it is very small, and increases with temperature attaining a maximum, and declines afterwards[16].

Bueche and White performed video tensile fractures on several rubbers [17]. They found that the propagation rate of a tear or a crack in elastomers reaches an upper limit. Maximum velocities of crack propagation in different rubbers showed to act as in a material with modulus and density in glassy region. This result led them to conclude that during rupture, rubbers behave like a glass, i.e. a brittle material. It was, as well, observed that the crack is created at low speed under stress, and increases as the speed of propagation increases with the strain. In another research, Thomas and Whittle [18] have studied the temperature dependence of rupture of natural rubber crosslinked by DCP and sulfur. They observed that the break mechanism follows two different pathways on the both sides of a critical temperature T_c , which depends on the nature of the chains and crosslinking degree. They explained

that above T_c the break is going through a tear process while, below T_c , the rupture is due to cracks growth.

1.2 Crosslinking by peroxides

1.2.1 Introduction

At their initial state, elastomers show low mechanical properties. In order to ameliorate this latter, a crosslinking step, which results in creation of inter-chain chemical bonds, is performed on raw elastomer gum. For the time being, based on the use of extrinsic species or energy sources, three major methods are being used to crosslink elastomers:

1. Sulfur compounds
2. Peroxides
3. Ionizing radiation

Historically, it is well-known that the first people who used rubber were Aztecs. They obtained rubber latex from rubber tree after mixing it with another plant's sap as solidifier [19]. However, solidification of rubber, via chemical reactions, was not formulized until the 19th century when Charles Goodyear and Thomas Hancock, separately but at the same period, crosslinked natural rubber by heating a rubber/sulfur mixture [20]. The crosslinking of rubber by sulfur is better known as vulcanization.

Organic peroxides, on the other hand, were not known as crosslinking agents until 1915 when Ostromislensky [21] used benzoyl peroxide to crosslink natural rubber. Actually, a wide range of organic peroxides can be used for curing, almost, all types of elastomers, in particular saturated gums. The advantage of using peroxides instead of sulfur as crosslinking agent is the higher thermal stability of C – C – C bonds in comparison with C – S – C bonds. However, sulfur vulcanisates show higher initial mechanical properties. It has also been demonstrated that the incorporation of sulfur compounds during peroxide crosslinking would lead to a rise in mechanical properties [22].

The first two methods of crosslinking, i.e. with sulfur and peroxides, are chemically induced while the third one, radiation, is physically induced. High energy rays such as γ , excimer laser, electron beam, etc., can create free radicals in elastomer and crosslinks can be formed by recombination of macroradicals. This method produces radicals randomly all over the chains and, in some cases, can cause the scission of chains as well. One of the semi-crystalline polymers widely cured by ionizing radiation is polyethylene where the crosslinking happens in its rubbery amorphous phase [23].

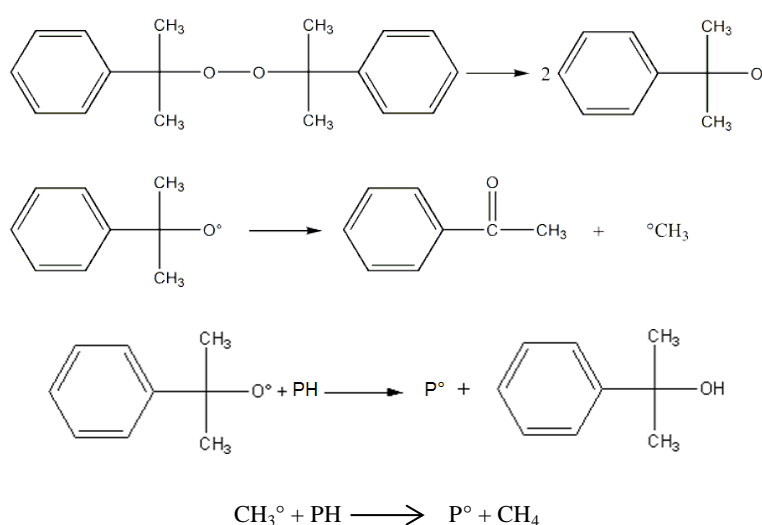
In this study, dicumyl peroxide will be used as crosslinking agent. The most important issue after crosslinking of EPDM with peroxide is the lack of knowledge on residual concentration of double bonds and their further effect on aging. In addition, the relative concentration of other monomer units, i.e. ethylene and propylene, may be another key parameter of the aging kinetics

In the following parts, a brief but complete mechanistic scheme of peroxide crosslinking of EPDM will be presented. First, the initiation by dicumyl peroxide (DCP), propagation and termination reactions will be detailed in the case of ethylene propylene copolymer (EPR). Then, the role of double bonds (EPDM) will be introduced in the crosslinking scheme.

1.2.2 Initiation by DCP

DCP incorporated into elastomer matrix goes through a homolytic scission under thermal stress to form two cumyloxy radicals [24]. These radicals can abstract a hydrogen atom on polymer chain or can reorganize via a chain scission, better known as β -scission, to create a ketone (acetophenone) and a methyl radical. This latter can also abstract a hydrogen atom from polymer chain and form a macroradical and a methane molecule (Scheme 1-4). The rate of β -scission depends solely on temperature [25]. In contrast, the rate of hydrogen abstraction depends on the nature of hydrocarbon substrate and the temperature. For instance, Bailey and Godin [26] determined the acetophenone/alcohol ratio formed from DCP decomposition in cumene. The results show that this ratio increases with temperature (Table 1-1).

It is clear that: higher the substrate reactivity, lower the molar ratio of ketone/alcohol. Thereby, a comparison of this ratio for a series of substrates having different types of labile hydrogen can be used to estimate their relative reactivity.



Scheme 1-4: Homolytic scission of DCP and β -scission of cumyloxy radical followed by hydrogen abstraction

Temperature (°C)	111	123.5	136.5	145	160
Acetophenone/alcohol	0.68	0.93	1.17	1.57	1.95

Table 1-1 :Ketone/alcohol molar ratio for DCP decomposition in cumene at various temperatures^[26]

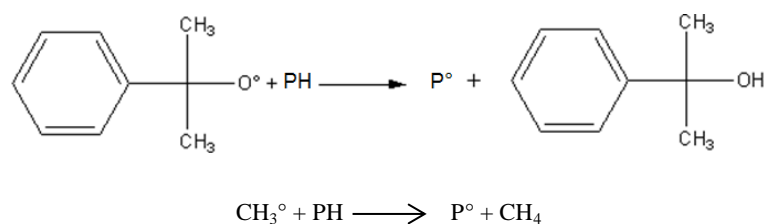
The thermal decomposition of DCP dispersed in kaolin and dissolved in a hydrocarbon solvent (di-n-butyl phthalate) have been studied by Brazier and Schwartz [27]. The effect of the substrate, as well as the heating rate, has been clarified and the results are presented in Table 1-2. Considering experimental errors, one can realize that the overall enthalpy of DCP degradation is independent of heating rate. The values found for kaolin are slightly lower than those in di-n-butyl phthalate because of the catalytic effect of argil.

Heating rate (°C/min)	$\Delta H_d \pm 5$ (kJ/mol)	$E_a \pm 8$ (kJ/mol)
Dicumyl peroxide		
20	217	140
10	212	142
5	216	138
40 wt% DCP on kaolin		
20	277	125
10	273	121
5	276	122
9,1 wt% DCP in di-n-butyl phthalate		
20	276	132
10	268	142
5	270	136

Table 1-2: Decomposition enthalpy (ΔH_d) and activation energy (E_a) for DCP in different reactive media^[27]

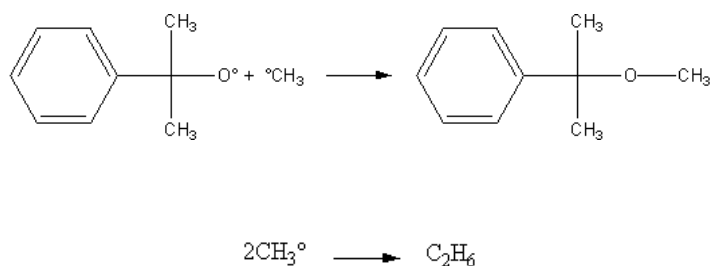
Hydrogen abstraction by produced radicals from macromolecular chain creates a macroradical. The abstraction takes place on the most labile hydrogen. Thus, the facility of hydrogen abstraction will vary in the order: allylic > tertiary > secondary > primary, while the reactivity of respective formed radicals will be sorted in the inverse order [28].

The DCP crosslinking efficiency of ethylene based copolymers, having different chemical composition, has been studied by Robinson et al. [29]. These authors used swelling test to measure the crosslink density of the cured samples. They have considered two principal hydrogen abstractions, first by cumyloxy radical to form a cumyl alcohol, and second by methyl radical to form methane (Scheme 1-5):



Scheme 1-5: Hydrogen abstraction by DCP radicals on a macromolecular chain

Both types of radicals formed from DCP decomposition have also the possibility to react together to form an ether linkage or an ethane molecule (Scheme 1-6). Since these two molecules are produced in very low concentrations, their formation is in general neglected.



Scheme 1-6: Side products of DCP decomposition

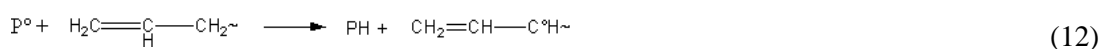
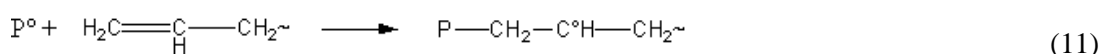
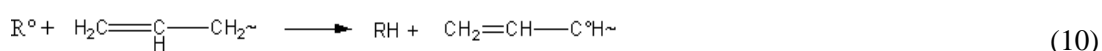
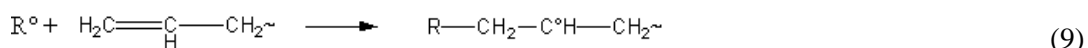
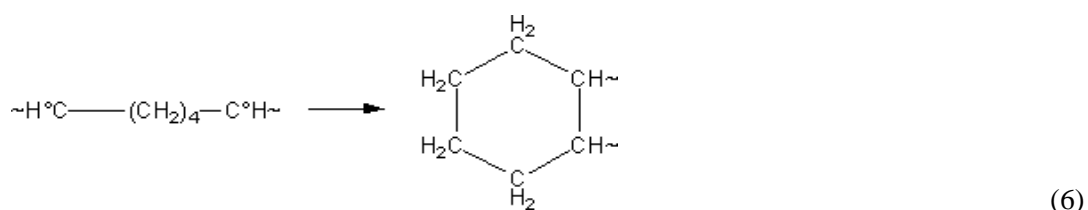
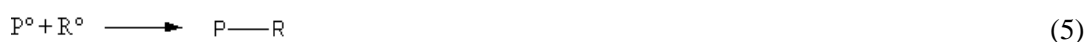
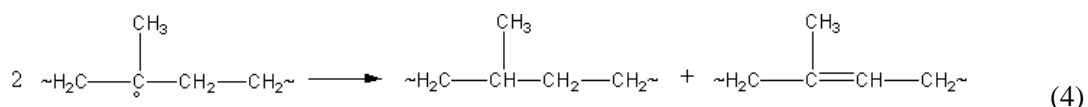
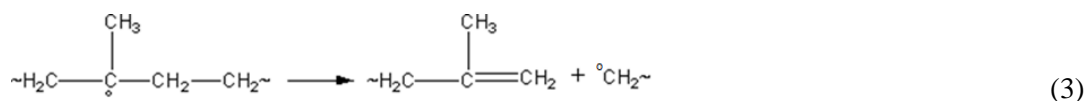
As a result, the two main reactions of Scheme 1-5 are in competition, and the ratios between the reaction products depend on the chemical structure of the polymer matrix and temperature. But it has been already demonstrated that, in the conventional crosslinking temperature range, the decomposition fraction of DCP into acetophenone and methyl radical is higher than the formation of cumyl alcohol [30].

1.2.3 Ethylene-Propylene Copolymers (EPR)

For a better understanding of EPDM crosslinking, a scanning review on saturated ethylene-propylene rubber (EPR) could be useful.

An EPR rubber possesses methyne (tertiary hydrogen), methylene (secondary hydrogen) and methyl (primary hydrogen) groups. The probability of primary hydrogen abstraction is very low because of its high bond dissociation energy ($E_D \sim 415 \text{ kJ}\cdot\text{mol}^{-1}$). Therefore the hydrogen donation competition remains between methyne groups of propylene units ($E_D \sim 378 \text{ kJ}\cdot\text{mol}^{-1}$) and methylene groups of ethylene units ($E_D \sim 393 \text{ kJ}\cdot\text{mol}^{-1}$). However, the observed selectivity depends not only on lability of hydrogens, but also on reactivity of radicals. Thus, depending on curing temperature, various

mechanistic pathways can be envisaged for crosslinking. Loan has proposed the following mechanism (Scheme 1-7) for peroxide crosslinking of EPR [31, 32]:



Scheme 1-7: Crosslinking mechanism for EPR [31, 32]

where R° is alkoxy radical, PH labile hydrocarbon chain, P° alkoxy radical, and P'° , P''° , P'''° primary, secondary and tertiary radicals from EPR.

In the case of an EPR, the potential coupling reactions may have a steric hindrance. To overcome this barrier, a radical needs an appropriate rotation so the radical combination could be achieved. Radicals, produced by hydrogen abstraction from methylene groups of ethylene gain in reactivity due to their

accessibility, and can easily couple with each other to produce a tetrafunctional crosslink. Consequently, coupling between the methylene radicals in ethylene sequences occurs easily. The DCP crosslinking efficiency of a polyethylene has been estimated close to unity, which means one crosslink for one DCP molecule [33]. However, methylene radicals can undergo disproportionation instead of coupling which decreases the crosslinking efficiency and creates unsaturated bonds. Disproportionation is improved by steric hindrance, availability of transferable hydrogens, and increasing the temperature.

Tertiary hydrogens of propylene units can as well be abstracted by radicals. A methyl group attached to this macroradical creates steric hindrance and makes the coupling difficult. This can lead to a chain scission that creates a double bond and a radical at chain's extremity [34, 35]. Chain scission decreases the network density and although, the formed terminal double bonds can get involved in crosslinking, the overall effect of β -scission remains the diminution of crosslink density. Additives can be added to the system in order to decrease chain scissions but this subject is out of interest of this study.

The EPR samples studied by Loan [22], containing (58 ± 5 mol%) and (65 ± 5 mol%) of ethylene, were crosslinked by dicumyl peroxide. He established the relationship between the density of chemical crosslinking and the parameter C_1 , i.e. the elastic term in the Mooney-Rivlin equation. Loan found that C_1 increases linearly with the peroxide concentration, as well as ($C_1 + C_2$). C_1 was determined from compression modulus at low deformation on swollen specimens in the range of 0-6% DCP. Consequently, it was deduced that the apparent efficiency of crosslinking is independent of peroxide concentration.

Based on what preceded, most of possible bimolecular reactions mentioned in Loan's mechanism (Scheme 1-7) have been considered to be negligible. The entire crosslinking chemistry has been experimentally and kinetically adapted to the fact that: all methylenic macroradicals participate mainly in effective crosslinking, while all methynic macroradicals end up into chain scissions. Macroradicals produced by chain scissions combine with methylenic radicals to form tri-functional crosslinks, or between each other to form a chain extension.

1.2.4 Ethylene Propylene Diene Terpolymers (EPDM)

In order to increase the crosslink density, a third monomer, containing double bonds on side chain, has been introduced into the EPR chains. The double bonds of the resulting EPDM can be opened by macroradicals to form crosslinks.

Harpell and Walrod have compared the peroxide crosslinking of EPDM with EPR and PE [36]. They followed the crosslinking reaction using torque measurement for several peroxide concentrations (Figure 1-4). The results showed that the torque gap between crosslinked and linear PE ($M_H - M_L$),

increases linearly with the concentration of peroxide. This result is not valid for EPR and EPDM rubbers because of the presence of propylene units. By increasing the concentration of DCP, the concentration of tertiary macroradicals increases as well and leads to a growth in β -scission. In the same Figure 1-4, one can recognize the effect of double bonds on the crosslinking progress of EPDM.

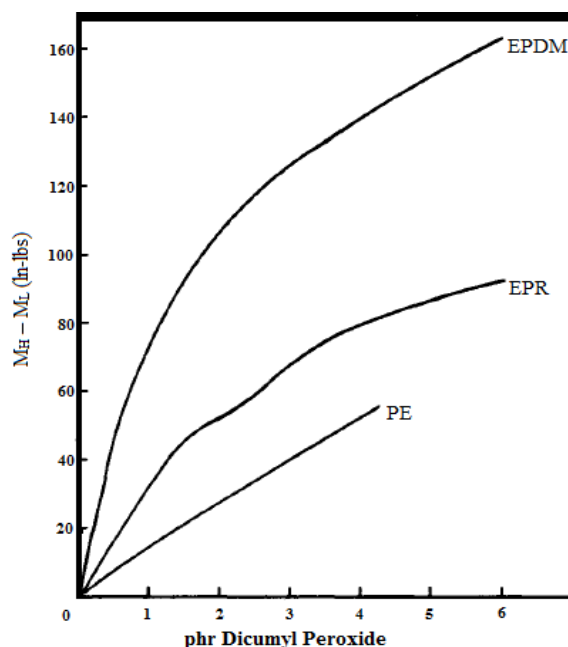


Figure 1-4: Mechanical response of PE, EPR, and EPDM during crosslinking.^[36]
 M_H : high torque (crosslinked polymer), M_L : low torque (un-crosslinked polymers)

In EPDM, macroradicals can propagate in two ways:

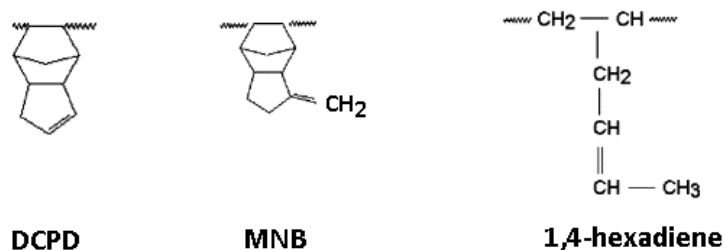
- I. By addition onto the double bonds,
- II. By abstraction of allylic hydrogens.

The first pathway is favored when double bond is terminal [28]. The radical produced by addition reaction on a terminal double bond is very reactive and, in the absence of steric hindrance, can react with another double bond to create a tetrafunctional crosslink without radical destruction. Thus, terminal double bond can provide the conditions to attain high crosslinking efficiency and high functionality of crosslinks. The addition of a radical to an internal double bond on the side chain does not lead to chain reaction due to steric hindrance. Thus, such an addition would have, mostly, a tendency to abstract a hydrogen atom from another unit, or to couple with another radical to form a crosslink. On this basis, one should expect that EPDM containing internal double bonds should attain the efficiency of crosslinking close to 1, i.e. one macroradical can open only one double bond [37]. The molecule with an internal double bond tends to react more by abstraction of allylic hydrogens, which produces radicals stabilized by resonance, and this stability leads to a decrease in the crosslinking yield [37]. In summary, the polymerisability of unsaturated segments is determined by the

position of the double bond (internal or terminal), the concentration of allylic hydrogens, their accessibility and the relative stability of resulting allylic radicals [38].

In addition to the question of crosslinking efficiency, it may be important to know if crosslinking takes place by the coupling of radicals or by an addition reaction of radicals on double bonds. In the latter case, the double bond is saturated, whereas in the former case, it remains intact. The final concentration of allylic hydrogens could be a key parameter of the vulcanisate aging kinetics. Indeed, the allylic hydrogens are more labile than methynic and methylenic ones, so the induction time of the autocatalytic oxidation would considerably reduce if allylic hydrogens are present [39].

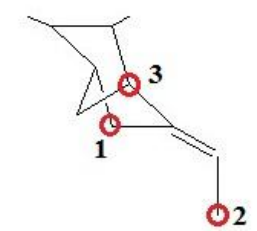
Wataya and Fujimoto [40] showed that the type of double bonds can as well affect the crosslinking mechanism. They compared three different EPDMs containing methylene-norbornene (MNB), dicyclopentadiene (DCPD), and 1,4-hexadiene (HD) (Scheme 1-8) crosslinked by 2.7 phr of peroxide. Crosslinking was carried out at 140°C for 100 minutes. The results of double bonds consumption were 85 mol.-%, 40 mol.-% and 29 mol.-% respectively for MNB, DCPD and 1,4-HD. MNB has a terminal vinylidene double bond, and thus the addition reaction predominates. The DCPD has an internal double bond and bears two active allylic hydrogens, while 1,4-HD has an internal double bond and bears five active allylic hydrogens. Logically, one would expect that 1,4-HD will induce a crosslinking by coupling of allylic radicals.



Scheme 1-8: Different types of diene monomer in an EPDM

It is licit to assume that ENB (ethylidene-norbornene) would tend to behave more like 1,4-HD than DCPD, due to their internal double bond. ENB has six hydrogens in α -position from the double bond (Scheme 1-9). Although position 3 is α from double bond, the formation of allylic radicals at this position cannot take place according to Bredt's rule¹ [41]. Thereby, ENB contains five active hydrogens: Two in the hexagonal cycle (position 1) and three on the methyl group (position 2).

¹ From IUPAC: "A double bond cannot be placed with one terminus at the bridgehead of a bridged ring system unless the rings are large enough to accommodate the double bond without an excessive strain."



*Scheme 1-9: Allylic positions in ENB unit.
(Position 1: two hydrogens, position 2: three hydrogens, position 3: one hydrogen)*

Few researchers tempted to demonstrate the position of an allylic crosslinking through an indirect method. For instance, Baldwin [42] exposed a crosslinked swollen EPDM-ENB to ozone at low temperature to obtain cleavage of the remaining double bonds. If the crosslink is in position 2, then the cleavage of double bond leads to a chain scission and reduces the crosslink density. In contrast, if the crosslink is on position 1, the cleavage of double bonds destroys the dangling double bond and leaves the elastically active chains intact. By this technique, it was reported that the methyl groups of ENB in α -position from double bond are involved in the crosslinking process up to 24%.

Other authors tried to demonstrate the position of crosslinks by a direct way, in particular by detecting the radical species formed during the crosslinking of EPDM initiated by DCP. As an example, Zachary [37] used electron paramagnetic resonance spectroscopy in order to detect allylic radicals. The percentages of allylic radicals were 90 mol.-% on position 1 and 10 mol.-% on position 2.

We know that a fraction of double bonds are consumed during peroxide crosslinking, but we do not know exactly how. Orza *et al.* [43, 44] studied the peroxide crosslinking of EPDM-ENB by using solid-state NMR. They found that the crosslink density is higher than the conversion of ENB over the total duration of crosslinking, even at the end of the crosslinking reaction (Figure 1-5). In other words, crosslink density increases faster than the conversion of ENB. However, at the end of crosslinking, ENB conversion continues, while the formation of crosslinks is stabilized. It was concluded that the crosslinking is initially dominated by bimolecular termination of macroradicals produced after peroxide decomposition, while at the end, the addition of macroradicals on ENB double bond takes over. Thus, the ratio between the rates of bimolecular termination of radicals and addition of radicals on double bonds, during peroxide crosslinking, changes over time. In addition, a peroxide yield of 50 mol.-% and a diene conversion of 40 mol.-% have been obtained, while the contribution of addition reactions to the total crosslinks was reported to be about 40 mol.-%.

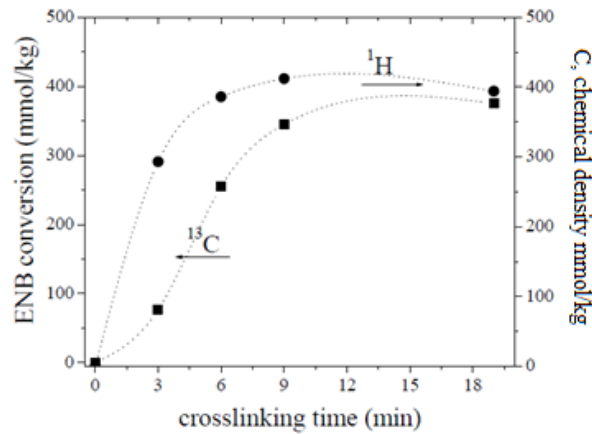
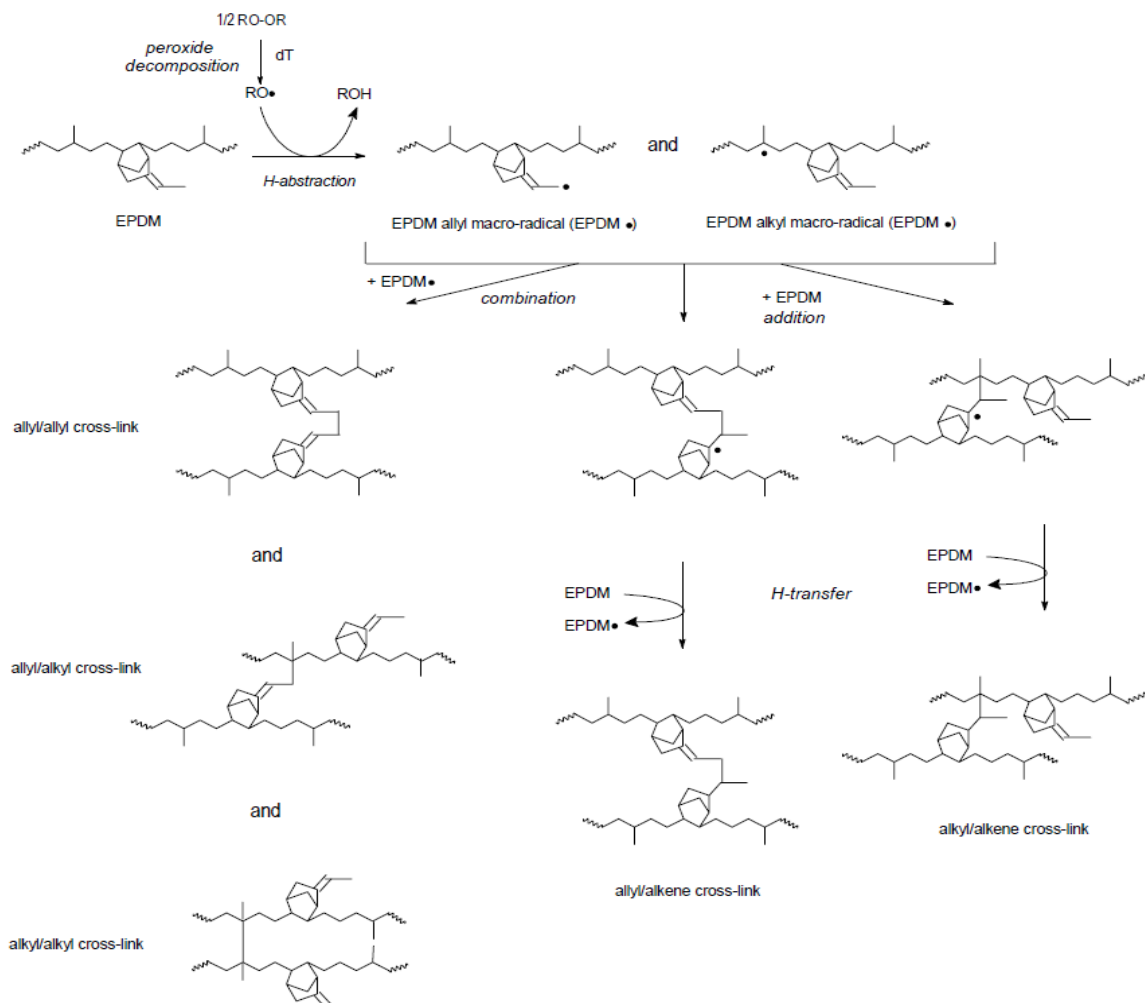


Figure 1-5: Increase in crosslink density (^1H NMR) and consumption of ENB double bonds (^{13}C NMR) for an EPDM-peroxide mixture ^[43]

^{13}C NMR and ^1H NMR spectroscopies allowed the authors to propose the following crosslinking mechanism (Scheme 1-10) of EPDM-ENB by peroxide [44]:



Scheme 1-10: EPDM-ENB peroxide crosslinking mechanism proposed by Orza (2008) ^[44]

For the moment, the presented crosslinking mechanism is generally accepted. It involves the most important elementary reactions. Although all the possible (secondary) reactions are not considered in the mechanism, their omission does not gravely affect the crosslinking kinetics.

1.3 Fillers

A crosslinked elastomer normally presents low mechanical properties. In order to achieve higher properties for industrial usage, fillers are introduced into elastomeric matrices. Particulate filled polymers show higher modulus, ultimate properties, hardness, tear resistance, etc. Some type of fillers, in the same time, can deliver other properties to the composite material such as fire retardancy or aesthetic aspects. In addition, high contents of low priced fillers, comparing to other components, decrease considerably the body costs.

1.3.1 Criteria for choosing fillers

Choosing filler depends on several criteria like their contribution to elastomer properties and evolution of these properties at long-term. The most important characteristics of fillers are:

a. Chemistry and composition

The chemistry of filler in bulk may or may not have an influence on overall characteristics and properties. Based on the chemical functions existing, filler can be active or inert facing external stresses. For instance, aluminum trihydrate (gibbsite) reacts as a fire retardant in temperatures over 200°C, by freeing molecules of water.

Going from the bulk to the surface of filler, the chemistry becomes more effective. Chemical properties of surface are determinant for mixing and processing operations. In some cases, a better interaction between the filler and the polymer chains is expected, and in order to achieve a better adhesion, surface reactive agents are added to the mixture. Surface agents can be single active, i.e. they can only be attached chemically to the filler, and have physical interaction with the polymer. They also can be dual reactive, so they can create chemical bonds between filler surface and polymer matrix and, thus, ensure a chemical continuous interphase. An example for the first case is stearic acid which improves the rheological properties when added to polyethylene or polypropylene, because of a better interaction between the organic structure of acid and the polymer chains[45]. An example for the second type is 3-(trimethoxysilyl)-propyl methacrylate which is used as coupling agent in thermoset or thermoplastic matrix composites, where it gets involved at filler/matrix interface to make a chemical continuous interphase [46].

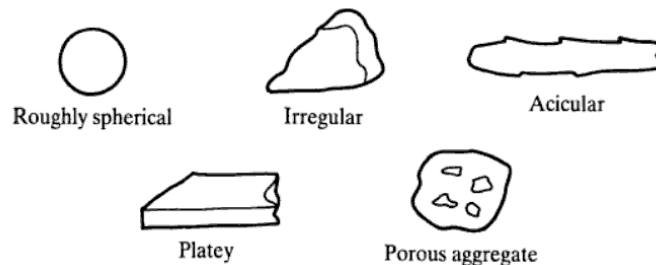
The interaction between the matrix and the filler is of great importance for obtaining better properties and good wettability and dispersion. Sometimes the organic nature of the polymer is not compatible with the mineral nature of the filler, for which surfactants are used.

Furthermore, there is usually an important gap between the thermal expansion coefficients of the filler and matrix. When the composite is used at temperatures well below the crosslinking temperature, this difference generates a high thermal residual stress at the filler/matrix interface, which has a direct effect on mechanical properties.

The properties of a composite can also be affected by the presence of impurities in filler [47]. These impurities can be naturally present in filler, i.e. a natural molecule from mine, or it can be introduced during the processing of filler, and can decrease the oxidation induction time. When the impurity is inert and its concentration is low, its effect is negligible.

b. Shape and size

Properties of a polymer can be adjusted by the introduction of fillers capable to contribute to some sought properties. This characteristic of fillers is, to some extent, related to their shape and morphology which can modify tensile properties, stiffness, rigidity and rheological properties of the composite. A natural filler form and shape depends on its crystalline structure while for a synthetic product it is defined by its chemical structure. This latter gives the possibility to produce different particle shapes for the same chemistry of filler.



Scheme 1-11: Several forms of filler particles^[48]

The two main geometrical factors of fillers are the particle size and specific surface (Scheme 1-11). These two parameters, which are somehow related, play a major role in determination of the final composite properties. There are several methods for measuring particle size such as optical scattering and diffraction or sieving. The issue to consider is that, in a composite, the filler exists in different form of accumulation that goes from primary particles to agglomerates and large aggregates. The final properties of the composite are strongly dependent on the dispersion level of particles, in particular their accumulation form (Figure 1-6).

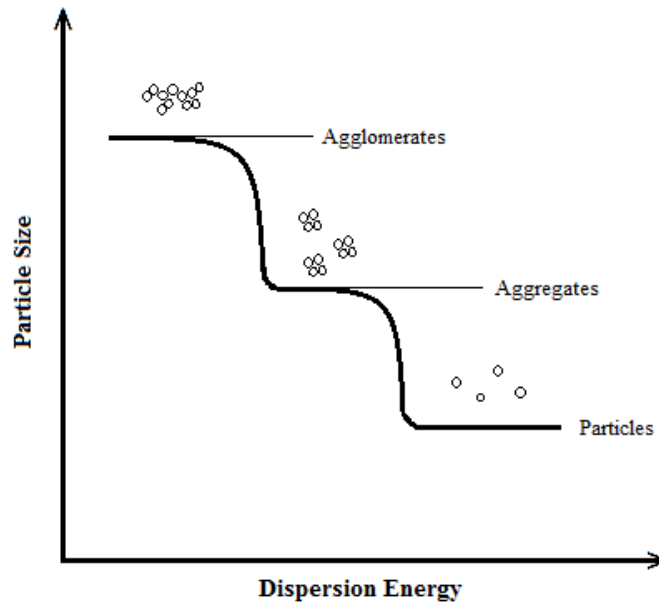


Figure 1-6: Dispersion energy of fillers vs. particle size^[48]

The specific surface is the surface per mass of fillers accessible to polymer matrix. It is obvious that the smaller the particle size or the lower the filler accumulation, the higher the specific surface. The importance of measuring the particle size and specific surface comes from the fact that the role of the filler is to trap polymer macromolecules on its surface. Therefore, the higher the specific surface, the more effective the composite reinforcement. Low polymer interaction with filler particles results in a phenomenon known as dewetting, which is the process of losing filler/matrix contact and beginning of cavitation.

1.3.2 Fire retardant filler

1.3.2.1 Aluminum trihydrate

Several types of filler are recommended for combustion inhibition such as Aluminum trihydrate (ATH), zinc borate, halogenated hydrocarbons, magnesium hydroxide, etc. ATH is one of the most widely used fire retardants [49], which plays the role of fire suppressant as well. The appellation gibbsite refers to a monoclinic crystal system of ATH with a sheet structure. The crystallites have a pseudo hexagonal platelet shape. Each sheet is composed of nominal charge (Al^{3+}) arranged between two layers of (HO^{-}) ions (Figure 1-7) [50].

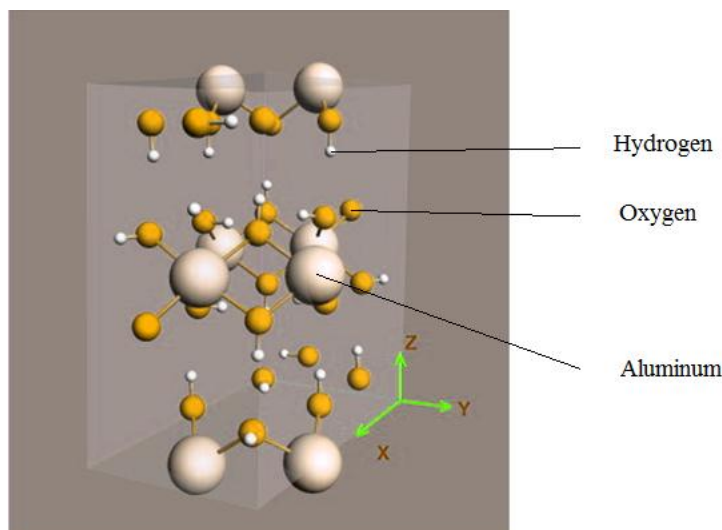
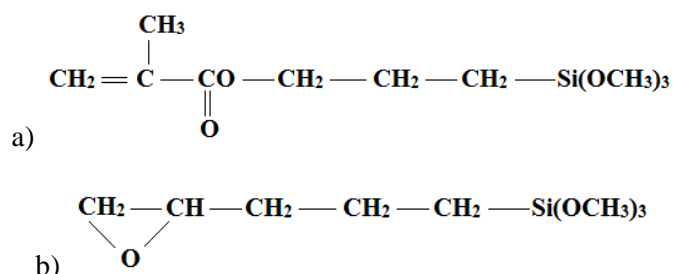


Figure 1-7: Structure of aluminum trihydrate ^[50]

This white, non-toxic filler decomposes at temperatures above 200°C into aluminum oxide and water through a complex reaction. Considering this latter, it is evident that ATH would be hard to use for polymers having processing temperature around 200°C. Gibbsite decomposition passes through an intermediate stage at really high temperatures that forms boehmite (AlO(OH)), i.e. aluminum hydroxyl oxide, which reduces fire the retardancy efficiency. The formation of boehmite increases with gibbsite particle size [51].

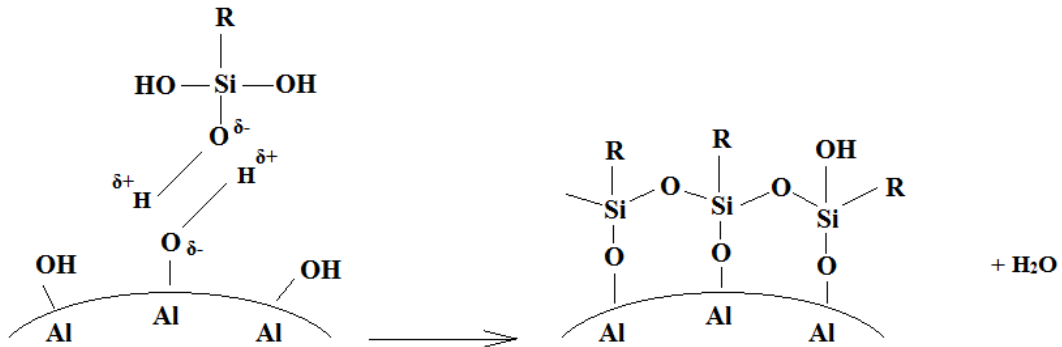
1.3.2.2 Chemical surface treatment

The particles of ATH go through surface modifications in order to ameliorate their interactions with polymeric matrices. The most common surface treatments are organo-silanes that can get both involved with mineral fillers, and be compatible with organic matrices [52]. Two examples of these coupling agents are methacryloxy-propyl-trimethoxy-silane (Scheme 1-12a), and glycidoxy-propyl-trimethoxy-silane (Scheme 1-12b).



Scheme 1-12 : Examples of organo-silane coupling agents

The first step to functionalize the surface of ATH is hydrolysis of the coupling agent [53] in an acidic or alkali solution (Equation 1-11). The resulting triol function can then be attached on the surface of the filler through a condensation reaction (Scheme 1-13). H_2O



Scheme 1-13 : Condensation phenomenon of organo-silane coupling agents on filler surface (Adapted from condensation of the same coupling agent onto silica)^[53]

The condensation step is normally carried out in a water-ethanol mixture containing up to 5 wt.-% of acid, and can form a multi-layer coating (up to 10 layers) [53].

1.3.3 Matrix/filler interactions

As previously mentioned, fillers are introduced into polymer matrices as reinforcements to obtain better mechanical properties. The adsorption of polymer chains onto particle surface can be considered as physical crosslinks because of strong interactions. Although the molecular models obtained through well-controlled technologies, such as sol-gel, can give some elucidations on reinforcement mechanism, the totality of modeling remains hypothetical to a high extent [54, 55].

Several authors have studied the effect of fillers, proposing theories describing particulate reinforcement. This latter depends on mutual interactions between polymer chains, between polymer chains and filler particles and between filler particles as well. Empirical relationship equivalent to Einstein's equation for the viscosity of colloidal solutions, is proposed by Smallwood [56] to account for the effect of fillers on elastic properties:

$$E = E_0(1 + 2.5\varphi) \quad 1-12$$

where E_0 is the modulus of unfilled polymer and φ the volume fraction of fillers. It is necessary to point out that this equation is valid for low concentrations of filler (no interactions between filler particles), the composite being assimilated to a suspension of filler particles in the matrix.

Guth and Gold [57, 58] have proposed a model using an polynomial equation (1-13) with an amplification factor considering higher fractions of filler in the matrix. They tried to model the effect of interactions between spherical fillers on mechanical properties of the matrix, and the matrix modulus in particular. Supposing the fillers as rigid particles, they proposed:

$$E = E_0(1 + 2.5\phi + 14.1\phi^2) \quad 1-13$$

Nevertheless, the real network modulus is higher than the values found by this model. This deviation is mainly due to filler-rubber interactions behaving as extra crosslinks which are not considered in the model. Kerner's equation (1-14) is frequently used for experimental data evaluation where it considers the Poisson coefficient of the matrix, ν_m :

$$E = E_0 \left(1 + \frac{\phi 15(1-\nu_m)}{(1-\phi)(8-10\nu_m)} \right) \quad 1-14$$

There are several other models which are used such as Chow, Nielsen, Nicolais-Narkis, Landon, etc. As an example, this latter, in addition to the effect of filler fraction on tensile stress, takes the effect of particle size (d) into account:

$$\sigma_c = \sigma_m(1 - \phi) - k\phi d \quad 1-15$$

where σ_c and σ_m are composite and matrix tensile strength respectively, and k is a constant.

When an elastomer network is subjected to large strains, large growth in modulus is observed due to non-Gaussian effects arising from limited extensibility of short chains [59]. The presence of filler particles increases the number of short chains and decreases the average length of chains. This phenomenon is referred to as strain amplification. Several proposals have been made to access to the amplification factor, by calculating the extension ratio in the rubber, α [60, 61]. The real extension ratio is proposed to be:

$$\alpha_r = \frac{\alpha - \phi}{1 - \phi} \quad 1-16$$

with α_r the extension ratio in rubber and α , the macroscopic extension ratio of composite.

Nielsen [62], in his works on filled polymers, proposed simplified equations to calculate stress-strain properties. He supposed a perfect adhesion between matrix chains and filler particles for elongation at break, but no adhesion for tensile strength (Figure 1-8).

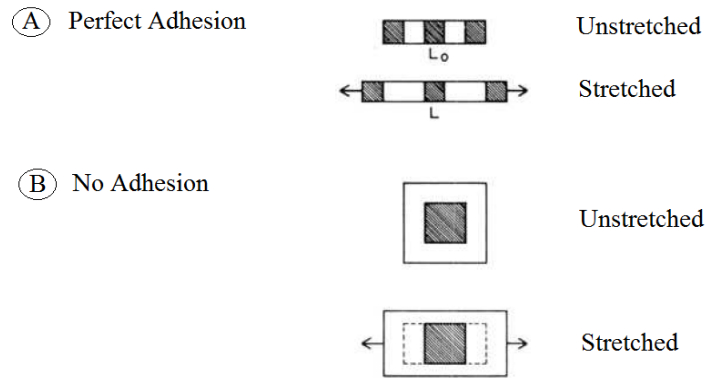


Figure 1-8: Deformation of a filled polymer for a) perfect adhesion and b) no filler/matrix adhesion^[62]

Considering these two boundary cases and assuming that the polymer matrix breaks at the same elongation in the filled system as in the unfilled system, the elongation at break would be:

$$\frac{\varepsilon_b(\text{filled})}{\varepsilon_b(\text{unfilled})} = 1 - \varphi^{1/3} \quad 1-17$$

This relationship is plotted in Figure 1-9.

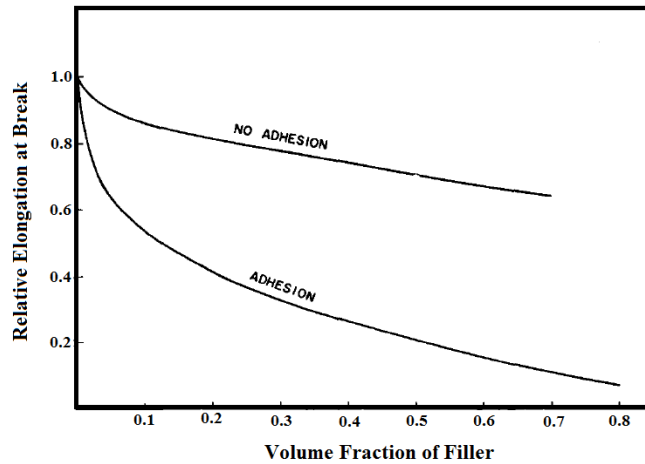


Figure 1-9: Effect of filler fraction on elongation at break^[62]

The Equation 1-17 proposes that the introduction of fillers into polymer matrix decreases the elongation at break. Although for several polymers this equation goes well with experimental results [63, 64], it is not a general rule. For instance, in the works of Poh et al., this effect is clearly shown [65]. Two different grades of natural rubber were mixed by carbon black, silica and calcium carbonate particles, and eventually vulcanized. Tensile strength of carbon black and silica filled elastomers increases with filler fraction, while the effect is inverted for calcium carbonate filled elastomers (Figure 1-10a). The effect of fillers on elongation at break is the opposite for the tensile strength, i.e. it

decreases as carbon black and silica fractions increase, and increases when calcium carbonate fraction increases (Figure 1-10b).

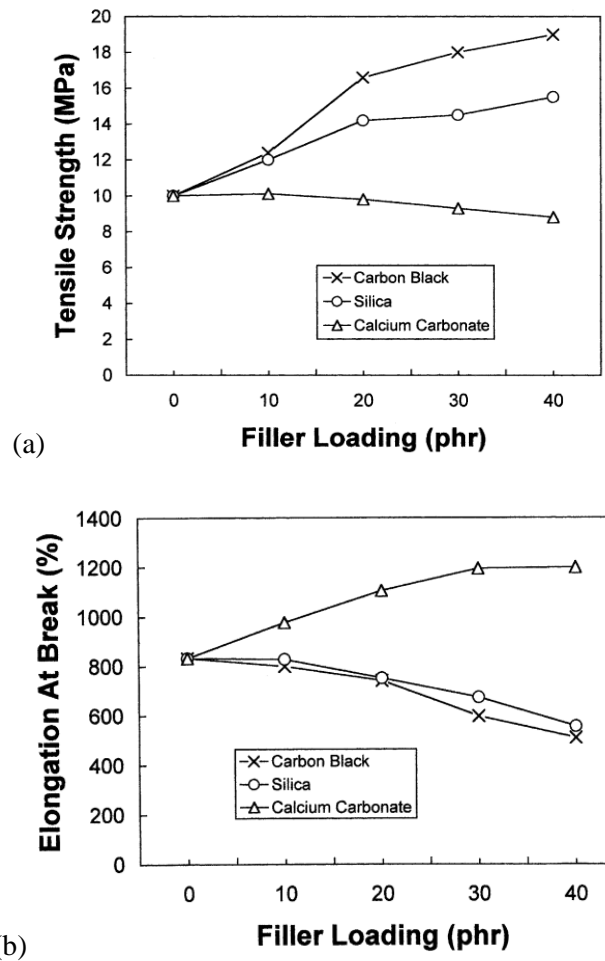


Figure 1-10: Effect of several filler fraction on a) tensile strength and b) elongation at break of EPDM composite^[65]

The effect of ATH on EPDM matrices was studied by Planes *et al.* where they showed that ATH has similar effect on EPDM as silica on natural rubber [66].

1.3.4 Swelling of filled elastomers

Introduction of fillers into a polymer matrix has been shown to increase the mechanical properties of the elastomer. The polymer chains are partially adsorbed onto filler surface, such as carbon black or silica, leading to reinforcement and improvement of mechanical properties [67]. This adsorption can be really strong and quasi-irreversible, so it can be considered as a physical crosslink [68]. In addition, in some cases, the filler contains chemically active surface treatments that can establish chemical bonds with polymer chains in order to form chemical junctions.

The Flory-Rehner equation has shown to be a reliable method for equilibrium swelling calculations in order to find the crosslink density of the crosslinked matrix. The introduction of fillers into the matrix creates huge complications and, depending on the hypothesis made about the filler-matrix interactions, as well as the type of network, the results can be diversified. Some authors made the assumption that the swelling of a filled network is similar to that of an unfilled vulcanisate and the fillers play the role of extra crosslinking sites[69, 70]. In the same perspective Lorenz has proposed that the swelling of a filled matrix is similar to an unfilled matrix, except in the vicinity of the particles interface, where the polymer chains in contact with filler particle behaves as an elastomer shell [71].

In a study on the filler-matrix interactions and the swelling behavior of composite, Kraus explains the effect of these interactions [72]. Introducing the parameter q as linear swelling coefficient and φ as the volume fraction of fillers, the final volume of swollen rubber would be $(1 - \varphi)q^3$ in the case where no filler-matrix interactions exist at swollen state. By swelling the rubber, it forms a “*vacuole*”² around each particle, which will be filled with solvent. The total volume of vacuoles is $\varphi(q^3 - 1)$. As a result, the volume swelling ratio Q will be:

$$Q = v_r^{-1} = (q^3 - \varphi)(1 - \varphi) = (v_{r0}^{-1} - \varphi)(1 - \varphi) \quad 1-18$$

with v_r the apparent volume fraction of the elastomer in the swollen gel and v_{r0} the true volume fraction of elastomer in the swollen gel, i.e. in absence of filler.

In the case of filler-matrix permanent interactions, equation 1-18 will be replaced by a more complicated one, and this is because the swelling in the vicinity of the interface is complex. Anyhow, the final equation is:

$$\frac{Q}{Q_0} = \frac{(q^3 + \Delta V)}{q^3} = 1 + [1 - q^{-3} - 3c(1 - q^{-1})] \left(\frac{\varphi}{1 - \varphi} \right) \quad 1-19$$

where Q_0 is the volume swelling ratio of unfilled polymer and c a function of particles diameter. ΔV is defined as below:

$$\Delta V = q_0^3 [1 - q_0^{-3} - 3c(1 - q_0^{-1})] \frac{\varphi}{1 - \varphi} \quad 1-20$$

In this approach, the network model is supposed to be affine. In the affine theory, the junction points of the network are assumed to be embedded in the network. As a result, components of each chain vector transform linearly with macroscopic deformation. The ultimate form of Kraus equation to calculate the concentration of elastically active chain is:

² A vacuole is an enclosed compartment including solvent that encompass the filler particle

$$\nu = \frac{V_{r0} \ln(1-V_r) + \chi V_r^2 + V_r}{V_S \quad 0.5V_r - V_r^{1/3} V_{r0}^{2/3}} \quad 1-21$$

where V_S is the molar volume of solvent and χ the Huggins solvent/polymer interaction parameter.

A parallel theory has been developed by James and Guth [73] who have supposed that the junction points “fluctuate over time without being hindered by the presence of neighboring chains”. The extent of fluctuations is not affected by the macroscopic state of deformation. The fluctuation ability of the junctions is the reason why this theory is called *phantom*. Considering phantom theory in Flory-Rehner equation, Erman and Mark derived the “Flory-Erman” equation (1-22) to calculate the concentration of elastically active chains ν in a filled polymer [54, 74]:

$$\nu = \frac{\ln(1-V_r) + \chi V_r^2 + V_r}{\rho(1-\frac{2}{\phi})V_r^{1/3}V_S} \quad 1-22$$

with V_r the molar volume fraction of polymer in gel, V_S the molar volume of solvent, χ the Huggins solvent/polymer interaction parameter and ρ the polymer volumic mass.

Vacuole formation can happen when the filler/matrix interactions are purely physical. When the interactions have a chemical origin, they cannot be undone by solvent penetration and therefore, no vacuole can be formed and the swelling ratio of the material tends to lower values, as shown by Berriot et al. [75].

1.4 Aging of polymers

The polymeric materials, used as miscellaneous parts of diverse structures, are sometimes exposed to harsh conditions such as thermal, irradiation or chemical stresses. Under these conditions, polymers tend to age and degrade more rapidly, which reduces their life-time and, eventually, the life-time of the structure. These modifications in a polymer can be costly and, occasionally, hazardous, and that is why attempts have been brought to the life-time prediction and aging modeling.

1.4.1 Methods for life-time prediction

It is more than 50 years that English researchers, Boland and Gee [76-78], have done the first attempts to model the aging of saturated elastomers in a study on materials aging kinetics. Since, several methods of life-time prediction have been developed. In what follows, the three most developed methods are presented.

1.4.1.1 Arrhenius method

Arrhenius law of time-temperature equivalency is the common approach for life-time prediction in industry. This method is based on the idea that the same state of a degraded material can be reached through accelerated aging tests at temperatures higher than use condition. This method is applicable by assuming that the aging mechanism, thus the aging pathway, at higher temperatures remains identical to the one of material use condition. The life-time of a material t_f can be defined by the duration for attaining a critical value a predefined chemical, physical or mechanical property such as carbonyl index, oxidation induction time or elongation at break [79].

The Arrhenius law is expressed as:

$$t_f = t_{f_0} \exp\left(-\frac{E}{RT}\right) \quad 1-23$$

with:

- t_{f_0} : pre-exponential factor
- E : apparent activation energy
- R : perfect gas constant
- T : absolute temperature in Kelvin

Once the endlife criterion is chosen and the accelerated tests are fulfilled, the life-time is plotted as a function of the absolute temperature on an Arrhenius diagram known as "thermal endurance diagram" (Figure 1-11).

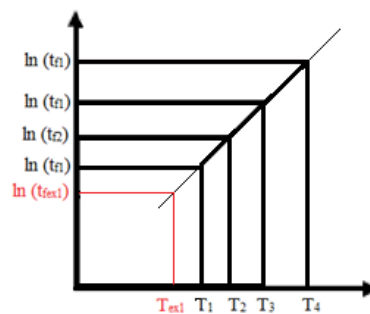


Figure 1-11: Thermal endurance diagram

Once the Arrhenius straight-line is plotted, the life-time can be predicted for any temperature by extrapolation (T_{ex1} , $\ln(t_{fex1})$).

In the case of PE, for instance, several authors have used this method to predict its life-time at ambient temperature. As an example, Hsuan et al. have determined the Arrhenius law of oxidation induction

time, as the endlife criterion, between 55°C and 75°C in natural atmosphere [80]. They claimed that the life-time of PE is between 122 and 172 years at 20°C.

A common endlife criterion in industry is attaining 50% of the initial value of elongation at break. However, 3 – 4% of weight loss is also frequently used due to the ease of utilization. For the time being, several researchers apply this methodology to study the thermal stability and degradation of polymeric materials by using a thermo-gravimetric analysis (TGA) apparatus. Further methods are cited in the literature such as cristallinity, carbonyl index, stiffness, etc. [81].

Nonetheless, several authors have published results indicating the thermal endurance profile, for oxidation induction time for instance, is not always linear [82-85]. This disagreement comes from the fact that changes in use properties do not obey, in general, an Arrhenius law. Indeed, these changes are due to a complex combination of several elementary chemical reactions. Although the elementary reactions obey an Arrhenius law, their combination does not essentially act upon an Arrhenius law. As an example, if the overall rate of degradation is described by the algebraic sum of these Arrhenius laws, the resulting equation do not follow the foresaid law [86] . As a result, this method can just be used for approximate estimation of life-time, but is not able to determine the causes of degradation, or to propose possible solutions. For instance, the studies made by Achimsky [83] on non-stabilized PP revealed a rupture in the Arrhenius diagram of the oxidation induction time, which leded the authors to propose a change in the degradation mechanism by a temperature rise. Celina et al. [87], by compiling these results and other data obtained by other authors on PP and PE, claimed that in all cases of thermo-oxidation, the degradation kinetics show a non-Arrhenian behavior above a critical temperature, and over-accelerates as the temperature increases. Similarly, Khelidj et al. [88] noted a discontinuity at 80°C in the Arrhenius diagram of non-stabilized PE oxidation induction time, as well as the maximum oxidation rate. They have found that the activation energy of the maximal oxidation rate increases from 75 kJ.mol⁻¹ to 138 kJ.mol⁻¹ above 80°C.

1.4.1.2 Acceleration factor method

This approach is based on the general hypothesis that by choosing suitable conditions of accelerated aging, i.e. simulating satisfactorily the natural aging, the homotheticity of the corresponding degradation kinetics leads to definition of an acceleration factor AF , which depends only on the chosen accelerated aging conditions (temperature, irradiation dose rate, etc.):

$$t_N = AF \cdot t_A \tag{1-24}$$

where t_N and t_A are the life-times determined for natural and accelerated aging, respectively. In simple words, Q hours of accelerated aging corresponds to $AF \cdot Q$ hours of natural aging [89].

Barois-Oudin et al. [90] have used this method for the weathering degradation of sulfur vulcanized EPDM-ENB. By using infrared spectrophotometry, they observed the formation of the same products for natural and accelerated agings. By studying the natural aging in climatically different places, they reported an acceleration factor varying between 10 and 20.

While this method is simple to use, it can cause serious inconveniences. The degradation mechanism of a material consists of several chemical reactions which have different activation energies. Therefore, the assumption of the unchanging mechanism, and ratios between the different degradation products, sounds absurd. In addition, this method may be applicable to some cases where degradation happens tolerably fast, but it remains hard to apply to other cases who could take several decades [91]. Similarly, it seems difficult to predict the applicability of this method in different cases [89]. For instance, can the same FA be applied to all grades and all form of PE or PP? Moreover, can the effects of antioxidants be neglected? Finally, accelerated testing is highly variable in terms of temperature, wavelength, intensity of radiation and relative humidity. Thus, it seems that each accelerated test has its own acceleration factor towards a given natural aging [92].

1.4.1.3 Non empirical methods

Based on the barriers of two previous methods, it is necessary to acquire a method which can include the modifications at different scales caused by degradation. The application of the non-empirical method requires the knowledge of an endlife criterion for the use property under consideration, and the changes of this latter as a function of imposed stresses.

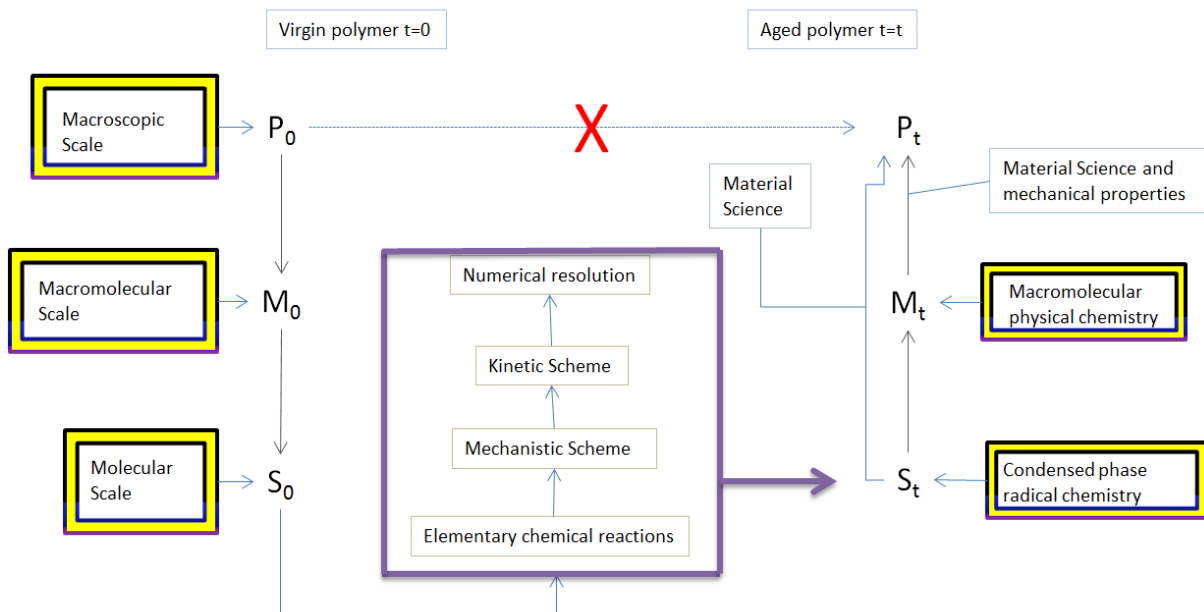


Figure 1-12: Principles and general scheme of non-empirical method for life-time prediction

Here, the main objective is to predict the effect of aging on properties at macroscopic scale. But, as illustrated Figure 1-12, it is impossible to directly access the final properties. To do so, the following steps should be taken into account:

- I. Decomposition of the complex phenomenon to a series of elementary steps at which we can apply simple dependence law for imposed stresses. This decomposition is based on an accepted and well defined mechanistic scheme that can be found in literature or be determined by performing analytical investigations. A kinetic scheme is then derived from the chosen mechanism to calculate the structural changes at the pertinent scales during exposure. The exactitude and applicability of final results represent the accuracy and the efficiency of the mechanism.
- II. Determination of every parameter of the model through experiments or, if already done, from literature. Once the model is complete, the aging conditions can be applied and the results can be extrapolated.
- III. Life-time prediction by imposing a structural end-life criterion.

The interconnection of these different scales requires a good knowledge of structure/property relationships. The very first general kinetic model was proposed by Bolland [76] for low temperature radio and thermo-oxidation of ethyl linoleate. The model was derived from the standard oxidation scheme established by spectrometric analyses (FTIR, UV, NMR, etc.) of the samples taken regularly during radiochemical or thermal aging. Rate constants of elementary reactions are determined by using the model as an inverse method [93, 94], i.e. by adjusting experimental data (e.g. concentration of oxidation products). For instance, Colin et al. [94] constructed a non-empirical kinetic model for radiochemical oxidation of ethylene propylene copolymers.

Fayolle *et al.* [95] studied the thermal oxidation of polyethylene by uniaxial tensile testing. They found that embrittlement results from a predominant chain scission process and occurs when the weight average molecular weight M_w reaches a critical value (M_{wc}) of about $70 \text{ kg}\cdot\text{mol}^{-1}$. The critical number of chain scission (n_c) was predicted from the following equation (1-25):

$$n_c = \frac{2}{M_{wc}} - \frac{2}{M_{w0}} \quad 1-25$$

1.4.2 Aging at molecular scale

1.4.2.1 Generalities on modifications at molecular scale

Reaction of dioxygen molecules with polymer chains leads to the formation of various carbonyl and hydroxyl bearing chemical species. These groups are detectable via several spectrochemical methods

such as infrared spectrophotometry or nuclear magnetic resonance, and chemical treatments. Oxidation products can also leave the system as small volatile molecules. The most frequent volatile products of oxidation are carbon monoxide CO and dioxide CO₂ and water. The grafting of oxygen onto the polymer chain, and volatile products emission induces mass changes. Delprat et al. [96], in their paper on photo-oxidation of ethylene propylene copolymers, measured the two most distinctive oxidation products, carbonyls and hydroxyls, by FTIR spectrophotometry (Figure 1-13). They also detected acetone molecules in gas phase, which they relate to oxidation of tertiary carbons of propylene unities.

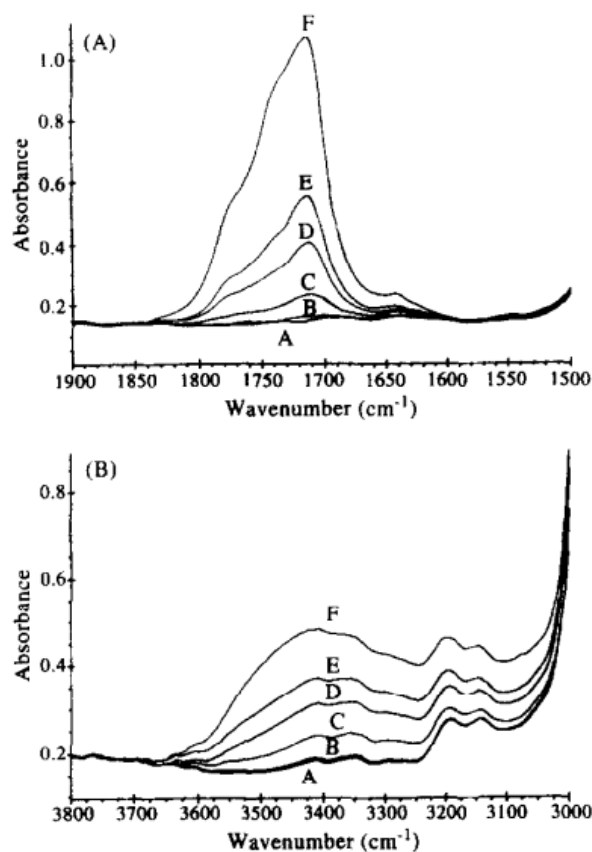


Figure 1-13: Build-up of oxidation products during EPR photo -oxidation:
A) carbonyls and B) hydroxyls^[96]

The reaction which seems the most probable in formation of volatile products is β -scission of radicals in chain-ends. In this case, the reaction product is a small molecule which can be released by the polymer.

Another interesting phenomenon of polymer oxidation, resulting from the formation of oxygenated products, is chemiluminescence. When an oxygen atom establishes a double bond to a carbon atom (in particular a ketone group), it moves from an excited to a stable state by emitting photons, who can be detected by adapted receptors [97, 98]. The intensity of chemiluminescence depends on the rate and amount of carbonyl product formation. For instance, Verdu et al. found that the chemiluminescence

from thermal aging of polyisoprene increases with the oxygen partial pressure in the surrounding atmosphere (Figure 1-14).

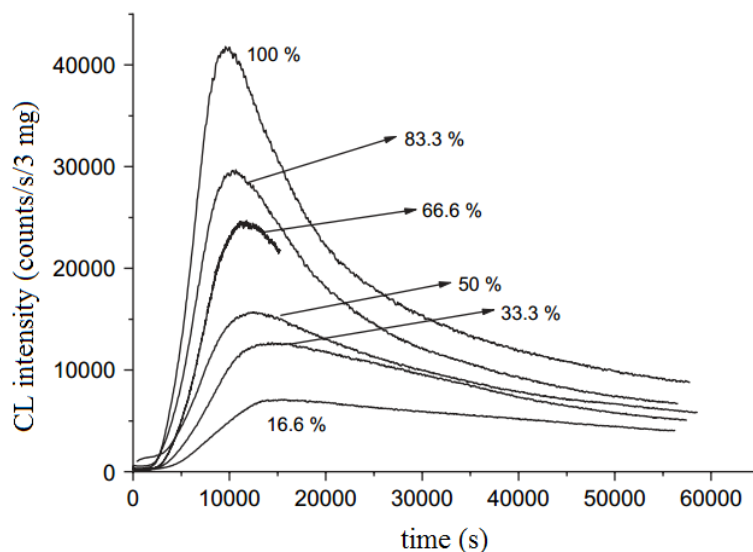


Figure 1-14: Effect of oxygen partial pressure (in percentage of atmospheric pressure) on chemiluminescence signal for polyisoprene thermal aging^[97, 98]

This result confirms that the formation of oxidation products, and consequently the chemiluminescence intensity, increases by increasing in oxygen concentration.

1.4.2.2 Aging mechanism

Oxidation is the main degradation mechanism of ethylene copolymers (EPR) and terpolymers (EPDM) subjected to thermal and radiochemical agings. It is a "radical chain reaction" composed of three main steps: initiation, propagation, and termination.

1.4.2.2.1 Initiation

Oxidation initiates by creation of radicals. This step consists in an energy absorption by the polymer chains, of which the weakest chemical bonds decompose to macroradicals:

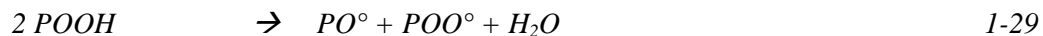
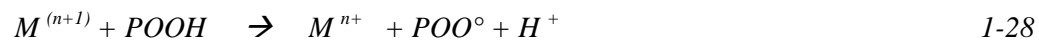


Initiation can happen in several ways depending on the energy source. This study is limited to radiochemical and thermal initiations.

1.4.2.2.1.1 Thermal and radiochemical initiation

The main difference between thermal and radiochemical aging, for a given polymer substrate, is the mode of initiation. Thermal aging is initiated by presence of instabilities in the polymer:

- Dissociation of existing weak chemical bonds in polymer under thermal stress. The probability of this type is directly related to the bond dissociation energies. At low to moderate temperatures (typically for $T < 200^{\circ}\text{C}$), O – O bond (about $140\text{-}150 \text{ kJ}\cdot\text{mol}^{-1}$) is more probable to break, and thus initiate chain reactions, than C – H ($E > 345 \text{ kJ}\cdot\text{mol}^{-1}$) and C – C ($E > 350 \text{ kJ}\cdot\text{mol}^{-1}$), due to its lower dissociation energy.
- Presence of impurities such as catalyzers (some metallic ions, Fe^{2+} , Cu^{2+} , etc.) can facilitate the initiation by reducing activation energies. Hydroperoxides, for example, as auxiliary source of radical, are highly effected by this presence [99-101]:



For moderate temperatures, hydroperoxide decomposition is the main source of radicals, and obviously happens in oxidized layer of the sample. From this point of view, the oxidized layer, at extremities, protects the interior bulk of sample from oxidation [102].

Radiochemical aging is initiated by extrinsic energy sources [103-105]:

- Electromagnetic rays: γ , UV, X
- Particle rays: electron, proton ...

Irradiation energy is normally much higher than bond energies, and although the absorptivity of polymers is low, the absorption in the matrix is not selective. Production of radicals can happen homogeneously in the sample thickness of some millimeters, and the abundance of a radical type depends on its concentration. For the sake of simplicity, it is generally considered that the main source of radicals is the chemical bonds with the highest concentration.

For pure radiochemical aging, the decomposition of hydroperoxides is neglected. However, it cannot be excluded that, at long term, above a critical hydroperoxide concentration, their thermal decomposition is activated, and radiochemical aging is pursued by thermal aging.

What has been explained above is the general idea of mechanism definition and kinetics deriving of oxidation phenomena. Evidently, this method, like any other method of life-time prediction, is jointed to some disadvantages such as heterogeneity of aging or complexity in considering all primary and secondary chemical reactions. That is why, in order to diminish the complications and saving time, case dependent simplifying hypotheses are considered [88].

Decomposition of polymer can happen through environmental stresses such as thermal, radiochemical or photochemical. These stresses provide enough energy to break chemical bonds and create radicals. The more the energy provided, the higher the formation rate and concentration of radicals.

1.4.2.2.1.2 Unimolecular decomposition of hydroperoxides

Since O–O bond presents the lowest dissociation energy, it is licit to suppose that the thermal oxidation is initiated by hydroperoxide decomposition. Two different modes of decomposition compete: Unimolecular and bimolecular. Unimolecular decomposition writes:



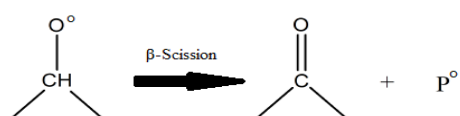
k_{1u} represent the unimolecular decomposition rate. ${}^\circ OH$ radical is highly reactive, and reacts whether by hydrogen abstraction or by combination with another radical. The eligibility of this reaction was shown by Achimsky *et al.* where they found that a polypropylene decomposes much more rapidly in presence of oxygen than under neutral atmosphere [101].

The decomposition rate constant k_{1u} obeys an Arrhenius law. The activation energy E_{1u} is around 140 $\text{kJ}\cdot\text{mol}^{-1}$ and temperature rise activates this reaction. Examples for values of k_{1u0} and E_{1u} are given in the following Table 1-3.

Polymer	Polyethylene [106]	Polypropylene [107]	Polyisoprene [108]
$k_{1u0} (\text{s}^{-1})$	8.0×10^{12}	1.2×10^{11}	9.3×10^{12}
$E_a (\text{kJ}\cdot\text{mol}^{-1})$	140	135	134

Table 1-3: Pre-exponential factors (k_{1u0}) and activation energies (E_a) for rate constant of POOH unimolecular decomposition

Alkoxy radical PO° is highly active as well. Along with hydrogen abstraction (and addition to a double bond in the case of polyenes), it can go through a β -scission (Scheme 1-14):



Scheme 1-14 : β -scission PO° radicals

The detailed mechanistic scheme of unimolecular POOH decomposition writes:



where γ is the carbonyl yield ranged between zero and unity.

1.4.2.2.1.3 Bimolecular decomposition of hydroperoxides

Bimolecular POOH decomposition reaction writes [109]:



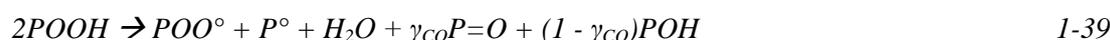
where k_{1b} represents the bimolecular decomposition of hydroperoxides.

The activation energy of bimolecular route is about 120 kJ.mol⁻¹, i.e. lower than unimolecular one.

Polymer	polyethylene ^[88]	polypropylene ^[89]	polyisoprene ^[107]	polybutadiene ^[110]
k_{1b0} (L.mol ⁻¹ .s ⁻¹)	2.8×10^9	2.0×10^{12}	1.2×10^{10}	3.5×10^{13}
E_a (kJ.mol ⁻¹)	105	100	102	137

Table 1-4: Pre-exponential factors (k_{1b0}) and activation energies (E_a) for rate constant of POOH bimolecular decomposition

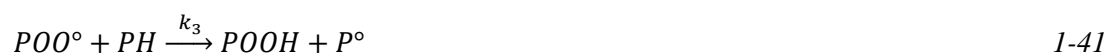
The same argument can be used for calculating the carbonyl yield in the bimolecular path. The detailed mechanistic scheme writes:



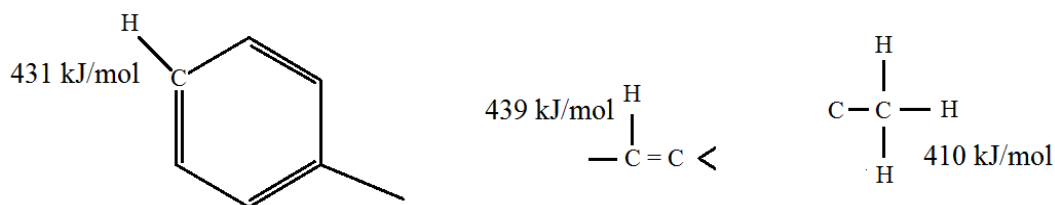
Creation and consumption of hydroperoxides are important reactions of thermal oxidation mechanistic scheme.

1.4.2.2.2 Propagation

As it was mentioned before, the oxidative aging of polymers is a chain reaction which constitutes the propagation stage. The propagation has two steps. The first step, i.e. oxygen consumption, is the grafting of O_2 molecules to macroradicals (Equation 1-40). The second step is hydrogen abstraction from the hydrocarbon substrate and formation of alkyl radical, which in its turn, reacts with oxygen to produce a peroxy radical (Equation 1-41):

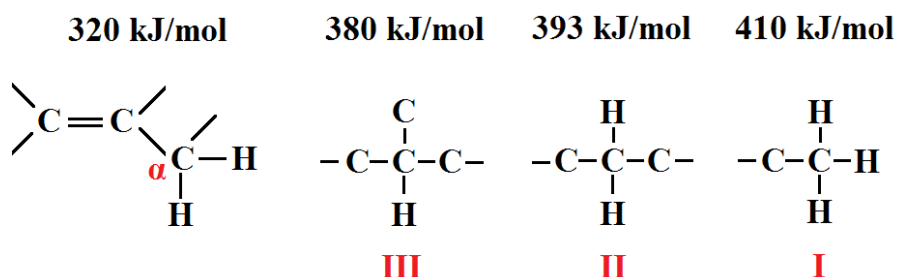


The rate of this reaction depends on the dissociation energy of the C – H bond (Scheme 1-15). In fact every hydrogen atom can be abstracted by radicals except for three types:



Scheme 1-15: Hard hydrogens to abstract in a radical reaction
(numbers beside Figures present the C – H bond dissociation energies)

Other C – H bonds are more or less reactive and get involved in reactions like secondary hydrogens in polyethylene or tertiary hydrogens in polypropylene. The facility of hydrogen abstraction in the common hydrocarbon structures varies in the following order (Scheme 1-16):

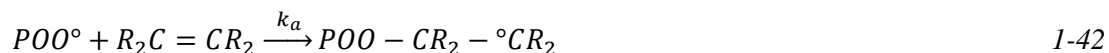


Allylic > *Tertiary* > *Secondary* > *Primary*

Scheme 1-16 : Classification of labile hydrogens according to the dissociation energy of corresponding C – H bond

Hydroperoxide groups formed in Equation 1-41 are also reactive and, under environmental stresses (high temperature), decompose into two radicals, so the chain reaction will not be stopped.

In the case of polymers containing double bonds, there exists another propagation mode via radicals attacking double bonds and creating a covalent bond. This reaction can continue in chain because another alkyl radical gets formed as well:



The double bond is frequently noted by “F” which transforms the equation 1-42 to a simpler notation:



Anyhow, after this step of propagation the resulting radical can abstract a hydrogen atom to create another macroradical. In excess of oxygen, the addition of P° to oxygen molecules is the fastest reaction and so the predominant. Thus, in the presence of double bonds mostly peroxide bridges are formed during addition to double bonds. But contrarily to this, when there is a lack of oxygen, the P° attack directly the double bonds. Coquillat *et al.* have shown that, in the case of polybutadiene, the rate of this reaction is of the order of 10⁴ s⁻¹ while the addition of peroxy radical to double bonds is around 24 s⁻¹ at 100°C [111, 112].

Another way of propagation is the rearrangement of radicals. For instance, methynic radical can undergo a chain scission (β-scission) in propylene, which reduces the molecular weight of the polymer [113].

1.4.2.2.3 Termination

The third and last step in a radical chain oxidation is the termination, where the radicals combine together to produce inactive products. Termination consists of three principal reactions corresponding to the different possibilities of macroradical pairs recombination:

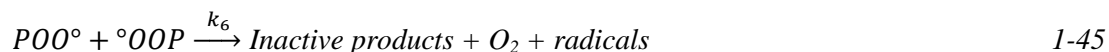
- i. Between two alkyl radicals:



- ii. Between one alkyl and one peroxy radical:



- iii. Between two peroxy radicals:



P° has the highest reactivity among other radicals and is active even at very low temperatures. It can move rapidly in the reactive medium by valence migration:

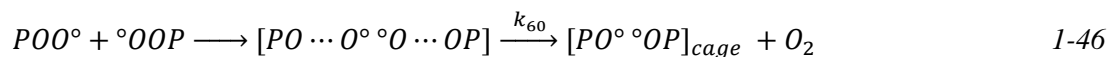


So, it is licit to suppose that the rate of reaction 1-43 is the highest among others [114].

Reaction 1-45 has two possibilities of termination: one through formation of alkyl – alkyl bridge and two, through hydrogen exchange. This second route is known as disproportionation and is well known in case of polyethylene[115].

The reaction 1-44 creates a peroxide molecule which is not totally inactive and can go through a homolytic scission to create two peroxy radicals. In addition, if P° possesses labile hydrogen, the reaction 1-44 can go through disproportionation, as well, and produce a hydroperoxide.

In third reaction of termination, the two radicals are more stable and they react in a different and more complex way. The combination of two POO° radicals results in a molecule having four consecutive oxygen atoms which is very instable. The rapid rearrangement of this molecule liberates a dioxygen molecule and two alkoxy radicals in a transition stage called “cage”:



Alkoxy radicals have three possibilities of recombination:

a) Addition (or coupling):



b) Disproportionation:

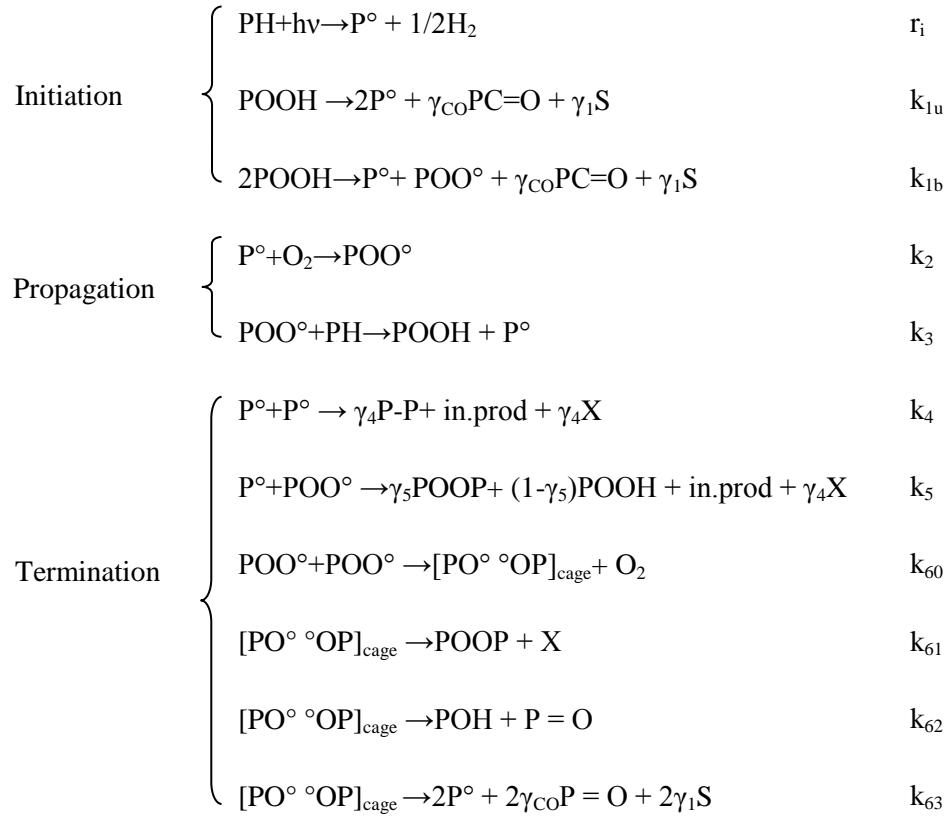


c) Escape from the cage and initiation of new radical oxidation chains:



1.4.2.3 Overall mechanism and kinetic scheme

Mechanism of aging clarifies the possible reactions in a system. In order to consider the set of experimental results found in the literature, Colin *et al.* have regrouped all the previous steps to schematize a global mechanism [116]. But, what is obvious is that the model improvement does not stop and is getting more and more complete by considering additional possible reactions [94, 117, 118]:



γ_1 is the chains scission yield, γ_4 alkyl – alkyl and γ_5 peroxide bridges yield.

Moving on from the aging mechanism to the kinetic scheme, a simplifying hypothesis is employed, which is the unicity of reactive sites [119, 120]. This hypothesis lets us, in a premier approach, to consider a unique C – H bond and avoid the complexities.

So, now that every elements of mechanism are present, the overall kinetic scheme can be written:

- $\frac{d[\text{P}^\circ]}{dt} = r_i + 2k_{1u}[\text{POOH}] + k_{1b}[\text{POOH}]^2 - k_2[\text{P}^\circ][\text{O}_2] + k_3[\text{POO}^\circ][\text{PH}] - 2k_4[\text{P}^\circ]^2 - k_5[\text{P}^\circ][\text{POO}^\circ] + 2k_{63}[\text{PO}^\circ\text{ }^\circ\text{OP}]_{\text{cage}}$
- $\frac{d[\text{POO}^\circ]}{dt} = k_{1b}[\text{POOH}]^2 + k_2[\text{P}^\circ][\text{O}_2] - k_3[\text{POO}^\circ][\text{PH}] - k_5[\text{P}^\circ][\text{POO}^\circ] - 2k_{60}[\text{POO}^\circ]^2$

- $\frac{d[POOH]}{dt} = -k_{1u}[POOH] - 2k_{1b}[POOH]^2 + k_3[POO^\circ][PH] + (1 - \gamma_5)[P^\circ][POO^\circ]$
- $\frac{d[PO^\circ OP]_{cage}}{dt} = k_{60}[POO^\circ]^2 - (k_{61} + k_{62} + k_{63})[PO^\circ OP]_{cage}$
- $\frac{dO_2}{dt} = -k_2[O_2][P^\circ] + k_{60}[POO^\circ]^2$

The rate constant (k) of each elementary reaction obeys an Arrhenius law (1-50):

$$k = k_0 \exp\left(-\frac{E_a}{RT}\right) \quad 1-50$$

where k_0 is the pre-exponential factor, E_a the activation energy of the reaction, R the universal gas constant and T the temperature in Kelvin. As k_0 , R , and E_a are constant, k becomes a decreasing function of temperature.

The rate constants of each elementary reaction for specific polymers are given in literature as well as radiochemical yield of each product formation. For instance, Khelidj et al. have determined this parameters for PE family [106].

1.4.2.4 Aging of ethylene-propylene copolymers at molecular scale

Aging of hydrocarbon polymers goes through specific chemical reactions that, in the presence of oxygen, produce several oxygen bearing chemical species. Precise determination and quantification of these products has been the field of endeavor to several researchers [121-125]. The team of Gardette brought an interest to determination of oxidation products of radiochemical aging of an EPDM and its corresponding ethylene-propylene copolymer (EPR) [125]. FTIR spectra uncover two main regions for oxidation products:

- I. 1600 – 1800 cm^{-1} (main peak at 1714 cm^{-1}) is the domain of carbonyls ($>C=O$)
- II. 3200 – 3600 cm^{-1} (main peak at 3400 cm^{-1}) is the domain of hydroxyls ($-OH$)

They found that the EPDM (containing double bonds) degrades more rapidly and more intensely than EPR. These results are shown in Figure 1-15. The graph shows the evolution in absorbance of carbonyls and hydroxyls as a function of received irradiation dose. As it can be seen, the accumulation of each product is greater for EPDM than EPR.

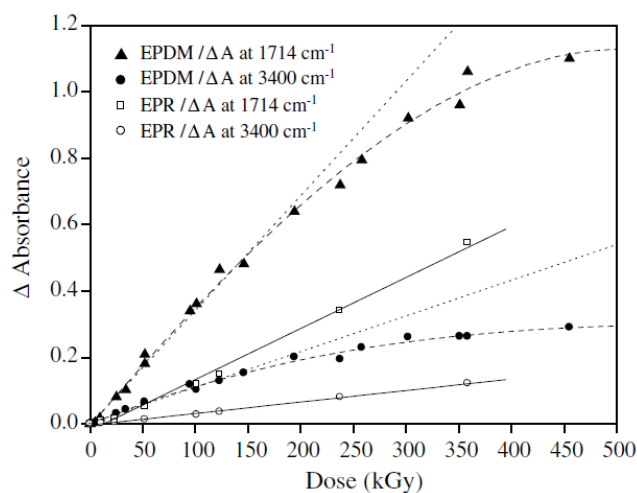


Figure 1-15: Build-up of oxidation products for an EPR and an EPDM^[125]
 (Δ Absorbance: $Absorbance(t) - Absorbance(t_0)$), (1 kGy/h, 20°C, 0.5 l.min⁻¹ pure oxygen flow)

Each oxidation product forms a family. For instance, carbonyl family contains ketones, aldehydes, carboxylic acids, esters, etc. and hydroxyl family contains hydroperoxides, alcohols, carboxylic acids, etc. The author tried to differentiate and quantify each type of these species by using chemical treatment methods such as SF₄ or NH₃ treatment. The results of radiochemical product formation yields are given in Table 1-5.

	POOH	Ketones	Acids	Alcohols	POOP
G(EPR)	6.0	3.0	2.0	2.0	0.2
G(EPDM)	15.0	13.9	4.4	4.1	0.3

Table 1-5: Radiochemical yield (G : mol.Gy⁻¹) of oxidation products for an EPR and an EPDM^[125]
 (1 kGy/h, 20°C, 0.5 l.min⁻¹ pure oxygen flow)

The only difference between the EPR and the EPDM is the presence of double bonds in the latter. The energy required to react with a double bond is much lower than the energy for hydrogen abstraction. So, it seems logic, for a free radical at the vicinity of a double bond or a C – H bond, to choose the addition route. In addition, allylic hydrogens are more labile than olefinic (methinic and methylenic) hydrogens, so their oxidation happens faster and more intensely.

In the same publication, the authors have also measured the consumption of double bonds (ethylidene norbornene in this case) with the time of exposure. As it is shown in Figure 1-16, the consumption of double bonds happens from the beginning of exposure and its rate decreases with time.

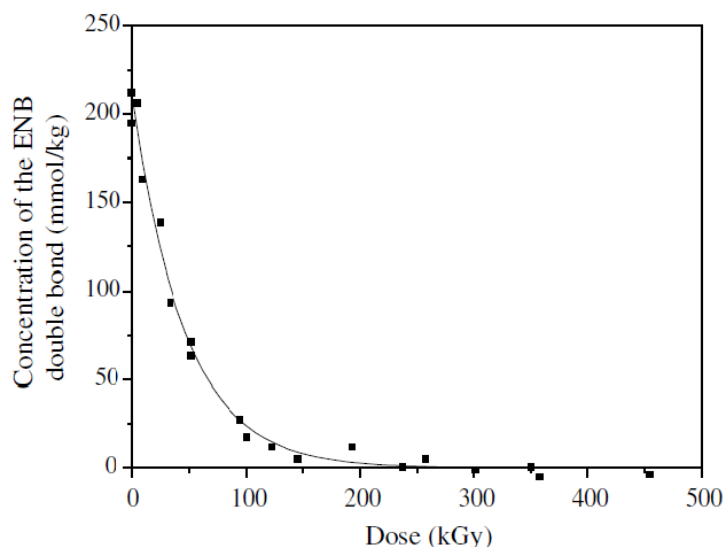


Figure 1-16: Consumption of ENB double bond as a function of received dose by sample^[125] (1 kGy/h, 20°C, 0.5 l.min⁻¹ oxygen flow)

Delor-Jestin et al., on the contrary, based their researches on photo- and thermal aging of EPDM-ENB [126, 127]. The aging was performed at 100 and 150°C, and the results are of quite interest. Carbonyls have been observed around 1700 cm⁻¹, as well as hydroperoxides at 3550 cm⁻¹ and alcohols at 3616 cm⁻¹ (Figure 1-17).

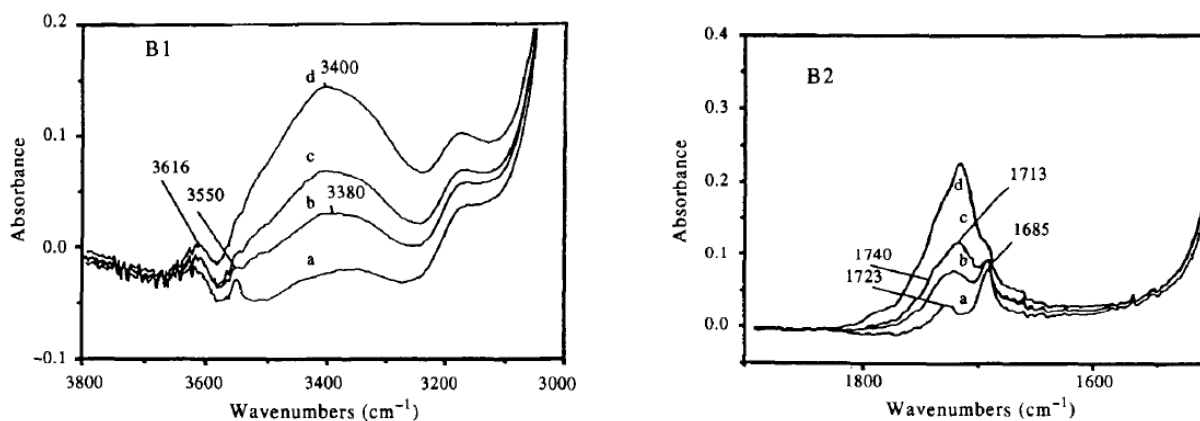


Figure 1-17: Formation of oxidation products detected by FTIR spectrophotometry: hydroxyls (left) and carbonyls (right)^[126, 127] (80°C, air under atmospheric pressure)

The evolution of oxidation product in thermal aging is no different from radiochemical aging. Concerning the consumption of ENB double bonds, they observe a diminution of the peak, but detect the appearing of a new band at 870 cm⁻¹. This apparition was argued as: “the double bonds are not simply consumed but, due to a shift, they absorb in a different region”.

In the same publication, the authors examined the thermo-oxidation of hydroperoxidized EPDM in order to study the role of hydroperoxides as initiators of oxidation. As we know, hydroperoxides decompose under thermal stress and create radicals that accelerate the oxidation. This was confirmed by the results of Delor *et al.* (Figure 1-18), demonstrating that the oxidation rate of a hydroperoxidized begins higher than raw (control) EPDM. As the aging continues, the rates for two species tend towards a same value.

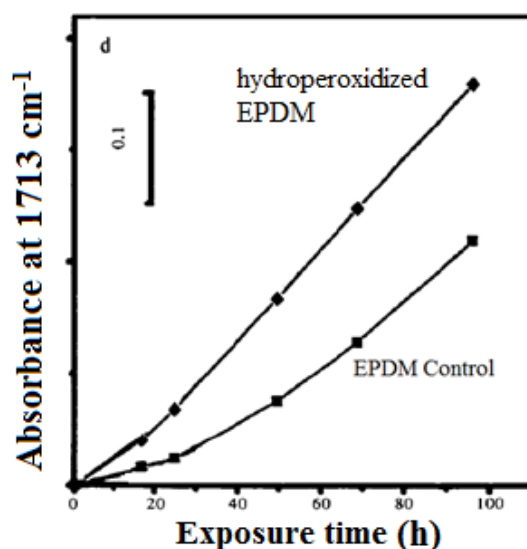


Figure 1-18: Creation of carbonyls for an EPDM and an EPDM hydroperoxide during UV irradiation^[126, 127] (80°C, air under natural atmosphere)

Macroradicals formed by thermal or radiochemical stress, react with di-oxygen molecules present in the system. Oxygen uptake measurements, by using manometric methods, throughout aging gives an index about the amount of oxygen reacted with matrix [128]. Zaharescu and Podina used oxygen uptake method to study the radiochemical stability of EPDM [129]. The effect of temperature at identical dose received by samples has been demonstrated in Figure 1-19. As the temperature increases, the oxygen uptake increases and reaches a constant value.

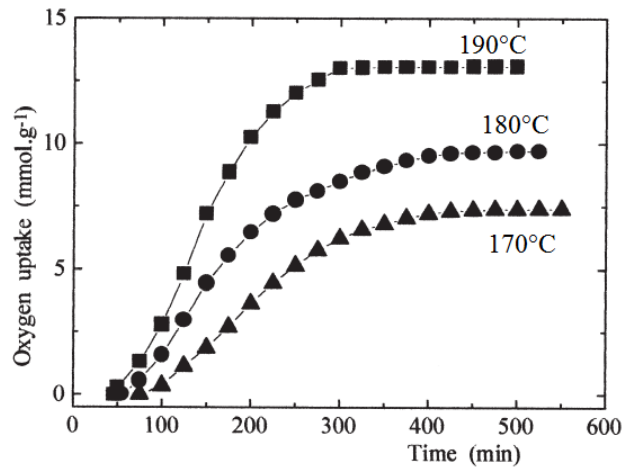


Figure 1-19: Oxygen absorption for an EPDM aged at different temperatures^[129] (170, 180 & 190°C, in air under atmospheric pressure)

In another publication, the same authors have brought out the same test on thermally aged EPDM and EPR [130]. The two materials possessing approximately the same content of ethylene and propylene was exposed to 165°C, 175°C and 185°C at a ventilated oven. The results disclose a considerable difference between uptake behavior of EPR and EPDM (Figure 1-20). This difference has been related to the presence of double bonds that offer lower activation energy for oxidation.

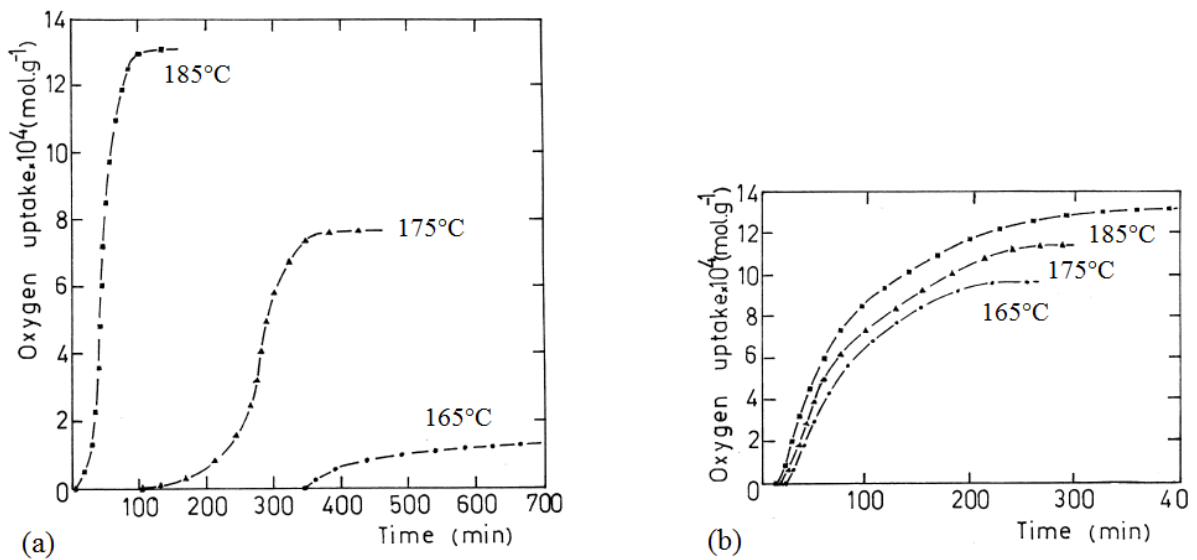


Figure 1-20: Gap of oxygen uptake between a) EPR and b) EPDM at different temperatures^[130] (165, 175 & 185°C, in air under atmospheric pressure)

In conclusion, one can conclude that the presence of double bonds, which do exist after EPDM crosslinking, is a more achievable position for radical attack and beginning of oxidation. But, is this

presence necessarily in disfavor of the elastomer or it can have also, in certain cases a favorable effect?

1.4.3 Macromolecular scale

1.4.3.1 Generalities on modifications at macromolecular scale

Macromolecules, i.e. long polymer chains, can undergo two types of modification under aging:

- I. Scission
- II. Inter or intra linking

These two can happen simultaneously in the system, and are important because they can change the physicochemical and mechanical properties of the polymer. For instance, polylactides are highly degradable by heating, which give them the ability of being totally recycled in addition to their biodegradability [131, 132]. When a macromolecule goes through chain scission, it creates two macromolecules with smaller molecular weight. The scission can continue up to procurement of oligomers or even monomers in the case of depolymerization. The number of chain scission in a linear polymer is given by:

$$S = \frac{1}{M_n} - \frac{1}{M_{n0}} \quad 1-51$$

with S the number of chain scissions, M_{n0} and M_n the number average molecular mass before and after aging, respectively.

Although chain scission happens more often in polymers than crosslinking, but this latter is of an importance as well. For instance, Khelidj [88] has shown that polyethylene under several γ -irradiation dose rates at 45°C in air goes through chain scission as much as it goes through crosslinking. This is while Bovey [133] categorizes polyethylene as a polymer dominated by crosslinking under ionizing irradiation at neutral atmosphere. In this case, chain scissions S and crosslink act X , simultaneously modify the polymer molecular structure based on Saito equations [134]:

$$S - X = \frac{1}{M_n} - \frac{1}{M_{n0}} \quad 1-52$$

And:

$$\frac{S}{2} - X = \frac{1}{M_w} - \frac{1}{M_{w0}} \quad 1-53$$

Different analytical methods are available to measure the amount of chain scissions in linear polymers. For instance, Bueche used the viscosity of molten polymer which can be easily measured with a rotary rheometer expressed as a function of molecular mass M_w [135]:

$$\eta = KM_w^{3.4} \quad 1-54$$

where K depends on temperature and chemical nature of the polymer.

In addition to rheometry, size exclusion chromatography (SEC) (or gel permeation chromatography) can be employed, where the results are expressed as distribution of molecular mass of polymer chains and average molecular mass. If the polymer chains are too long or branched, the efficiency of these methods decreases. In this case, more sophisticated methods, such as SEC at high temperature, can be employed.

For a tridimensional network of a polymer, the methods above are no more valid because the network is no more fusible or soluble in solvents. A tridimensional network is defined by its crosslinks and elastically active chains. In the case of an ideal network, for which every chain is elastically effective, the concentration of crosslinks is given by:

$$x = 2 \frac{v}{f} \quad 1-55$$

where x is the concentration of crosslinks, v the concentration of elastically effective chains and f the functionality of crosslinks.

One of the most common methods of measuring the concentration of elastically active chains (or crosslinks) is the swelling test. This method is based on affinity of solvent for dissolving polymer chains and the resistance of crosslinks which lead to a swelled state of the network. This method was formulized by Flory and Rehner in 1940s. Celina et al. [136] has used Flory – Rehner equation to calculate the average molecular mass of elastically active chains in PE crosslinked by dicumyl peroxide and silane (Figure 1-21). The results show a fall of average molecular mass of elastically active chains for low degrees of crosslinking, and negligible changes for high degrees of crosslinking.

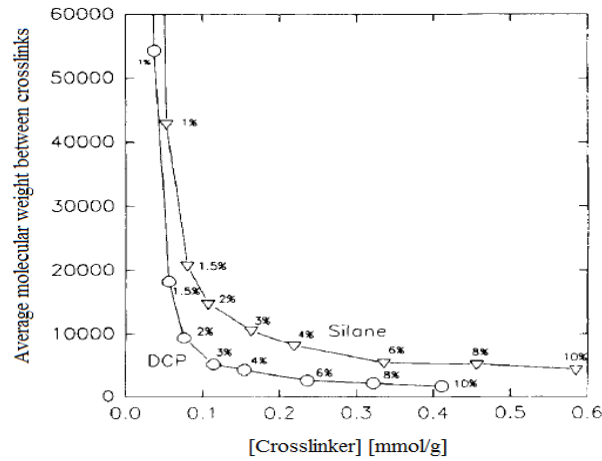
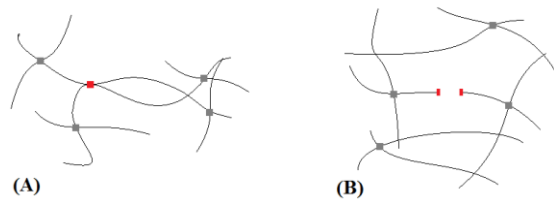


Figure 1-21: Effect of crosslinking agent concentration on average molecular weight of elastically active chains during polyethylene crosslinking^[136]

Concentration of elastically active chains can be measured by mechanical tests. The crosslink density of the network ν is related to whether shear (G) or Young's (E) modulus:

$$G = \frac{E}{3} = \nu \rho RT \quad 1-56$$

where R is universal gas constant, ρ is the volumic mass, and T is the absolute temperature.



Scheme 1-17 : A) crosslinking and B) chain scission in a tetrafunctional network

Based on Equation 1-56, the evolution in structure of a tridimensional network can be expressed by equation 1-57:

$$G - G_0 = \frac{E - E_0}{3} = (\nu - \nu_0) \rho RT \quad 1-57$$

Considering a chain scission in a tetrafunctional network (Scheme 1-17B), one can realize that one scission is equal to the loss of one elastically active chain ($S = \nu_0 - \nu$) so:

$$G - G_0 = \frac{E - E_0}{3} = S \rho RT \quad 1-58$$

On the other hand, the formation of a crosslink (Scheme 1-17A), produces as twice elastically active chains ($X = \frac{\nu - \nu_0}{2}$):

$$G - G_0 = \frac{E - E_0}{3} = 2X\rho RT \quad 1-59$$

Tridimensional networks, as well as linear polymers, can go through both crosslinking and chain scission. Assink et al. have followed the network evolution of an industrial EPDM during thermal aging [137]. The results revealed that the crosslink density of the network decreases by scission in the beginning of aging, but crosslinking takes over at the end (Figure 1-22).

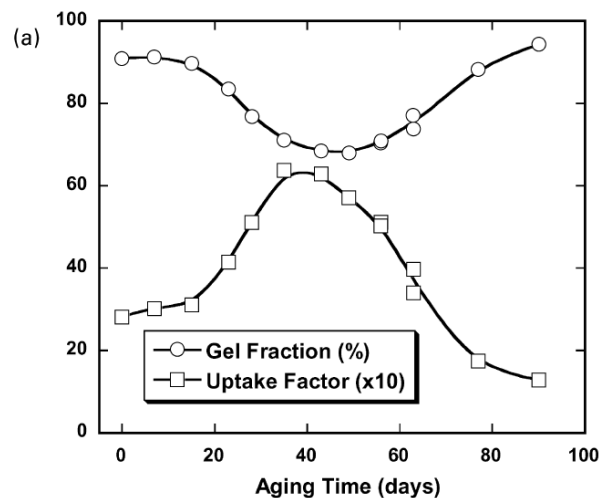


Figure 1-22: Competition between crosslinking and chain scissions, during EPDM thermal aging^[137] (air under atmospheric pressure, 140°C)

Modifications at macromolecular scale have direct effects on mechanical properties of material. Next section is dedicated to this type of modifications.

1.4.3.2 Aging of ethylene-propylene copolymers at macromolecular scale

Modifications in a tridimensional network have significant impacts on material properties, going from density and T_g to loss factor and swelling ratio.

Gillen et al. tried to measure the density changes as an index for aging of cable materials used in power plants, and more precisely crosslinked polyethylene. The samples were aged both thermally and thermo-radiochemically. They observed that density of samples rises with a comparatively constant rate. For samples presenting an aging induction time, also densities increased but more slowly until reaching the point of induction where the density increasing rate auto-accelerates. The results for crosslinked polyethylene have been presented in Figure 1-23. At low dose rates, density increases

homogeneously along the sample thickness. As the dose rate increases, the material seems to be more intact in the core. This effect is dependent on diffusion of oxygen molecules through the sample thickness. The oxidation rate increases with dose rate, so the oxygen molecules are consumed at layers closer to surface, leading to decrease of the thickness of oxidized layer [138].

Scission of chains in a polymer network reduces the real part of modulus (storage) and on the contrary increases the imaginary part (loss). Crosslinking of the network will have the opposite effect, and as the structure of the network tends to perfectness, the loss modulus approaches zero. In each case, the modifications can be shown by measuring the phase lag between the deformation and the stress, in form of $\tan \delta$ (G''/G' or E''/E'), which is also called the *loss factor*. Boiteux et al. have followed the changes in $\tan \delta$ of a crosslinked EPDM-hexadiene under thermal aging at 135°C in air [139]. The results in Figure 1-24 revealed two main changes:

1. Shift of $\tan \delta$ spectra to higher temperatures,
2. Decrease in α relaxation peak height that permits the quantification of degradation.

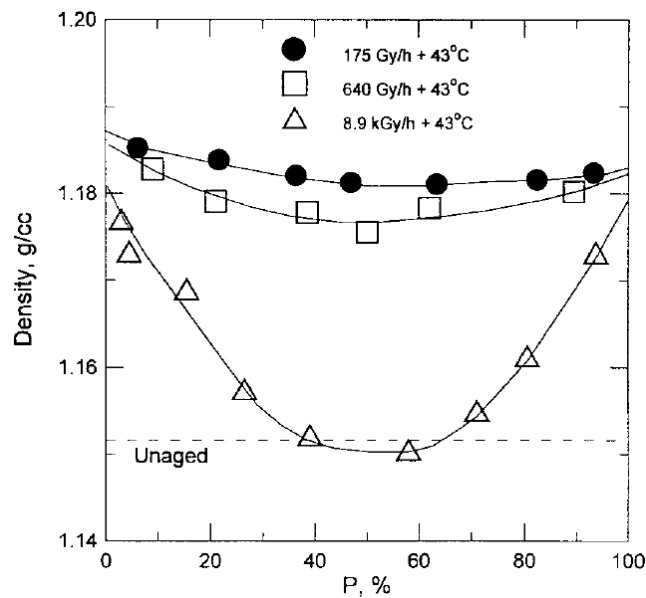


Figure 1-23: Density profile of XLPE in air at 43°C as a function of dose rate along the 0.8mm thickness of the sample [138]

They have also examined the radiochemical aging of the samples at 90°C under 0.1 kGy/h dose rate in air. Contrarily to thermal aging, it was seen that as the material gets irradiated, the α -relaxation peak height increases. These results are showing that, in the early stages of aging, the main phenomenon in thermal aging is the chain scission, while, in radiochemical aging, crosslinking is predominant. These results are in good agreement with those found by Gueguen et al. who worked on the same type of materials [140, 141].

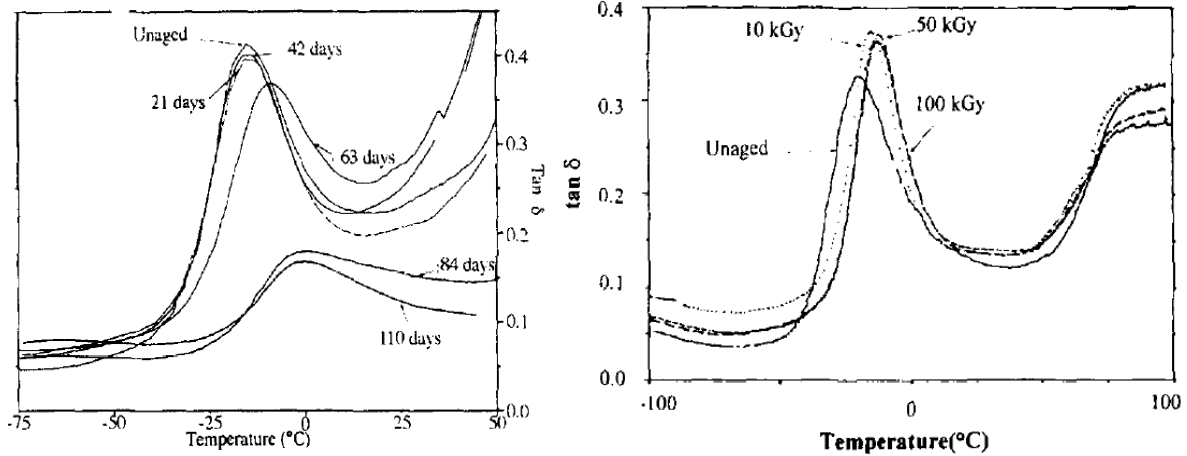


Figure 1-24: Variation of $\tan \delta$ for a crosslinked EPDM aged thermally in air at 135°C (left) and radiochemically under 0.1 kGy/h in air at 90°C (right) ^[139]

In their turn, Celette et al., did not stop EPDM radiochemical aging in the early stages, but continued up to higher doses of irradiation [142]. What they observed was that, identically to previous authors, EPDM goes through crosslinking in early irradiation times. By continuing further, the height of peak began to decrease. Thus, it was concluded that, after attaining a maximal crosslink density, the chain scission becomes prevalent and the network degradation begins.

Swelling test, by Planes et al., was used to study the effect of irradiation on property changes of EPDM-ENB [143]. Both linear and crosslinked samples were γ -irradiated with 1 kGy/h dose rate at room temperature under pure oxygen atmosphere for several doses. Swelling test has been brought to the samples using xylene as solvent. Results of swelling ratio and soluble fraction for both types of samples are presented in Figure 1-25.

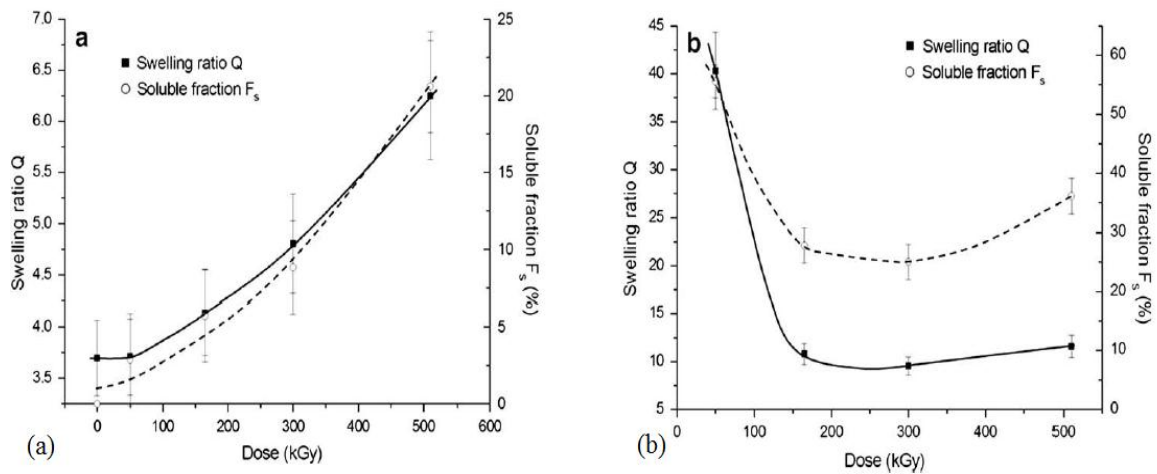


Figure 1-25: Changes at macromolecular scale during γ -irradiation of a) crosslinked and b) linear EPDM under ^[143] (1 kGy/h , room temperature, oxygen atmosphere)

In the case of crosslinked EPDM, at low received doses (0-50 kGy), the swelling ratio remains constant while soluble fraction increases. This was related to crosslinking of elastomer at early times of exposure. As the received dose increases, the swelling ratio increases as well, showing that the chain scission takes over. But, in the case of linear samples, both swelling ratio and soluble fraction show a dramatic fall up to doses around 300 kGy and begin to increase afterwards. This was interpreted as a high yield of crosslinking in the early periods of exposure (probably due to higher concentration of double bonds), and then followed by chain scission.

In the same review, the concentration of elastically active chains has been quantified by using the affine network theory. By measuring the modulus of both samples, the network changes at the macromolecular scale have been determined (Figure 1-26). The evolution of elastically active chains concentration matches with what preceded, i.e. the crosslinking of the material followed by chain scission.

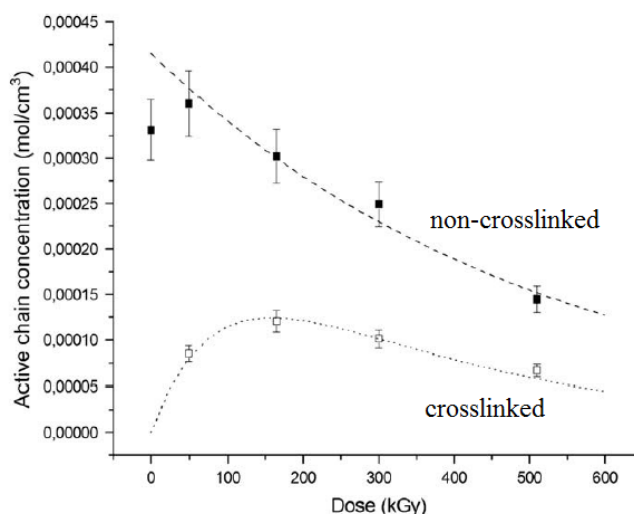


Figure 1-26: Evolution of the apparent crosslink density as a function of γ -irradiation dose for crosslinked and linear EPDM ^[143] (1 kGy/h, room temperature, oxygen atmosphere)

Mechanical properties (at macroscopic scale) are highly dependent on modifications at smaller scales. In next section these modifications are studied.

1.4.4 Macroscopic scale

1.4.4.1 Generalities on modifications at macroscopic scale

A linear polymer, subjected to chain scissions, will acquire lower molecular mass. This means lower concentration of physical entanglements, lower viscosity, more defects (chain ends), and practically lower mechanical properties. In the case of a tridimensional network, chain scissions lead to creation of more flaws. In addition, as the chain scissions are not selective, the resulting network would be

heterogeneous i.e. some areas with higher and some other with lower density of crosslinks. Crosslinking as well can change properties of the polymer in undesirable ways. In elastomers, for instance, where high deformability is required, extra crosslinks will reduce the ultimate elongation.

Polyethylene, as one of the most used polymers, has been the center of interest for researchers, and the modifications of its properties have been vastly studied [95, 144-146]. Fayolle et al. have exposed polyethylene to thermal aging at 80°C and 90°C in air under atmospheric pressure [147]. The evolution of the polymer has been determined by measurements of molecular weight by rheometry and tensile testing. The results showed that chain scissions are predominant and embrittlement occurs at a critical molecular mass ($M_w \approx 70 \pm 40 \text{ kg}\cdot\text{mol}^{-1}$, Figure 1-27).

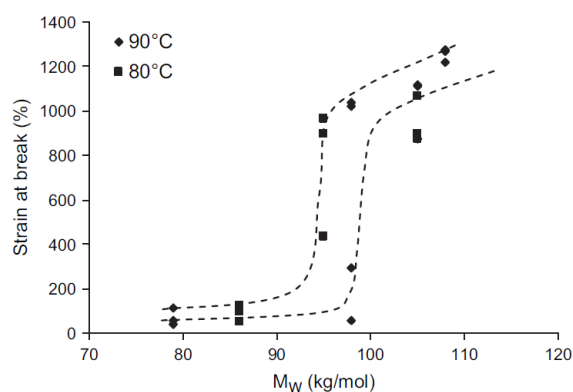


Figure 1-27: Embrittlement of PE under thermal aging at 80 – 90°C in air under atmospheric pressure. Changes in elongation at break as a function of weight average molecular mass^[148].

To give an example of changes in ultimate elongation, we can refer to the work of Celina et al. [149], on thermal aging of hydroxyl terminated Polybutadiene (HTPB) for temperatures ranged between 50 and 110°C under a pure oxygen atmosphere. They have observed the diminution of ultimate tensile elongation with aging time (Figure 1-28).

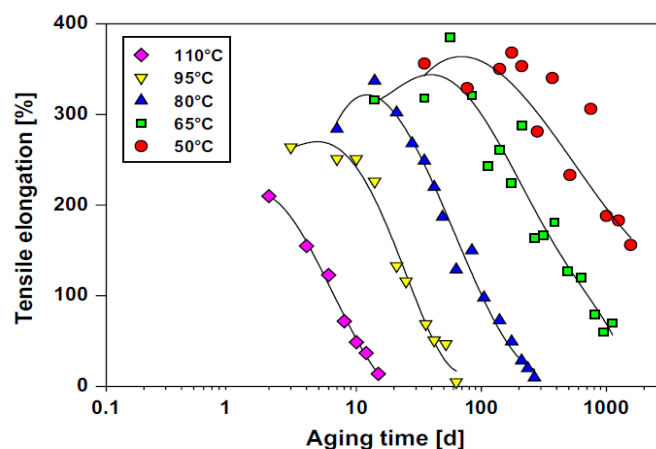


Figure 1-28: Changes in fracture behavior of HTPB under pure oxygen between 50 and 110°C^[149].

In the next section we will see how the modifications at macroscopic scale proceed in the case of ethylene copolymers and terpolymers.

1.4.4.2 Aging of ethylene-propylene copolymers at macroscopic scale

In several industries, elongation at break has been adopted as the endlife criterion. When the elongation at break of a polymer under aging attains 50% of its initial value, the polymer is considered to have reached the end of its life-time:

$$t = t_f \text{ when } \varepsilon_r = 0.5\varepsilon_{r_0}$$

In the relation above t_f is the life-time of the sample, ε_{r_0} and ε_r are elongation at break before and after aging.

By defining the failure envelope of an EPDM rubber, which is the stress/elongation at break diagram for different aging times, the modifications of mechanical properties can be schematized [150]. Gueguen et al., for instance, have plotted the failure envelope for EPDM-hexadiene under different γ dose rates (Figure 1-29) [141]. The two different behaviors of ultimate properties were attributed to the alteration of the predominant phenomenon by moving from high dose rates ($I > 0.5 \text{ kGy.h}^{-1}$), where the degradation is dependent on oxygen diffusion, to low dose rates ($I < 0.1 \text{ kGy.h}^{-1}$), where the dependence on oxygen diffusion becomes negligible.

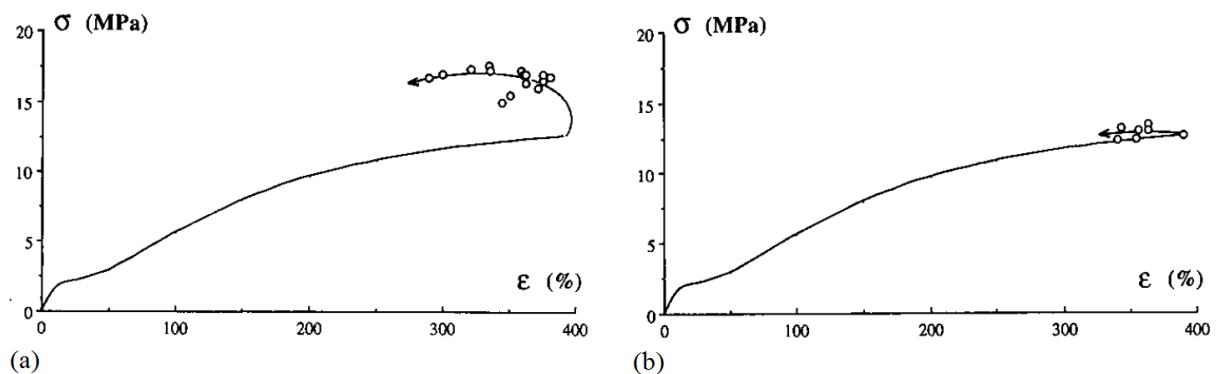


Figure 1-29: Failure envelope of EPDM subjected to a change in macromolecular structure^[141]:
a) $I > 0.5 \text{ kGy.h}^{-1}$ & b) $I < 0.1 \text{ kGy.h}^{-1}$, at 40°C , in air, atmospheric pressure.

The coexistence of both phenomena has been as well observed in radiochemical aging of polyethylene [151, 152]. In the case of thick samples under irradiation, the outer layers, which have enough oxygen at their disposition, go through chain scission and the oxidation products are formed. Inner core instead, which have received as much dose as outers but dispose no oxygen, go under crosslinking. Thus, the fact that oxidation is diffusion controlled leads the samples toward heterogeneity at high

dose rates, and an apparent predominance of crosslinking, which is manifested by higher ultimate stress of irradiated samples (Figure 1-29 a).

1.4.4.2.1 Oxidized layer

The possible variation in oxidized layer of a hypothetical sample has been shown in Figure 1-30. For samples thinner than the critical thickness L_C , the oxidation can be considered homogeneous. Alternately, for samples thicker than $L_C = 2T_{OL}$, a heterogeneous aging should be expected (the factor 2 is for the general case where diffusion takes place from both sides of the sample and T_{OL} is the thickness of oxidized layer). The critical thickness is defined as [153]:

$$L_C = 2T_{OL} = 2\left(\frac{DC}{r_C}\right)^{1/2} \quad 1-60$$

where D is the coefficient of oxygen diffusion, C the equilibrium value of oxygen concentration and r_C its consumption rate.

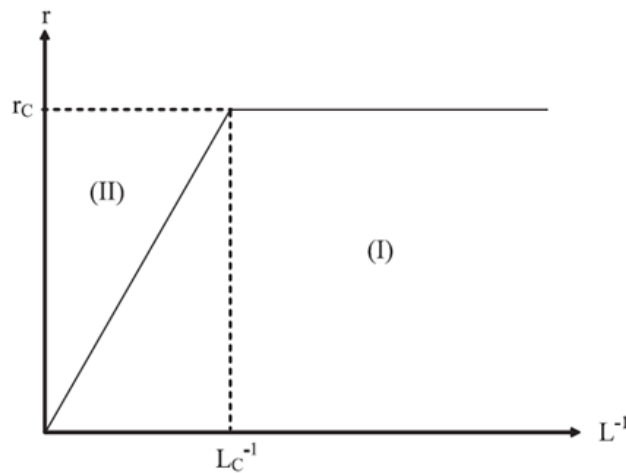


Figure 1-30: Dependence of oxygen consumption rate (r_c) as a function of reciprocal sample thickness^[153]

In given physical state (glassy or rubbery) oxygen diffusion and oxidation rate obey an Arrhenius law:

$$r_C = r_{C_0} \exp\left(\frac{-E_C}{RT}\right) \quad \& \quad D = D_0 \exp\left(\frac{-E_D}{RT}\right)$$

where r_{C_0} and D_0 are the pre-exponential factors, and E_C and E_D the activation energies of oxygen consumption and diffusion, respectively.

As this law can be written for both parameters, the Arrhenius law can be written as well for the oxidized layer:

$$L_C = L_{C_0} \exp\left(-\frac{E_L}{RT}\right) \quad 1-61$$

with L_{C_0} the pre-exponential factor $L_{C_0} = \left(\frac{D_0 C}{r_{C_0}}\right)^{0.5}$ and E_L the activation energy $E_L = \frac{1}{2}(E_D - E_r)$.

The reaction rate r_C depends also on irradiation dose rate (I). This dependence has been shown to follow a simple power law:

$$r_C = r_{C_0} \exp\left(\frac{-E_r}{RT}\right) I^\alpha \quad 1-62$$

Bykov *et al.* have studied the radio-oxidation of polyethylene under oxygen atmosphere at ambient temperature [154]. They have realized that, by increasing the dose rate the difference between oxidized and non-oxidized layer becomes more distinct. By measuring the thickness of oxidized layer for several dose rates, they have found a value equal to 0.5 for α [155].

1.4.4.2.2 Polyethylene and polypropylene

Polyethylene and polypropylene are among most used polymers, and their structural modifications have been well "decorticated". For instance, Fayolle *et al.* have studied the thermo-oxidation of polyethylene in air at 80°C and 90°C on thin films [148]. The prevalent mechanism of degradation has been detected to be chain scissions. By combining FTIR and tensile testing it was perceived that embrittlement of the samples happen after the oxidation induction time (Figure 1-31a). A critical molecular weight ($70 \pm 4 \text{ kg}\cdot\text{mol}^{-1}$) has been identified below which the polyethylene goes through a sudden embrittlement (Figure 1-31b).

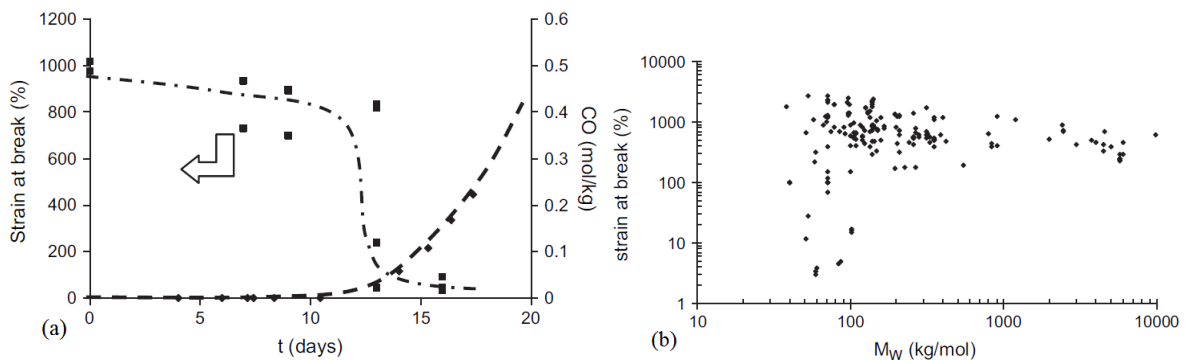


Figure 1-31: a) Evolution of oxidation products (carbonyls) and elongation at break for PE at 80°C in air under atmospheric pressure, b) Compilation of the results of elongation at break vs. molecular weight of several authors^[148]

The same authors have brought the same type of aging and characterization to polypropylene at 90°C [156]. It was observed that, contrarily to the case of polyethylene, the sudden embrittlement happens before the oxidation induction time (Figure 1-32). The explanation of this difference between

polyethylene and polypropylene would go back to their ability to crosslink. In the case of PE, the crosslink formation during oxidation hinders the embrittlement for a period of time. However, the only mechanism for polypropylene is chain scission, so the embrittlement happens before that one can observe oxidation products.

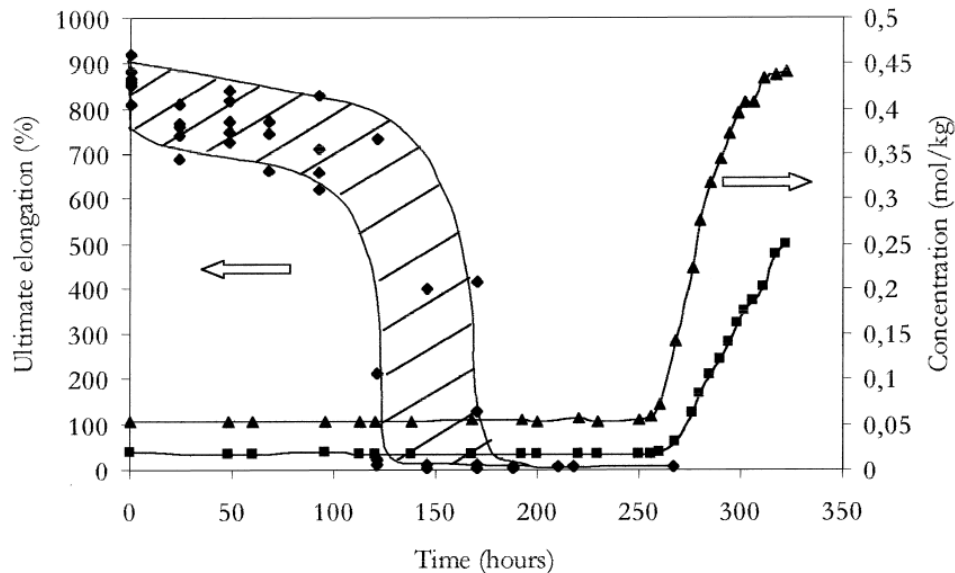


Figure 1-32: Evolution of oxidation products (carbonyls and hydroxyls) and elongation at break for PP at 90°C in air under atmospheric pressure ^[148, 156]

1.4.4.2.3 Ethylene propylene rubber

The predominance of chain scission in polyethylene and polypropylene has been approved in presence of oxygen. One may conclude that this mechanism should be valid for ethylene propylene copolymers, for which several researches have been carried out [157-159]. Gillen et al. have studied the long-term thermal aging of four industrial ethylene propylene copolymers (EPR) for a range of temperature varying from 100°C to 170°C [159]. The aging was performed both in air and neutral atmosphere (nitrogen). They have observed that the elongation at break of samples decreases slowly until achieving a so-called "induction time" and falls steeply afterwards (Figure 1-33a). As the temperature increases, the induction time decreases, but for all samples and all temperatures the allure of spectra remains the same. Contrarily to aging in presence of oxygen, where oxidation is dominant in polymer degradation, in nitrogen, the elongation at break of samples did not change significantly and the induction time was not observed at all (Figure 1-33b).

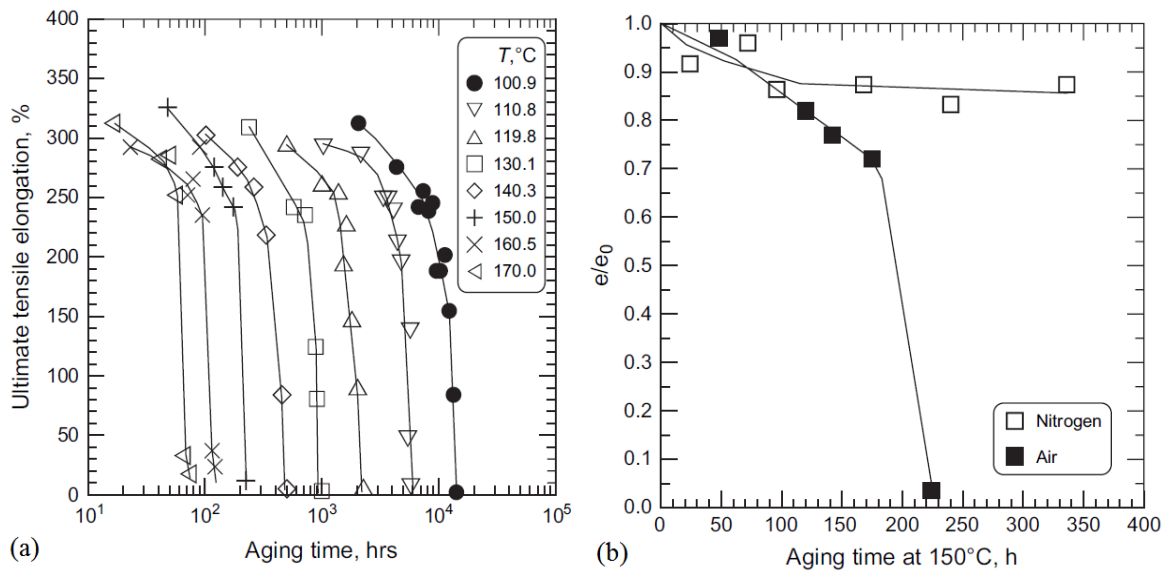


Figure 1-33: a) Elongation at break of thermally aged EPR between 100 and 170°C in air under atmospheric pressure b) Elongation at break of EPR aged at 150°C in air and in nitrogen under atmospheric pressure^[159]

Modifications of EPR properties under irradiation has also been the subject of several researches [121, 157, 160]. For instance, Clavreul has measured the variations of mechanical properties of an industrial EPR [157]. The results divulge, by a slow constant diminution in elongation at break, that in this case as well, chain scission is prevalent. The author has also studied the effect of temperature at a constant dose rate where he did not find any important effect (Figure 1-34a). This result, contrariwise, do not agree with general effect of temperature during irradiation which accelerates aging [161]. For instance, in their work on polyethylene, Clough and Gillen [162] have clearly shown this effect (Figure 1-34b).

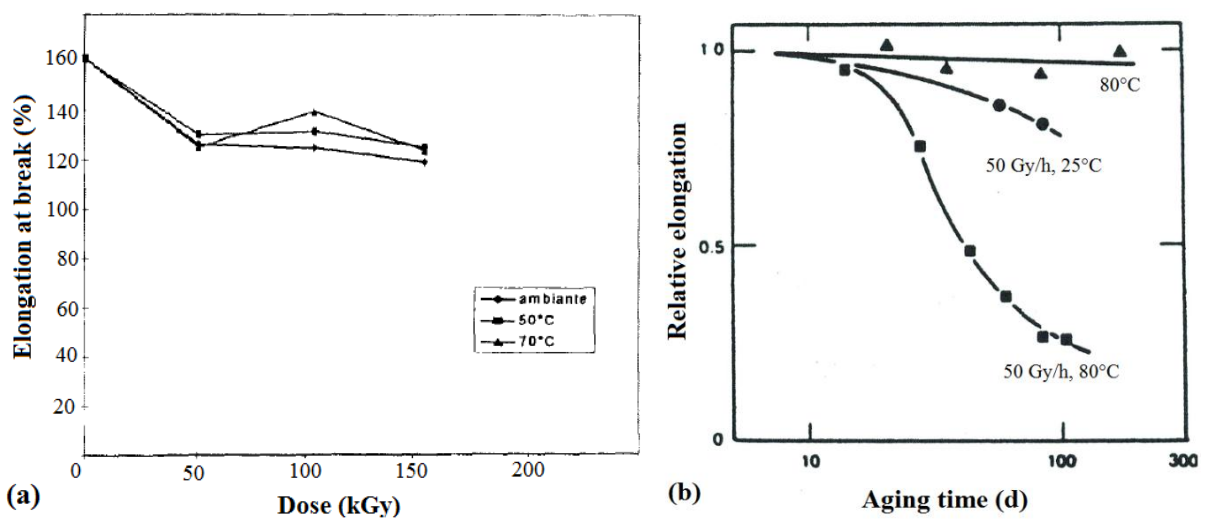


Figure 1-34: a) Effect of temperature during γ -irradiation of EPR (Clavreul 1997)^[157] b) Effect of temperature during irradiation of PE (Clough 1981)^[162] (under atmospheric pressure)

1.4.4.2.4 Ethylene propylene diene monomer

Planès used an EPDM rubber having the respective comonomer mass ratios of 70 : 29.5 : 0.5 for ethylene, propylene, and ENB [163]. The rubber was crosslinked with DCP during 10 minutes at 170°C. Crosslinked EPDM sheets, having a thickness of 1mm, were exposed to a thermal aging at 80°C in air. The results of tensile tests on thermally aged samples indicated that elastic modulus increases while elongation at break decreases (Figure 1-35). The author concludes that the samples are the subject of crosslinking phenomena and therefore, no chain scission happens at 80°C before 300h of aging.

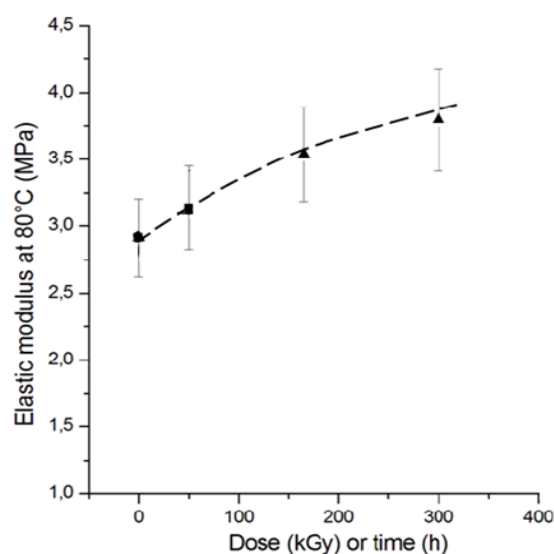


Figure 1-35: Elastic modulus evolution of crosslinked EPDM during thermal aging at 80°C in air under atmospheric pressure ^[163] (graph adapted from the PhD thesis of Planès, 2008)

Devenas *et al.* have done the same study on a slightly different EPDM (77.9% ethylene, 21.4% propylene, 0.7% diene) crosslinked likewise with DCP[142]. The results of thermal aging at 80°C in air have shown that, in this case, the crosslink density decreases during aging. Comparison of these two results indicates that thermal aging mechanism of crosslinked EPDM is more complicated than its predecessors and several factors (such as residual peroxide, residual double bonds, etc.) are involved.

Contrarily to low interest brought to thermal aging of EPDM, especially the mechanical properties, irradiation effects on this type of elastomer has been studied more widely [140-143, 164, 165]. In contrast to thermal aging, in this case there is a general agreement that EPDM elastomer goes through a crosslinking step in the early stages of irradiation which will be overcome by chain scission over time.

The results of Planès, for radiochemical aging of EPDM, are shown in Figure 1-36. The samples have been irradiated under 1 kGy/h irradiation dose rate in pure oxygen at room temperature. Aging under

irradiation decreases the elongation at break after 50 kGy of received dose, which is the same for the tensile strength. Such a behavior is interpreted as “no direct correlation between modulus and rupture behavior”.

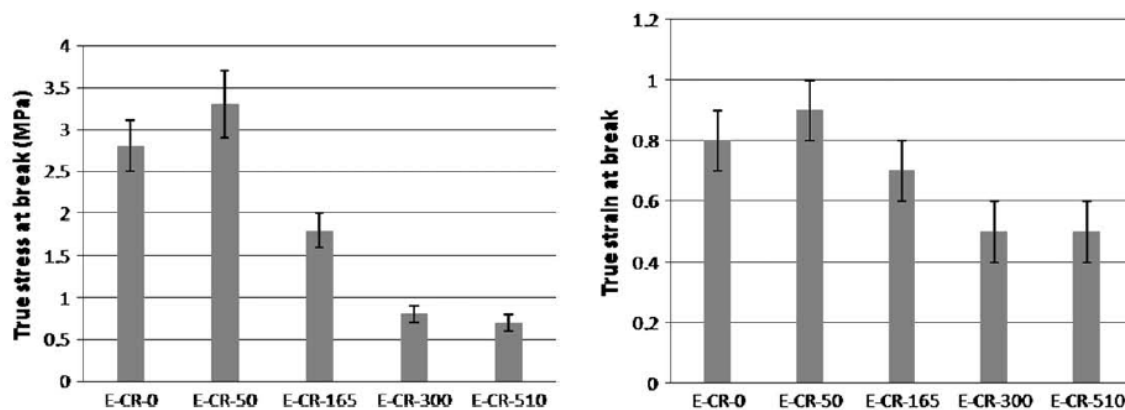


Figure 1-36: Evolution of a) stress and b) elongation at break of crosslinked EPDM during 1 kGy/h γ -irradiation in pure oxygen at room temperature (Planes 2008)^[163]

Albeit modifications in properties of crosslinked EPDM are important, but elastomers are, practically always, reinforced by fillers. The effects of these particles are discussed in next section.

1.4.4.3 ATH filled EPDM

Among very few researches brought on aging of ATH filled elastomers, we point out two of them in this section. Kim et al. studied the effect of γ -irradiation on properties of an ATH filled polyethylene-octene elastomer [166]. The samples containing 120 phr of ATH were sheets of 1 and 3mm thick. The irradiations were carried out under $0.6 \text{ kGy}\cdot\text{h}^{-1}$, at room temperature in air. The swelling and tensile testing have shown that for doses inferior to 100 kGy, the chain scission can be neglected as the gel fraction content and tensile strength increases with received dose. By increasing the irradiation time, the mechanical properties, as well as gel fraction, decreases confirming predominance of chain scissions above 100 kGy.

Planès et al. introduced the pristine ATH in their under-study rubber, plus another ATH having vinyl silane surface treatment [167]. Due to high cristallinity of the initial gum, they carried out the tensile tests at a temperature higher than the melting point of crystallites, i.e. 80°C . The ultimate behavior of samples, containing 150 phr of fillers, is shown in Figure 1-37.

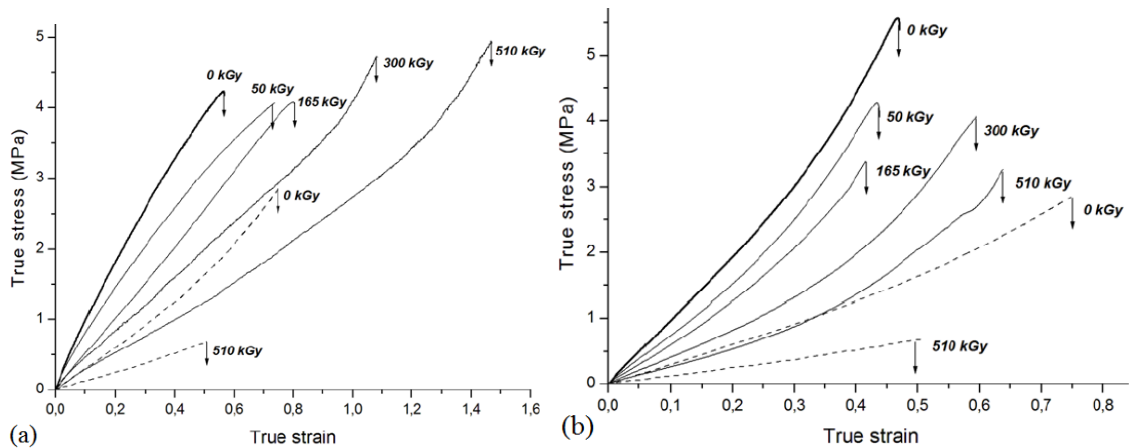


Figure 1-37: Evolution of tensile properties of EPDM containing 150 phr of a) untreated ATH and b) treated ATH for several γ -irradiation doses (dashed graphs represent unfilled elastomer, Planès) ^[167] (1 kGy/h, air, atmospheric pressure, 80°C)

In the case of pristine filler, the elongation at break increases by aging time while tensile at break remains roughly constant. The author relates the decrease of tensile strength to degradation of matrix phase. This behavior is different for surface treated fillers. For this latter, it was observed that the tensile and elongation at break decrease jointly, up to 165 kGy. At 300 kGy we see an abrupt increase both in tensile and elongation at break.

The difference between elongation at break of two fillers has been related to the capability of energy dissipation of composites by filler/matrix decohesion. This fact implies the degradation of matrix at filler vicinity or filler/matrix interphase. In fact, as the aging advances, the untreated ATH filled composite has more and more capacity of decohesion so the elongation at break increases. But, for treated ATH filled composite, decohesion cannot take place because of strong covalent bond between matrix and filler treatments. Thus, for treated filler, decohesion is not possible for doses below 300 kGy and the behavior resembles that of unfilled elastomer. But apparently, for doses higher than 300 kGy, decohesion can take place, so the induced stress relaxation lets the sample endure larger elongations to fracture.

Conclusion

The increasing usage of polymers in industry requires a global knowledge of this type of material and its behavior at various structural scales, as well as the connection between these scales. EPDM, as the main material of this study, has been the subject of many researches during the past half century. However, it has been developed less than PE, PP and EPR, presumably because of the complications due to the presence of a third unsaturated monomer. The modifications of EPDM's properties and life-time throughout aging highly depend on the initial state of the rubber after crosslinking. In fact, presence of residual double bonds, participating in radical reactions at molecular scale, can lead to alterations of EPDM behavior at macromolecular and macroscopic scales. For the time being, the lack of a thorough study, which concatenates these three general aspects, is felt.

In addition, the effect of ubiquitous fillers seems to be taken of less importance. Surface active fillers are capable of getting involved in curing of rubber, which indeed can modify the mechanism of network formation, as well as the structure of the network at the filler/matrix interphase. Furthermore, the degradation of this latter is an extra factor to consider while studying the changes in mechanical properties throughout aging. In fact, losing physical interactions at the interface reduces the reinforcement role of filler particles. These interactions can be replaced by chemical covalent bonds between the polymer chains and filler particles.

In this work, we try to keep a multi-scale view on crosslinking and oxidative aging of EPDM matrices. Based on what has been reviewed, the principal axes will be:

- Crosslinking of EPDM with peroxide, composition and structure of the tridimensional network and its mechanical properties,
- Effect of fillers and their chemical reactivity on curing of EPDM matrix and its properties at different structural scales,
- Aging of EPDM network under thermal and radiochemical exposures and the consequences on mechanical properties,
- The effect of fillers on aging process.

In the following chapters, we will to keep a balance between chemical, physicochemical and mechanical aspects of EPDM matrix by investigating at molecular, macromolecular and macroscopic scales.

References:

1. Mark, J.E., A. Eisenberg, and W.W. Graessley, *Physical properties of polymers*. 1993: American Chemical Society.
2. Gough, J., *A description of a property of Caoutchouc, or Indian rubber*. Mem. Lit. Phil. Soc. Manch. S, 1805. **2**(1): p. 288-295.
3. Meyer, K.H., G.V. Susich, and E. Valko, *Elastizität des kautschuks*. Kolloid-Zeitschrift, 1932. **61**(3): p. 370-371.
4. Meyer, K.H. and C. Ferri, *Sur l'élasticité du caoutchouc*. Helvetica Chimica Acta, 1935. **18**(1): p. 570-589.
5. Joule, J.P., *On Some Thermo-Dynamic Properties of Solids*. Phil. Trans. R. Soc. Lond., 1859. **149**: p. 91-131.
6. Treloar, L.R.G., *The physics of rubber elasticity*. 1975: Oxford University Press, USA.
7. Francois, D., A. Pineau, and A. Zaoui, *Mechanical behaviour of materials*. 2012: Springer.
8. Guth, E. and H. Mark, *Zur innermolekularen, Statistik, insbesondere bei Kettenmolekülen I*. Chemical Monthly, 1934. **65**(1): p. 93-121.
9. James, H.M. and E. Guth, *Theory of the elastic properties of rubber*. Chemical Physics, 1943. **11**(10): p. 455.
10. Flory, P.J. and J. Rehner, *Statistical mechanics of cross-linked polymer networks I. rubberlike elasticity*. Chemical Physics, 1943. **11**(11): p. 512.
11. Treloar, L.R.G., *The elasticity of a network of long-chain molecules*. Transactions of the Faraday Society, 1943. **39**: p. 83-94.
12. Verdu, J., *Elasticité caoutchoutique*. 1995.
13. Mooney, M., *A theory of large elastic deformation*. Applied Physics, 1940. **11**(9): p. 582 - 592
14. Rivlin, R.S., *Large elastic deformations of isotropic materials*. Philosophical Transactions of the Royal society of London, 1948. **241**(835): p. 379-397.
15. Bueche, F., *The tensile strength of elastomers according to current theories*. Rubber Chemistry and Technology, 1959. **32**(5): p. 1269-1285.
16. Halpin, J.C., *Molecular view of fracture in amorphous elastomers*. Rubber Chemistry and Technology, 1965. **38**(5): p. 1007-1038.
17. Bueche, A.M. and A.V. White, *Kinematographic study of tensile fracture in polymers*. Applied Physics, 1956. **27**: p. 980.
18. Thomas, A.G. and J.M. Whittle, *Tensile rupture of rubber*. Rubber Chemistry and Technology, 1970. **43**(2): p. 222-228.
19. Kaufman, R., *Aztec, Maya Were Rubber-Making Masters?* National Geographics, 2010.
20. Mark, J.E., B. Erman, and F.R. Eirich, *Science and Technology of Rubber*. 2005.
21. Ostromislensky, I.I., Russian Physics and Chemistry Society, 1915. **47**.
22. Loan, L.D., *The role of sulfur in peroxide cured ethylene-propylene rubber*. Polymer Science, 1964. **2**.
23. Perez, C.J., E.M. Vallés, and M.D. Failla, *The effect of post-irradiation annealing on the crosslinking of high-density polyethylene induced by gamma-radiation*. Radiation Physics and Chemistry, 2010. **79**(6): p. 710-717.
24. VanDuin, M. and H.G. Dikland, *Effect of third monomer type and content on peroxide crosslinking efficiency of EPDM*. Rubber Chemistry and Technology, 2003. **76**(1): p. 132-144.
25. Brazier, D.W. and G.H. Nickel, *Thermoanalytical methods in vulcanizate analysis*. Rubber Chemistry and Technology, 1975. **48**.
26. Bailey, H. and G.W. Godin, *The thermal decomposition of dibenzoyl and di-acumyl peroxides in cumene*. Transaction of the Faraday Society, 1956. **52**(52): p. 68-73.
27. Brazier, D.W. and N.V. Schwartz, *The cure of elastomer by dicumyl peroxide as observed in differential scanning calorimetry*. Thermochemica Acta, 1980. **7**.

28. Vallat, M.F., F. Ruch, and M.O. David, *A structural study of EPDM networks—the influence of the crosslinking mode on their microscopic structure*. *European Polymer Journal* 2004. **40**(7): p. 1575–1586.
29. Robinson, A.E., J.V. Marra, and L.O. Amberg, *Ethylene-propylene rubber vulcanization with aralkyl peroxide and coagents*. *Industrial & Engineering Chemistry*, 1962. **1**(2): p. 78–82.
30. Nanushyan, S.R., G.I. Pashintseva, and V.V. Severnyi, *Mass spectroscopic investigation of radical polymerization initiated by dicumyl peroxide*. *Polymer Science U.S.S.R.*, 1975. **18**(3): p. 593–597.
31. Loan, L.D., *The role of sulfur in peroxide cured ethylene-propylene rubber*. *Polymer Science*, 1964. **2**(1): p. 59–62.
32. Loan, L.D., *Peroxide crosslinking of ethylene-propylene rubber*. *Polymer Science*, 1964. **2**(7): p. 3053–3066.
33. Rijke, A. and L. Mandelkern, *Irradiation of Linear Polyethylene. Partitioning between Sol and Gel*. *Macromolecules*, 1971. **4**(5): p. 594–599.
34. Borsig, E., et al., *Solid-state polypropylene grafting as an effective chemical method of modification*. *Macromolecules Symposium* 2001. **176**(1): p. 289–298.
35. Dickens, B., *Thermal degradation study of isotactic polypropylene using factor-jump thermogravimetry*. *Polymer Science*, 1982. **20**(5): p. 1169–1183.
36. Harpell, G.A. and D.H. Warold, *Organic peroxides for cure of ethylene-propylene rubbers*. *Rubber Chemistry & Technology*, 1973. **46**(2): p. 238–254.
37. Zachary, M., et al., *EPR study of persistent free radicals in cross-linked EPDM rubbers*. *European Polymer Journal*, 2008. **44**(2099–2107).
38. Dikland, H.G., *Influence of chemical composition and molecular structure of EPDM on peroxide crosslinking efficiency*. *Kautschuk Gummi Kunststoffe*, 1996. **49**(6): p. 413–417.
39. Waters, W.A., *Mechanisms of oxidation of organic compounds*. 1964.
40. Fujimoto, K. and K. Wataya, *The study of polymer by high-temperature ATR spectroscopy*. *Applied Polymer Science*, 1961. **13**(12): p. 2513–2526.
41. Bredt, J., *Über sterische hinderung in brückenringen (Bredtsche Regel) und über die meso-trans-stellung in kondensierten ringsystemen des hexamethylens*. *European Journal of Organic Chemistry*, 1921. **437**(1): p. 1–13.
42. Baldwin, F.P., et al., *The influence of residual olefin structure on EPDM vulcanization*. *Rubber Chemistry & Technology*, 1970. **43**(3): p. 522–548.
43. Orza, R.A. and M.V. Duin, *Investigation of peroxide crosslinking of EPDM rubber by solid-state NMR*. 2008.
44. Orza, R.A., et al., *Mechanism for peroxide cross-linking of EPDM rubber from MAS 13C NMR spectroscopy*. *Macromolecules*, 2009. **42**(22): p. 8914–8924.
45. Papirer, E., J. Schultz, and C. Turchi, *Surface properties of a calcium carbonate filler treated with stearic acid*. *European Polymer Journal*, 1984. **20**(12): p. 1155–1158.
46. Paunikallio, T., M. Suvanto, and T.T. Pakkanen, *Grafting of 3-(trimethoxysilyl)propyl methacrylate onto polypropylene and use as a coupling agent in viscose fiber/polypropylene composites*. *Reactive and Functional Polymers*, 2008. **68**(3): p. 797–808.
47. Morlat-Therias, S., et al., *Photooxidation of ethylene-propylene-diene/montmorillonite nanocomposites*. *Polymer degradation and stability*, 2005. **90**(1): p. 78–85.
48. Rotheron, R.N., *Particulate-Filled Polymer Composites*. 2003: Rapra Technology Limited.
49. Wierenga, A.M., T.A.J. Lenstra, and A.P. Philipse, *Aqueous dispersions of colloidal gibbsite platelets: synthesis, characterisation and intrinsic viscosity measurements*. *Colloids and Surfaces A: Physicochemical and Engineering Aspects*, 1998. **134**(3): p. 359–371.
50. Thilagam, A., et al., *Interaction of gibbsite with oleic acid*. *Mineral Processing*, 2012. **104**(105): p. 24–30.
51. Sobolev, I. and E.A. Woycheshin, *Handbook of fillers for plastics*. 1987.
52. Cárdenas, M.A., et al., *Mechanical and fire retardant properties of EVA/clay/ATH nanocomposites – Effect of particle size and surface treatment of ATH filler*. *Polymer Degradation and Stability*, 2008. **93**(11): p. 2032–2037.

53. Philipse, A.P. and A. Vrij, *Preparation and properties of nonaqueous model dispersions of chemically modified, charged silica spheres*. Journal of colloid and interface science, 1989. **128**(1): p. 121-136.
54. Erman, B. and J.E. Mark, *Structure and properties of rubberlike networks*. 1997: Oxford University Press.
55. Mark, J.E. and B.Erman, *Rubberlike elasticity: A molecular primer*. 2007: Cambridge.
56. Smallwood, H.M., *Limiting law of the reinforcement of rubber*. Journal of Applied Physics, 1944. **15**(11).
57. Guth, E., *Theory of filler reinforcement*. Applied Physics, 1945. **16**(1): p. 20- 25
58. Guth, E. and O. Gold, *On the hydrodynamical theory of the viscosity of suspensions*. Physical Review, 1938. **53**.
59. Bokobza, L., *Application of vibrational spectroscopy for the analysis of polymer composites*, in *Macromolecules symposium*. 2004. p. 61–70.
60. Bueche, F., *Mechanical degradation of high polymers*. Applied polymer Science, 1960. **4**(10): p. 101–106.
61. Mullins, L. and N.R. Tobin, *Stress softening in rubber vulcanizates. Part I. Use of a strain amplification factor to describe the elastic behavior of filler-reinforced vulcanized rubber*. Applied Polymer Science, 1965. **9**(9): p. 2993–3009.
62. Nielsen, L.E., *Simple theory of stress-strain properties of filled polymers*. Applied Polymer Science, 1966. **10**(1): p. 97–103.
63. Montezin, F., et al., *Flame retardant and mechanical properties of a copolymer PP/PE containing brominated compounds/antimony trioxide blends and magnesium hydroxide or talc*. Fire and Materials, 1997. **21**(6): p. 245–252.
64. Vlasova, N.N., et al., *Influence of the degree of filling and the properties of the fillers on the strain-strength properties of synthetic polyethylene composites*. Polymer Science U.S.S.R, 1988. **30**(7): p. 1487–1494.
65. Poh, B.T., H. Ismail, and K.S. Tan, *Effect of filler loading on tensile and tear properties of SMR L/ENR 25 and SMR L/SBR blends cured via a semiefficient vulcanization system*. Polymer Testing, 2002. **21**(7): p. 801–806.
66. Planes, E., et al., *Influence of fillers on mechanical properties of ATH filled EPDM during ageing by gamma irradiation*. Polymer Degradation and Stability, 2010. **95**(6): p. 1029–1038.
67. Boonstra, B.B., *Role of particulate fillers in elastomer reinforcement: a review*. Polymer, 1971. **20**(6): p. 691–704.
68. Warrick, E.L., et al., *Silicon elastomer developments*. Rubber Chemistry and Technology, 1971. **52**(3): p. 437-525.
69. Bueche, A.M., *Interaction of polydimethylsiloxanes with swelling agents*. Polymer Science, 1955. **15**(79): p. 97–103.
70. Kraus, G., *Degree of Cure in Filler-Reinforced Vulcanizates by the Swelling Method*. Rubber Chemistry and Technology, 1956. **30**(3): p. 928-951.
71. Lorenz, O. and C.R. Parks, *The crosslinking efficiency of some vulcanizing agents in natural rubber*. Polymer Science, 1961. **50**(154): p. 299–312.
72. Kraus, G., *Swelling of filler-reinforced vulcanizates*. Applied Polymer Science, 1963. **7**.
73. James, H.M. and E. Guth, *Theory of increase in rigidity of rubber during curing*. Chemical Physics, 1947. **15**(9): p. 669-684.
74. Mark, J.E. and B. Erman, *Rubber elasticity. A molecular primer*. 1988: Wiley InterScience.
75. Berriot, J., et al., *Reinforcement of model filled elastomers: experimental and theoretical approach of swelling properties*. Polymer, 2002. **43**(23): p. 6131-6138.
76. Bolland, J.L., *Kinetic studies in the chemistry of rubber and related materials. I. The thermal oxidation of ethyl linoleate*. Proceedings of the Royal Society of London, 1946. **186**(1005): p. 218-236.
77. Bolland, J.L. and G. Gee, *Kinetic studies in the chemistry of rubber and related materials. II. The kinetics of oxidation of unconjugated olefins*. Transactions of the Faraday Society, 1946. **42**(42): p. 236-243.

78. Bolland, J.L. and G. Gee, *Kinetic studies in the chemistry of rubber and related materials. III. Thermochemistry and mechanisms of olefin oxidation*. Transactions of the Faraday Society, 1946. **42**: p. 244-252.
79. Huy, M.L. and G. Evrard, *Methodologies for lifetime predictions of rubber using Arrhenius and WLF models*. Die Angewandte Makromolekulare Chemie, 1999. **261-262**(1): p. 135-142.
80. Hsuan, Y. and M. Li, *Temperature and pressure effects on the oxidation of high-density polyethylene geogrids*. Geotextiles and Geomembranes, 2005. **23**(1): p. 55-75.
81. Koerner, R.M., A.E. Lord, and Y.H. Hsuan, *Arrhenius modeling to predict geosynthetic degradation*. Geotextiles and Geomembranes, 1992. **11**(2): p. 151-183.
82. Bernstein, B.S. and P.N. Lee, in *International Wire and Cable Symposium*. 1975.
83. Achimsky, L., *Etude cinétique de la thermo-oxydation du polypropylène*. 1996.
84. Gugumus, F., *Effect of temperature on the lifetime of stabilized and unstabilized PP films*. *Polymer degradation and stability*. Polymer Degradation and Stability, 1999. **63**(1): p. 41-52.
85. Gillen, K.T., et al., *Extrapolation of accelerated aging data: Arrhenius or erroneous?* Trends in Polymer Science, 1997. **5**(8): p. 250-257.
86. Langlois, V., et al., *Thermooxidative aging of crosslinked linear polyethylene: stabilizer consumption and lifetime prediction*. Polymer Degradation and Stability, 1993. **40**(3): p. 399-409.
87. Celina, M., K.T. Gillen, and R.A. Assink, *Accelerated aging and lifetime prediction: Review of non-Arrhenius behavior due to two competing processes*. Polymer Degradation and Stability, 2005. **90**(3): p. 395-404.
88. Khelidj, N., *Vieillissement d'isolant de cables en polyéthylène en ambiance nucléaire*. 2006.
89. Richaud, E., *Durabilité des Géotextiles en Polypropylène*. 2006.
90. Barrois-Oudin, N., C. Cardinet, and F. Delor-Jestin, *Vieillissement photochimique des caoutchoucs EPDM*. 1997.
91. Faure, Y.H., et al., *Analysis of geotextile filter behaviour after 21 years in Valcros dam*. Geotextiles and Geomembranes, 1999. **17**(5-6): p. 353-370.
92. Tireau, J., *Propriétés à long terme des gaines de polyéthylène haute densité utilisées pour les ponts à haubans*. 2011.
93. Colin, X., L. Audouin, and J. Verdu., *Determination of thermal oxidation rate constants by an inverse method. application to polyethylene*. Polymer Degradation and Stability, 2004. **86**(2): p. 309-321.
94. Colin, X., et al., *Kinetic modelling of radiochemical ageing of ethylene-propylene copolymers*. Radiation Physics and chemistry, 2010. **79**(3): p. 365-370.
95. Fayolle, B., et al., *Mechanism of degradation induced embrittlement in polyethylene*. Polymer Degradation and Stability, 2007. **92**(2): p. 231-238.
96. Delprat, P., X. Duteurtre, and J.L. Gardette, *Photooxidation of unstabilized and HALS-stabilized polyphasic ethylene-propylene polymers*. Polymer Degradation and Stability, 1995. **50**(1): p. 1-12.
97. Tcharkhtchi, A., et al., *Oxyluminescence of polyamide 12*. Polymer Degradation and Stability, 1994. **44**(3): p. 335-341.
98. Verdu, J., et al., *Chemiluminescence from the thermal oxidation of polyisoprene and polybutadiene I. Influence of oxygen pressure on the chemiluminescence of polyisoprene during its oxidation*. Polymer Degradation and Stability, 2006. **91**(6): p. 1387-1394.
99. Hoàng, E.M., et al., *The thermo-oxidative degradation of metallocene polyethylenes. Part 1: Long-term thermal oxidation in the solidstate*. Polymer Degradation and Stability, 2006. **91**(6): p. 1356-1362.
100. Sánchez, K.D.T., et al., *Effects of type of polymerization catalyst system on the degradation of polyethylenes in the melt state. Part 1: Unstabilized polyethylenes (including metallocene types)*. Journal of Vinyl and Additive Technology, 2011. **17**(1): p. 28-39.
101. Achimsky, L., L. Audouin, and J. Verdu, *Kinetic study of the thermal oxidation of polypropylene*. Polymer Degradation and Stability, 1997. **57**(3): p. 231-240.
102. Verdu, J., *Vieillissement oxydant des polymères*. 2012.
103. Bovey, F.A., *The effects of ionizing radiation on natural and synthetic high polymers* Applied Polymer Science, 1958. **1**.

104. Seymour, R.B., *Radiation physics and chemistry of polymers* (Makhlis, F. A.). Chemical Education, 1976. **53**(2): p. A138.
105. Clough, R.L. and S.W. Shalaby, *Radiation effects on polymers*. Vol. 475. 1991: ACS Publications.
106. Khelidj, N., et al., *Oxidation of polyethylene under irradiation at low temperature and low dose rate. Part I. The case of "pure" radiochemical initiation*. *Polymer Degradation and Stability*, 2007. **91**(7).
107. Colin, X., L. Audouin, and J. Verdu, *Kinetic modelling of the thermal oxidation of polyisoprene elastomers. Part 1: Unvulcanized unstabilized polyisoprene*. *Polymer Degradation and Stability*, 2007. **92**(5): p. 886–897.
108. Richaud, E., et al., *Effect of oxygen pressure on the oxidation kinetics of unstabilised polypropylene*. *Polymer Degradation and Stability*, 2006. **91**(2): p. 398–405.
109. Colin, X., et al., *Vieillissement thermo-oxydant des polymères. Un pas vers la modélisation cinétique*. *Vieillissement et durabilité des matériaux*. 2003.
110. Coquillat, M.G., *vieillissement des propergols à matrice polybutadiene: modélisation cinétique d'oxydation*. 2007.
111. Coquillat, M., et al., *Thermal oxidation of polybutadiene. Part 1: Effect of temperature, oxygen pressure and sample thickness on the thermal oxidation of hydroxyl-terminated polybutadiene*. *Polymer Degradation and Stability*, 2007. **92**(7): p. 1326–1333.
112. Coquillat, M., et al., *Thermal oxidation of polybutadiene. Part 2: Mechanistic and kinetic schemes for additive-free non-crosslinked polybutadiene*. *Polymer Degradation and Stability*, 2007. **92**(7): p. 1334–1342.
113. Tüdös, F. and M. Iring, *Polyolefine oxidation: Rates and products*. *Acta polymerica*, 2003. **39**(1-2): p. 19-26.
114. Ranby, B. and H. Yoshida, *Electron spin resonance studies of polyethylene and polypropylene irradiated by ultraviolet light*. *Polymer Science*, 1966. **12**(1): p. 263–276.
115. Turner, D.T., *Role of free radicals in the radiation chemistry of polymers*. *Polymer Science*, 1971. **5**(1): p. 229–383.
116. Colin, X., *Modélisation cinétique de la thermo-oxydation de matériaux polymères et composites à hautes performances thermomécaniques*. 2000.
117. Colin, X., C. Marais, and J. Verdu, *A new method for predicting the thermal oxidation of thermoset matrices: Application to an amine crosslinked epoxy*. *Polymer Testing*, 2001. **20**(7): p. 795–803.
118. Decelle, J., N. Huet, and V. Bellenger, *Oxidation induced shrinkage for thermally aged epoxy networks*. *Polymer Degradation and Stability*, 2003. **81**(2): p. 239–248.
119. Verdu, J., *Vieillissement oxydant des polymères*. 2012: Lavoisier.
120. Rincon-Rubio, L.M., et al., *A general solution of the closed-loop kinetic scheme for the thermal oxidation of polypropylene*. *Polymer degradation and stability*, 2001. **74**(1): p. 177–188.
121. Decker, C. and F.R. Mayo, *Aging and degradation of polyolefins. II. γ -initiated oxidations of atactic polypropylene*. *Polymer Science*, 1973. **11**(11): p. 2847–2877.
122. Decker, C., F.R. Mayo, and H. Richardson, *Aging and degradation of polyolefins. III. Polyethylene and ethylene-propylene copolymers*. *Polymer Science*, 1973. **11**(11): p. 2879–2898.
123. Niki, E., C. Decker, and F.R. Mayo, *Aging and degradation of polyolefins. I. Peroxide-initiated oxidations of atactic polypropylene*. *Polymer Science*, 1973. **11**(11): p. 2813–2845.
124. Dely, N., et al., *Oxygen consumption in EPDM irradiated under different oxygen pressures and at different LET*. *Beam Interactions with Materials and Atoms*, 2005. **236**: p. 145-152.
125. Rivaton, A., S. Cambon, and J.L. Gardette, *Radiochemical ageing of EPDM elastomers. 2. Identification and quantification of chemical changes in EPDM and EPR films gamma-irradiated under oxygen atmosphere*. *Beam Interactions with Materials and Atoms*, 2005. **227**(3).
126. Delor, F., et al., *Ageing of EPDM—2. Role of hydroperoxides in photo- and thermo-oxidation*. *Polymer Degradation and Stability*, 1998. **60**(2-3): p. 321–331.

127. Delor-Jestin, F., et al., *Photo-, thermal and natural ageing of ethylene-propylene-diene monomer (EPDM) rubber used in automotive applications. Influence of carbon black, crosslinking and stabilizing agents*. *Polymer Degradation and Stability*, 2000. **67**(3): p. 469–477.
128. Zaharescu, T., R. Vilcu, and C. Podina, *Some kinetic and thermodynamic aspects of thermal degradation of lightly stabilised elastomers*. *Polymer Testing*, 1998. **17**(8): p. 587–596.
129. Zaharescu, T. and C. Podina, *Radiochemical stability of EPDM*. *Polymer Testing*, 2001. **20**(2): p. 141–149.
130. Zaharescu, T., R. Vilcub, and C. Podinab, *Some kinetic and thermodynamic aspects of thermal degradation of lightly stabilised elastomers*. *Material Behaviour*, 1998. **17**.
131. Signori, F., M.B. Coltellib, and S. Broncoa, *Thermal degradation of poly(lactic acid) (PLA) and poly(butylene adipate-co-terephthalate) (PBAT) and their blends upon melt processing*. *Polymer Degradation and Stability*, 2009. **94**(1): p. 74–82.
132. Clapper, J.D., et al., *Development and characterization of photopolymerizable biodegradable materials from PEG–PLA–PEG block macromonomers*. *Polymer Degradation and Stability*, 2007. **48**(22): p. 6554–6564.
133. Bovey, F.A., *The effects of ionizing radiation on natural and synthetic high polymers* *Applied Polymer Science*, 1959. **1**(2): p. 250.
134. Dole, M., *Radiation chemistry of macromolecules. Volume II*. 1973.
135. Bueche, F., *Derivation of the WLF equation for the mobility of molecules in molten glasses*. *Chemical Physics*, 1956. **24**(2): p. 418.
136. M. Celina, G.A.G., *Characterisation and degradation studies of peroxide and silane crosslinked polyethylene*. *Polymer Degradation and Stability*, 1995. **48**.
137. Assink, R.A., K.T. Gillen, and B. Sanderson, *Monitoring the degradation of a thermally aged EPDM terpolymer by 1H NMR relaxation measurements of solvent* *Polymer*, 2002. **43**(4): p. 1349–1355.
138. Gillen, K.T., M. Celina, and R.L. Clough, *Density measurements as a condition monitoring approach for following the aging of nuclear power plant cable materials*. *Radiation Physics and Chemistry*, 1999. **56**(4): p. 429–447.
139. Boiteux, G., et al., *Dielectric and mechanical spectroscopies for the study of thermal and radiochemical ageing of polymers*. *Beam Interactions with Materials and Atoms*, 1997. **131**(1-4): p. 172–179.
140. Gueguen, V., et al., *Lifetime prediction in the case of radiooxidative ageing of an ethylenepropylene rubber used for electrical insulation*. *Polymer degradation and stability*, 1994. **46**(1): p. 113-122.
141. Gueguen, V., et al., *Radiochemical oxidation of an ethylene-propylene-hexadiene terpolymer*. *Radiation Physics and Chemistry*, 1994. **44**(6): p. 557–565.
142. Celette, N., et al., *Relaxation behaviour of radiochemically aged EPDM elastomers*. *Beam Interactions with Materials and Atoms*, 2001. **185**(1-4): p. 305–310.
143. Planes, E., et al., *Evolution of EPDM networks aged by gamma irradiation – Consequences on the mechanical properties*. *Polymer*, 2009. **50**(16): p. 4028–4038.
144. Basfar, A.A. and K.M.I. Ali, *Natural weathering test for films of various formulations of low density polyethylene and linear low density polyethylene*. *Polymer Degradation and Stability*, 2006. **91**(3): p. 437–443.
145. Naddeo, C., et al., *Mechanical and transport properties of irradiated linear low density polyethylene*. *Polymer Degradation and Stability*, 2001. **72**(2): p. 239–247.
146. Colin, X., C. Monchy-Leroy, and J.Verdu, *Effect of gamma irradiation on tensile properties of low molecular weight polyethylene samples*. *Radiation Physics and chemistry*, 2011. **80**(8): p. 895-901.
147. Fayolle, B., et al., *Review: degradation-induced embrittlement in semi-crystalline polymers having their amorphous phase in rubbery state*. *Journal of materials science*, 2008. **43**(22): p. 6999-7012.
148. Fayolle, B., et al., *Mechanism of degradation induced embrittlement in polyethylene*. *Polymer Degradation and Stability*, 2007. **92**(2).

149. Celina, M., et al., *Chemiluminescence as a condition monitoring method for thermal aging and lifetime prediction of an HTPB elastomer*. *Polymer Degradation and Stability*, 2006. **91**(10): p. 2365–2374.
150. Verdu, J., *Effect of aging on the mechanical properties of polymeric materials*. *Macromolecular Science*, 1994. **31**(10): p. 1383-1398.
151. Makhlis, F.A., *Radiation physics and chemistry of polymers*. 1972: John Wiley and Sons.
152. Emanuel, N.M. and A.L. Buchachenko, *Chemical physics of polymer degradation and stabilization*. Vol. 1. 1982: VSP Books.
153. Colin, X., G. Teyssedre, and M. Fois, *Ageing and degradation of multiphase polymer systems*, in *Handbook of Multiphase Polymer Systems*. 2011, Wiley.
154. Bykov, Y.V., Y.V. Bystritskaya, and O.N. Karpukhin, *Evaluation of the thickness of the radiation-oxidized layer of irradiated polyethylene*. *Polymer Science USSR*, 1987. **29**(7): p. 1479–1485.
155. Khelidj, N., et al., *A simplified approach for the lifetime prediction of PE in nuclear environments*. *Nuclear Instruments and Methods in Physics Research Section B: Beam Interactions with Materials and Atoms*, 2005. **236**(1): p. 88-94.
156. Fayolle, B., et al., *Oxidation induced embrittlement in propylene a tensile testing study*. *Polymer Degradation and Stability*, 2000. **70**(3): p. 333–340.
157. Clavreul, R., *Evolution of ethylene propylene copolymers properties during ageing*. *Beam Interactions with Materials and Atoms*, 1997. **131**.
158. Y.Suna, S.L., K.Watkinsc, C.P. Wongb, *Electrical approach to monitor the thermal oxidation aging of carbon black filled ethylene propylene rubber*. *Polymer Degradation and Stability*, 2004. **88**(2).
159. K.T. Gillen, R.B., R.L. Clough, M. Celina, *Lifetime predictions for semi-crystalline cable insulation materials: I. Mechanical properties and oxygen consumption measurements on EPR materials*. *Polymer Degradation and Stability*, 2006. **91**.
160. Carlsson, D.J., *Degradation and stabilisation of polymers subjected to high energy radiation*, in *Atmospheric Oxidation and Antioxidants, Vol. II*. 1993.
161. James, J.E., *Physical Properties of Polymers Handbook*. 2006: Springer.
162. R.L.Clough, K.T.G., *Combined environment aging effects*. *Polymer Science*, 1981. **19**.
163. E.Planes, *Influence des charges sur l'évolution des propriétés mécaniques des EPDM chargés lors de leur vieillissement par irradiation*. 2008, Ecole doctorale : Matériaux de Lyon: Lyon.
164. Davenas, J., et al., *Influence of the molecular modifications on the properties of EPDM elastomers under irradiation*. *Nuclear Instruments and Methods in Physics Research Section B: Beam Interactions with Materials and Atoms*, 2003. **208**: p. 461-465.
165. Davenas, J., et al., *Stability of polymers under ionising radiation: The many faces of radiation interactions with polymers*. *Nuclear Instruments and Methods in Physics Research Section B: Beam Interactions with Materials and Atoms*, 2002. **191**(1): p. 653-661.
166. Chonung Kim¹, Tao He³, Pingkai Jiang^{3,*}, Ping Wei³, Xingyi Huang³, Zhijian Jin⁴, *Dielectric properties of γ -irradiated POE highly filled with aluminum hydroxide*. *Polymer Engineering & Science*, 2006. **46**.
167. E.Planes, L.C., G.Vigier, J.Fournier, I.Stevenson-Royaud, *Influence of fillers on mechanical properties of ATH filled EPDM during ageing by gamma irradiation*. *Polymer Degradation and Stability*, 2010. **95**(6).

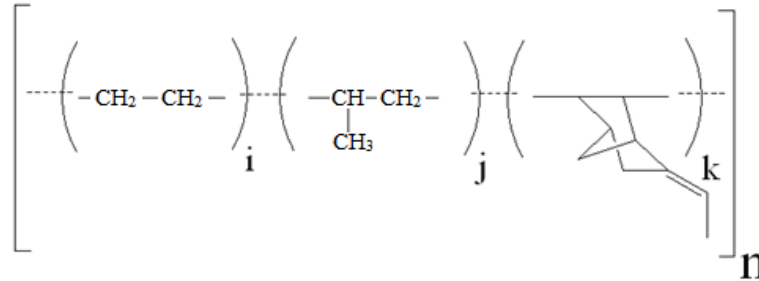
CHAPTER II

2 Materials & Experimental Techniques

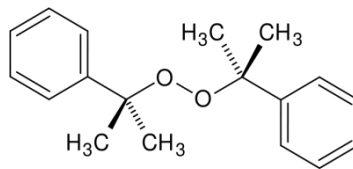
Extended abstract (in French language)

Dans ce chapitre, les matériaux bruts utilisés dans cette étude sont présentés :

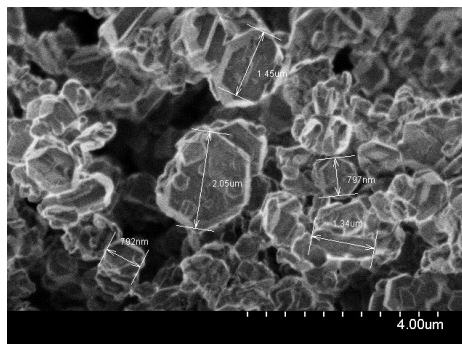
- Les EPDMs linéaires:



- L'agent de réticulation (le peroxyde de dicumyle) :



- Et les charges ATH $[\text{Al}(\text{OH})_3]$ d'un diamètre moyen de $1,3 \mu\text{m}$, vierges et traitées en surface par un agent de couplage de type vinyle-silane:



Il présente ensuite les matériaux de l'étude réalisés à partir des matériaux bruts précédents :

- Les matrices EPDM pures
- Les matrices EPDM chargées de particules ATH vierges
- Les matrices EPDM chargées de particules ATH traitées en surface

Nous avons choisi les appellations suivantes pour la matrice Nordel 4640 pure et chargée par différentes fractions de particules ATH vierges (PATH) et traitées en surface (TATH) :

	Nordel 4640 (wt.-%)	PATH (wt.-%)	TATH (wt.-%)	DCP (phr)
4640-N	100	-	-	3
33phr-PATH	75	25	-	3
33phr-TATH	75	-	25	3
100phr-PATH	50	50	-	3
100phr-TATH	50	-	50	3

Ce chapitre détaille enfin les différentes méthodes d'essai et les approches utilisées pour caractériser les matériaux de l'étude avant et après vieillissement thermique et radiochimique. Le vieillissement thermique sera réalisé à 90, 110 et 130°C dans l'air. Le vieillissement radiochimique sera réalisé sous les rayons γ à $40 \pm 5^\circ\text{C}$ dans l'air sous les débits de dose de 0,1, 1 et 10 $\text{kGy}\cdot\text{h}^{-1}$.

Les méthodes de caractérisation sont classées en fonction de l'échelle structurale d'analyse:

Echelle moléculaire :

- Spectrophotométrie infrarouge
- Résonance magnétique nucléaire à l'état solide
- Calorimétrie différentielle à balayage

Echelle macromoléculaire :

- Chromatographie d'exclusion stérique
- Essai de gonflement
- Analyse thermogravimétrique
- Rhéométrie à l'état fondu

Echelle Macroscopique :

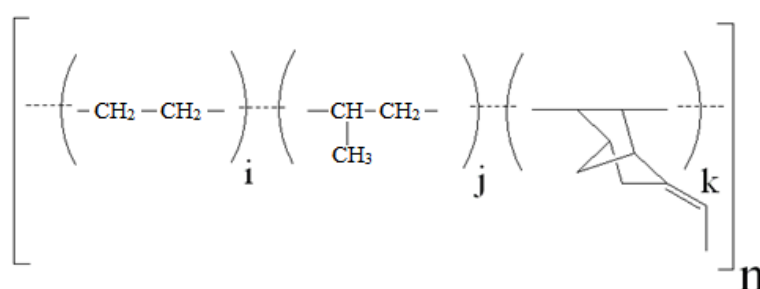
- Essai de traction

Ces méthodes, classées dans un ordre chronologique, visent à élucider la structure aux échelles moléculaire, macromoléculaire et microscopique, en vue d'établir des relations structure – propriétés mécaniques. Dans chaque catégorie, on a essayé de donner des informations brèves mais complètes sur ces techniques et leurs conditions expérimentales choisies pour la caractérisation des matériaux.

2.1 Raw materials

2.1.1 Elastomer

Three EPDMs (Scheme 2-1) having industrial appellations of “Nordel” and identifiers of “4520”, “4640” and “4570”, have been supplied by *Dow Chemicals Company* for this study. The nominal content of each monomer (ethylene, propylene and ENB), as given in EPDM industrial technical sheet, are presented in Table 2-1. All three EPDMs contain closely the same content of ENB and approximately the same content of the two other monomers. Thus, the main difference between these linear polymers is their molecular weight (M_w) which may clarify the effect of dangling chains on initial and long-term behavior of crosslinked network.



Scheme 2-1: General structure of an EPDM

	Ethylene (wt.-%)	Propylene (wt.-%)	ENB (wt.-%)	Cristallinity (%)	Mw (g.mol⁻¹)
NORDEL IP 4520	50	45.1	4.9	<1	115000
NORDEL IP 4570	50	45.1	4.9	<1	210000
NORDEL IP 4640	55	40.1	4.9	<4	160000

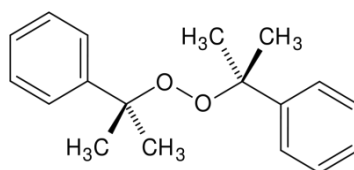
Table 2-1: Data from Dow Chemical's technical sheets

In this study, the three EPDMs are considered as totally amorphous i.e. the small fraction of cristallinity ($X_C < 4\%$) will be neglected in every case.

2.1.2 Crosslinking agent

The crosslinking agent is dicumyl peroxide (DCP, Scheme 2-2) with a purity superior to 99% provided by *Sigma-Aldrich*®. The concentration of DCP recommended by NEXANS NRC for crosslinking of three linear EPDMs is 3phr (3 grams of peroxide Per Hundred grams of Resin). But, in this study,

other concentrations (2.75, 5.5, 10 and 17 phr) have been used to analyze the effect of DCP concentration on crosslinking, and physical and mechanical properties of crosslinked networks.



Scheme 2-2: Molecule of dicumyl peroxide (N° Cas: 80-43-3)

2.1.3 Filler

Aluminum trihydrate (ATH) which is better known as gibbsite has been provided by *Nabaltec* society. The two grades of ATH chosen for this study are Apyral 40 CD (pristine ATH or PATH) and Apyral 40 Vs1 containing tri-ethoxy-vinyl-silane grafted to the surface of filler particles as coupling agent (treated ATH or TATH). Some information concerning the physicochemical properties of these fillers has been given in Table 2-2.

	Apyral 40 CD (PATH)	Apyral 40 Vs1(TATH)
Al (OH) ₃	99.5%	98.5%
Bulk density	400 kg/m ³	350 kg/m ³
Density	2.4 g/cm ³	2.4 g/cm ³
Specific surface area	3.5 m ² /g	3.5 m ² /g

Table 2-2: Some physicochemical properties of ATH fillers

2.2 Samples

2.2.1 Neat samples

Two routes have been employed to introduce DCP into the EPDM matrices:

a) Solution route:

In order to study the crosslinking of EPDM with dicumyl peroxide, several concentrations of this latter have been introduced into EPDM via a solution path. Fresh powder of DCP, obtained by grinding of DCP crystallites, is introduced into a solution of EPDM in 2:1(vol : vol) solvents mixture of cyclohexane and dichloromethane and stirred until thorough dissolution of DCP at 40°C. Then, the solution is poured in clean glass petri dishes at room temperature to evaporate the solvents. The obtained EPDM+DCP film is then put under vacuum at 40°C to evaporate all residual solvents.

b) Mixer route:

The second path to introduce DCP is by using industrial mixers appropriate for producing large quantities of mixture. EPDM gum is premixed for 10 minutes at 140°C and then the temperature is lowered to 110°C for peroxide introduction. The blend is then mixed for 2 minutes at 120°C before cooling down to the room temperature.

In this method, the only concentration of DCP has been 3phr, which corresponds to the current concentration in industrial formulations. Prior to production of crosslinked samples for aging purposes, small quantities of EPDM-DCP blend have been sampled for crosslinking analyses.

Crosslinking has been carried out by means of a laboratory scale hot press at 170°C for 15 minutes. The obtained crosslinked films and plates were of 50 to 100 µm and 2-3 mm thick, respectively.

2.2.2 Filled samples

The mixer route has been used to fabricate high quantities of ATH filled EPDM. The protocol of fabrication is as follows:

- Premixing of EPDM gum for 10 minutes at 140°C
- Introduction of filler and mixing for 5 minutes at 150°C
- Cooling down the mixture and introducing the peroxide at 110°C
- Mixing for 2 minutes at 120°C

Contents of fillers in matrices have been chosen 25 wt.-% (corresponding to 33 phr) and 50 wt.-% (corresponding to 100 phr) for all EPDMs except for Nordel IP 4570. For this latter, due to its high molecular weight and high melt viscosity, incorporation of 50 wt.-% of fillers was not possible.

Nordel IP 4640 has been chosen for aging studies. The appellations chosen for these formulations are presented in Table 2-3.

	Nordel 4640 (wt.-%)	PATH (wt.-%)	TATH (wt.-%)	DCP (phr)
4640-N	100	-	-	3
33phr-PATH	75	25	-	3
33phr-TATH	75	-	25	3
100phr-PATH	50	50	-	3
100phr-TATH	50	-	50	3

*Table 2-3: Materials for aging tests
(N: Neat, PATH: Pristine ATH, TATH: Treated ATH)*

ATH filled EPDM sheets of 2-3 mm thick have been processed with hot pressing at 170°C for 15 minutes. In order to assure over 99% consumption of DCP molecules. The applied pressures were around 120 bars for thin films and 200 Mbar for thick plates. Samples, after preparation, were conserved at -20°C in order to decrease thermal effects.

2.3 Aging conditions

2.3.1 Thermal aging

Neat and filled crosslinked EPDM samples have been aged thermally in air ventilated ovens at 90°C, 110°C and 130°C having $\pm 1^\circ\text{C}$ error.

2.3.2 Radiochemical aging

Radiochemical aging has been carried out at SCK·CEN, the Belgian nuclear research center using a ^{60}Co irradiation source.

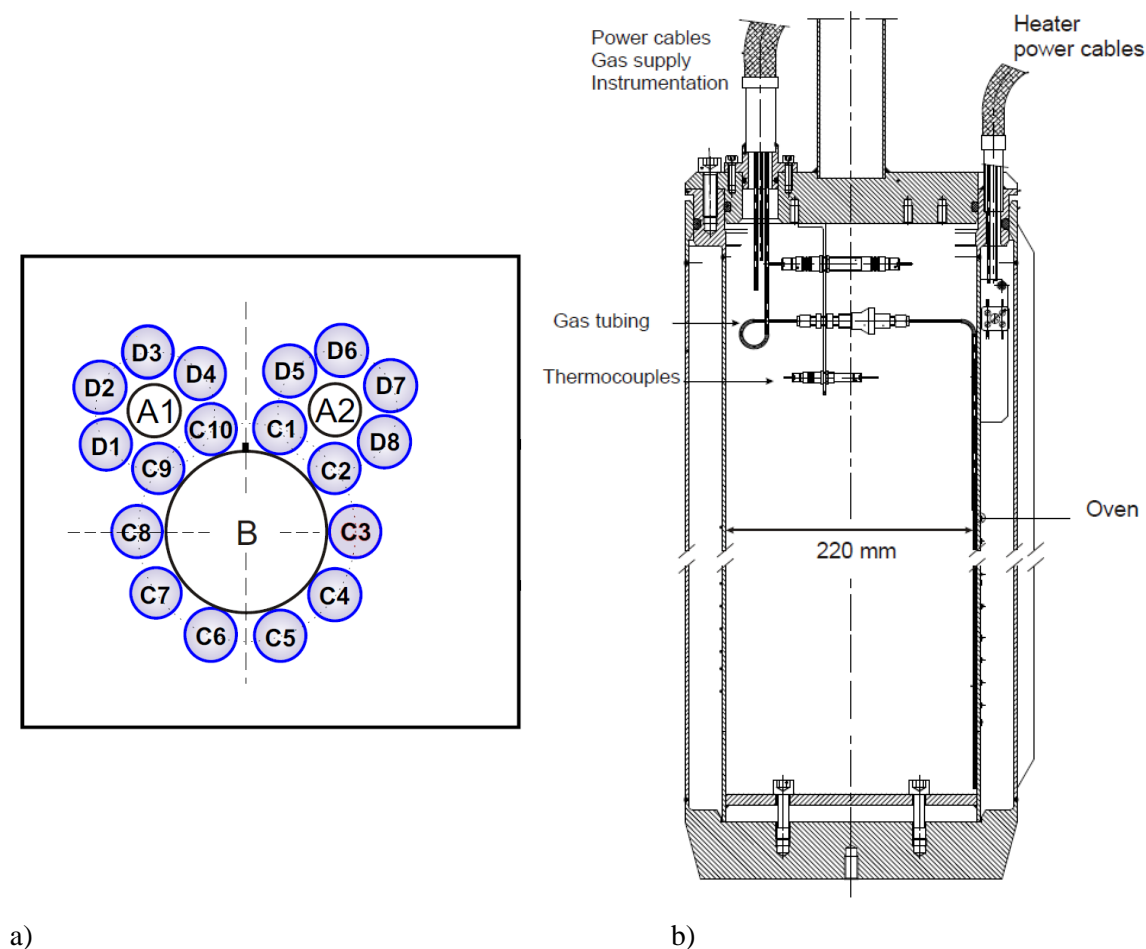


Figure 2-1 : a) Schematization of Brigitte facility, b) Longitudinal cross-section of the irradiation container B (see text)

The underwater high dose rate Gamma irradiation facility used for this study is named Brigitte. Three irradiation containers (B, A1 and A2) are installed on a rack of lattice shaped holders (Figure 2-1a). The samples are irradiated at position B. The oven, thermocouples, wirings and gas tubing of container B are depicted in Figure 2-1b. Positions labeled C₁ – C₁₀ and D₁ – D₈ are containers of radioactive fuel rods. The samples are irradiated under a dried air flow at a temperature ranged between 35°C and 45°C, presumably depending on the gamma dose rate. Irradiation conditions are detailed in Table 2-4.

Dose rate (kGy.h ⁻¹)	Received dose (kGy)						
0.1	15	30	50	80	–	–	–
1	15	50	100	150	300	500	800
10	15	50	100	150	300	500	800

Table 2-4: γ dose rates and received doses

The dose rates present an error less than 5%.

2.4 Characterization methods

In this part, the test methods and approaches used to characterize the initial EPDM gums, and the neat and filled crosslinked samples before and after aging are presented and explained. These methods, categorized in a chronologic order, are aimed to elucidate the structure at the molecular, macromolecular and microscopic scales, and to establish some important structure – property relationships. In each category, it has been tried to give brief but complete information about the technics and experimental conditions chosen for the material characterization.

2.4.1 Molecular scale

FTIR spectroscopy has been the principle method for characterization and quantification of chemical groups in neat samples. The consumption of these chemical groups as well as the formation of new compounds has been determined by this method. In order to confirm these results, complimentary experiments were performed by ¹³C and ¹H NMR spectrometry on some samples.

DSC has been used to measure the enthalpic variations during the peroxide curing of EPDM gums. These variations are due to exothermic or endothermic chemical reactions that take place during crosslinking. Such an analysis justifies the classification of DSC in the molecular scale category.

2.4.1.1 Fourier Transition Infrared Spectrophotometry

FTIR method, as the main tool to understand the modifications at molecular scale, has been used in three different modes. Conventional FTIR method consists in recording of a single spectrum in transmission mode per test run. Real-time FTIR method permits to visualize chemical groups modifications in real time thanks to the insertion of a local device in the measure chamber of the spectrophotometer. Imaging FTIR method consists in an edge-to-edge scanning of the sample cross-section. Each mode and related conditions are detailed in the following sections.

2.4.1.1.1 Conventional FTIR spectrophotometry

Among various spectrochemical characterization methods, FTIR spectrophotometry is a relatively simple analytical tool based on the detection of characteristic vibration modes of chemical bonds. It can thus be used to analyze and quantify the chemical functions present in the material, and their modifications during exposure time.

The concentration of each chemical function, which is directly proportional to the spectral absorption intensity, can be calculated by the common Beer-Lambert law:

$$OD = \epsilon l C \quad 2-1$$

where OD is the optical density (or absorbance), l is the thickness or the IR ray path length, i.e. the sample thickness (in cm), ϵ is the molar absorptivity or molar extinction coefficient (in $L \cdot mol^{-1} \cdot cm^{-1}$), and C is the concentration of the considered chemical species (in $mol \cdot L^{-1}$).

In general we are interested in concentrations:

$$C = OD / \epsilon l \quad 2-2$$

A *Perkin Elmer Frontier* FTIR spectrophotometer that functions in both transmission and attenuated total reflectance (ATR) mode in wavelength range of $400-4000 \text{ cm}^{-1}$ with a nominal resolution of 4 cm^{-1} , was used for analyzing the thin EPDM films of 50 and 100 μm thick deposited on KBr pellets (Figure 2-2).



2.4.1.1.2 *Figure 2-2 : Thin film samples deposited on KBr pellets*

The use of KBr pellets is justified by the fact that the surface of the samples becomes completely sticky after long durations of oxidative aging, which complicates the handling of the samples.

2.4.1.1.3 *Real-time FTIR spectrophotometry*

A specific device was inserted in the measure chamber of the FTIR spectrophotometer for monitoring the real-time evolution of chemical functions throughout the curing process. This device consists of a pair of KBr windows lodged in a heating cell, while the temperature is controlled by aid of a thermocouple (Figure 2-3). Once the device is set up, a sample film measuring about 100 μm thick is positioned between KBr windows and heated to the curing temperature at 170°C. A 16 scan spectra is obtained in transition mode every 30 seconds during the stay of sample at curing temperature. The test duration, which is 30 minutes, is chosen to be two times the conventional curing period to detect any possible changes.

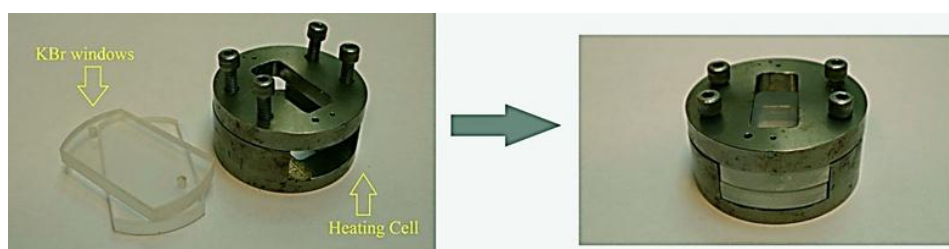


Figure 2-3: Real-time FTIR spectrophotometry device

2.4.1.1.4 *Imaging FTIR spectrophotometry (FTIR microscopy)*

This method has been used in the case of thick sample sheets in order to determine the oxidation profile products in the sample thickness or, in other words, the thickness of oxidized layer. The FTIR microscope employed for this analysis is a *Spectrum Spotlight 300 FTIR Microscope* which has the capability of taking FTIR spectra in a 15 x 15 μm^2 cell.

Once the sample is positioned at its emplacement, a magnified image of sample's cross-section taken by the microscope helps to determine the pathway of the infrared emitting probe along the sample's width (Figure 2-4). The probe then scans the cross-section along the pathway with a defined precision of 16 scans per spectrum and a determined constant step length of 20 μm .

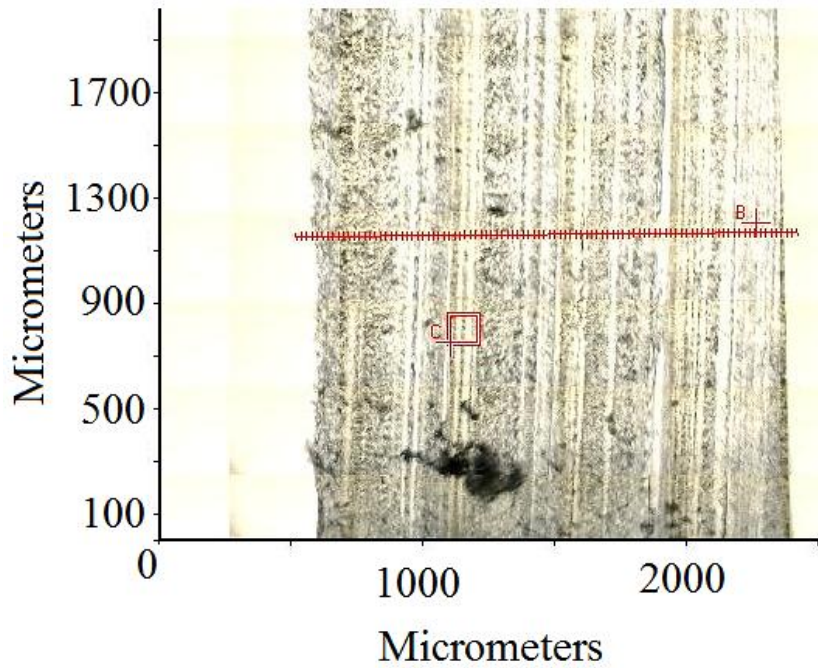


Figure 2-4: Magnified image of sample's cross-section - Definition of an FTIR scanning pathway

Sample preparation has been performed with a cryogenic microtome functioning at temperatures as low as -120°C thanks to liquid nitrogen injection (Figure 2-5).

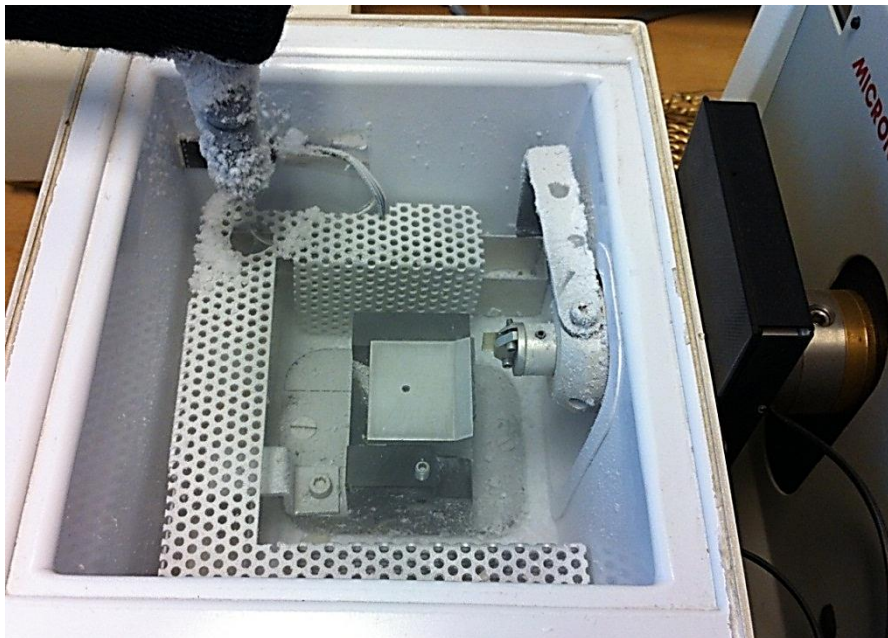


Figure 2-5: Cryogenic microtome

This apparatus lets us work at temperatures below samples' T_g , which facilitates the processing of sample slices. Thickness of samples is about $30\text{-}40\ \mu\text{m}$.

2.4.1.2 Nuclear magnetic resonance spectrometry

NMR tests have been carried out at the *National Center of Scientific Research (CNRS) Thiais-France*. ^1H NMR and ^{13}C NMR spectrometers have been used to determine the chemical composition of the elastomers before and after crosslinking. This method has helped, to some extent, to verify some modifications throughout aging as well.

Solid state NMR spectrometry has been performed with an *Avance III Bruker* spectrometer, using a 9.4 T magnetic field. This condition induces a precession frequency of 400.4 MHz for ^1H and 100.7 MHz for ^{13}C . In both cases, a 4.0 mm double resonance MAS probe has been used for spectra acquisition.

^1H spectra have been acquired at 343 K by applying simple pulse for a t_{90° ³ impulsion period of 2.7 microseconds with a repetition delay of 5 seconds. This latter time is higher than five times of the proton spin relaxation time in order to reassure the quantitative quality of obtained spectra. The angular velocity for these experiments was 8 or 10 kHz.

^{13}C NMR spectra have been registered by direct polarization at 303 K with a t_{90° of 4 microseconds, a repetition delay of 5 to 10 seconds and an angular velocity of 5 kHz. During the ^{13}C NMR spectra acquisition, a proton dipolar decoupling of 66 kHz has been applied.

2.4.1.3 Differential Scanning Calorimetry (DSC)

DSC technique is based on measuring the difference in heat flow of a sample with an inert reference during an imposed thermal change. Chemical reactions are endothermic or exothermic, inducing enthalpy variations in the thermal spectra.

A *TA Instruments Q1000* calorimeter was used for measuring the residual enthalpy of crosslinking and the T_g during a $10^\circ\text{C}\cdot\text{min}^{-1}$ ramp from -72°C to 235°C under nitrogen flow. Non-crosslinked EPDM samples containing dicumyl peroxide, weighing from 5 to 10 mg were placed in standard aluminum capsules and the test procedure was:

- i. Ramp from -72°C to 170°C at $10^\circ\text{C}\cdot\text{min}^{-1}$
- ii. Isotherm at 170°C up to 60 minutes
- iii. Rapid cooling down to -72°C
- iv. Ramp from -72°C to 235°C at $10^\circ\text{C}\cdot\text{min}^{-1}$

³ t_{90° is the time necessary for magnetization vector to rotate clockwise 90° about the axis of pulsed magnetic field.

This protocol let us to determine the consumption of DCP as a function of residence time at 170°C. The crosslinking enthalpy measured via this protocol is the sum of different contributions: initiation by dicumyl peroxide, coupling and disproportionation of macroradicals (cf. Section 3 chapter I). The final results are expressed as the enthalpy per one gram of DCP:

$$\Delta H_{crosslinking} = \frac{\Delta H_i}{[DCP]} \left(\frac{J \text{ or } cal}{g} \right)$$

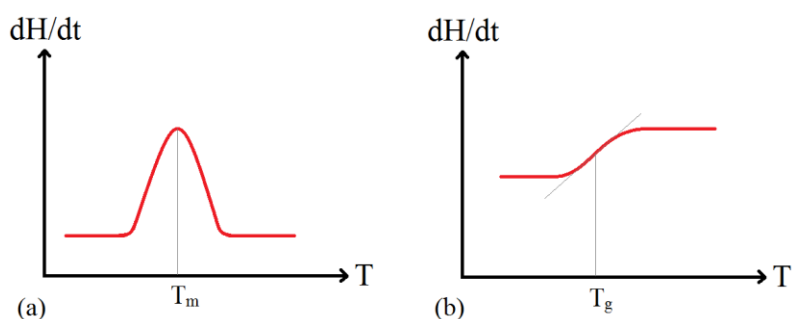
where ΔH_i is the enthalpy measured for samples and $[DCP]$ is the concentration of DCP in one gram of samples in grams.

DSC helps us, as well, to measure the hydroperoxide build-up through aging. The hydroperoxide groups that are formed along the polymer chains in both thermal and radiochemical aging decompose by under thermal stress. The exothermic peak of this chain scission has a maximum around 175°C. By measuring the enthalpy of this reaction in a temperature ramp up to 230°C, the concentration of hydroperoxide can be measured. The rate of heating used for this protocol was also 10°C.min⁻¹. Subsequently, the concentration of hydroperoxides can be calculated by following equation:

$$[POOH] = \frac{\Delta H_d}{\Delta H_t}$$

with ΔH_d the experimental enthalpy measured by DCS and ΔH_t the theoretical enthalpy calculated for decomposition of one mole of hydroperoxide. More explicit explanation for this method is provided in Chapter IV.

DSC is also used for macromolecular scale (which is more developed in following section) to determine the first and second order physicochemical phenomena, such as melting point and glass transition temperature (Scheme 2-3). These transition phenomena are visualized with enthalpy changes and are responsible for variations in thermal properties of polymer, such as heat capacity.



Scheme 2-3 : Schematized enthalpic diagrams of a) melting point T_m and b) T_g

Complementary to crosslinking protocol at molecular scale, the T_g was measured after each isotherm. The value of T_g demonstrates the crosslinking state of the matrix after each stay time at crosslinking temperature.

2.4.2 Macromolecular scale

Properties of a crosslinked elastomer, before and after aging, depend, to some extent, on initial properties of corresponding gum. The molecular weight (M_n , M_w) of raw gums are determined by high-temperature size exclusion chromatography, and are subsequently used to determine the concentration of dangling chains in the crosslinked network. Rheometry test, DSC (cf. previous section) and swelling test are employed to identify the structure of EPDM's tridimensional network, the concentration of elastically active chains ν and their mass M_c . The weight variations are followed by thermogravimetric analysis. The direct effect of modifications at macromolecular scale, i.e. crosslinking and chain scission is then visualized by mechanical tests.

2.4.2.1 Size Exclusion Chromatography (High-Temperature Gel permeation Chromatography)

Size (or steric) exclusion chromatography is used to determine the molecular weight of polymeric chains at their linear initial state. In this method the polymer is fractionated according to the size of solvate (rather than the true molecular weight). The empirical Mark-Houwink equation relates the intrinsic viscosity of a polymer to its molecular weight:

$$[\eta] = KM^a \quad 2-3$$

where $[\eta]$ is the intrinsic viscosity and K and a are the constants of a polymer-solvent couple at a specific temperature.

Grubisic et al. have shown that the product of $[\eta] \cdot M$ plotted as a function of elution volume for any polymer, independent of its chemical nature, is placed on a universal calibration curve [1]. This achievement is translated to Equation 2-4, for polymer 1 and polymer 2.

$$[\eta]_1 \cdot M_1 = [\eta]_2 \cdot M_2 \quad 2-4$$

Therefore, by combining Equations 2-3 and 2-4, we obtain:

$$K_1 M_1^{(a_1+1)} = K_2 M_2^{(a_2+1)} \quad 2-5$$

Equation 2-5 is used to calculate the molecular weights in GPC method. The results are expressed as "equivalent" molecular weights and would normally be presented in the form of weight and number

average molecular weight and polydispersity. The superposition of calculated molecular weight curves is used to emphasize the similarities or differences in the molecular weight distributions of the samples of interest.

HT-GPC measures the average molecular weight and its distribution for polymers which are not perfectly soluble in conventional solvents and temperatures. Polyethylene and its copolymers are usually included in this category.

In our case the samples are prepared by adding 15mL of eluent to 15 mg of EPDM and heating at 190°C for 20 minutes. The solutions were allowed to cool to 160°C and were then filtered through a 1.0 µm glass-fiber mesh. The solutions were filtered directly into auto-sampler vials and injection of samples was carried out automatically.

The instrument was an *Agilent PL GPC220* equipped with an *Agilent PLgel Olexis* guard column with a refractive index detector. The eluent is 1,2,4-trichlorobenzene with antioxidant. The nominal flow rate is 1.0 mL.min⁻¹ at 160°C and the data have been collected and analyzed using *Agilent cirrus* software. HT-GPC tests have been carried out at *Smithers-Rapra*, England.

A conventional GPC has been used as well for determination of relative molecular weight of soluble fraction for aged samples. The device is a *Water 717 plus auto-sampler*, accompanied with a *2998 photodiode* detector and a *Styragel column HR 4E*. The samples are prepared in THF at 25°C and are injected with a flow rate of 1.0 mL.min⁻¹. The columns are calibrated with polystyrene samples.

2.4.2.2 Swelling test

A linear polymer in appropriate solvent absorbs this latter and swells until the total separation of macromolecular chains and formation of a solution. A crosslinked polymer as well absorbs solvent and swells, but the chains cannot be dissociated due to covalent bonds between chains. In this case each elastically active chain will be extended until equilibrium establishment between solvent/polymer interaction forces and retracting forces of chains.

The swelling measurement of a crosslinked polymer in an organic solvent is an efficient method to determine the network structure. The swelling ability depends on the interactions between solvent molecules and polymer chains, and the chain length between crosslinks (or their concentration).

The swelling theory of Flory-Rehner [2-4] gives access to the concentration of elastically active chains:

$$\nu = \frac{V_{r0} + \chi * V_{r0}^2 + \ln(1 - V_{r0})}{V_s * \left(\frac{2V_{r0}}{f} - V_{r0}^{1/3} \right)} \quad [in \text{ mol. cm}^{-3}] \quad 2-6$$

with:

- V_{r0} : volume fraction of polymer in swelled gel
- V_s : molar volume of solvent
- χ : Huggins solvent-polymer interaction parameter
- f : functionality of crosslinks

This approach is based on a homogeneous network, where the result is an indicator of an average value of the crosslink density. The volume fraction of swollen gel in the network V_{r0} is related to the solvent absorption factor k [5]:

$$V_{r0} = \frac{1}{1 + \frac{(k-1)\rho_{pol}}{\rho_s}} \quad 2-7$$

where ρ_{pol} is the volumic mass of polymer and ρ_s the volumic mass of solvent. k is calculated by:

$$k = \frac{W_{sw}(\text{weight of swollen gel})}{W_{gel}(\text{weight of gel})} \quad 2-8$$

and the gel content is:

$$\%gel = \frac{W_{gel}(\text{weight of gel})}{W_{ini}(\text{initial weight})} \cdot 100 \quad 2-9$$

W_{gel} is the weight of gel (crosslinked elastomer) in the sample and W_{ini} is the initial weight of the sample.

The solvent - polymer interaction parameter is the sum of enthalpic and entropic components:

$$\chi = \chi_H + \chi_s \quad 2-10$$

χ_H is the enthalpic interaction factor which can be calculated by:

$$\chi_H = (V_s/RT)(\delta_{pol} - \delta_s)^2 \quad 2-11$$

with δ_{pol} and δ_s , the solubility factors of components polymer and solvent, respectively.

χ_s is a constant of about 0.35 ± 0.1 and, for a non-polar solvent, is normally equal to 0.34 [6, 7]. So, the accepted equation will be:

$$\chi \approx 0.34 + (V_s/RT)(\delta_{pol} - \delta_s)^2 \quad 2-12$$

To obtain a solution, the solubility parameters, which depend on the chemical structures of polymer and solvent, should be quasi-similar [8]. The discrepancy between the values of δ_{pol} and δ_s tends to decrease the dissolution.

The swelling test in this study has been carried out on 2mm plates of crosslinked EPDM. The samples were cut into 30-50 mg cubic pieces (W_{ini}) and then were swelled in cyclohexane for 72h at 25°C. The cubes were then removed from solvent, weighed in their swelled state (W_{sw}), and then put under vacuum at 40°C to evaporate the solvent. After 48h under vacuum, the samples were removed and weighed in their un-swollen state (W_{gel}).

2.4.2.3 Thermogravimetric Analysis

High temperature is an activator of chemical reactions, especially in presence of oxygen. During thermal oxidation, a polymer can gain on weight by grafting oxygen molecules and, at the same time, lose weight by losing volatile products. Thermogravimetric analysis is a simple method to access these weight variations.

Samples are weighed manually at precise intervals over a defined period on a common laboratory microbalance. The Thermogravimetry test has been performed on thin film samples under thermal aging that were used for FTIR spectrophotometry analysis. This approach helps to correlate the samples' weight changes with chemical modifications at molecular scale.

Variations of samples weight can also be continuously measured on the plateau of a microbalance installed in a sealed chamber with a controlled atmosphere (e.g. nitrogen) and connected to a computer. The TGA machine used for this second is a *TGA Q500* from *TA Instruments* having the possibility of integral mass flow control and gas switching. The sealed chamber provides the test possibility under controlled atmosphere while the heating furnace can heat the sample up to 1000°C. The tests are performed in a high resolution dynamic mode.

2.4.2.4 Rheometry

Rheometry is performed to study the changes in viscoelastic properties during the crosslinking of EPDM/DCP blends. The used device is an *ARES* from *Rheometrics Scientific*. The test is conducted with parallel plate geometry of 25 mm diameter at 170°C, in nitrogen, with an intra-plates gap of (1.1 ± 0.1 mm). With temperature rise, three-dimensional network is formed and the value of the storage modulus G' increases while the loss modulus G'' decreases. At the end of crosslinking the G' curve reaches a constant value on a plateau and this final modulus is considered as a physical characteristic of the network structure.

For a temperature well above T_g (e.g. $T_g + 50^\circ\text{C}$), the shear modulus at small deformations is related to average molecular mass of elastically active chains by the Flory's equation [2, 9]:

$$G' = \frac{\rho RT}{M_c} \text{ (in Pa)} \quad 2-13$$

with:

- ρ : density ($\text{kg}\cdot\text{m}^{-3}$)
- T : temperature (K)
- M_c : mass of elastically active chain ($\text{g}\cdot\text{mol}^{-1}$)
- R : universal gas constant ($8.314 \text{ J}\cdot\text{K}^{-1}\cdot\text{mol}^{-1}$)

The Equation 2-13 can be rewritten as a function of the elastically active chains concentration (v):

$$G' = v\rho RT \quad 2-14$$

Therefore, v can be calculated from final value of G' on the plateau.

2.4.3 Macroscopic scale – Tensile testing

Tensile testing is the conventional method to measure the mechanical properties of materials such as the Young modulus E' and the elongation at break ϵ_r . The determination of this latter is of quite importance because it represents the industrial endlife criterion. Tensile test can show how the network structure and, consequently, the mechanical properties evolve throughout aging.

In this study, tensile testing is performed with an *Instron 4301* machine using pneumatic grips attached to a *2525 series* drop-through statistic load cell supporting up to 100 kN (Figure 2-6). Dumbbell shaped samples were cut to the following dimensions (Figure 2-7):

- Length: 40 mm
- Width: 4mm
- Length of grip section: 10mm
- Thickness: 2-3 mm
- Gage length: 20 mm



Figure 2-6: Tensile machine

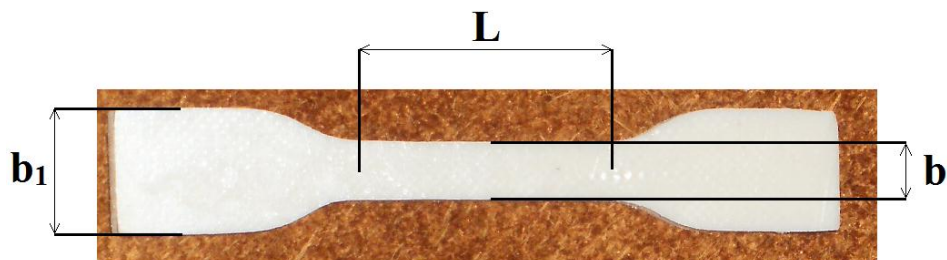


Figure 2-7 : Dumbbell shaped specimen used for tensile testing. L : Gage length (20mm), b : width (4mm), b_1 : length of grip section (10mm)

Tests have been carried out in standard room conditions, i.e. at temperature equal to 20°C and relative humidity of 50%. For each aging condition and each EPDM formulation, 10 specimens have been considered among which 6-8 present low flaws, to assure the exactitude of measurements. Furthermore, some samples happened to break outside of the gage length, for which the results are not taken into consideration (Figure 2-8).

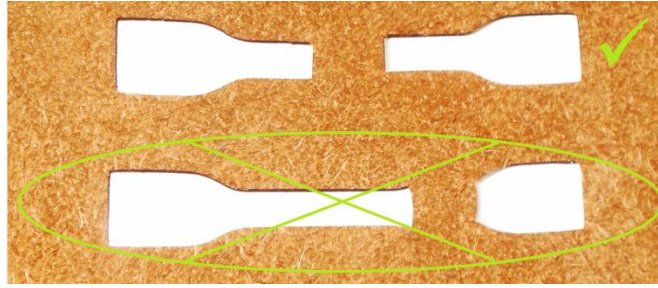


Figure 2-8 : Demonstration of samples eligibility

The deformation rate was preliminary determined by scanning a large range of deformation rates between 0.25 and 12.5 s^{-1} , and a deformation rate equal to $50 \text{ mm}\cdot\text{min}^{-1}$ has been chosen (see chapter III). This deformation rate is also equal to the one used at EDF for tensile testing on elastomers.

References

1. Grubisic, Z., P. Rempp, and H. Benoit, *A universal calibration for gel permeation chromatography*. Journal of Polymer Science Part B: Polymer Physics, 2003. **34**(10): p. 1707-1713.
2. Flory, P.J., *Principles of polymer chemistry*. 1953: Cornell University.
3. Flory, P.J., *Thermodynamics relations for high elastic materials*. Transaction of Faraday Society, 1961. **57**: p. 829-838.
4. Flory, P.J., *The elastic free energy of dilatation of a network*. Macromolecules, 1979. **12**(1): p. 119-122.
5. Celina, M. and G.A. George, *Characterisation and degradation studies of peroxide and silane crosslinked polyethylene*. Polymer Degradation and Stability, 1995. **48**(2): p. 297-312.
6. Blanks, R.F. and J.M. Prausnitz, *Thermodynamics of polymer solubility in polar and non-polar systems*. Industrial and Engineering Chemistry Fundamentals, 1964. **3**(1): p. 1-8.
7. Scott, R.L. and M. Magat, *Thermodynamics of high-polymer solutions. Swelling of cross-linked rubber*. Polymer Science, 1949. **4**(5): p. 555-571.
8. Miller-Chou, B.A. and J.L. Koenig, *A review of polymer dissolution*. Progress in Polymer Science, 2003. **28**(8): p. 1223-1270.
9. Verdu, J. and X. Colin, *Structures macromoléculaires tridimensionnelles*. 1993: Ed. Techniques Ingénieur.

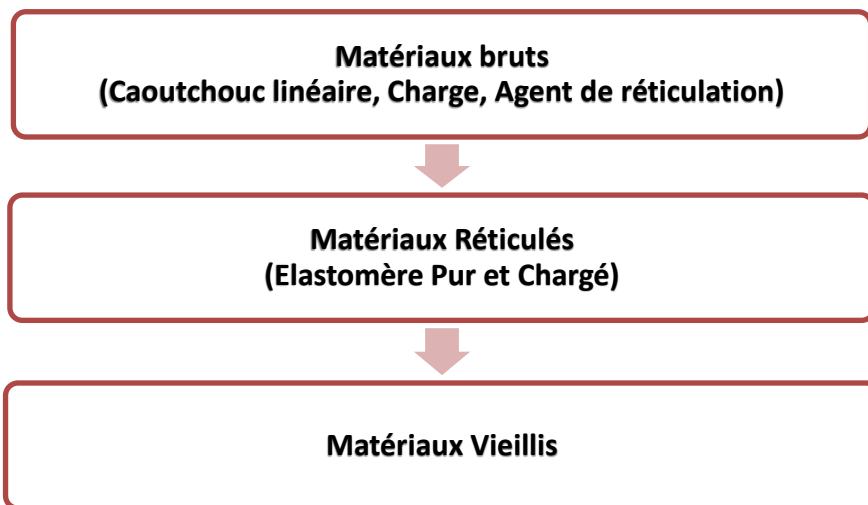
CHAPTER III

3 Initial Characterization

Extended abstract (in French language)

Les matrices EPDM de cette étude sont destinées à être utilisées en tant que matériaux isolants dans les câbles électriques de faible à moyenne tension dans les centrales nucléaires. Les principaux ingrédients des formulations industrielles, en plus du caoutchouc, sont les agents de réticulation, les charges et les antioxydants. Dans cette étude, une attention particulière est portée aux effets de la réticulation et des charges.

Les matrices sont d'abord réticulées, puis vieilles, ce qui implique la présence de trois états structuraux distincts:



Dans ce chapitre, les deux premiers états sont étudiés. Dans une première étape, les caractéristiques initiales des principaux ingrédients, i.e. l'EPDM linéaire, les particules de charges ATH avec et sans traitement de surface et l'agent de réticulation, sont déterminées. Dans une seconde étape, le mécanisme et la cinétique de réticulation de l'EPDM linéaire par le peroxyde sont étudiés. La dernière partie est consacrée à la détermination de l'effet des charges ATH sur la cinétique de réticulation d'EPDM linéaire, et la structure macromoléculaire de la matrice EPDM. L'étude de vieillissement thermique et radiochimique sera développée dans les deux chapitres suivants.

Les résultats obtenus dans ce chapitre détaillent le mécanisme et la cinétique de réticulation, ainsi que la structure du réseau obtenue. Premièrement, la réticulation de l'EPDM par le peroxyde a été étudiée par différentes méthodes caractéristiques, à différentes échelles structurales. Un schéma mécanistique de réticulation a été proposé. Il repose sur deux approches différentes à l'échelle moléculaire: par spectrophotométrie IRTF et calorimétrie différentielle à balayage (DSC). Les résultats obtenus par ces deux méthodes sont, de manière convaincante, très proches. Succédant à ce mécanisme de réticulation, un schéma cinétique a été dérivé et le système d'équations différentielles correspondant a été résolu numériquement. Les résultats de la simulation numérique, basés sur des données de la littérature, sont

en bon accord avec les résultats expérimentaux. A titre d'exemple, la courbe cinétique de consommation des doubles liaisons ENB a été tracée sur la Figure I.

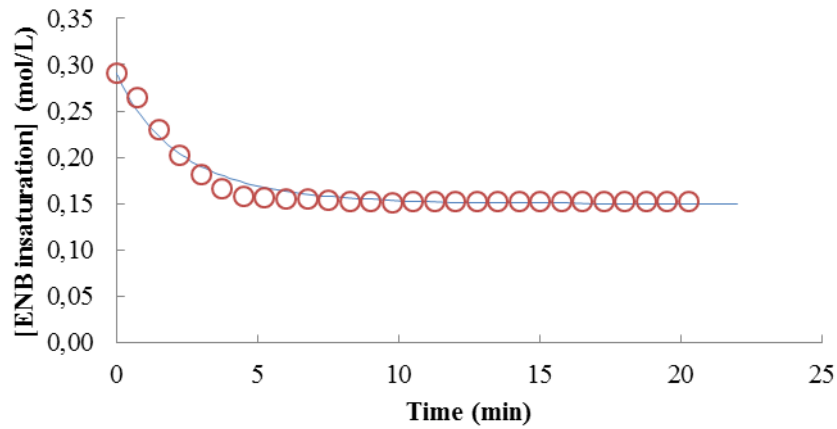


Figure 1 : Consommation des doubles liaisons ENB pendant la réticulation à 170°C avec 3 phr de DCP. Les ronds représentent les résultats expérimentaux et la ligne continue représente les résultats du modèle cinétique

Afin de déterminer la structure du réseau EPDM réticulé, les densités de réticulation des trois matrices EPDM de l'étude ont été mesurées au moyen de trois méthodes différentes à l'échelle macromoléculaire. Ces trois méthodes conduisent à des résultats très proches. En outre, la densité de réticulation calculée numériquement avec le modèle cinétique se place dans l'intervalle d'erreur de mesure des résultats expérimentaux.

L'effet des charges ATH dépend de la présence de molécules chimiquement actives sur leur surface. La charge vierge n'a pas d'effet sur le mécanisme de réticulation de la matrice EPDM. En revanche, dans le cas de la charge ATH traitée en surface, les molécules d'ensimage participent à la réaction de réticulation, conduisant à des densités de réticulation plus élevées.

L'effet de renforcement des charges ATH dans les composites ATH/EPDM n'a pas pu être modélisé par les théories empiriques conventionnelles. Un nouveau modèle qui est basé sur une interphase bi-phasique a été utilisé. Un schéma simple de cette interphase est montré sur la Figure II.

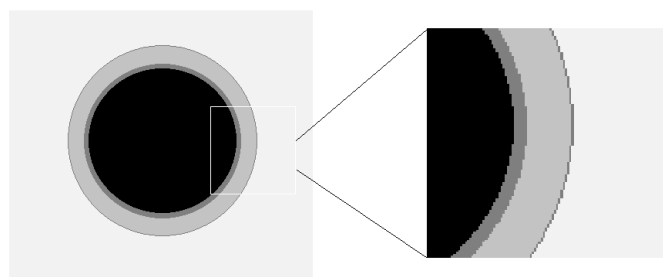


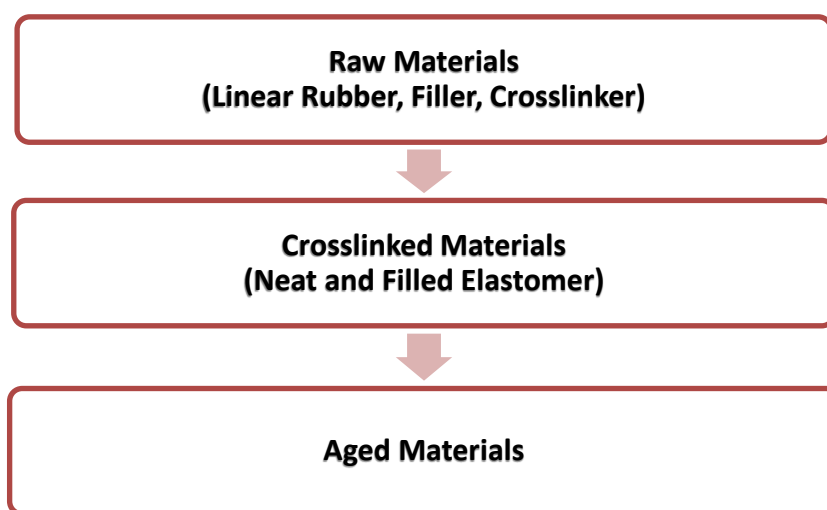
Figure II : Schématisation de l'interphase bi-phasique

Ce modèle a permis, en effet, de démontrer de façon satisfaisante la capacité de renforcement des particules de charge. Ce modèle sera plus détaillé dans les chapitres suivants lorsqu'il sera appliqué à l'étude du vieillissement des composites ATH/EPDM. Grâce à ce modèle, une nouvelle méthode est proposée pour calculer l'épaisseur et le module d'Young de l'interphase charge/matrice polymère.

Introduction

The EPDM matrices under study are intended to be used as insulation materials in low to medium voltage cables in nuclear power plants. The main ingredients of industrial formulations, in addition to rubber, are the crosslinking agent, fillers and antioxidants. In this study, a special stress is put on crosslinking and filler effects.

The EPDM matrices will be first crosslinked and then aged, which implies the presence of three distinct states:



In this chapter, the two first states are studied. Afterward, the two following chapters will be devoted to thermal and radiochemical aging of neat and filled EPDM matrices.

3.1 Characterization of raw materials

The raw elastomers are first to be mixed with peroxide and fillers, then crosslinked and subsequently, exposed to aging criteria. The characterization of raw materials is necessary to understand the mechanism and kinetics of crosslinking, and define as well the structural state of samples after curing and before aging. Indeed, the knowledge of this state provides an opening to the aging studies. In the case of filled materials, determination of fillers' initial state helps to better understand the filler matrix interactions. This section is dedicated to characterization of raw EPDM rubbers and ATH fillers.

3.1.1 Linear EPDM

The information available in technical data sheets are nominal values. The real values can change from one batch to another. Thus, in order to be more accurate in this study and avoid any unexplainable phenomenon, the physicochemical properties under interest have been verified through available laboratory techniques.

3.1.1.1 Determination of chemical structure by FTIR spectrophotometry

3.1.1.1.1 Generalities

Modifications in materials can be followed by measuring the changes in concentration of reactive groups during a chemical reaction. The initial concentrations of ethylene, propylene and ethylidene-norbornene are measured with infrared spectrophotometry, by applying the Beer-Lambert law.

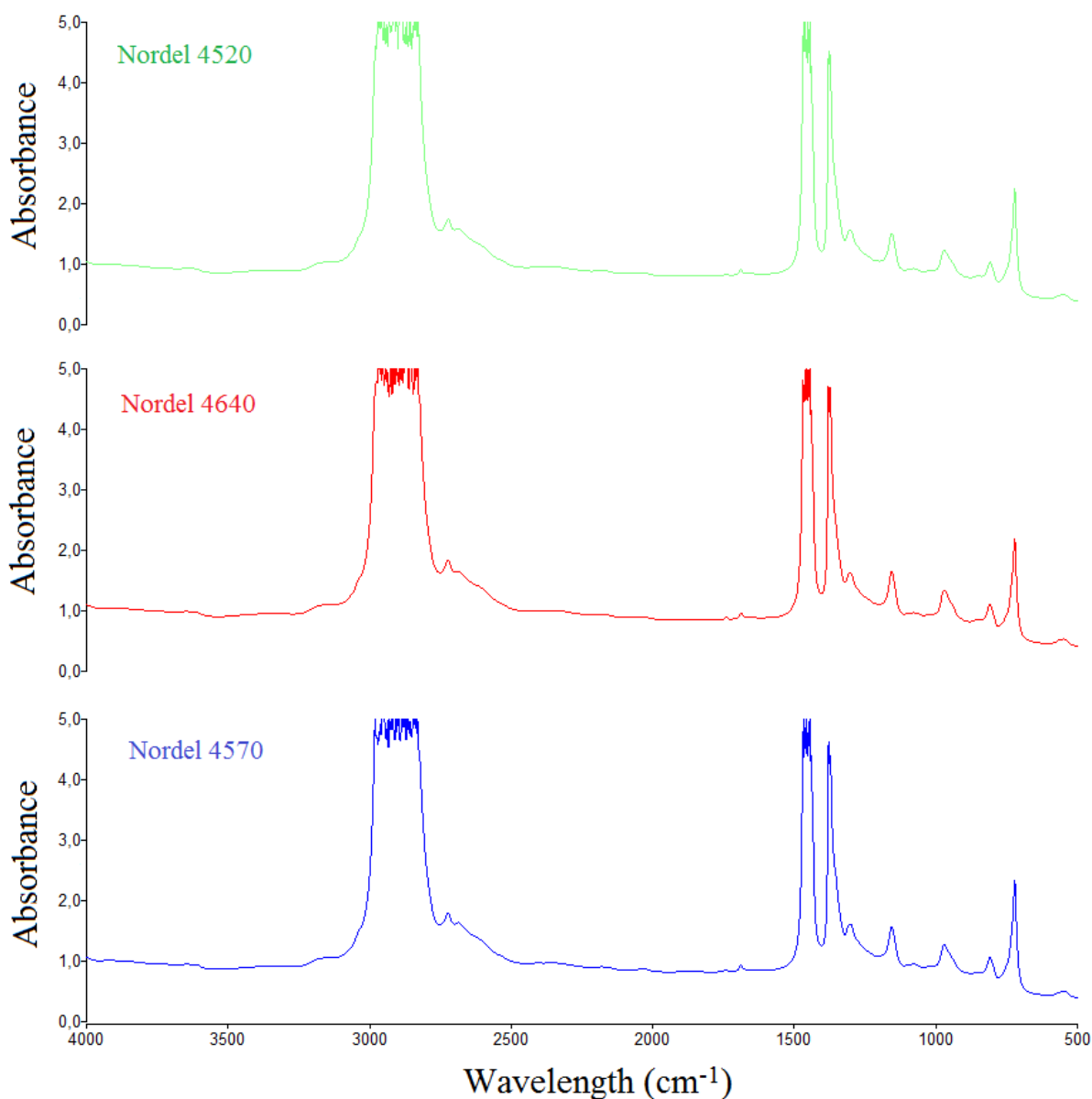


Figure 3-1 : Infrared spectra of approximately 100 μm thick films of three EPDM Nordels under study

The concentration of each monomer can be determined if the following information is available:

- I. Wavenumber at which the corresponding chemical group shows an absorption peak,
- II. Optic density (height) of the absorption peak regarding to an approved baseline,
- III. Molar extinction, or absorptivity, coefficient ϵ of the corresponding absorbing entity,
- IV. Pathlength of the IR beam in the sample.

The FTIR spectra of the three EPDMs under study are shown in Figure 3-1. The chemical structure and their monomer fractions in three Nordels are approximately the same, resulting in similarity of the three spectra.

Absorption Frequency (cm⁻¹)	Chemical species attribution
3000 – 2800	Symmetrical and asymmetrical stretching of C – H bonds of methyl and methylene groups, stretching of C – H groups [1]
2732	Combination of CH symmetric deformation and CH ₃ symmetric deformation of propylene [2]
1687	Stretching of ENB double bond [3]
1464 (saturated)	Symmetrical bending of CH ₃ [4], Scissoring of CH ₂ [1]
1377 (saturated)	Symmetric bending of CH ₃ [1]
1156	Methyl groups of propylene units [5]
971	Skeletal stretching of C – C [6]
809	CH adjacent to double bond of ENB units [5, 7]
722	CH ₂ sequences of ethylene units [5]

Table 3-1: Chemical species attribution of IR absorption bands of EPDM

A chemical compound can exhibit several IR absorption peaks for which the wavelengths and intensities depend on nature of chemical bonds, their vibration modes and their concentration. This means that the presence of a chemical bond can be recognized from the absorption wavenumber, and the concentration of each chemical bond can be quantified thanks to the peak intensity. The attributions of each absorbing wavenumber to the corresponding chemical bonds of an EPDM are presented in Table 3-1.

Subsequent to determination of IR characteristic peaks, the corresponding intensities can be measured under certain circumstances. In order to quantify the concentration of a given chemical bond in the sample, the absorbance should not exceed the saturation limits and, at the same time, the intensity should be strong enough to avoid the nuisances of the baseline ($0.1 < \text{Functional Absorbance} < 4$).

Considering these remarks, the characteristic peaks chosen to determine the concentration of three monomers of EPDM are (Figure 3-2):

- i. 722 cm^{-1} : CH_2 sequences of ethylene units
- ii. 809 cm^{-1} : CH adjacent to double bond of ENB units⁴
- iii. 1156 cm^{-1} : methyl groups of propylene units

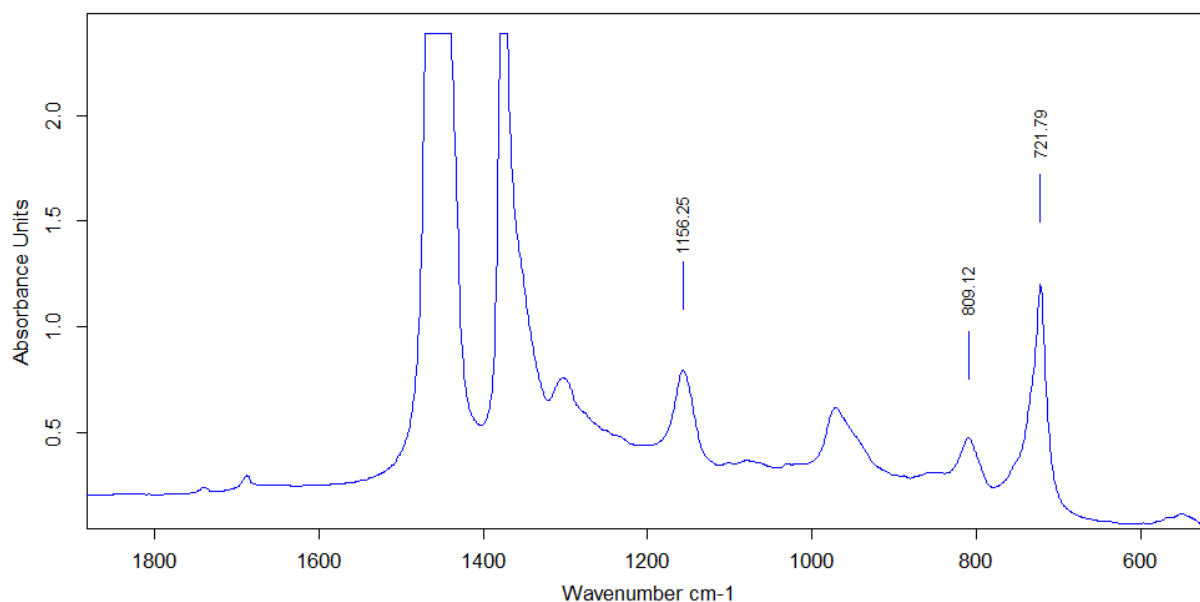


Figure 3-2: FTIR spectra of 100 μm thick film of EPDM Nordel IP 4520,

Despite the fact that the chemical bond attributions of the chosen characteristic peaks are correct at their individual state, in the case of EPDM, these peaks cannot be used directly because of the multiple absorptions of different monomers at similar wavenumber. For instance, methylene groups of propylene absorb at the same wavenumber as ENB C – H adjacent to double bond (809 cm^{-1}). ENB molecule, in its turn, absorbs at 722 cm^{-1} which overlaps with methylene groups of ethylene. It is clear that the use of raw optical density values for these peaks will lead to inaccurate estimations. Thus, a deconvolution of overlapping peaks seems necessary, to get to the concentration of chemical groups.

Deconvolution of overlapping peaks requires the knowledge of all corresponding molar absorption coefficients. Most of these coefficients are accessible in literature, but those who are not known must be determined by a standard calibration.

⁴ For the sake of facility, the term "CH adjacent to double" bond will be replaced by "double bond" for the peak absorbing at 809 cm^{-1} .

3.1.1.1.2 Standard calibration

Values of molar extinction coefficients of frequently sought groups, i.e. methyl groups of propylene, double bond of ENB and methylene group of ethylene, are regrouped in Table 3-2.

Chemical group	ϵ (L.mol ⁻¹ .cm ⁻¹)	Absorption (cm ⁻¹)
-CH ₃ (from propylene)	5 ^[5]	1156
-CH ₂ - (from ethylene)	2.6 ^[5]	722
-C=C- (from ENB)	17.5 ^[8]	809

Table 3-2: Molar extinction coefficient of EPDM chemical groups

ϵ of polypropylene's methylene group has been determined by standard calibration of the peak at 809 cm⁻¹ of an atactic polypropylene. Several PP films have been analyzed with FTIR spectrophotometry in transmission mode and the optical density at 809 cm⁻¹ has been measured. The concentration of methylene groups in PP equals 20.2 mol.L⁻¹, and the concentration measured with FTIR corresponds solely to amorphous part of the matrix. The thickness of films and the optical densities are known. Therefore the molar absorptivity can be calculated by application of the Beer-Lambert law (Figure 3-3).

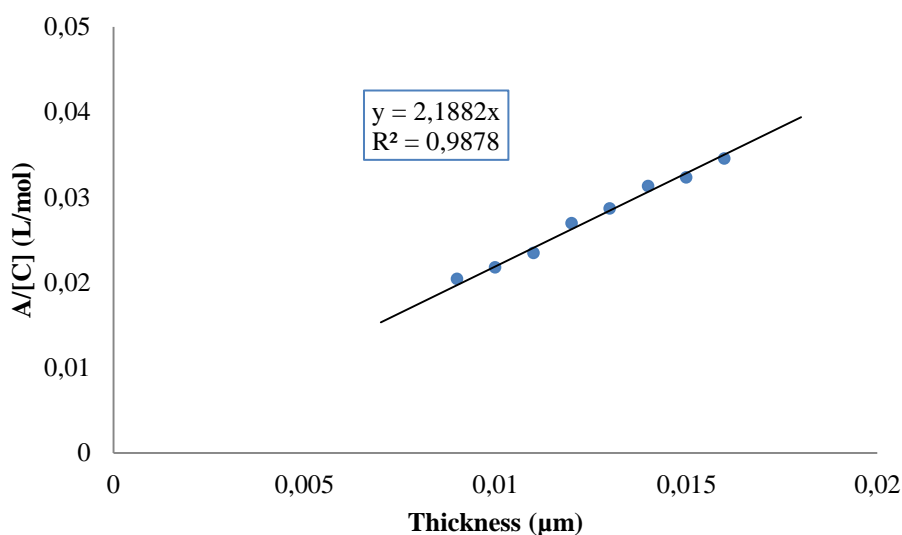


Figure 3-3: Determination of the molar extinction coefficient of methylene groups of polypropylene according to the Beer-Lambert law

The last unknown value to determine is the contribution of ENB to the peak absorbing at 722cm⁻¹, commonly attributed to methylene groups of ethylene units. For this purpose, the ratio of $[\epsilon(722\text{cm}^{-1}) /$

$\varepsilon(809\text{cm}^{-1})$] can be used to retrace the absorbance contribution of ENB and determine the absorbance of ethylene units. This ratio has been determined to be of the order of 1.5 using FTIR spectra of ENB.

3.1.1.1.3 Monomer percentage

For a better understanding of the employed method, hereby is presented a more expanded explanation of the method in a more explicit way. To begin, the absorbance of ENB at 809 cm^{-1} is calculated by retraceing the contribution of methylene groups of propylene units:

$$A_{(P\ 809\text{ at } cm^{-1})} = A_{(P\ 1156\text{ at } cm^{-1})} \cdot \frac{\varepsilon_{(P\ 809\text{ at } cm^{-1})}}{\varepsilon_{(P\ 1156\text{ at } cm^{-1})}} \quad 3-1$$

$$A_{(ENB\text{ at } 809\text{ cm}^{-1})} = A_{(809\text{ cm}^{-1})} - A_{(P\text{ at } 809\text{ cm}^{-1})} \quad 3-2$$

By the results of Equations 3-1 and 3-2, and using $[\varepsilon_{(ENB\text{ at } 722\text{ cm}^{-1})}/\varepsilon_{(ENB\text{ at } 809\text{ cm}^{-1})}]$ ratio, the absorbance of ENB and ethylene at 722 cm^{-1} will be:

$$A_{(ENB\ 722\text{ at } cm^{-1})} = A_{(ENB\text{ at } 809\text{ cm}^{-1})} \cdot \frac{\varepsilon_{(ENB\text{ at } 722\text{ cm}^{-1})}}{\varepsilon_{(ENB\text{ at } 809\text{ cm}^{-1})}} \quad 3-3$$

$$A_{(E\text{ at } 722\text{ cm}^{-1})} = A_{(722\text{ cm}^{-1})} - A_{(ENB\text{ at } 722\text{ cm}^{-1})} \quad 3-4$$

where P and E designate propylene and ethylene, correspondingly.

Now that every single absorbance is quantified, the concentration of each component will be determined with the Beer-Lambert equation and its ε :

$[Ethylene] = \frac{A_{(E\text{ at } 722\text{ cm}^{-1})}}{l \cdot (\varepsilon_{(CH_2\text{ at } 722\text{ cm}^{-1})} \cdot 2)}$	3-5
$[Propylene] = \frac{A_{(P\text{ at } 1156\text{ cm}^{-1})}}{l \cdot \varepsilon_{(P\text{ at } 1156\text{ cm}^{-1})}}$	3-6
$[ENB] = \frac{A_{(ENB\text{ at } 809\text{ cm}^{-1})}}{l \cdot \varepsilon_{(ENB\text{ at } 809\text{ cm}^{-1})}}$	3-7

Table 3-3 : Application of the Beer-Lambert law for concentration determination of the three monomers (l is the thickness of the sample)

Values of ε in Table 3-2 for ethylene monomers correspond, to methylene units ($-\text{CH}_2-$). Thus, to obtain the concentration of ethylene units, this value should be divided by 2. We recall that the elastomer is considered as practically amorphous, so no cristallinity is taken into account.

Once the concentration of each monomer is determined via FTIR spectrophotometry, the percentage of each component can be obtained by equations of Table 3-4. The resulting weight percentages then can be compared with those reported by Dow Chemicals in the technical data sheet.

EPDM	Molar%	Weight%
Ethylene	$\frac{[E]}{[E] + [P] + [ENB]}$	$\frac{[E] \cdot Mn_E}{[E] \cdot Mn_E + [P] \cdot Mn_P + [ENB] \cdot Mn_{ENB}}$
Propylene	$\frac{[P]}{[E] + [P] + [ENB]}$	$\frac{[P] \cdot Mn_P}{[E] \cdot Mn_E + [P] \cdot Mn_P + [ENB] \cdot Mn_{ENB}}$
ENB	$\frac{[ENB]}{[E] + [P] + [ENB]}$	$\frac{[ENB] \cdot Mn_{ENB}}{[E] \cdot Mn_E + [P] \cdot Mn_P + [ENB] \cdot Mn_{ENB}}$

Table 3-4 : Determination of molar and weight percentages of monomers in EPDM

The molar percentages are simply calculated by dividing the molar concentration of each monomer to the sum of molar concentrations of all monomers. Weight percentages are then obtained by multiplying the molar concentration by the molecular weight (Table 3-5) of each monomer.

Chemical group	M _n (g.mol ⁻¹)
Ethylene	28
Propylene	42
ENB	120

Table 3-5: Molecular weight of EPDM components

The EPDM samples used in this case have a thickness of 100-150 μm. They were obtained by hot pressing at 110°C for 30 seconds. Each FTIR spectrum is built up of 32 scans in a transmission mode. The monomers concentrations are given in Table 3-6. The corresponding molar and weight percentages are given in Table 3-7.

EPDM	Ethylene (mol.l ⁻¹)	Propylene (mol.l ⁻¹)	ENB (mol.l ⁻¹)
Nordel 4520	15.80	9.10	0.29
Nordel 4640	15.00	7.40	0.32
Nordel 4570	14.50	8.60	0.32

Table 3-6: Monomers concentration by FTIR for the three EPDM Nordels under study

EPDM	%molar			%weight		
	Ethylene	Propylene	ENB	Ethylene	Propylene	ENB
Nordel 4520	62.75	36.09	1.16	51.51	44.44	4.05
Nordel 4640	66.16	32.46	1.38	54.78	40.32	4.90
Nordel 4570	62.00	36.62	1.38	50.47	44.71	4.82

Table 3-7: Molar and weight percentages of monomers in the three EPDM Nordels under study

By comparing the monomers concentrations found through FTIR spectroscopy with those reported in technical data sheet (Chapter II. Section 1.1), a good agreement can be found.

3.1.1.2 Determination of molecular weight

3.1.1.2.1 Standard calibration

The molecular weight and its distribution are determinants of polymers' physical properties such as T_g , viscosity, etc. Consequently, the molecular weights of three EPDMs and their distribution are determined.

Measurements of molecular weights are carried out by using a high-temperature SEC (or GPC). The GPC system was calibrated by polystyrene (PS) standards and corrected by Mark-Houwink equations for polyethylene (the reason of this correction is the assumption that an EPDM with a high ethylene concentration in GPC testing is relatively close to a polyethylene). The calibration permits to draw the linear plot of $\log(M_w)$ as the function of elution time (or volume) and subsequently, interpolate the molecular weight of samples.

The Mark-Houwink (see Chapter II) parameters of polystyrene and polyethylene are presented in Table 3-8.

	Polystyrene (calibrants)	Polyethylene (sample)
a	0.707	0.725
$K \cdot 10^{-4}$	1.21	4.06

Table 3-8: Mark-Houwink parameters used for calculation of molecular weight

3.1.1.2.2 Molecular weight of raw EPDM

Standard calibration method has been applied to the three EPDMs and the results are summarized as the calculated average molecular weight and polydispersity index (M_w/M_n) in Table 3-9:

Nordel	M_w	M_n	Polydispersity
4520	114,000	46,100	2.5
4640	147,000	53,300	2.7
4570	187,000	85,400	2.2

Table 3-9: Weight and number average molecular weights and polydispersity index for the three EPDM Nordels under study

Triplicate runs were carried out for each sample solution but results have only been reported for the duplicate runs giving best graphical agreement with respect to the computed molecular weight distributions.

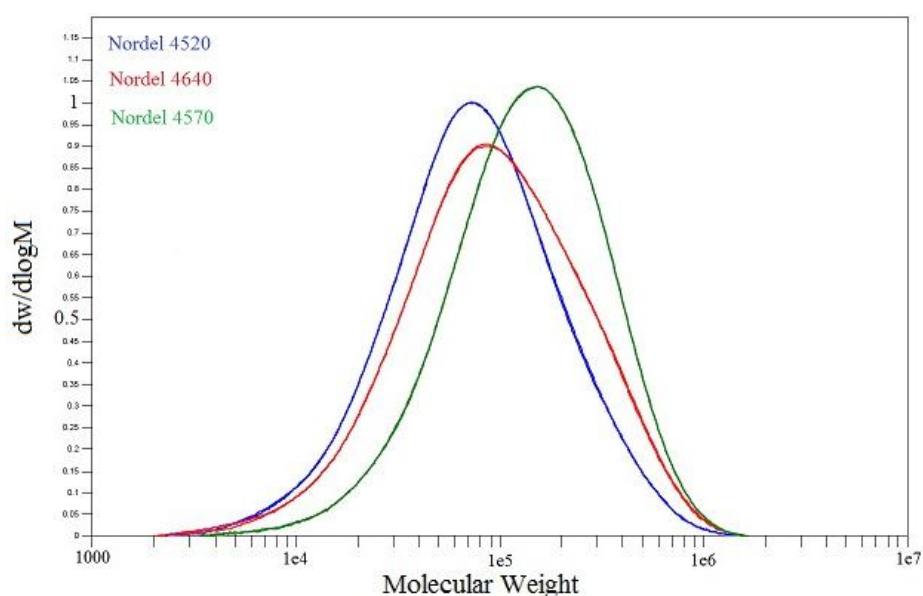


Figure 3-4: Molecular weight distribution (two runs per sample presented)

Figure 3-4 shows an overlay of the computed molecular weight distributions for the duplicate runs of the three samples, which are perfectly superposed. The plots are all normalized with respect to area, the y-axis being a function of weight fraction. All plots are to the same scales.

3.1.1.2.3 Molecular weight after mixing

The processing of EPDM matrices by an industrial mixer exert high shear stresses and, at processing temperatures up to 150°C, can induce mechano-scission and therefore modify the molecular weight of the polymers. In order to examine these effects, the mixing protocols (cf. Chapter II) of filled and unfilled samples have been applied to three EPDMs and then they were analyzed by HT-GPC. No filler or peroxide was added to the matrices. Samples mixed according to unfilled protocol have the suffix P-I and filled protocol the suffix P-II.

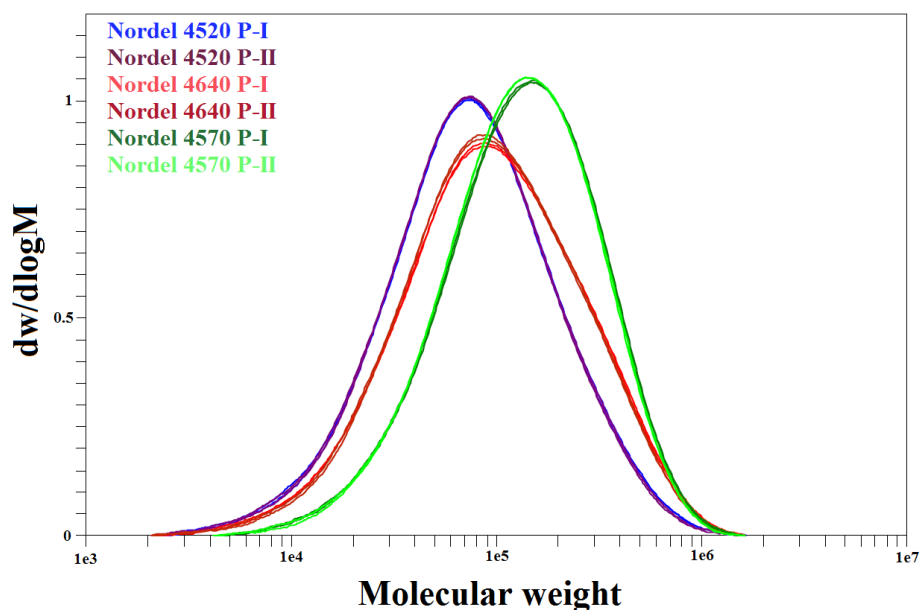


Figure 3-5 : Molecular weight distribution of processed EPDMs (two runs per sample presented)

The molecular weight distributions of processed EPDMs are shown in Figure 3-5. All the process and calculations for mixed samples are the same as unmixed ones. In protocol-I, samples are mixed for 10 minutes at 140°C and 2 minutes at 110°C while in protocol-II the samples are mixed, in addition to two previous steps, for 5 minutes at 150°C.

EPDM	M_w	M_n	Polydispersity
4520	114,000	46,100	2.4
4640	150,000	55,100	2.7
4570	183,000	85,400	2.2

Table 3-10 : Weight and number average molecular weights and polydispersity index for the three EPDM Nordels under study after mixing – unfilled protocol (P-I)

Table 3-10 contains the results of molecular weight measurements after P-I mixing. The comparison between the values of molecular weights and polydispersity indices shows that this protocol induces no mechano-scissions. Based on these results, we can claim that P-I processed samples possess identical molecular size as initial EPDMs.

EPDM	M_w	M_n	Polydispersity
4520	113,000	46,100	2.4
4640	146,000	55,400	2.6
4570	180,000	85,300	2.1

Table 3-11 : Weight and number average molecular weights and polydispersity index for the three EPDM Nordels under study after mixing – filled protocol (P-II)

The results of applying the second protocol on EPDMs, presented in Table 3-11, confirms that the protocol P-II, similarly to P-I, does not cause considerable modifications in molecular weight. The slight difference in M_w values of Nordel 4570, which has the highest M_w among two others, can be attributed to the sporadic mechano-scission of long chains. Anyhow, these slight changes are negligible even without considering instrumental errors.

3.1.2 Fillers

3.1.2.1 Surface treatment measurement by elemental analysis

Elemental analysis on Apyral 40 Vs1 (TATH), performed at *Elemental Analysis Service of CNRS France*, revealed 0.12 – 0.14 wt.-% of silicon grafted to hexagonal ATH particles (Figure 3-6). We know that one vinyl group is attached to one silicon group, which means by measuring the concentration of silicon atoms on the surface of filler particles, the concentration of available double bonds can be determined.

In order to facilitate the calculations, filler particles are assimilated to spheres for which the density and specific surface are $2.4 \text{ g}\cdot\text{mm}^{-3}$ and $3.5 \text{ m}^2\cdot\text{g}^{-1}$, respectively. By these data, the average values of geometric properties of a filler particle are (Table 3-12):

Volume (nm^3)	Specific surface (nm^2)	Mass (g)
1.1×10^9	9.8×10^6	2.8×10^{-12}

Table 3-12 : Average physical characteristics of a filler particle

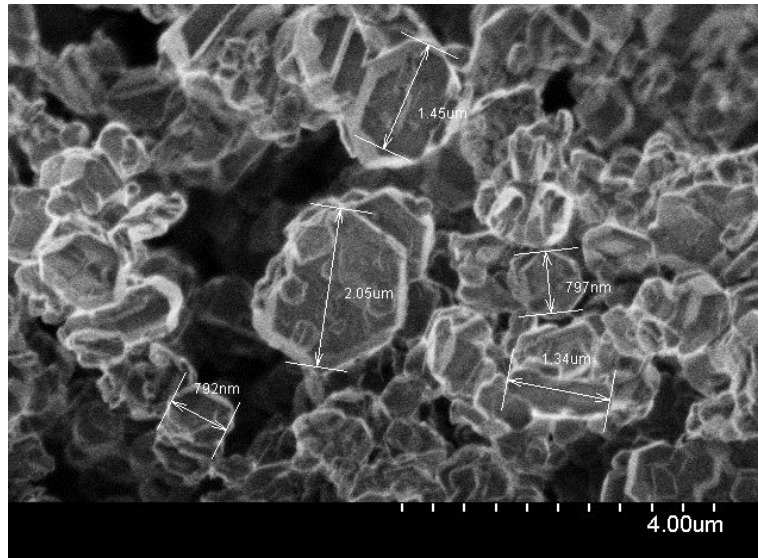


Figure 3-6 : SEM image of TATH particles

An average value of 0.13 wt.-% of silicon was used to calculate the number of surface treatment molecules (ST) per filler particle (molecular weight of Si = 28.1 g.mol⁻¹). Having the specific surface area of particle (Table 3-12), the concentration of ST can be determined (Table 3-13).

Mole of Si (or ST) per gram of ATH	4.6×10^{-5}
Mole of Si (or ST) per particle	1.3×10^{-16}
Number of Si (or ST) per particle ($N_A=6.022 \times 10^{23} \text{ mol}^{-1}$)	7.7×10^7
Number of Si (or ST) per (nm ²)	7.9

Table 3-13 : Experimental ST concentration on TATH particles surface

ST molecules occupy a defined volume in which other molecules cannot penetrate. This volume is better known as Van der Waals (VDW) volume and can be determined for any individual group of atoms. In a first approach, by assuming that a first layer covers thoroughly a particle's surface and then the second layer is formed, according to Figure 3-7 and the structure of R, the ST molecule is considered as a cylinder. The radius of this cylinder is dependent of the volumes occupied by one silicon atom and one oxygen atom (each oxygen atom is shared out between two silicon atoms).

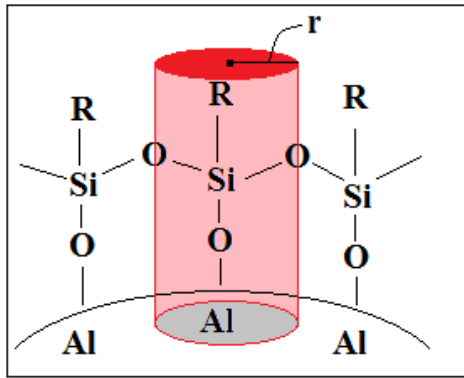


Figure 3-7 : Representation of the volume occupied by a ST molecule

The VDW volume of silicon and oxygen are given in table (Table 3-14). Considering these remarks, the VDW volume of a ST and its projected surface area on filler surface are calculated in the same table. The projected surface is then used to define the theoretical maximum number of ST per unit of filler surface.

Oxygen VDW volume ($\text{cm}^3 \cdot \text{mol}^{-1}$)	5 ^[9]
Silicon VDW volume ($\text{cm}^3 \cdot \text{mol}^{-1}$)	16.6 ^[9]
Cylinder effective volume (nm^3 per ST)	0.036
Projected surface area (nm^2 per ST)	0.13
ST molecules possible per nm^2	7.7

Table 3-14 : Theoretical ST concentration on the surface of TATH particles

From Table 3-13 we experimentally know that 7.9 ST per nm^2 exist, and from theoretical calculation, we know that maximum number of 7.7 ST molecules can be branched to nm^2 of particle surface, if only the ST is mono-layered. This shows that slightly more than one layer of ST may exist per filler particle, which is equal to:

- ✓ 7.6×10^7 ST molecules per particle
- ✓ Or 1.26×10^{-16} moles of ST per particle
- ✓ Or 4.51×10^{-5} moles of ST per gram of ATH.

The results above give an indication on the average concentration of surface treatment molecules per mass unit of filler, but it provides no information about the dispersion pattern or number of layers per particle and thus, they should be taken with caution.

3.1.2.2 Thermal response of fillers

The fire retardancy of aluminum trihydrate is due to the endothermic decomposition of filler particles once exposed to high temperatures. This endothermic decomposition helps the fire retardancy in two ways:

- i. Absorption and dissipation of the heat released by polymer combustion.
- ii. Formation and release of water molecules, which in addition to heat absorption create a barrier against oxygen diffusion.

The overall mechanism of ATH decomposition is as follows:

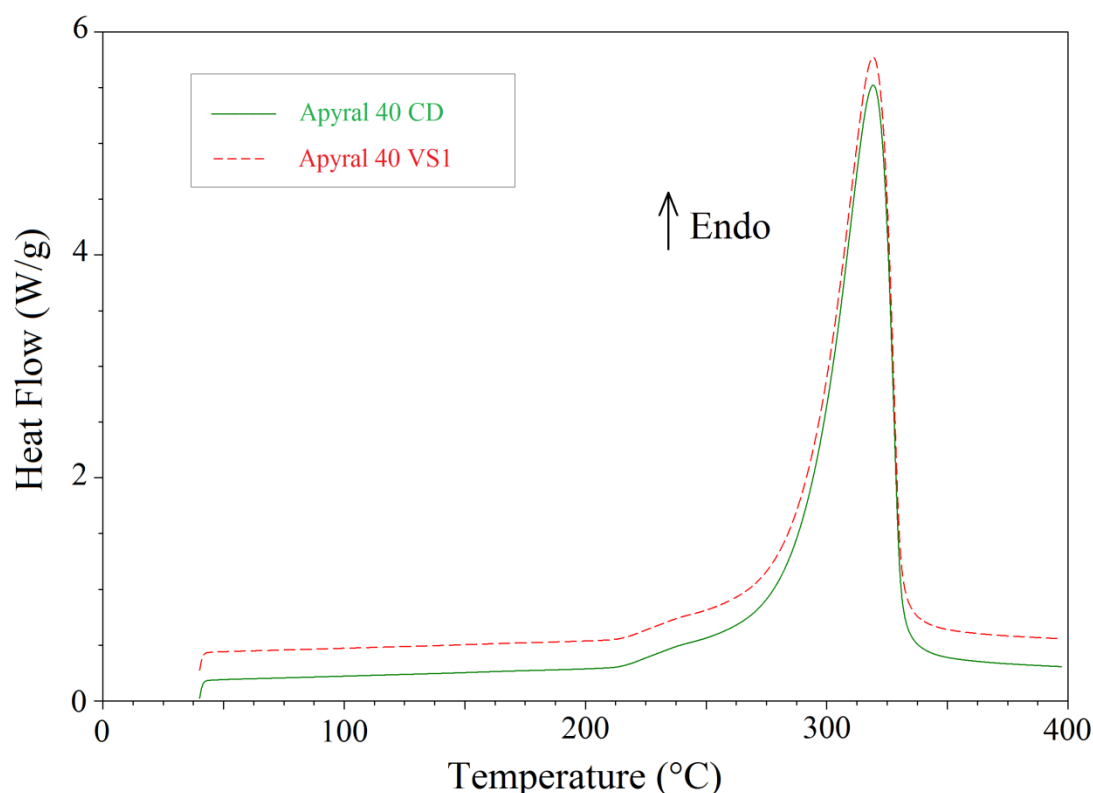


Figure 3-8 : DSC thermograms of PATH (40 CD) and TATH (40 VS1) ($10^{\circ}C.min^{-1}$, in N_2)

Samples of fillers with and without surface treatment have been exposed to a heat ramp from ambient up to $400^{\circ}C$ in inert atmosphere. The DSC curve of fillers thermal decomposition shows two endotherms. The first change in the spectra happens around $220^{\circ}C$ which is attributed to evaporation of free water molecules attached at filler particles surface. The second change happening around $310^{\circ}C$ is the endothermic decomposition peak of $Al(OH)_3$ molecules. The decomposition heat measured by calculating the under peak area, is about $1.1 kJ.g^{-1}$.

3.1.2.3 Gravimetric response of fillers to the heating

Decomposition of aluminum trihydrate frees water molecules, leaving the molecules of aluminum oxide as residual product (cf. Equation 3-8). Molecular weight calculations of ATH total decomposition, according to decomposition mechanism, leads to the remaining of 65.4% of initial weight, which corresponds to residual of Al_2O_3 .

Samples of the both fillers have been decomposed thermally at $5^\circ\text{C}/\text{min}$ under nitrogen in high resolution dynamic mode of TGA and the weight changes have been recorded. The tests are continued up to 800°C in order to attain total decomposition of ATH particles. As it is demonstrated in Figure 3-9, the weight loss of both pristine and treated fillers are identical and reach 65% of their initial values, which is very close to the theoretical weight loss. In addition, no variation related to the departure of ST molecules is observed.

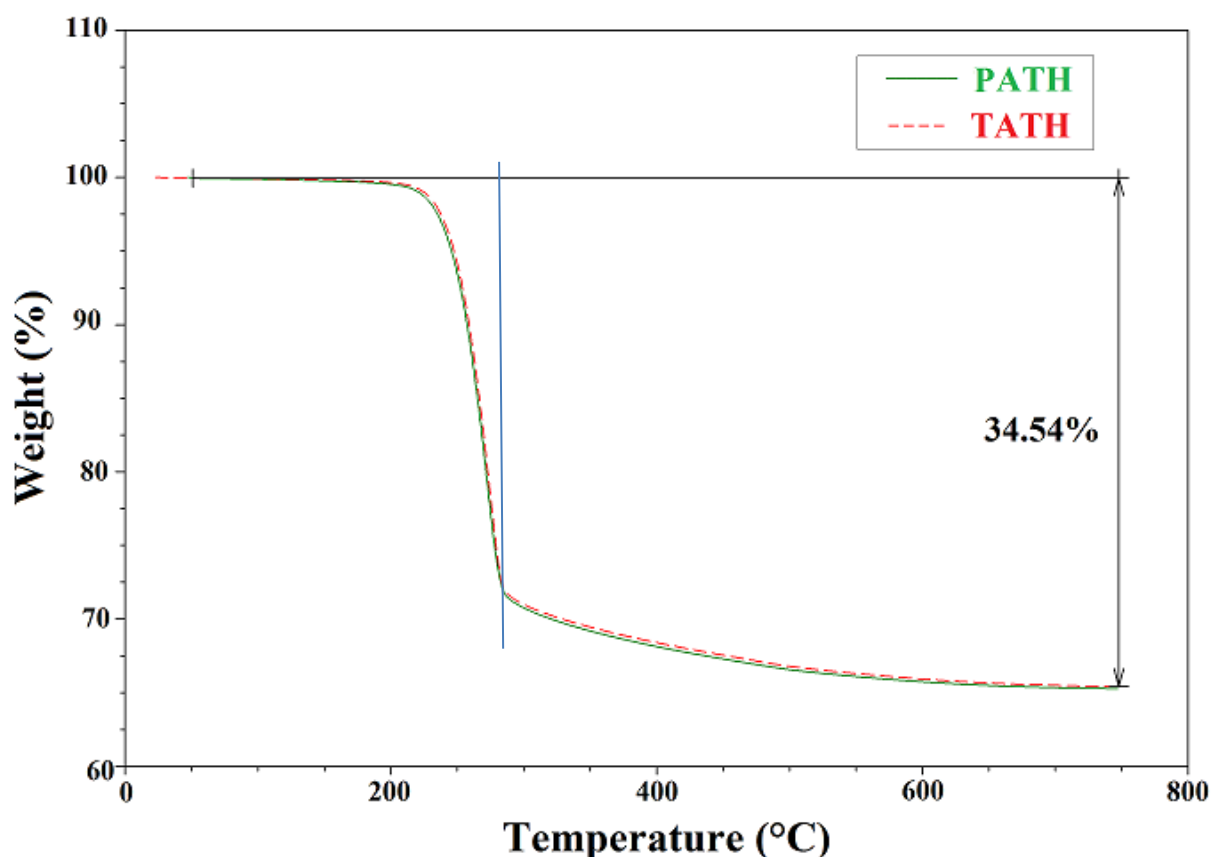


Figure 3-9 : TGA thermograms of PATH and TATH fillers ($5^\circ\text{C}\cdot\text{min}^{-1}$, N_2)

Although by quantification of weight changes between initial and final state of test, a convincing correlation is found between theoretical and experimental results. It is obvious from Figure 3-9 that two distinct regimes of mass loss coexist in this reaction. The first regime begins at around 200°C and falls steeply up to 287°C . The second regime becomes clearer after 287°C , where the slope of mass

loss changes radically. These variations are related to the mechanism of ATH dehydration. In fact, the ATH molecules are thermally converted to aluminum oxide hydroxide (AlO(OH) or boehmite), which is manifested by first-order temperature derivative peak in Figure 3-10. The boehmite molecules are then dehydrated, giving aluminum oxide molecules [10]:



The transformation of gibbsite to boehmite theoretically represents 23 wt.-% of total mass loss, leaving 11.5 wt.-% for the second regime. However, the experimental result shows a value equal to 29.0 wt.-% for the first regime and 5.7 wt.-% for the second. Therefore, it can be concluded that both steps of dehydration are not totally separated (the further discussion of this phenomenon is out of interest of this study).

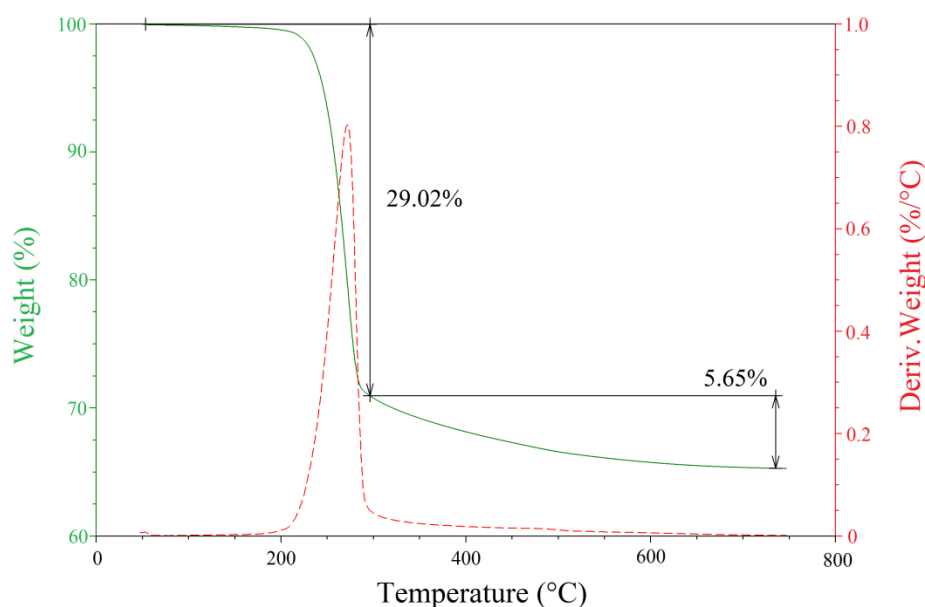
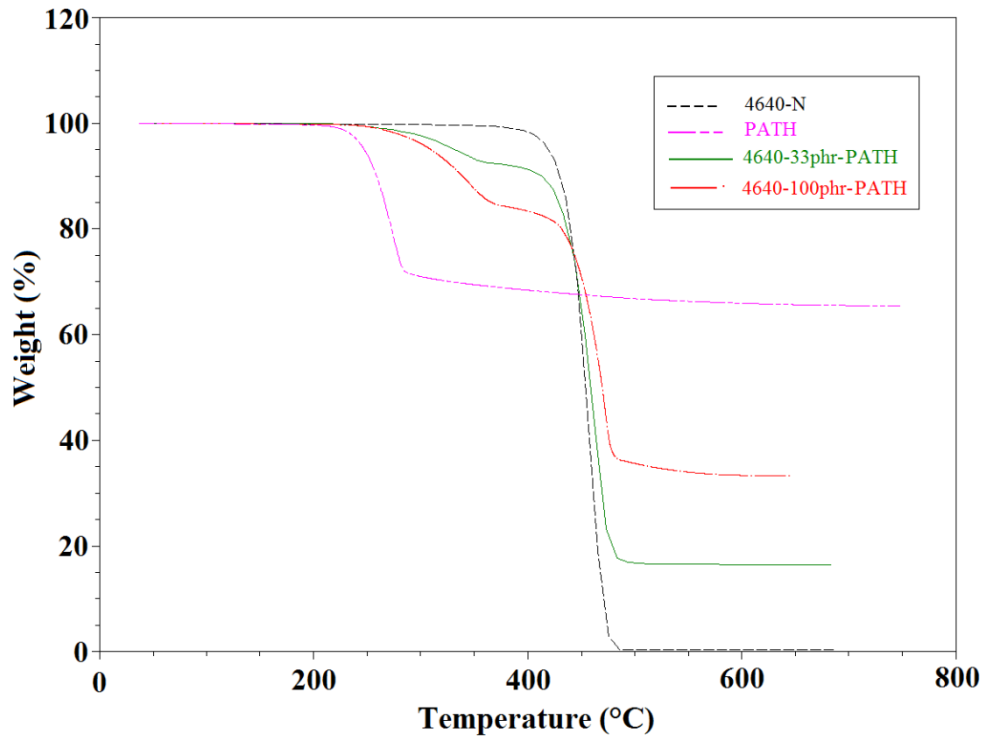
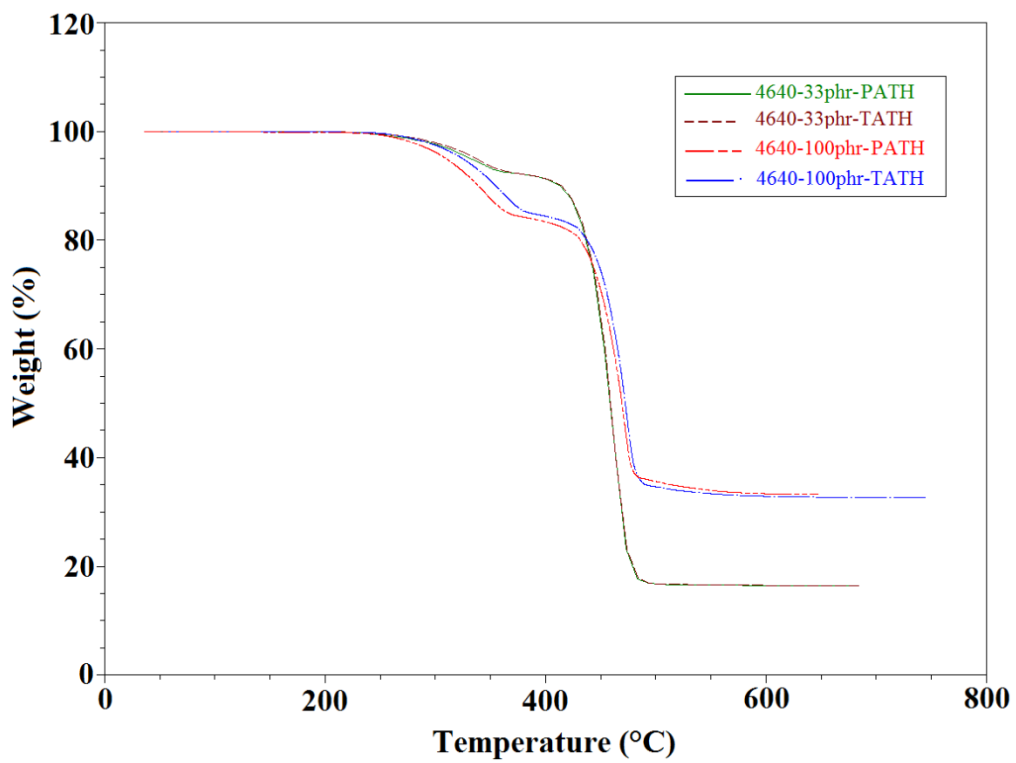


Figure 3-10 : Second derivative TGA thermogram PATH

The thermogravimetric analysis results of filler thermal decomposition are subsequently used to verify the filler content in filled samples. The filler content in each filled sample can as well be verified by this method. The thermolysis of EPDM begins at 400°C (Figure 3-11a), which is distinctively higher than ATH thermal decomposition (220°C). Figure 3-11b confirms that no significant difference is detectable between pristine and treated fillers.



a)



b)

Figure 3-11 : TGA thermograms of different materials under study. a) All materials
 b) filled EPDM samples only ($5^{\circ}\text{C}\cdot\text{s}^{-1}$, N_2)

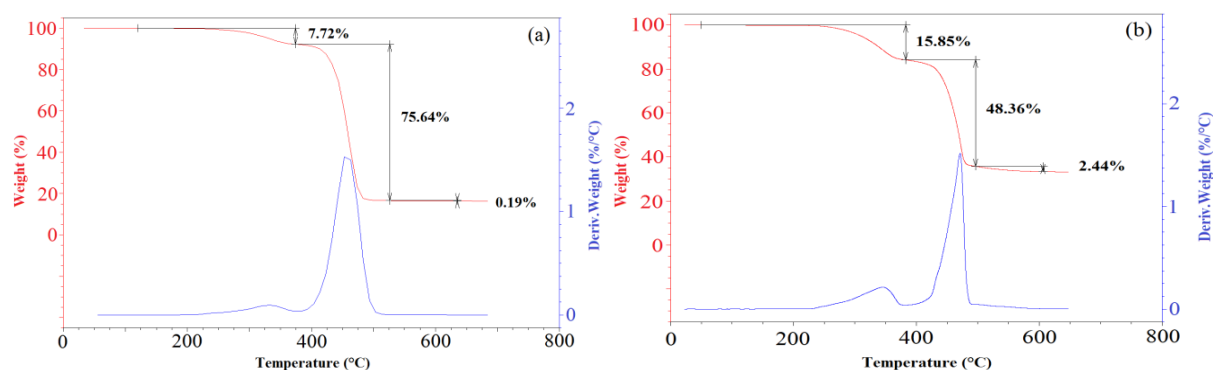


Figure 3-12 : Second derivative of TGA thermograms of a) 33phr and b) 100phr PATH filled EPDM samples ($5^{\circ}\text{C}\cdot\text{s}^{-1}$, N_2)

Samples filled by 33 phr of ATH lose 83.6 wt.-% of their initial mass regarding to theoretical value of 83.8 wt.-% (Figure 3-12a), and samples containing 100phr of ATH lose 66.7 wt.-% comparing to 67.5 wt.-% of theoretical mass loss (Figure 3-12b).

This test has been run several times for each batch, so the homogeneity of fillers dispersion could be approved.

3.2 Kinetic analysis of EPDM crosslinking by DCP

3.2.1 Molecular scale

3.2.1.1 FTIR spectrophotometry

To have a better understanding of crosslinking phenomena, the real-time changes in characteristic IR peaks of EPDM and DCP are taken into consideration. In this method, thin films ($\sim 150\ \mu\text{m}$) of linear EPDM / DCP mixture are prepared and positioned between a pair of KBr windows. This installation is then integrated in a heating temperature controlled cell where an FTIR spectrum is acquired every 30 seconds throughout crosslinking at the imposed temperature of 170°C .

The peaks of our interest according to the general crosslinking mechanism (Chapter I, Section 3) are:

- $809\ \text{cm}^{-1}$: Double bond of ENB^[5]
- $855\ \text{cm}^{-1}$: O-O bond of DCP^[1]
- $1690\ \text{cm}^{-1}$: C=O bond of acetophenone ^[1]

In the overall mechanism of crosslinking, the ethylene and propylene units are consumed. However, the number of these participating units in crosslinking reactions is undetectable and negligible comparing to their initial concentration. But, the three characteristic peaks mentioned above are in

measurable range of absorption and their concentration can be determined. Figure 3-13 shows the real-time concentration changes for EPDM Nordel 4520 at 170°C. A similar behavior has been observed for two other Nordels under study.

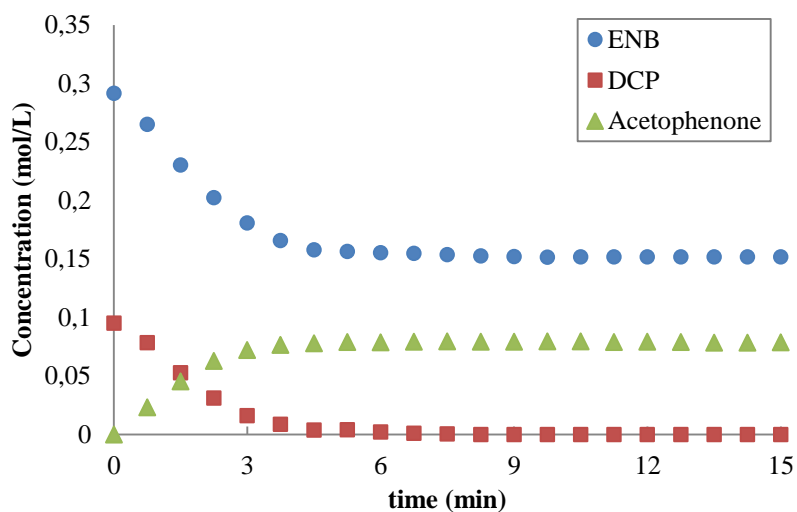


Figure 3-13: Real-time concentration monitoring of ENB, DCP and acetophenone variations during the crosslinking of Nordel 4520 at 170°C

The results of crosslinking of three Nordels under study suggest that:

- i. Consumption of ENB double bonds begins from the very early period of crosslinking with a maximal rate during first 5 to 10 minutes, and then slows down gradually until the end of the crosslinking. This behavior is very similar for the three EPDMs. The maximal amounts of consumed ENB double bonds are given in Table 3-15.

Nordel	Consumed ENB / Introduced DCP (mol/mol)
4520	1.5 ± 0.1
4640	1.6 ± 0.1
4570	1.3 ± 0.1

Table 3-15 : Normalized concentration of consumed ENB double bonds per initial concentration of DCP introduced in the reactive medium

- ii. The concentration of DCP in mixtures is 3 phr, which is equal to 0.096 mol.L⁻¹. The consumption of DCP begins with a sudden decrease and, in an interval between 10 and 15 minutes, the concentration approaches zero.
- iii. The molecules of acetophenone are formed parallel to DCP consumption. However, it should be precised that the concentration on the final plateau does not represent the maximum

concentration but the ultimate limit of IR apparatus detection sensitivity. The real concentration is presumably superior to this latter. The molecules of acetophenone are volatile but voluminous and leave the matrix very slowly, only at the periphery of KBr windows. Thus, these molecules can be trapped in the matrix for long time. So, once the crosslinking is finished, the samples were put under vacuum to tentatively evaporate every ketone molecules to avoid any interference and overlapping with IR peaks.

The presence of residual double bonds after crosslinking has been reported by several authors (cf. Chapter I. section 3). For instance, Kranenburg *et al.* followed the crosslinking of an EPDM containing 48 wt.-% ethylene and 9.0 wt.-% of ENB (almost twice of our materials), with a (*t*-butylperoxy-isopropyl) benzene in solution in cyclohexane as a solvent at 175°C [11]. The crosslinking was followed by Raman infrared spectrophotometry. Consumption of double bonds as a function of crosslinking time and peroxide concentration has been detected. The consumption of ENB with 2 phr peroxide after 20 minutes was reported to be about 20 – 25 mol.-%.

3.2.1.2 Differential calorimetry

Several authors have tried to determine the mechanism of dicumyl peroxide curing of elastomers [12-15]. The decomposition enthalpy of dicumyl peroxide has been determined in several researches. For instance, Lu *et al.* [16] or Wu *et al.* [17] have found an enthalpy equal to 750 J/g (203 kJ/mole). However, the enthalpy measured by DSC during crosslinking is the resultant of several elementary reactions involved in a general chemical mechanism. This enthalpy has been measured for a range of residence times at curing temperature (Chapter II, Section 4.1.3). The enthalpy measured at the second ramp is an index of the unreacted DCP concentration which is not consumed during the stay time at 170°C (Figure 3-14). As it is shown in Figure 3-14, the active molecules of DCP are totally consumed after 15 minutes at 170°C. A kinetic approach for lifetime determination of DCP is possible considering the first order decomposition reaction of DCP. In the literature, an activation energy equal to 140 kJ.mol⁻¹ and a pre-exponential factor equal to 1.85×10^{14} is found [18]. With these data we obtain a half-life of 2 minutes for DCP at 170°C. Consequently, the conversion of DCP after 15 minutes at 170°C is higher than 99%.

It is noteworthy to precise that the residual value is not capable to give any quantitative information about the concentration of consumed residual peroxide, and reveals only the time needed for total consumption of DCP molecules and the total heat of crosslinking.

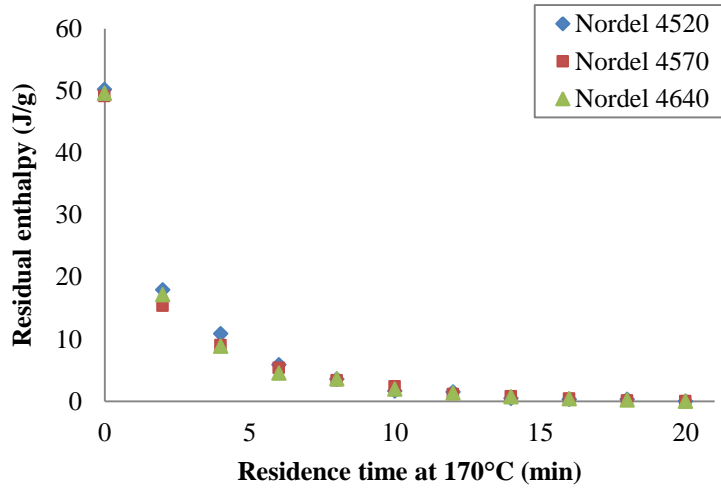


Figure 3-14 : Residual enthalpy of crosslinking as a function of residence time at 170°C (results for an initial concentration of 5.5phr of DCP)

In this study, several concentrations of DCP have been introduced into EPDM matrices. The total crosslinking enthalpy remains constant per mole of peroxide for concentrations inferior to 10 phr. Beyond this concentration, the total enthalpy per mole of peroxide decreases. This deviation has been previously reported in the works of Schwartz where it was shown that the deviation occurs for butyl rubber and nitrile butadiene rubber for concentrations above 5 phr of peroxide [18].

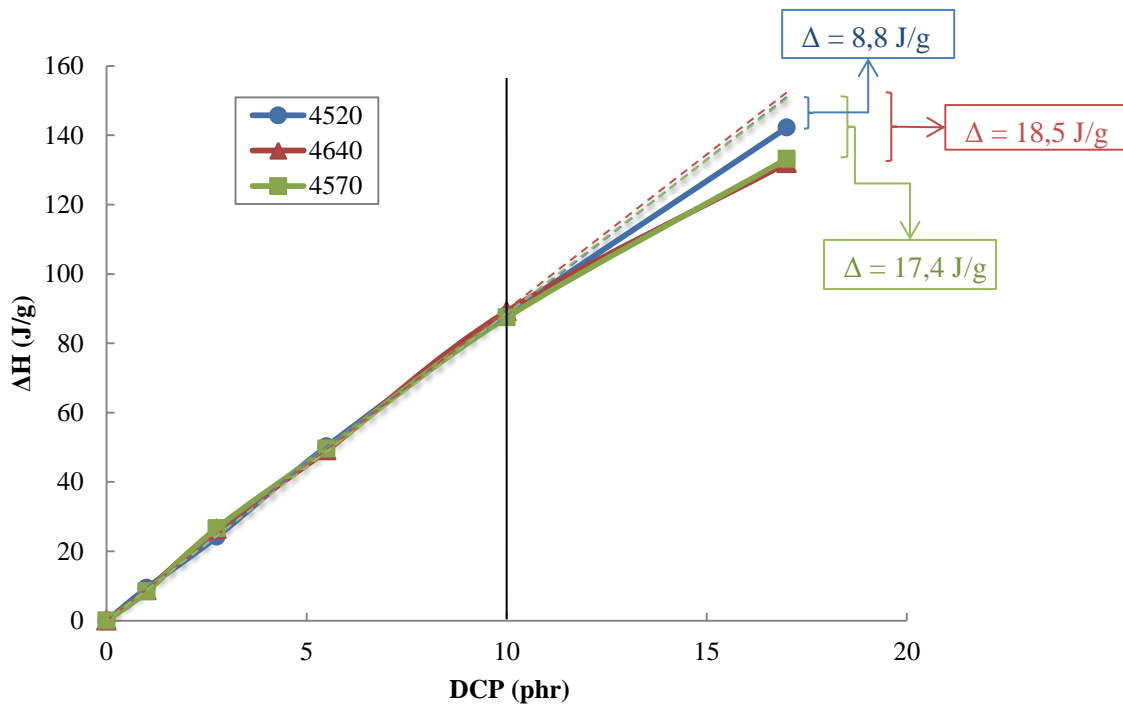


Figure 3-15 : Enthalpy of crosslinking as a function of DCP concentration at 170°C

The deviation from linearity beyond 10 phr of DCP is related to dispersion state of peroxide in the matrix. In fact, at low concentrations the peroxide molecules are homogeneously dispersed among polymer chains. However, as the concentration increases, the DCP molecules get closer and form clusters. Above 10 phr, a change in the consumption kinetics of DCP is evidenced in Figure 3-15.

3.2.1.3 Thermochemistry of crosslinking

As mentioned in previous section, the total enthalpy of crosslinking measured by DSC is a linear combination of the several elementary reactions. Therefore, by considering common kinetic rules and thermochemistry concepts, one should be able to define a general crosslinking mechanism for EPDM.

The radicals formed from decomposition of DCP can attack hydrocarbon chains and abstract labile hydrogens on three principal sites:

- 1) Secondary hydrogen of ethylene
- 2) Tertiary hydrogen of propylene
- 3) Allylic hydrogen of ENB

Hydrogen abstraction capability is often defined by the dissociation energy of C – H bonds. This makes allylic hydrogens more sensitive to radical attack than methynic and methylenic hydrogens. However, according to common kinetic concepts, hydrogen abstraction capability depends not only on values of rate constants, but also on concentration of involved species. According to the Arrhenius law, the rate constant k at temperature T is related to pre-exponential factor k_0 and, activation energy E_a by:

$$k = k_0 \exp\left(\frac{-E_a}{RT}\right) \quad 3-10$$

with R ideal gas constant.

The concentration of involved chemical groups in crosslinking has been determined for the three elastomers (Section 3.1.1), and the kinetic parameters are found in previous works performed in PIMM laboratory, and listed in Table 3-16.

Hydrogen type	E_a (kJ.mol ⁻¹)	k_0 (s ⁻¹ or mol.L ⁻¹ .s ⁻¹)	k (170°C)
Secondary ^[19-21]	73	1.5×10^{10}	37
Tertiary ^[22]	66	3.0×10^8	6
Allylic ^[23]	63	5.6×10^9	209

Table 3-16: Literature values for kinetics parameters of EPDM crosslinking

The fourth column of the table above contains the rate constants calculated for 170°C (curing temperature). The rate constant for allylic hydrogen of ENB is not easily accessible in literature, and therefore, was replaced by values found for polyisoprene, for which the molecular structure is close to ENB.

The hydrogen abstraction rate r for each species can be calculated by Equation 3-11:

$$r = k \cdot [R^\circ] \cdot [PH] \quad 3-11$$

with R° the attacking radical and PH the hydrocarbon substrate.

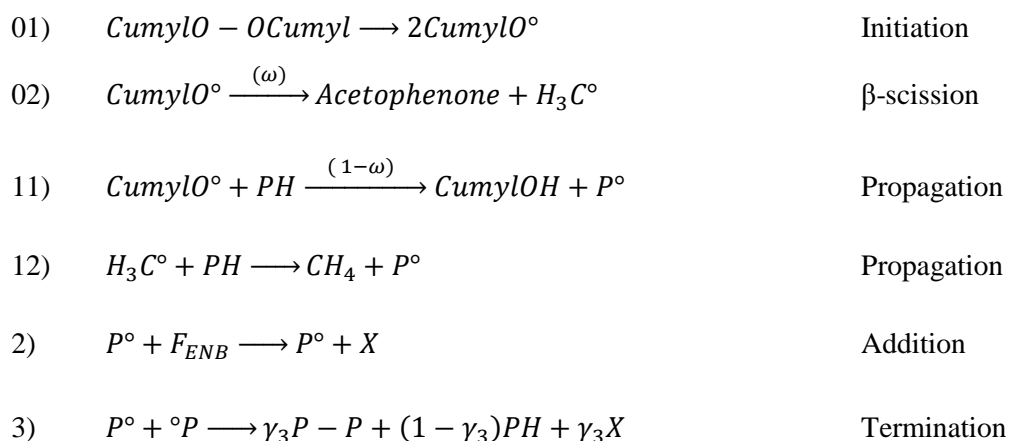
Considering the rate constants of Table 3-16 and the concentrations of Table 3-6, the abstraction probability for each type of hydrogen is determined in Table 3-17. The concentration of R° is considered identical in all cases.

Nordel	Secondary	Tertiary	Allylic
4520	91.2%	4.0%	4.8%
4640	91.1%	3.5%	5.4%
4570	90.3%	4.1%	5.6%

Table 3-17: Participation of each species in crosslinking at 170°C

These results propose that over 90 mol.-% of formed macroradicals are secondary, implying the predominance of junctions formed on ethylene units. This approach is used in thermochemical calculations by considering all the macroradicals as secondary.

We write the general crosslinking mechanism of EPDM by DCP, based on ethylene units, as follow:



where ω is the conversion rate of cumyloxy radical to acetophenone, F the ENB double bond, γ_3 the C - C bridges formation yield and $(1-\gamma_3)$ the disproportionation yield in termination.

A rapid review of available data on organic chemistry gives the formation enthalpy of the bonds involved in the mechanism above [23-25]. These values are listed in Table 3-18.

Chemical Bond	ΔH (kJ.mol ⁻¹)
CumylO – OCumyl	148
β -scission of CumylO°	10
P - H	393
CumylO – H	460
H ₃ C – H	415
Addition on - C = C -	12
- C – C -	328
Disproportionation of - CH ₂ - °CH -	303

Table 3-18: Bond formation energies [23-25]

The enthalpy balance for each reaction per mole of reactive group can be calculated from the data of Table 3-18:

$$\Delta H_{01} = 148$$

$$\Delta H_{02} = 10$$

$$\Delta H_{11} = 393 - 460 = -67$$

$$\Delta H_{12} = 393 - 415 = -22$$

$$\Delta H_2 = -12$$

$$\Delta H_3 = -328 \gamma_3 - 303 (1 - \gamma_3)$$

Considering the global crosslinking mechanism, the overall enthalpy is written as:

$$\Delta H_{\text{total}} = \Delta H_{01} + 2 \cdot (\omega) \cdot \Delta H_{02} + 2 \cdot (1 - \omega) \cdot \Delta H_{11} + 2 \cdot (\omega) \cdot \Delta H_{12} + x_{\text{ENB}} \cdot \Delta H_2 + \Delta H_3$$

with x_{ENB} the consumption ratio of double bonds per mole of peroxide. By replacing the enthalpy values, the total crosslinking enthalpy becomes:

$$\Delta H_{\text{total}} = 148 + 2 \cdot (\omega) \cdot 10 + 2 \cdot (1 - \omega) \cdot (-67) + 2 \cdot (\omega) \cdot (-22) - x_{\text{ENB}} \cdot 12 - 328 \cdot \gamma_3 - 303 \cdot (1 - \gamma_3)$$

The molecules of alcohol are not detectable by spectrophotometry techniques, while absorption peak of ketone attains saturated limits very fast, leaving the parameter ω undefined. However, a compilation of literature data in Figure 3-16 was employed to quantify the conversion rate of cumyloxy radical to acetophenone [26].

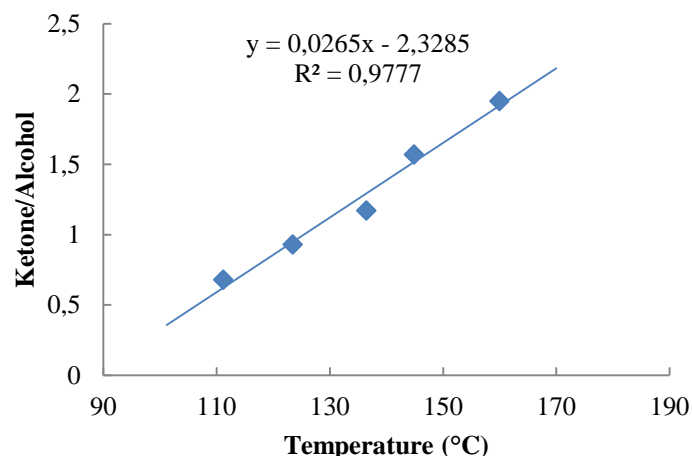


Figure 3-16 : Ketone/alcohol ratio of thermal decomposition of DCP in cumene ^[26]

Extrapolation of the linear regression to 170°C suggest an ω equal to 0.685 at 170°C, which is used for enthalpy calculation. In addition, it is shown in the literature that γ_3 for PE is equal to 0.5 [27]. Subsequently, the total enthalpy of crosslinking is:

$$\Delta H_{total} = -225 - 12x_{ENB} \quad 3-12$$

This last equation proposes that the total enthalpy of crosslinking is a function of double bond consumption ratio.

<i>DCP (phr)</i>	<i>Nordel 4520</i>	<i>Nordel 4640</i>	<i>Nordel 4570</i>
10	238	241	236
5.5	247	241	244
2.75	238	249	262
1	254	237	227
ΔH_{total} (average)	246 ± 8	243 ± 6	240 ± 15

Table 3-19: Crosslinking enthalpy (in $\text{kJ} \cdot \text{mol}^{-1}$ of DCP)

The total enthalpy of crosslinking per mole of DCP has been measured by DSC for several DCP concentrations (Table 3-19) making possible the regeneration of experimental values by theoretical equations of thermochemistry. The introduction of these experimental values into the Equation 3-12 gives the number of consumed double bonds throughout crosslinking (Table 3-20).

Nordel	Consumed ENB/ introduced DCP (mol/mol)
4520	1.1 – 2.4
4640	1.0 – 2.0
4570	0.8 – 1.7

Table 3-20 : Consumption Range of ENB double bonds throughout crosslinking at 170°C in air

The overall enthalpy and consumed ENB double bonds are in the same order for three EPDM Nordels. This coherence was naturally expected due to close chemical structure of the samples. Furthermore, the accuracy of the proposed mechanism is approved by comparing the values of Table 3-15 and Table 3-20, where a good coherence between FTIR spectroscopy and calorimetric outcomes is distinct. Furthermore, the solid state NMR tests on Nordel 4640 measured double bond molecules consumption equal to 50%, which is very close to 48% found by FTIR spectrophotometry.

3.2.1.4 Toward a general kinetic model

Based on the crosslinking mechanism proposed in previous section, the following system of differential equations can be derived:

$$\frac{d[POOP]dt}{dt} = -k_{01}[POOP] \quad (1)$$

$$\frac{d[PO^\circ]}{dt} = 2k_{01}[POOP] - k_{02}[PO^\circ] - k_{11}[PO^\circ][PH] \quad (2)$$

$$\frac{d[H_3C^\circ]}{dt} = k_{02}[PO^\circ] - k_{12}[H_3C^\circ][PH] \quad (3)$$

$$\frac{d[P^\circ]}{dt} = k_{11}[PO^\circ][PH] + k_{12}[H_3C^\circ][PH] - 2k_3[P^\circ]^2 \quad (4)$$

$$\frac{d[F_{ENB}]}{dt} = -k_2[P^\circ][F_{ENB}] \quad (5)$$

$$\frac{d[P=O]}{dt} = k_{02}[PO^\circ] \quad (6)$$

$$\frac{d[CH_4]}{dt} = -k_{12}[H_3C^\circ][PH] \quad (7)$$

$$\frac{d[POH]}{dt} = k_{11}[PO^\circ][PH] \quad (8)$$

$$\frac{d[X]}{dt} = k_2[P^\circ][F_{ENB}] + \gamma_3 k_4 [P^\circ]^2 \quad (9)$$

The boundary conditions at t = 0 can be written:

- $[POOP] = [POOP]_0$ (i)
- $[PO^\circ] = [H_3C^\circ] = [P^\circ] = 0$ (ii)
- $[F_{ENB}] = [F_{ENB}]_0$ (iii)
- $[PH] = [PH]_0$ (iv)

The proposed mechanism, which is derived from the thermochemistry of crosslinking, is based on some simplifying hypotheses explained in the previous section, for which the legitimacy must be proven. To do so, we attempt to validate the model through a numerical simulation, which is the subject of the following section.

3.2.1.5 Numerical simulation of EPDM crosslinking kinetics

In this method, the system of differential equations established in Section 3.2.1.4 is implemented in the MATLAB software and resolved by ODE23s solver. The resulting simulation curves are obtained using the kinetic parameters found in the literature. These results are then plotted and compared with the ones found by real-time FTIR spectrophotometry (here presented for Nordel 4520). The advantage of this approach is that if the numerical simulation curves fit the experimental data without introducing additional assumptions or parameter, the validity of the proposed model is proven.

The first step of crosslinking, i.e. the homolytic scission of DCP molecules to form two alkoxy radicals, has been the subject of several studies [28-31]. These research works propose a range of $10^{12} - 10^{14} \text{ s}^{-1}$ for the pre-exponential factor and, $120 - 146 \text{ kJ.mol}^{-1}$ for activation energy. The kinetic parameters of this reaction depend solely on temperature and the concentration of DCP, and are independent of any other chemical species in the system. Therefore, the values can be calculated directly by fitting the experimental results. The best fit (Figure 3-17) was found for a k_{010} equal to 2.7×10^{12} and E_{01} equal to 122 kJ.mol^{-1} , which are very close to the results of Dixon's [29]. Considering these values, the rate constant of the reaction k_{01} at 170°C is equal to $1.13 \times 10^{-2} \text{ s}^{-1}$.

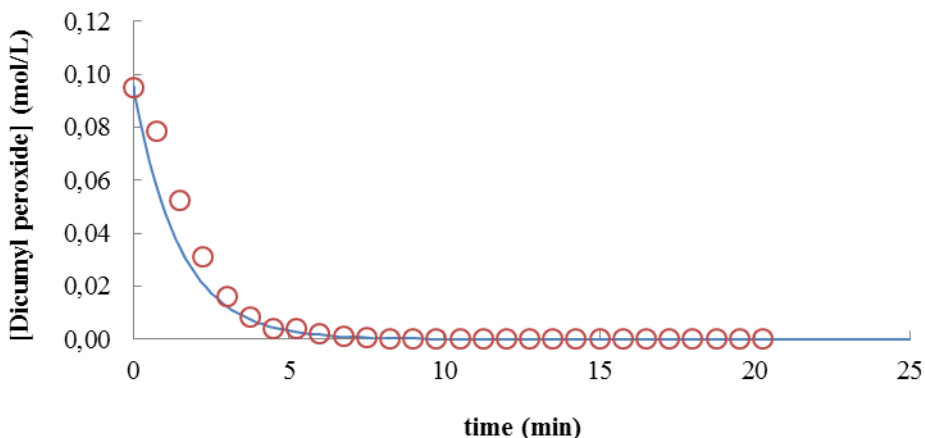


Figure 3-17 : Change in the DCP concentration at 170°C (results for 3 phr of DCP)
Hollow circle: experimental data. Continuous line: kinetic modeling.

In the next step, the beta cleavage of cumyloxy radicals leads to formation of acetophenone molecules. This reaction also is well studied [32, 33]. The results found by Bagnée et al. [33] is the closest to the experimental results, where a value of 1.7×10^{13} for k_{020} and $64 \text{ kJ}\cdot\text{mol}^{-1}$ for E_{02} defines the k_{02} equal to $4.9 \times 10^6 \text{ s}^{-1}$.

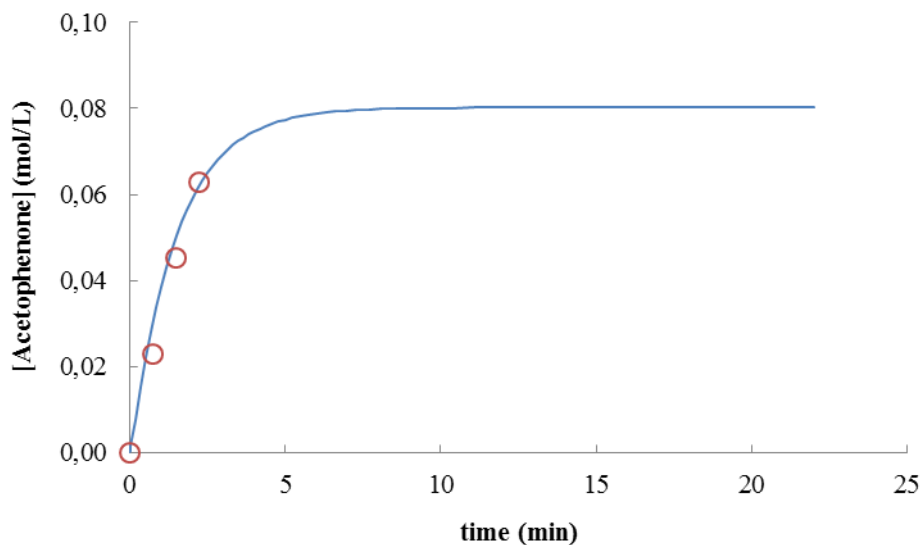


Figure 3-18 : Change in concentration of acetophenone at 170°C (results for 3 phr of DCP)
Hollow circle: experimental data. Continuous line: kinetic modeling.

The result for acetophenone is provided in Figure 3-18, where one can realize that the model convincingly fits the first points of experimental results. Beyond this fraction of time, the experimental results cannot be referenced due to the inaccuracy of FTIR spectrophotometry, where the characteristic peak of acetophenone absorbance at 1690 cm^{-1} attains its saturation limit. Furthermore, acetophenone

is volatile and leaves the system during crosslinking. Therefore, the kinetic curves of acetophenone concentration for longer periods are not plotted.

The side-product of acetophenone formation is methyl radical which, based on proposed mechanism, holds the same kinetic parameters as acetophenone.

Cumyloxy radical can, as well, directly attack the hydrocarbon chains and abstract a hydrogen atom to form a cumylalcohol molecule and a macroradical. A rate constant equal to $4.2 \times 10^4 \text{ L}\cdot\text{mol}^{-1}\cdot\text{s}^{-1}$ at 170°C is found by applying 7.5×10^{10} for k_{110} and $53 \text{ kJ}\cdot\text{mol}^{-1}$ for E_{11} [34]. These parameters result in an approximate maximum alcohol concentration of $1.1 \times 10^{-1} \text{ mol}\cdot\text{L}^{-1}$ (Figure 3-19), which remains fairly low and explains the difficulties in detecting the corresponding FTIR peak.

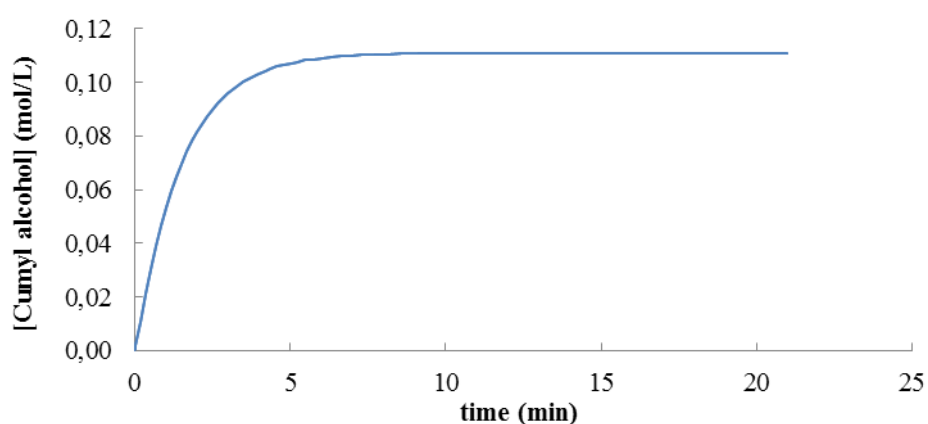


Figure 3-19: Change in cumylalcohol concentration at 170°C (results for 3 phr of DCP)

Methyl radicals resulting from β -scission of cumyloxy can either abstract a hydrogen atom to form a methane molecule and a macroradical, or combine with another methyl radical to form an ethane molecule. These two molecules are highly volatile and can easily evaporate out of system. The formation ratio between these two products has not been determined, but regarding to the low concentration of methyl radical, it is licit to conclude that the concentration of methane would be higher than ethane. Anyhow, the kinetic parameters of this reaction are given in Table 3-21.

Consumption of ENB double bonds is the result of radical attack of previously formed macroradicals. As previously mentioned, ENB has a molecular structure close to polyisoprene and, therefore, the kinetic parameters of this latter have been employed to calculate the corresponding rate constant. Colin et al. have determined a k_{30} and E_3 respectively equal to 2.3×10^6 and $11 \text{ kJ}\cdot\text{mol}^{-1}$ for non-crosslinked, non-stabilized polyisoprene [35]. These values result in a rate constant k_3 equal to $5.1 \times 10^4 \text{ mol}\cdot\text{L}^{-1}\cdot\text{s}^{-1}$, which satisfactorily fits the experimental results (Figure 3-20).

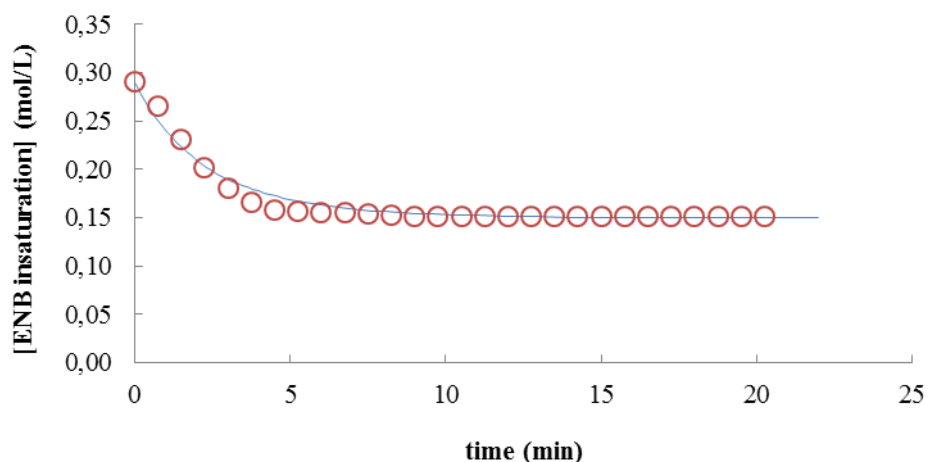


Figure 3-20: Changes in the ENB double bond concentration at 170°C (results for 3 phr of DCP)
Hollow circles: experimental data. Continuous line: kinetic modeling.

Addition of a macroradical onto an ENB double bond creates a macroradical and a crosslink. This latter can also be created by combination of secondary radicals formed from ethylene units. Therefore, the total number of crosslinks can be calculated by summing these two contributions. The simulation results of crosslink concentration as a function of exposure time has been presented in Figure 3-21.

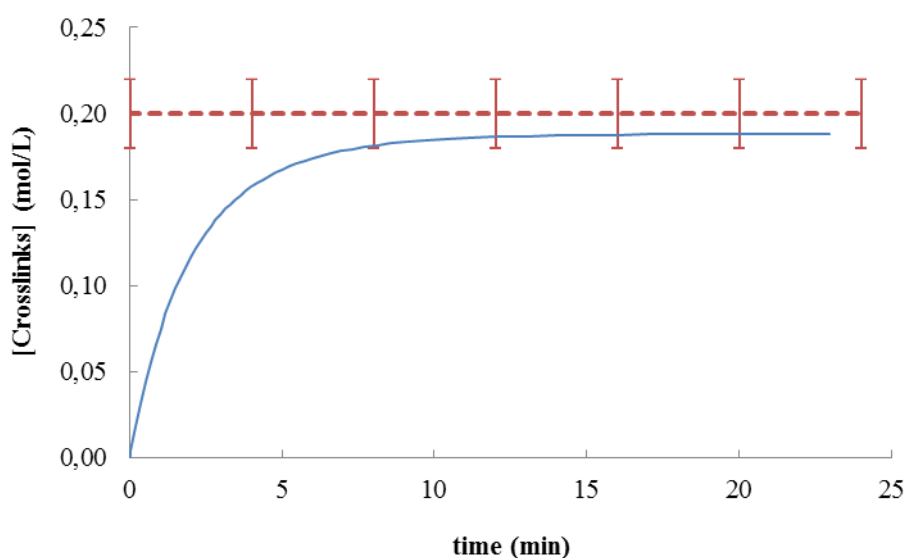


Figure 3-21: Change in the crosslinks concentration at 170°C (results for 3 phr of DCP)
Dashed line: average experimental crosslink density. Continuous line: kinetic modeling.

The simulation results reveal that the crosslink density arrives to 98% of its final value after 10 minutes, and the final EPDM network is built after 15 minutes. This final value has been compared to experimental results (dashed line) found by swelling test, which is subsequently discussed in Section

2.2.3. These result shows that the final theoretical value is placed in the error margin of experimental data.

Reaction (i)	Ref	Pre-exponential Factor k_{i0} (s^{-1} or $mol.L^{-1}.s^{-1}$)	Activation Energy E_i ($kJ.mol^{-1}$)	Rate Constant (170°C) k_i (s^{-1} or $mol.L^{-1}.s^{-1}$)
01	[29]	2.7×10^{12}	122	1.1×10^{-2}
02	[33]*	1.7×10^{13}	64	4.9×10^6
11	[34]	7.5×10^{10}	53	4.2×10^4
12	[36]	1.6×10^{15}	58	2.3×10^8
2	[35]	2.3×10^6	14	5.1×10^4
3	[19]*	1.8×10^{11}	0	1.8×10^{11}

Table 3-21: Kinetic parameters of EPDM crosslinking by DCP
(*Values are adapted by slight modifications)

The proposed mechanism has been shown to satisfactorily model the crosslinking of EPDM by DCP. This approach is based on compilation of literature kinetic parameters, but does not prevent a more precise approach through experimental determination of the parameters in the future.

3.2.2 Macromolecular scale

3.2.2.1 Differential calorimetry

3.2.2.1.1 Plasticizing effect of DCP

The T_g of linear EPDM containing DCP is lower than the T_g of matrix alone. This difference is evoked by plasticizing effect of DCP. The equation proposed by Kelley and Bueche [37] gives the T_g of a polymer/plasticizer mixture:

$$T_g = \frac{(1-\phi_S).T_{gP}.\Delta\alpha_P + \phi_S.T_{gS}.\Delta\alpha_S}{(1-\phi_S).\Delta\alpha_P + \phi_S.\Delta\alpha_S} \quad 3-13$$

where ϕ_S is the volume fraction of plasticizer, α is the free volume expansion coefficient and the indices P and S correspond to polymer and plasticizer, respectively. This equation can be rewritten in the form of Equation 3-14, which reduces the initial equation to apparent variables of polymer's T_g and volume fraction of plasticizer:

$$T_g = T_{gP} \left(\frac{1-\Delta.\phi_S}{1-\gamma\phi_S} \right) \quad 3-14$$

with:

- $A = (\alpha_p.T_{gp} - \alpha_s.T_{gs})/\alpha_p.T_{gp}$
- $\gamma = (\alpha_p - \alpha_s)/\alpha_p$

For softening effect of small molecules (dicumyl peroxide in this case), the information on plasticizer parameters of this equation, which are α_s and T_{gs} , are rarely available. Simha and Boyer [38] proposed experimental data for expansion coefficients of several polymers in their glassy and rubbery states. By considering the glass transition temperature of polymers as an iso-free volume state, they concluded that $(\alpha_l - \alpha_g).T_g = K_1$ and $\alpha_l.T_g = K_2$, where α_l and α_g are the cubic expansion coefficients for a 100% amorphous polymer above and below T_g and K_1 and K_2 are constants. The results were 0.113 for K_1 and 0.164 for K_2 . Later, Verdu [39] proposed to apply these coefficient values in the case of a plasticized polymer by supposing that $\alpha_p.T_{gp} \sim \alpha_B.T_{gB} \sim 0,113$, which results in $\Lambda \sim 0$. This simplifications leads to the following equation for plasticizing effect:

$$\frac{1}{T_g} = \frac{1}{T_{gp}} + \kappa\phi_S \tag{3-15}$$

where κ is a constant.

The plasticizing effect of DCP on the three linear EPDMs under study is demonstrated in Figure 3-22. Two different regions are detectable: First, DCP phr < 2.75, where the plasticization does not follow a well-defined path and certainly not the mixtures law. Second, beyond 2.75 phr of DCP, where T_g evolves linearly with DCP. The introduction of the values of T_{gp} and the concentrations of DCP into the Equation 3-15, gives an average κ value equal to $-1.2 \times 10^{-3} \text{ (K}^{-1}\text{)}$ for the three linear EPDMs.

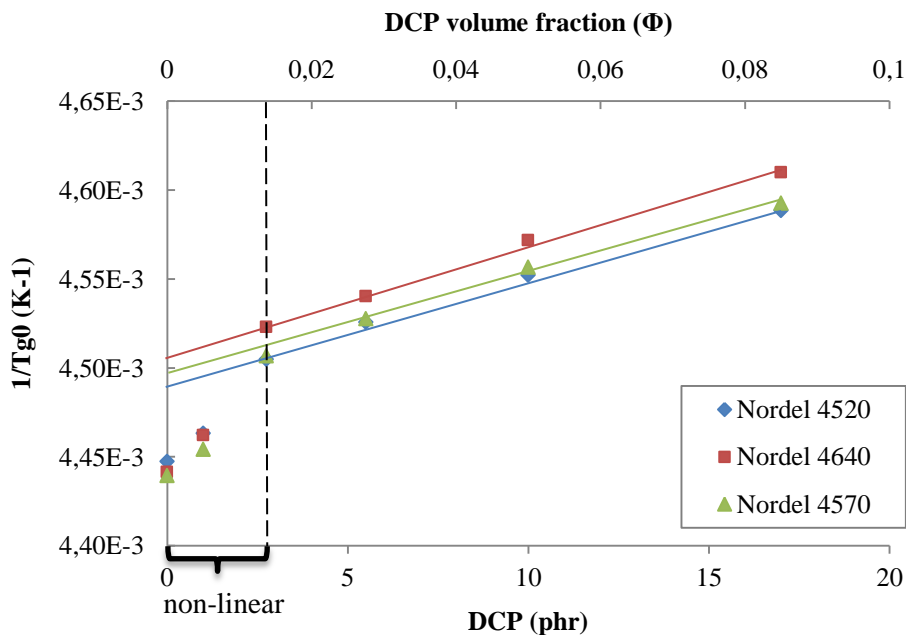


Figure 3-22: Plasticizing effect of DCP the three linear EPDMs under study

One other interesting information that we can obtain from calorimetric data is the relation between the T_g of the elastomer and its molecular weight. Fox and Flory have studied the influence of molecular weight on "second-order transition temperatures" of polystyrene [40]. It was claimed that, in each case of study, the T_g was a reciprocal function of M_n (number average molecular weight), which led them to propose the following equation (3-16) to relate these two quantities:

$$T_g = T_{g\infty} - \frac{k_{FF}}{M_n} \quad 3-16$$

where $T_{g\infty}$ is the limit value of the T_g when the sequence number of monomer repetitions in a polymer chain tends to infinity and k_{FF} , a constant dependent to the nature of the polymer.

Bicerano [41], by compiling the bibliographic data, proposed an empirical relationship between $T_{g\infty}$ and k_{FF} , where this latter is assumed to be proportional to $T_{g\infty}$ to the power of three:

$$k_{FF} = 0.002715 T_{g\infty}^3 \quad 3-17$$

which transforms the Fox-Flory equation into :

$$T_g = T_{g\infty} - 0.002715 \frac{T_{g\infty}^3}{M_n} \quad 3-18$$

The introduction of experimental values of M_n given in Section 3.1.1.2 (HT-GPC) in the Bicerano's approach leads to values of $T_{g\infty}$ presented in Table 3-22.

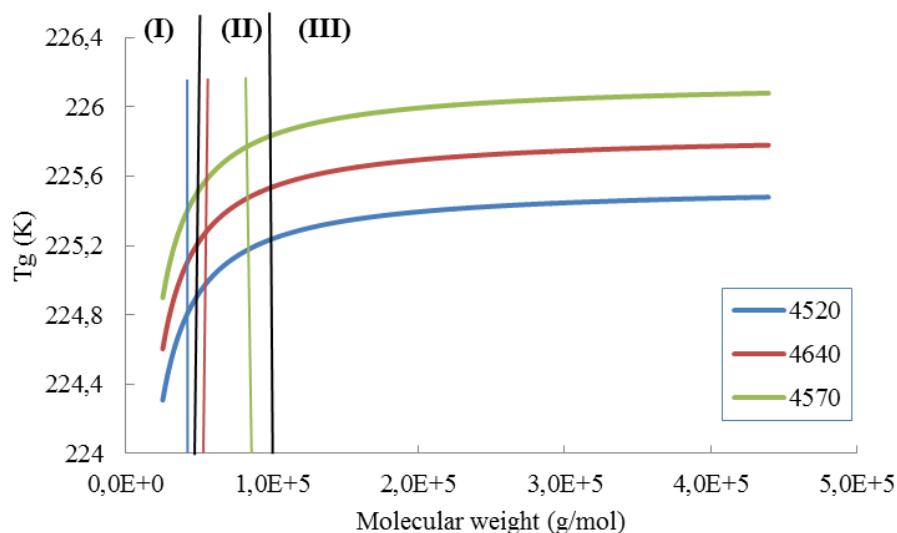


Figure 3-23 : T_g as a function of (M_n) according to Fox-Flory equation modified by Bicerano's approach

Nordel	T _g	T _{g∞}	M _n	K _{FF}
4520	- 48.4	- 47.6	46,100	3.7 x 10 ⁴
4640	- 48.0	- 47.3	53,250	3.7 x 10 ⁴
4570	- 47.2	- 47.0	85,400	1.7 x 10 ⁴

Table 3-22: Values of $T_{g\infty}$ calculated from Fox-Flory equation modified by Bicerano's approach using T_g and M_n as parameters

The values of k_{FF} calculated for the Nordel 4520 and 4640 are equal to 3.7×10^4 , while that of Nordel 4570 is equal to 1.7×10^4 . This nonconformity is related to the real molecular weight of the three samples. In fact, at low molecular weights, T_g increases rapidly with molecular weight up to a specific limit (region I) and slows down afterwards (region III, Figure 3-23). This transition range for the three linear EPDMs under study is located between 5×10^4 and $10^5 \text{ g}\cdot\text{mol}^{-1}$ (region II). By positioning the T_g of samples on the curves of Figure 3-23, it can be observed that Nordel 4520 and 4640 are closer to region I while 4570 is closer to region III.

The region I corresponds to Fox-Flory equation, but in region II, M_n gets rather closer to the theoretical $M_{n\infty}$ value. In region III however, the T_g can be considered constant and equal to $T_{g\infty}$. Therefore, in region III, the changes in T_g with M_n are negligible and deviate from Equation 3-21.

3.2.2.1.2 Crosslinking kinetics

Kinetic study of crosslinking by DSC has been carried out for 2.75, 3, 5.5 10, and 17 phr of DCP. The introduction of 3 phr of DCP has been made via an industrial mixer, while other concentrations were introduced via the solution route. Samples of 5-10 mg of linear EPDM/DCP mixture were placed in standard aluminum pans and crosslinked in nitrogen at 170°C.

It can be observed that after total consumption of DCP (~15 minutes), the T_g tends toward higher values (Figure 3-24). The increasing of T_g , once the DCP molecules are thoroughly consumed, indicates the presence of residual macroradicals and the formation of crosslinks up to 40 minutes, beyond which T_g reaches an asymptotic value, $T_{g \text{ max}}$.

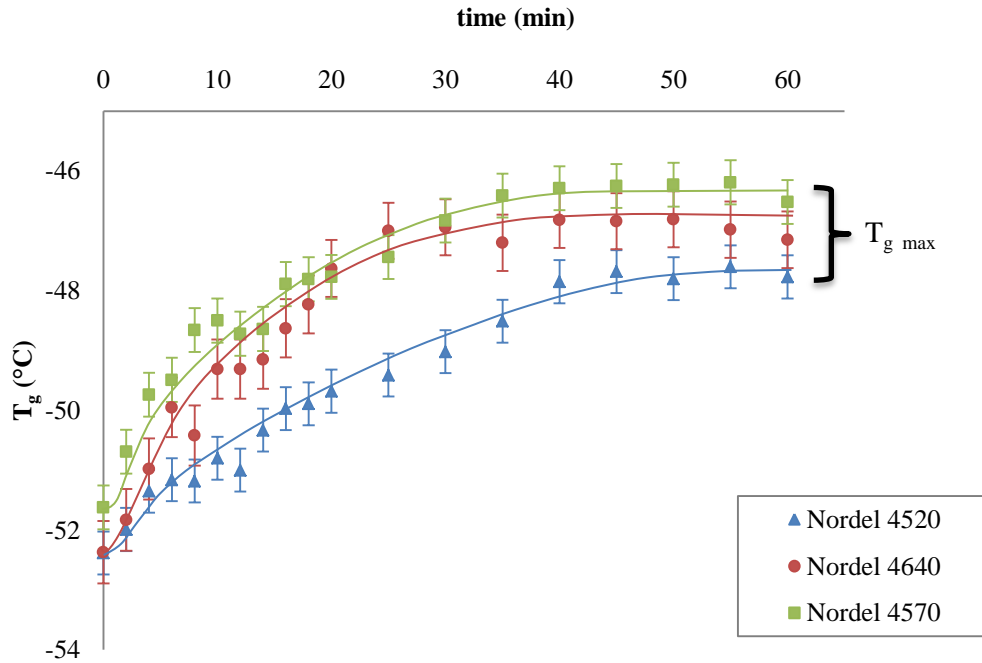


Figure 3-24: Evolution of T_g as the EPDM networks being formed throughout crosslinking (results presented for samples containing 5.5 phr of DCP, at 170°C)

The crosslink density increases with the concentration of peroxide, which pushes the T_g plateau to higher values. Figure 3-25 shows the changes in the inverses of T_{g-max} as a function of crosslinker concentration. According to Equation 3-16, T_{g-max} is supposed to increase with concentration of active chains. From a physical point of view, this evolution is due to a reduction of polymer chains' mobility. However, a quick glance at the Figure 3-25 shows that the Di Marzio's equation is not applicable to low concentrations of crosslinks. This discrepancy comes from the fact that in the presence of a high number of entanglements in linear samples, the concentration of crosslinks becomes effective above a certain critical value [42]. In addition, as the chemical crosslinks get formed, the entanglements are replaced by chemical junctions. This substitution induce a predominance transition at around 2.75 phr of DCP (corresponding to around 0.2 mol.kg^{-1} of crosslinks), where the chemical crosslinks becomes more important than physical entanglements.

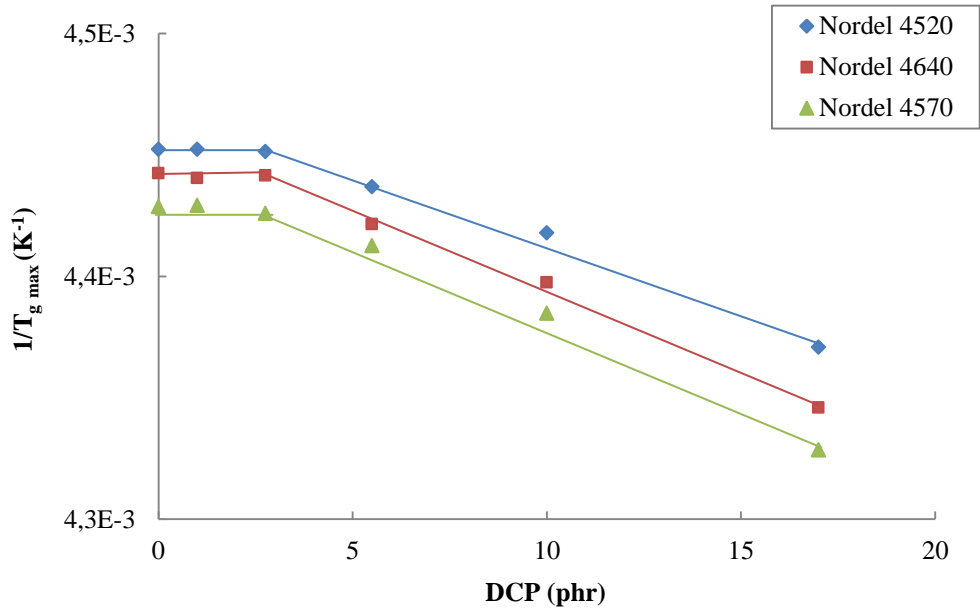
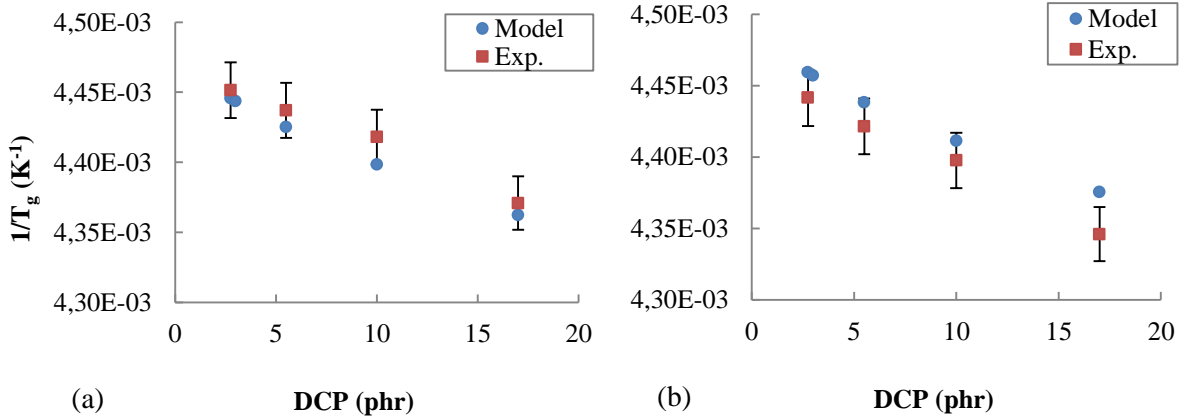


Figure 3-25: Crosslinked network T_g as a function of DCP concentration

The T_g of crosslinked samples in Figure 3-25 are empirically determined through calorimetry tests. We recall from section 3.2.1.5 that the theoretical crosslink density of the network can be measured through numerical simulation of the crosslinking model. Therefore, by replacing the numerically determined x in Di Marzio's equation, the numerical T_g of the crosslinked network (T_{gn}) with different concentration of DCP can be calculated.



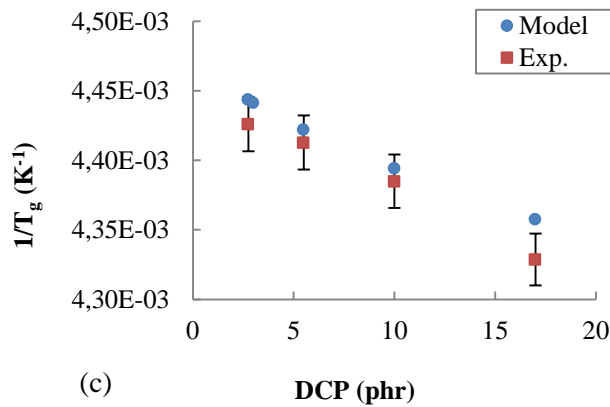


Figure 3-26: Comparison between experimental and numerical simulation results the of crosslinked network T_g as a function of introduced DCP: a) Nordel 4520, b) Nordel 4640 & c) Nordel 4570

Figure 3-26 presents the diagrams comparing the experimental T_g of networks measured by calorimetry and the theoretical values calculated by numerical simulation. Although the numerical method does not superpose the experimental data, these results are convincingly positioned in the error margins of the experience, and the crosslinking model has been approved once again.

3.2.2.2 Rheometry

Formation of crosslinks restrains the chains mobility in material bulk and increases the Young's modulus as well. Figure 3-27 shows that the crosslinking can be started at temperatures lower than the conventional temperature of curing (170°C). By heating beyond 135°C the effect of temperature rise becomes more important and the rate of peroxide decomposition and, consequently, the global crosslinking rate will be accelerated.

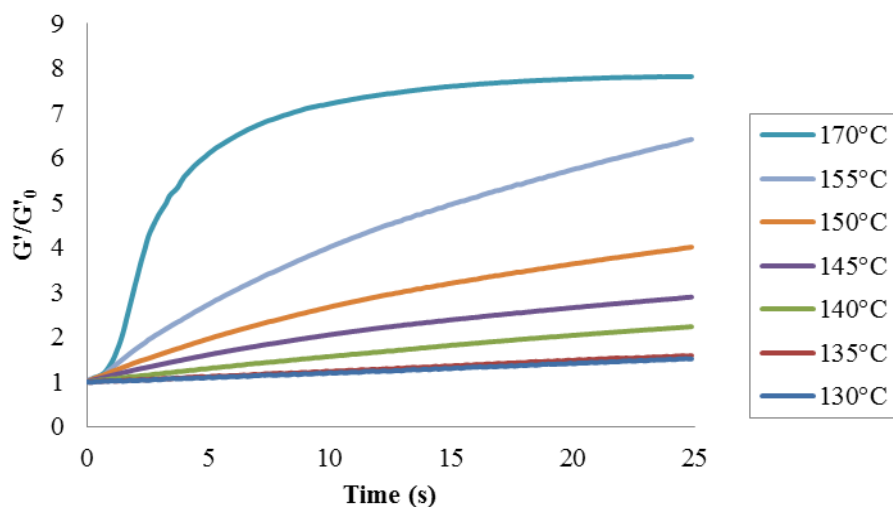


Figure 3-27: Changes in storage modulus as a function of crosslinking time at different temperatures in air (for Nordel 4520)

Flory [43] indicated that shear modulus is related to the concentration of elastically active chains by:

$$G' = \nu \rho RT \quad 3-19$$

In the case of an ideal network, this concentration is equal to the reciprocal average mass of the active chains M_C :

$$\nu = 1/M_C \quad 3-20$$

However, for a non-ideal network the effect of chain-ends, which do not participate in overall modulus of the network and can have a plasticizing effect, should be considered. In each initial linear EPDM chain, there are two ends who do not participate in the macromolecular network formation and remain as dangling chains with an average concentration of $2/M_n$. As a result, Equation 3-20 becomes:

$$\nu = \frac{1}{M_C} - \frac{2}{M_n} \quad 3-21$$

It can be seen, from Equation 3-21, that the effect of chain-ends becomes negligible for initial linear polymers of high molecular weight (M_n).

The Figure 3-28 shows the evolution of storage modulus during crosslinking of Nordel 4520, between the two parallel plates of a rheometer at 170°C. The storage modulus rises rapidly in the beginning of the exposure to reach an asymptotic value. This final plateau represents the thoroughly crosslinked network from which the crosslink density can be determined according to Equation 3-19. This figure clarifies, as well, that after 15 minutes at 170°C, the modulus has attained around 98% of its final value.

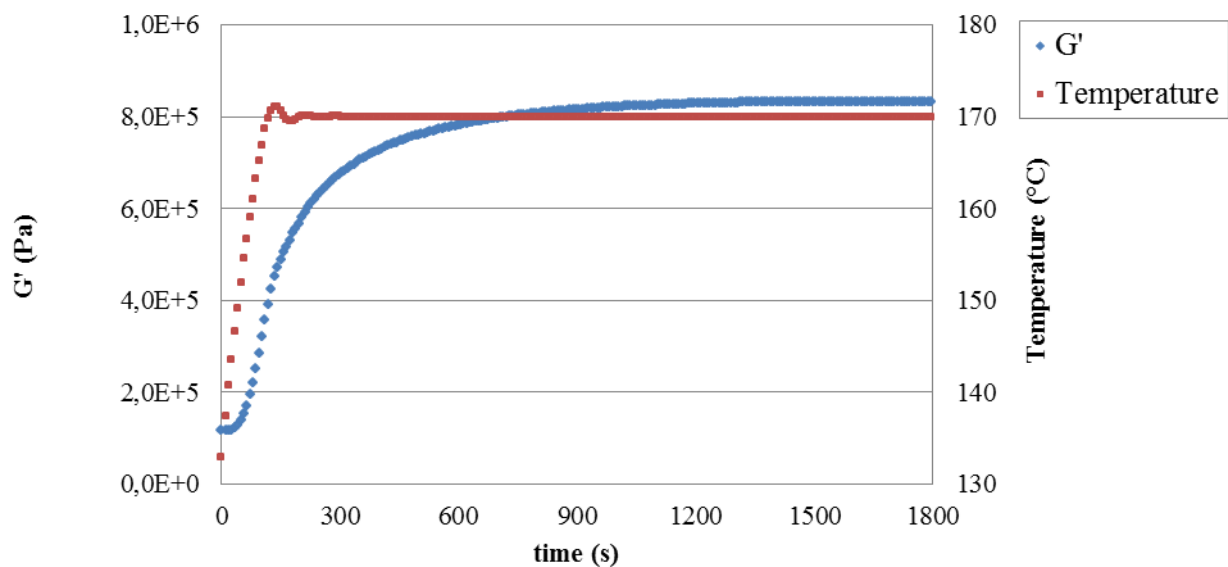


Figure 3-28: Evolution of storage modulus during crosslinking of Nordel 4520 at 170°C

Before calculating the crosslink density of the network through rheometry results, the eventual effect of temperature has to be considered. Although the term of temperature is included in the equation of Flory, it is only related to the molecular mobility. Nevertheless the density of the material is affected by temperature as well. The volumic mass of the material depends on the linear thermal expansion coefficient (α_l) and the test temperature variations (ΔT). For a tridimensional expansion, the volumic mass at temperature T is given by:

$$\rho_T = \frac{\rho_{ambient}}{1+3\alpha_l\Delta T} \quad 3-22$$

Equation 3-22 results in a density equal to 0.78 g.cm^{-3} at 170°C for The EPDMs under study.

A simple application of Flory equation allows calculating of the maximal crosslink density for each network from the asymptotic values of storage modulus (Table 3-23).

Nordel	$M_n \text{ (g.mol}^{-1}\text{)}$	$G'_0 \text{ (MPa)}$	$G'_{max} \text{ (MPa)}$	$\nu \text{ (mol.L}^{-1}\text{)}$
4520	4.60×10^4	0.16	1.13	4.38×10^{-1}
4640	5.32×10^4	0.17	0.95	3.70×10^{-1}
4570	8.54×10^4	0.30	0.99	3.84×10^{-1}

Table 3-23: Elastically active chains' concentration of the three EPDM Nordels crosslinked at 170°C with 3phr of DCP

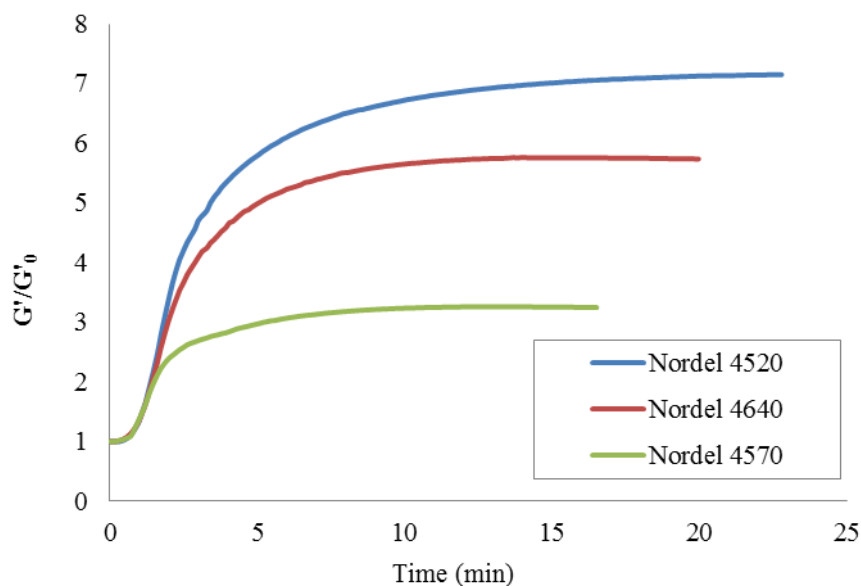


Figure 3-29: changes in G'/G'_0 throughout the crosslinking of the three Nordels under study containing 3 phr of DCP at 170°C

Although the variations of modulus for the three samples are similar, the value at the plateau varies in following order: 4520 > 4640 > 4570 (Figure 3-29). This order is presumably due to different entanglement concentrations of the three linear EPDMs at their non-crosslinked state. Therefore, although the crosslinking states of elastomer are almost the same, the G'/G'_0 values are different due to their initial modulus.

3.2.2.3 Swelling test

In intention of swelling test, plates of 2-3 mm of the three EPDMs were fabricated by press molding at 170°C with 3phr of DCP. Then, cubic samples of 30-50 mg were machined cut out of plates and subsequently swelled in cyclohexane at room temperature for 72 hours. Table 3-24 shows the gel fractions of the three EPDMs under study which attain to the values higher than 98%.

Nordel	f	%Gel
4520	3.04	98
4640	3.08	98
4570	3.05	98

Table 3-24: Solvent uptake factor (f) and gel content for three crosslinked EPDMs under study in cyclohexane at 25°C

The solubility parameters for EPDM and cyclohexane are presented in Table 3-25. It is well-known that two organic substances are mutually soluble when their solubility parameters are close, which here is the case for EPDM and cyclohexane.

$\delta_{EPDM} (MPa)^{1/2}$	$\delta_{cyclohexane} (MPa)^{1/2}$	$V_{ms\ cyclohexane} (cm^3 \cdot mol^{-1})$
16.3 – 18.0	16.7	108

Table 3-25: Solubility parameters of EPDM and cyclohexane

As it was mentioned previously (Chapter II, Section 4.2.2), the solvent/polymer interaction factor, which is composed of enthalpic and entropic contributions, has to be introduced to the Flory-Rehner equation to calculate the gel fraction. The parameters of this latter are defined (Table 3-25), so the concentration of elastically active chains in each EPDM network can be calculated by aforesaid equation (Table 3-26). The results have been presented as minimum, maximum and average values corresponding to an uncertainty interval for solubility parameter.

Nordel	v_{\min} (mol.L ⁻¹)	v_{\max} (mol.L ⁻¹)	v_{average} (mol.L ⁻¹)
4520	3.80×10^{-1}	4.90×10^{-1}	4.35×10^{-1}
4640	3.60×10^{-1}	4.80×10^{-1}	4.20×10^{-1}
4570	3.80×10^{-1}	4.80×10^{-1}	4.30×10^{-1}

Table 3-26: Concentration of elastically active chains for EPDM crosslinked with 3 phr of DCP at 170°C

3.2.2.4 Tensile Test – Small deformation

The tensile properties as well as ultimate properties, i.e. properties at break, are properly measured by tensile testing. In our case, elongation at break and the tensile (or Young's) modulus have been followed as mechanical properties. Conventionally, modulus is expressed whether as tangent modulus at the origin of stress-strain curve or at 100% of deformation. In this study, for the reason that the ultimate strain does not attain 100%, the moduli are measured at the origin (Figure 3-30).

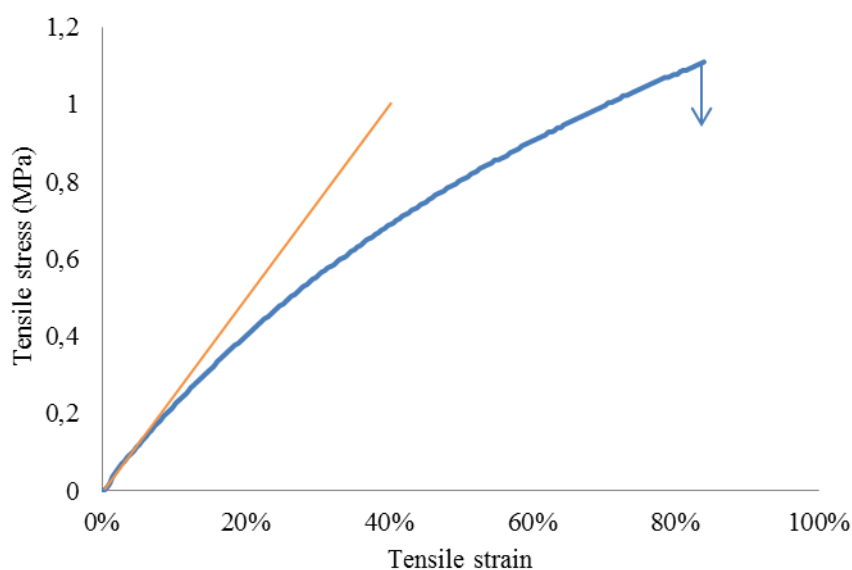


Figure 3-30 : Stress-strain curve of crosslinked Nordel 4640

Tensile testing on neat crosslinked elastomer has been performed in a scanning range of deformation rate from 0.25s^{-1} to 12.5s^{-1} . The ultimate elongation, as well as tensile modulus, remains constant up to 7s^{-1} (Figure 3-31). The values in this linear region are taken as corresponding initial values for unaged samples.

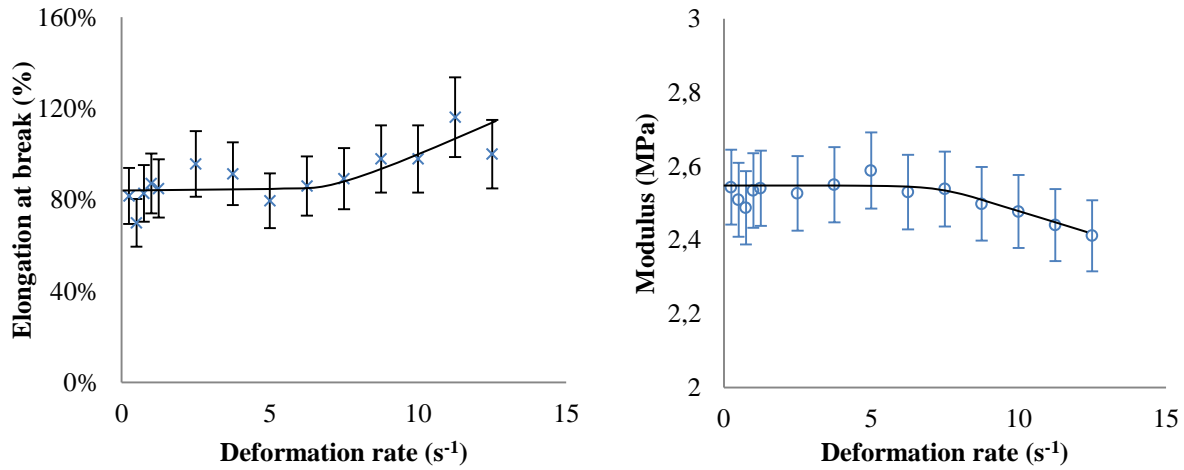


Figure 3-31 : Variations in Young's modulus (right) and elongation at break (left) as functions of deformation rate (4640-N)

The tensile modulus is explained as the ratio of uniaxial stress (σ) over uniaxial strain (ϵ) and is the index of stiffness (resistance to deformation) of material. This relation for extension ratio (λ) and uniaxial strain, which are related as ($\lambda = \epsilon + 1$), is presented in Equation 3-23:

$$\sigma = \frac{\rho RT}{M_e} \cdot \epsilon \left(\frac{1}{1+\epsilon} + \epsilon + 2 \right) \quad 3-23$$

Equation 3-23 shows that the tensile modulus is dependent on uniaxial strain, so it changes during the test. However, as previously mentioned, the tensile modulus is measured at the origin which means when the deformation tends to zero. So the Young's modulus can be derived as:

$$E' = \lim_{\epsilon \rightarrow 0} \frac{\sigma}{\epsilon} = 3 \frac{\rho R t}{M_e} = 3\nu\rho RT \quad 3-24$$

The terms of equation (3-24) shows that the concentration of elastic active chains can also be calculated through tensile test. A quick comparison between equations (3-19) and (3-24) reveals the relation between shear and tensile modulus:

$$E' = 3G' \quad 3-25$$

It is important to emphasize that the equation 3-25 is valid only at low deformation, and as the uniaxial strain increases a deviation is observed.

The value for Young's modulus has been measured equal to $2.54 \pm 4\%$ MPa for 4640-N samples. Insertion of Young's modulus, found by tensile testing for Nordel 4640, into Equation 3-24 gives a ν equal to $(0.404 \pm 0.016) \text{ mol.L}^{-1}$.

3.2.3 Final network structure

A polymeric tridimensional network can be presented by a constitutional repetitive unit, which is called the Structural Unit of Network (SUN). The whole network can be build up by SUN because it represents the most important details at molecular scale, such as type and concentration of different chemical groups, and at macromolecular scale, such as mesh dimensions of the network [44]. SUN should accurately clarify the stoichiometry and functionality of constituting monomers.

The concentration of ENB molecules in the three samples of study is fairly low comparing to other monomers. Therefore, it is licit to assume that the double bonds are dispersed along the chains and no two ENB units are intra-chain neighbors.

Contrarily to ENB, ethylene and propylene units can be located whether in form of block sequences of each monomer or a complete statistical form. Several authors have studied the structure of these terpolymers [45-48]. The polymerization condition of Nordel (Ziegler-Natta vanadium catalyzer) implies a statistical structure. Thus, the global scheme of an EPDM macromolecular chain can be sketched as presented in Scheme 3-1.



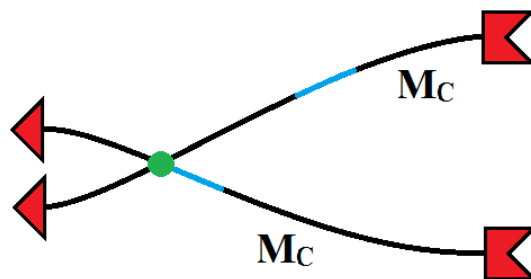
Scheme 3-1: scheme of a linear EPDM chain

As it was previously mentioned in Chapter I, the intern double bonds of ENB can participate in formation of just one crosslink due to steric hindrance. Thus, the crosslinks have to be weather between one ENB and one ethylene monomers or between two ethylene monomers. The participation of ENB can takes place either by its double bond or by its allylic hydrogen. Anyhow, it is experimentally shown that the amount of residual double bonds remains over 50%, leaving the rest of double bonds to get involved in crosslinking.

A crosslink between two monomers other than ENB have no mass, so it is a tetrafunctional junction. Contrariwise, the crosslink made on an ENB has a mass equal to the mass of an ENB (120 g.mol^{-1}). This mass is a part of four active chains, leaving 30 g.mol^{-1} for each. However, the mass of the crosslink is much lower than the mass of an effective chain ($M_C > 2000 \text{ g.mol}^{-1}$), and as a result, the mass of crosslink can be neglected and the crosslink can be presumed tetrafunctional.

When an ENB creates a crosslink on its allylic position, the double bond remains intact. One may conclude the possibility of creating more than one crosslink on an ENB, which results in a functionality more than four. However, the macroradicals cannot easily reach the double bond because

of steric hindrance. Hence, even if such a reaction could take place, the concentration would be too low to be taken into account.



Scheme 3-2: General EPDM SUN (blue dashes represent ENB units)

To sum up, all crosslinks are trifunctional, and by the provided data the SUN of crosslinked EPDM network can be sketched (Scheme 3-2). On the other hand, the crosslink density and the number of consumed ENB units, and consequently number of ethylene units, participated in crosslinking can be calculated by the kinetic model. These theoretical results are presented in Table 3-27.

Nordel	Tri-mer mass ($\text{kg}\cdot\text{mol}^{-1}$)	x ($\text{mol}\cdot\text{kg}^{-1}$)	M_c ($\text{kg}\cdot\text{mol}^{-1}$)	ENB + Eth ($\text{mol}\cdot\text{kg}^{-1}$)	Eth + Eth ($\text{mol}\cdot\text{kg}^{-1}$)
4520	2.964	0.22	2.27×10^{-1}	0.17	0.05
4640	2.447	0.23	2.17×10^{-1}	0.17	0.06
4570	2.487	0.24	2.08×10^{-1}	0.16	0.08

Table 3-27: Theoretical values calculated by kinetic model at 170°C with 3phr of DCP (ENB + Eth and Eth +Eth: crosslink formed between one ENB and one ethylene and two ethylene units)

The M_c values found by kinetic model are inferior to the mass of the three EPDM tri-mers. This approves the aforesaid fact that two ethylene units solely are also responsible for creation of crosslinks. Furthermore, the knowledge of crosslink density and concentration of consumed ENB units will make it possible to calculate the number of crosslinks formed between two ethylene units. Consequently, thanks to the data provided in Table 3-27, the exact structure of Sun for each EPDM under study can be determined.

3.2.4 Tensile testing – Large deformation

At large deformations before fracture, the chains in the network are at their maximum extension, driving the hypothesis of Gaussian distribution of chains out of force. A chain, in order to follow Gaussian probability, has to extend infinitely. Nevertheless, the extensibility of a polymer chain has a limit and, therefore, deviates from Gaussian function.

In addition to limited extensibility, at large deformations, other phenomena can also intervene and amplify the deviation from rubber elasticity law. Two of these phenomena are:

- i. Crystallization: an elastomer is normally well above its melting point at testing temperature. Once exposed under large strains, the chains become extended and tend to be well oriented side by side in the same direction. This state considerably reduces the entropy of the system leading to higher melting points. Consequently, the oriented chains can form crystallites, which do not have the same tensile modulus as the amorphous system. However, EPDM is classed among non-strain crystallizing polymers, leaving this phenomenon out of interest [49].
- ii. Entanglements: in a statistical coil, the chains are twisted through each other and form entanglements. Once the elastomer is cured, a portion of entanglements are trapped between two crosslinks and cannot be undone. These entanglements are called permanent compared to temporary ones.

The tensile behavior models based on rubber elasticity are usually valid at very low deformation, where the behavior is considered as ideal. Mooney-Rivlin equation considers a second term for the deviation from the ideality:

$$\sigma = 2 \left(\lambda - \frac{1}{\lambda^2} \right) \left(C_1 + \frac{C_2}{\lambda} \right) \quad 3-26$$

where σ and λ are tensile stress and elongation, respectively, C_1 the elastic parameter and C_2 the deviation parameter. The Equation 3-26 can be regrouped as:

$$\frac{\sigma \lambda^2}{2(\lambda^3 - 1)} = \left(C_1 + \frac{C_2}{\lambda} \right) = f\left(\frac{1}{\lambda}\right) \quad 3-27$$

Application of equation 3-27 to the tensile results proves the linearity of the relationship and reveals the quantitative values for C_1 and C_2 of Nordel 4640 (Figure 3-32).

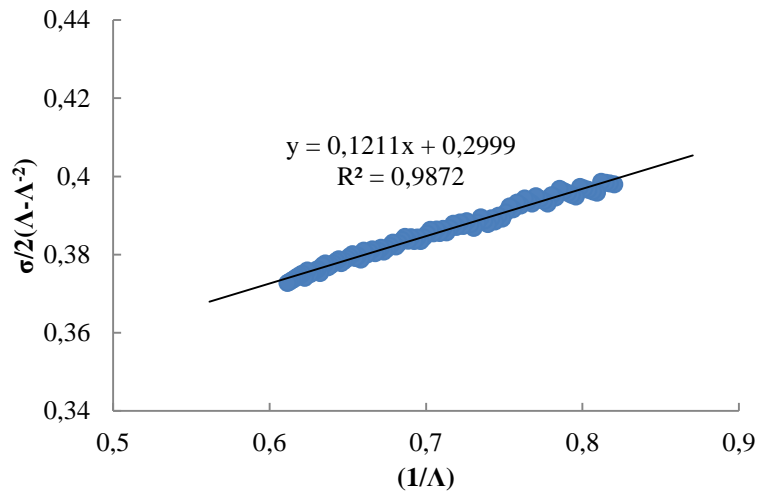


Figure 3-32: $\sigma/2(\lambda-\lambda^{-2})$ as a function of λ^{-1} for Nordel 4640

In the figure above, the Y-intercept and the slope represent the C_1 and C_2 , respectively. Logically, replacing these parameters in Mooney-Rivlin equation and tending the λ from 1 to higher values, should model the experimental tensile diagram, which indeed fits very suitably (Figure 3-33).

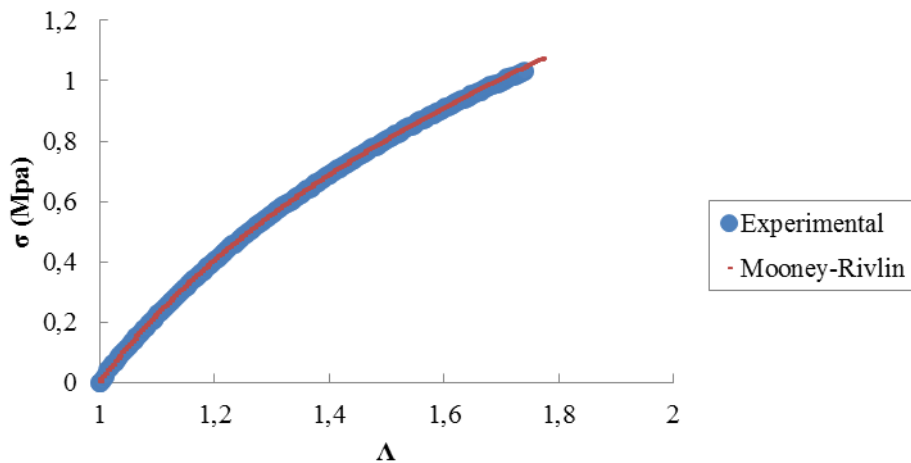


Figure 3-33: Experimental and theoretical tensile diagrams found by Mooney-Rivlin equation

The perfect fitting of the experimental results by Mooney-Rivlin equation, confirms the validity of the basic hypotheses for this method which are isotropy and incompressibility of the tridimensional EPDM network. Furthermore, it has been previously shown that this method is valid in a limited domain of elongation, i.e. 30-150% [50]. Anyhow, the ultimate elongation of the EPDM network under study is placed between the foresaid limits.

3.3 Effect of fillers on initial properties

The reinforcement effect of filler particles on mechanical properties of polymeric matrix has been known for long time (Chapter I), and for our samples we expect no exception. But, how does this presence affect the properties of samples at different scales (e.g. molecular, macromolecular macroscopic)? Does the crosslinked initial state of filled samples differ from that of non-filled ones? Does the presence of surface treatment have an effect, and if the answer is positive to what extend? In what follows, it has been tried to bring answers to questions above and to elucidate the effect of fillers at initial state before aging.

All the filled samples have Nordel 4640 as rubber. Therefore, henceforth we do not provide the name of the EPDM, except where it is necessary.

3.3.1 Molecular scale

3.3.1.1 FTIR Spectrophotometry

Superposition of characteristic peaks of ATH and EPDM made it impossible to study the filled samples through FTIR spectrophotometry.

3.3.1.2 Crosslinking enthalpy

The filled samples are crosslinked under the same conditions as neat samples. The values of residual enthalpies measured in the second ramp are plotted in Figure 3-34.

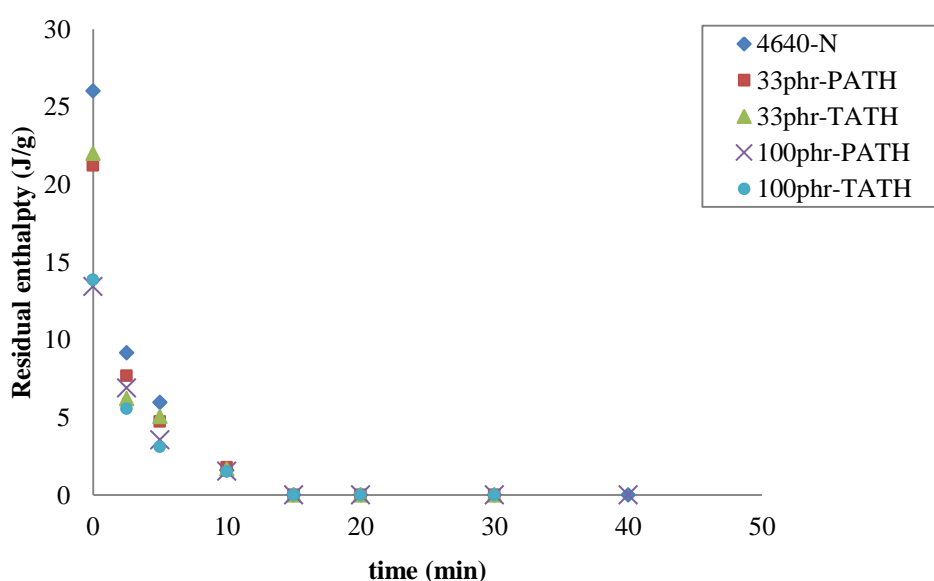


Figure 3-34 : Residual enthalpy of crosslinking as a function of residence time at 170°C

The residual enthalpies measured for 33 phr filled rubber are higher than those containing 100phr, while non-filled rubber retains the highest. However, one should consider that, contrarily to neat sample, the measured values for filled samples are expressed per mass unit of composite and not rubber. Thus, in order to have a comparable basis, the residual enthalpies of filled material must be expressed in joules per gram of rubber. To do so, we need simply to multiply measured values by $\frac{4}{3}$ and 2 for 33 phr and 100 phr filled samples, respectively. The corrected enthalpies are displayed in Figure 3-35.

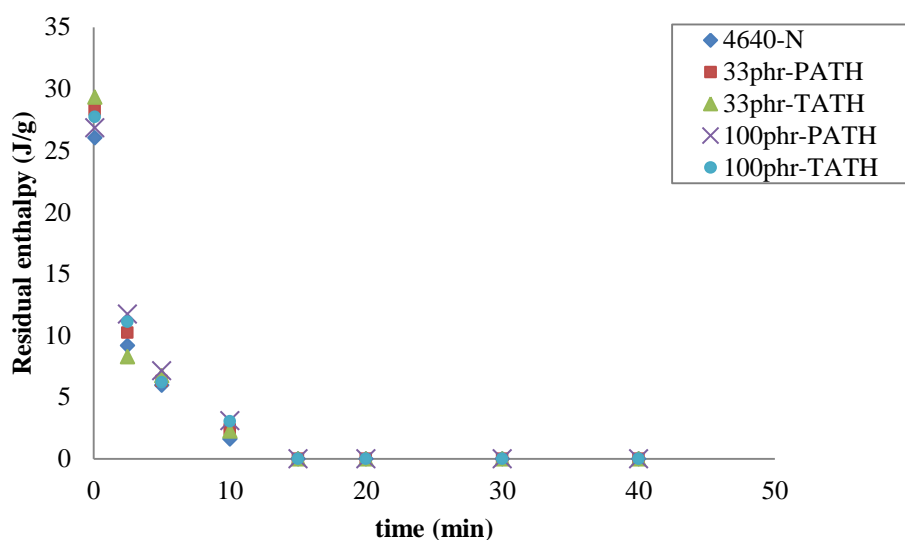


Figure 3-35 : Residual enthalpy of crosslinking corrected per gram of rubber as a function of residence time at 170°C

The corrected values for five different samples are practically the same by considering the measurement error, which attains approximately up to 8% (the error bars are omitted for sake of more clarity).

It may be asked about the participation of surface treatment's vinyl double bonds in overall mechanism of crosslinking. This question will be discussed later, but one point should be taken into consideration: the participation of double bonds consists of a radical addition to a double bond, which comparing to overall enthalpy of crosslinking, is of the second order. Anyhow, by comparing all the values for filled and neat samples, it is clear that the presence of fillers does not affect the crosslinking of the samples.

3.3.2 At macromolecular scale

Aging induced modifications scale cannot be well studied due to limitations of low sensitivity threshold of available techniques at molecular scale. However, some interpretation of what happens at molecular scale can be derived from samples characterization at macromolecular scale.

3.3.2.1 Differential calorimetry

The crosslinking kinetics of the neat gum shows that after 15 minutes at 170°C, more than 99% of dicumyl peroxide molecules have been consumed. However, we have seen in previous section that crosslinking does not terminate at this stage. Macroradicals persist up to 40 minutes of crosslinking, above which T_g reaches an asymptotic value. Filled samples present a similar behavior to neat gum (Figure 3-36).

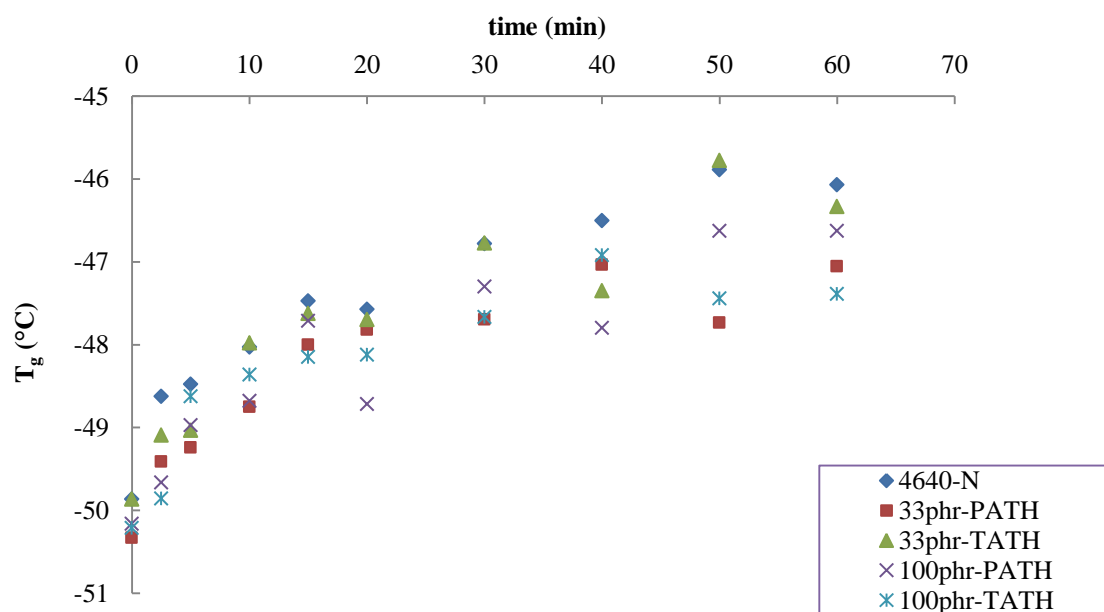


Figure 3-36 : Changes in T_g of neat and filled EPDM samples as a function of time at 170°C

The incorporation of fillers into the gum does not considerably change the value of T_g . It is also difficult to observe a significant difference between all samples for, at least, two reasons. First, values of T_g are fairly dispersed and second, the scattering range is approximately $\pm 1^\circ\text{C}$, which allows stating that all values are in the same order for a given residence time at 170°C.

3.3.2.2 Swelling test

There are two main interests to perform swelling test on filled materials:

- i. Fillers on global crosslinking state of elastomer matrix,
- ii. Surface treatment on filler/matrix interactions.

Swelling test for filled samples has been performed under the same condition as for neat samples. Cyclohexane in contact with aluminum trihydrate is inert, so every possible interaction between them can be neglected.

The Flory-Rehner equation of swelling modified by Kraus has been used to calculate the concentration of elastically active chains [51]:

$$\nu = \frac{V_{r0} \ln(1-V_r) + \chi V_r^2 + V_r}{V_s \cdot 0.5V_r - V_r^{1/3} V_{r0}^{2/3}} \quad 3-28$$

- V_{r0} : volume fraction of polymer in swelled gel
- V_r : apparent volume fraction of polymer in swelled composite
- V_s : molar volume of solvent
- χ : Huggins solvent-polymer interaction parameter

A chemically inert filler establishes pure physical interactions with polymer chains at solid state. During swelling test, the solvent molecules penetrate through polymer network and reach filler/matrix interphase, dissolve the chains in contact with and trapped at filler surface, and thus remove the physical interactions between the filler particles and the polymer matrix. Consequently, the swelling ratio of a filled elastomer will be limited to elastomer network and, obviously, equal to that of non-filled samples. This phenomenon happens for PATH filled samples. As it is shown in Figure 3-37, the concentrations of elastically active chains for 33 phr and 100 phr PATH filled samples are equal to that of neat sample.

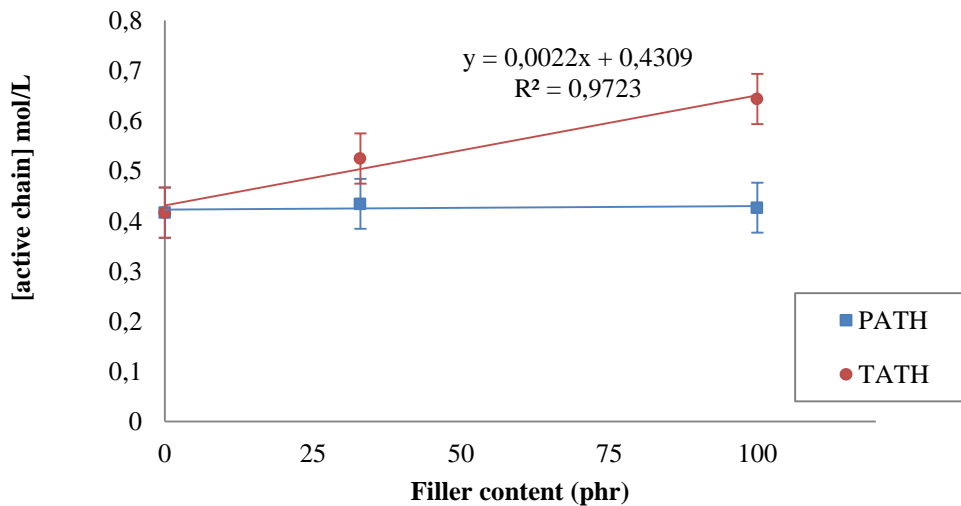
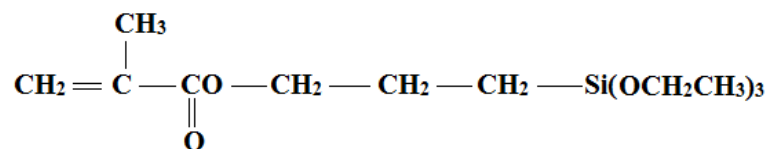


Figure 3-37 : Concentration of elastically active chains for neat and filled samples determined by swelling measurement

In the case of chemically reactive fillers, they can get involved in crosslinking network at filler/matrix interphase. As we can see in Figure 3-37, the concentration of apparent active chains increases with the concentration of incorporated fillers. Furthermore, this increasing shows to be linear and proportional to the fillers content. In fact, the increase in the number elastically active chains for 100

phr is twice that of 33 phr (we recall that 33phr and 100 phr represent 25 wt.-% and 50 wt.-% of filler, respectively).



Scheme 3-3: Vinyltriethoxysilane molecule (ATH surface treatment)

The difference between concentrations of elastically active chains for treated and pristine fillers, proposes the participation of surface treatment molecules (Scheme 3-3) in the crosslinking mechanism of filled gum. The double bond is at the extremity of the molecule and easily accessible by neighbor macroradicals. The crosslink made by opening the double bond, saves the radical. This reaction can be decomposed as follow:

- a) Transfer of the radical to a polymer chain by hydrogen abstraction and creating a macroradical,
- b) Addition of the radical to an ENB double bond, creating a crosslink and preserving the radical,
- c) Combination of radicals and crosslink formation.

The possibility of these three reactions can be accepted by considering the global mechanism of unsaturated elastomers, but the probability of each of them is not clear enough for the time being. Moreover, the surface treatment molecules can crosslink with their allylic hydrogens too.

The crosslinking mechanism on fillers surface is not clear yet. However, it was mentioned in chapter I that external double bonds (at the extremity of the chain) can reach a crosslinking yield superior than one. Therefore, one may conclude that the molecule in Scheme 3-3 can be responsible for more than one crosslink.

Through what has been discussed above, it can be concluded that the filler/matrix chemical interaction can form crosslinks at filler/matrix interface or at its vicinity. Anyhow, several questions remain still open: how dense is the concentration of crosslinking at filler matrix interphase? What is the functionality of these crosslinks? Are they influenced by filler's particle size? Etc.

3.3.2.3 Mechanical reinforcement by filler particles

Among diverse reasons for adding fillers into an elastomer, the most important is the improvement of elastomers' poor mechanical properties, which has a direct effect on the material's stiffness, and can

be quantified by measuring the Young's modulus. Several empirical equations have been proposed to model the reinforcing effect of filler particles in a composite material (see Chapter I, section 4) among which, the very best fittings are employed and compared with experimental data obtained from tensile testing. All approaches are the extensions of Smallwood's Equation (3-29) [52], which is an adaption of Einstein's colloidal solutions equation, for calculating the Young's modulus [53].

$$E = E_0(1 + 2.5\varphi) \quad 3-29$$

with:

- E : modulus of composite
- E_0 : modulus of rubber
- φ : filler volume fraction

The Smallwood's equation considers solely the hydrodynamic effect of the filler particles on polymer chains, and is applicable for low contents of filler. This model, as shown in Figure 3-38, obviously underestimates the reinforcing effect of fillers, and the deviation increases with filler volume fraction.

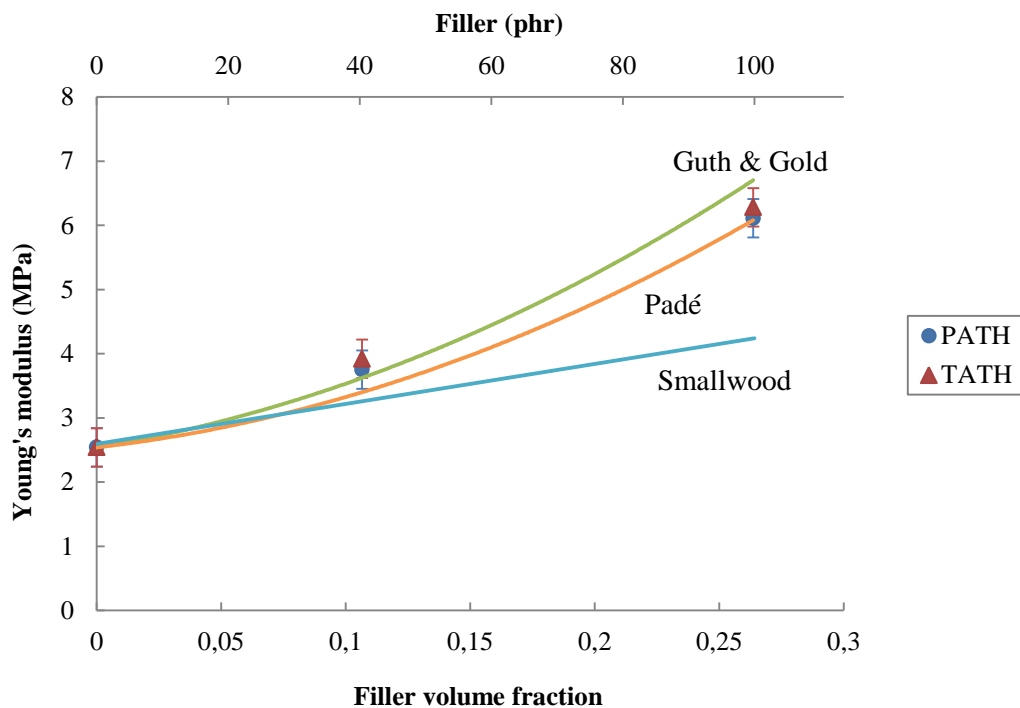


Figure 3-38 : Predictions of Young's modulus with frequently used mechanical theories for filled samples

To consider this deviation, a power series model was proposed, in which the second power term considers the interaction effect of particle pairs, the third power term the particle triplets, and so on [54]. The parameters of this model, however, are difficult to determine and depend on the shape of

fillers. In the simplest case, the particles are spherical and the factors have been numerically determined by Guth and Gold and validated for carbon black reinforced rubber [55] (Equation 3-30).

$$E = E_0(1 + 2.5\phi + 14.1\phi^2) \quad 3-30$$

Nevertheless, this model underestimates the reinforcement effect for 33 phr of ATH, and overestimates for 100 phr.

The best approximation, here, turns out to be a model of second order for which the factors are determined by a Padé approximation expressed as [56]:

$$E = E_0\left(1 + \frac{2.5\phi}{1-2\phi}\right) \quad 3-31$$

Although this model is the closest one and conveniently approximates the reinforcement at 100 phr, the underestimation at 33 phr prevents us to adopt this model, either. In fact, more careful examination of filler effect reveals a linear tendency in reinforcement effect of fillers in composites. This implies that in order to predict the toughening of the samples by a power series, the first power factor must be higher than 2.5 and the second power factor close to zero. The first power factor increases when the shape of filler particles recede from spherical, for examples, up to 8 for oblate particles [57]. However, in this study, the hexagonal ATH particles will be considered as spherical in a first approximation.

Another effect of fillers that has been the subject of several arguments is the study of polymer/matrix interphase. The properties and structure of fillers can affect the properties of polymer matrices at the vicinity of particles by forming a layer of matrix (interphase) around the particles which shows altered properties comparing to the matrix bulk. These effects can be due to physical interactions (polarity of filler surface), chemical interactions (formation of chemical bonds at the interface) or mechanical interactions (roughness), and can influence the global properties of composite. Determination of thickness and mechanical properties of this interphase, called "bound rubber" too, was the subject of several researches [56, 58-60].

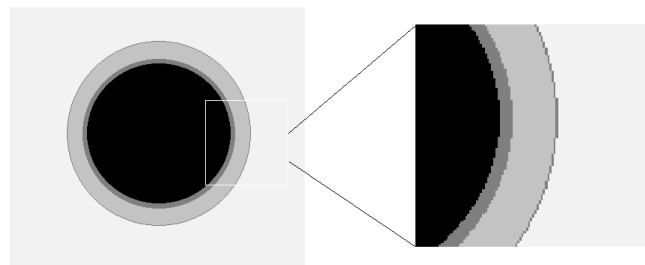


Figure 3-39: Two-layered "bound rubber"

In an almost recent paper, Fukahori proposed a two-phased bound rubber model which can convincingly explain some phenomena for elastomers under a tensile stress [61]. The principles of this model is based on existence of a first "glassy hard" thin layer of rubber in direct contact with filler surface, followed by a second thicker "sticky hard" rubber layer (Figure 3-39). An attempt has been made to adapt this model to our case.

The EPDM elastomer in ATH filled samples exists in three forms:

- 1) Matrix network: the fraction of EPDM in the composite whose properties are not affected by filler particles.
- 2) Interphase network: the fraction of EPDM in the composite affected by filler particles, which the same as sticky hard layer.
- 3) Glassy hard layer: the small fraction of EPDM in direct contact with filler particles.

At low strains, the presence of glassy hard layer acts similar as having chemically bonded interphase. This can explain the similar Young's moduli for both pristine and surface treated fillers.

Based on what has been explained, stress hardening in filled samples is dedicated to hydrodynamic effects of filler particles and higher modulus of sticky hard rubber network. Therefore, by eliminating the hydrodynamic effect, what remains is the superposition of double-phase (matrix plus interphase) polymer modulus E_p .

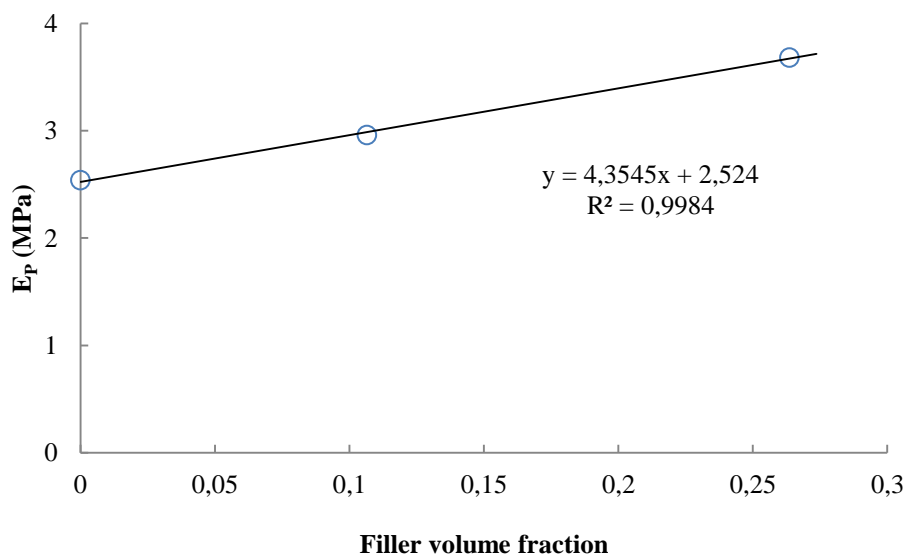


Figure 3-40: Young's modulus of double-phase polymer E_p as a function of volume fraction of filler ϕ

The evolution of E_p as a function of filler volume fraction is plainly linear (Figure 3-40), imposing that EPDM matrix, with its modulus E_M , and interphase, with its modulus E_i , are connected in a parallel system obeying Equation 3-32:

$$E_p = E_M \varphi_M + E_i \varphi_i \quad 3-32$$

where φ_M is the volume fraction of matrix and φ_i the volume fraction of interphase. Considering $\varphi_M + \varphi_i = 1$, the Equation 3-32 becomes:

$$E_p = E_M(1 - \varphi_i) + E_i \varphi_i$$

$$\Rightarrow E_p = (E_i - E_M) \varphi_i + E_M \quad 3-33$$

The validity of the argument above is evident by considering two interpenetrating network of polymer matrix and interphase, as shown in Figure 3-41.

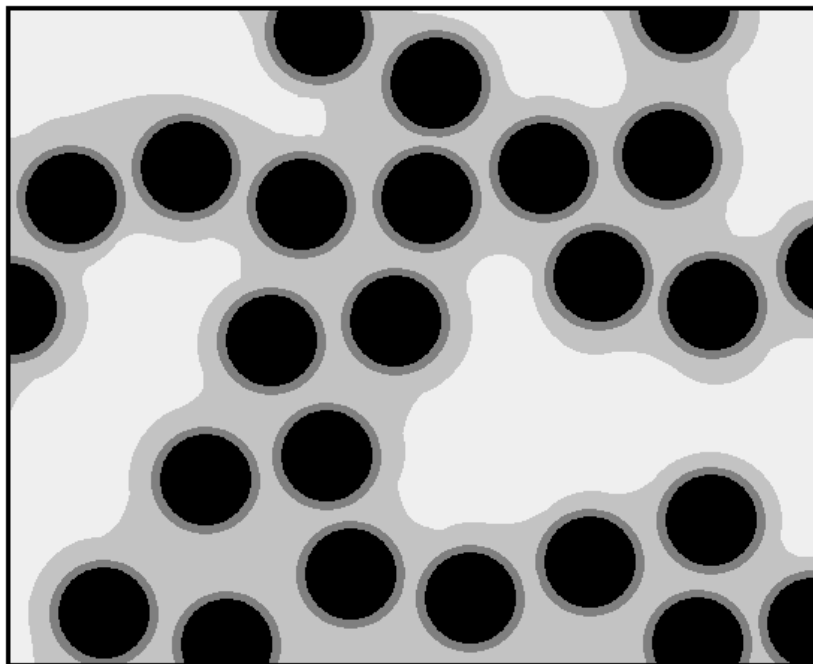


Figure 3-41: 2D presentation of interpenetrating networks of matrix and interphase according to literature data^[61, 62]

The calculation of modulus and thickness of interphase in a first approach is based on the following hypotheses:

- i. The modulus of the filler is much higher than those of matrix and interphase network that no deformation happens for rigid particles ($E_{ATH} = 70$ GPa).

- ii. The thickness of glassy hard rubber is very low compared to sticky interphase and rubber matrix, so its volume fraction is negligible.
- iii. The deformation happens only in the matrix and interphase networks.

The linearity of E_p with φ permits to write the following Equation (3-34):

$$E_p = \psi\varphi + E_{p_0} \quad 3-34$$

where ψ is the slope of the regression line in Figure 3-40 and E_{p_0} is equal to E_M .

On the other hand, if the average thickness of interphase on mono-dispersed spherical filler particle of diameter D is equal to i , then φ_i can be estimated by Equation 3-35:

$$\varphi_i = \varphi \frac{6i}{D} \quad 3-35$$

By replacing the value of φ_i in Equation 3-33 we finally have:

$$E_p = \frac{6i}{D}(E_i - E_M)\varphi + E_M \quad 3-36$$

Such a simplified model can be used to tentatively explain the elastic behavior of the filled EPDM under study. However, the thickness of the interphase and its modulus are not determined. Although some estimation will be subsequently proposed in the following chapter, it would be of a great interest for further studies to experimentally determine these parameters for EPDM samples filled with both pristine and treated ATH.

3.3.3 Macroscopic scale-Tensile testing

The effect of ATH fillers on tensile properties of EPDM composites is presented in Figure 3-42, in comparison with neat EPDM network, and the quantitative values are presented in Table 3-28.

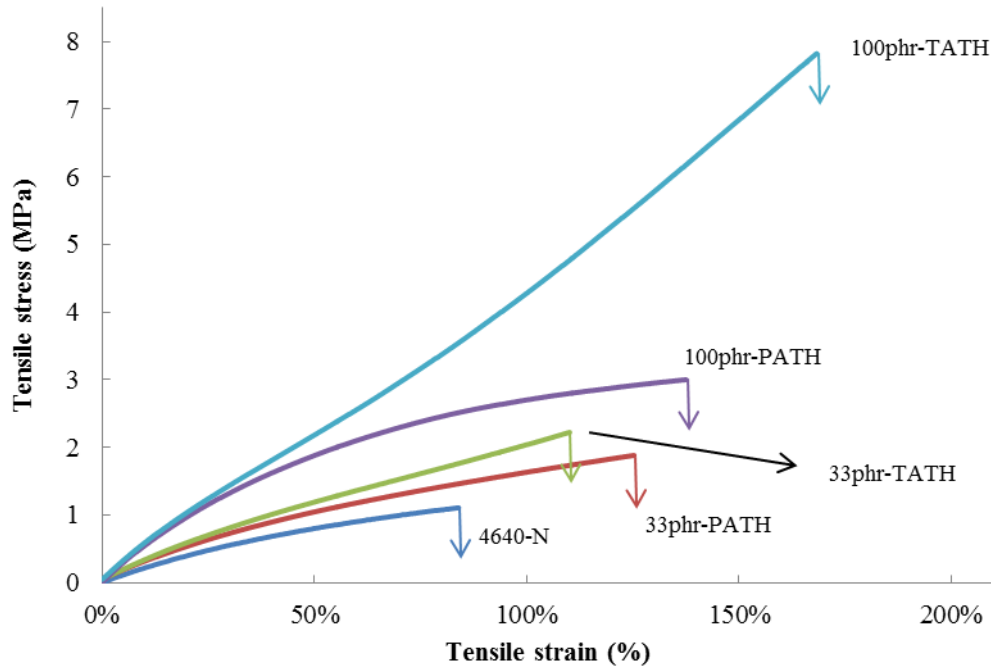


Figure 3-42 : Stress-strain curves of neat and filled EPDM samples

Introduction of 33phr of ATH particles slightly increases the Young's modulus comparing to neat samples. At low strains ($\epsilon < 20\%$), the stress-strain curves of PATH and TATH filled samples superpose, confirming the aforesaid idea that at low strains the glassy hard layer acts like chemical bonding. However, beyond 30% of strain, the curve of TATH filled sample begins to diverge to higher values of modulus. The same behavior is detectable for 100 phr filled samples. As the only difference between these two composite families is the absence or the presence of filler surface treatment, it is licit to attribute this divergence to covalent chemical bonds at the filler/matrix surface.

Sample	Young's Modulus (MPa)	Elongation at break
4640-N	2.54 ± 0.1	85 ± 10
33phr-PATH	3.75 ± 0.1	125 ± 14
33phr-TATH	3.92 ± 0.1	110 ± 18
100phr-PATH	6.11 ± 0.1	138 ± 26
100phr-TATH	6.28 ± 0.3	168 ± 31

Table 3-28 : Young's modulus and elongation at break for neat and filled EPDM samples

From a macromolecular point of view, the polymer chains and filler particles begin to move under the exerted force. Under the extension, the polymer chains tend to rearrange for stress relaxation, which leads to local movement of chains regarding to filler particles. In case of PATH filled EPDM, these local movements can lead to partial decohesion of chains from filler particles, which indeed facilitates

the stress relaxation. On the contrary, in the case of TATH filled samples, the strong covalent bonds allow no decohesion, and consequently no stress relaxation is observed. This will lead to a stress thickening phenomenon observed for TATH filled samples. In the same manner, the ultimate elongation at break increases with filler concentration.

Conclusion

In this chapter, the crosslinking of EPDM with peroxide has been studied with various methods at different structural scales. A crosslinking mechanistic scheme has been proposed based on two different approaches at molecular scale: FTIR spectrophotometry and differential scanning calorimetry. The results of these two methods have shown to be convincingly close. Succeeding to the crosslinking mechanism, a kinetic scheme has been derived and the corresponding system of differential equations has been numerically solved. The outcomes of numerical simulation were in a good agreement with the experimental data.

In order to determine the structure of the EPDM network, the crosslink densities of the three EPDMs matrices under study have been measured through three different methods at macromolecular scale. The results of these three methods have shown to be very similar. Furthermore, the crosslink density calculated by the kinetic model is placed within the measurement error interval of the experimental results.

The effect of ATH fillers on DCP crosslinking of EPDM has shown to be dependent on the presence of chemically active molecules at their surface. Pristine filler has no effect on the crosslinking mechanism of EPDM matrix in composite while, in the case of surface treated fillers, the sizing molecules get chemically involved in crosslinking, providing higher crosslink densities.

The reinforcement effect of ATH filler particles in ATH/EPDM composites could not be modeled by conventional empirical theories. A fairly new model, which is based on a two-phased interphase, was employed. It satisfactorily demonstrates the reinforcing ability of filler particles. This model will be more detailed in following chapters throughout aging of ATH/EPDM composites. Thanks to this model, a new method is proposed to calculate the thickness and Young's modulus of the corresponding interphase.

References

1. Silverstein, R.M., G.C. Basler, and T.C. Morill, *Identification spectrométrique de composés organiques*. 2004: De Boeck Université.
2. Lin, V.D., et al., *The handbook of infrared and raman characteristic frequencies of organic molecules*. 1991, Academic Press, New York. p. 68.
3. D3900, *Standard Test Methods for Rubber-Determination of Ethylene Units in Ethylene-Propylene Copolymers (EPM) and in Ethylene-Propylene-Diene Terpolymers (EPDM) by Infrared Spectrometry*. ASTM.
4. Lin, V.D., et al., *The handbook of infrared and raman characteristic frequencies of organic molecules*. 1991, Academic Press, New York.
5. McMurry, H.L. and V. Thornton, *Correlation of infrared spectra*. Analytical Chemistry, 1952. **24**(2): p. 318-334.
6. M. Avram, G.D.M., *Infrared spectroscopy: applications in organic chemistry*. 1972.
7. Rivaton, A., S. Cambon, and J.L. Gardette, *Radiochemical aging of ethylene-propylene-diene monomer elastomers. I. Mechanism of degradation under inert atmosphere*. Journal of Polymer Science Part A: Polymer Chemistry, 2004. **42**(5): p. 1239-1248.
8. Rivaton, A., S. Cambon, and J.L. Gardette, *Radiochemical ageing of EPDM elastomers.: 2. Identification and quantification of chemical changes in EPDM and EPR films gamma-irradiated under oxygen atmosphere*. Nuclear Instruments and Methods in Physics Research Section B: Beam Interactions with Materials and Atoms, 2005. **227**(3): p. 343-356.
9. Van Krevelen, D.W. and K. Te Nijhuis, *Properties of polymers: their correlation with chemical structure; their numerical estimation and prediction from additive group contributions*. 2009: Elsevier Science.
10. Zhu, B., B. Fang, and X. Li, *Dehydration reactions and kinetic parameters of gibbsite*. Ceramics International, 2010. **36**(8): p. 2493-2498.
11. Kranenburg, J.M., M. Van Duin, and U.S. Schubert, *High-Throughput Kinetic Study of Peroxide Curing of EPDM Rubber*. Rubber Chemistry and Technology, 2011. **84**(1): p. 101-113.
12. Brazier, D.W. and G.H. Nickel, *Thermoanalytical Methods in Vulcanizate Analysis I. Differential Scanning Calorimetry and the Heat of Vulcanization*. Rubber Chemistry and Technology, 1975. **48**(1): p. 26-40.
13. Van der Hoff, B.M.E., *Reactions between Peroxide and Polydiolefins*. Industrial & Engineering Chemistry Product Research and Development, 1963. **2**(4): p. 273-278.
14. Loan, L.D., *Crosslinking efficiencies of dicumyl peroxide in unsaturated synthetic rubbers*. Journal of Applied Polymer Science, 1963. **7**(6): p. 2259-2268.
15. Imoto, M., K. Takemoto, and M. Kono, *A kinetic study on the reaction of dicumyl peroxide with some low α -olefin rubbers*. Die Angewandte Makromolekulare Chemie, 1967. **1**(1): p. 78-91.
16. Lu, K.T., et al., *Investigation of the decomposition reaction and dust explosion characteristics of crystalline dicumyl peroxide*. Process Safety and Environmental Protection, 2010. **88**(5): p. 356-365.
17. Wu, K.W., H.Y. Hou, and C.M. Shu, *Thermal phenomena studies for dicumyl peroxide at various concentrations by DSC*. Journal of thermal analysis and calorimetry, 2006. **83**(1): p. 41-44.
18. Brazier, D.W. and N.V. Schwartz, *The cure of elastomers by dicumyl peroxide as observed in differential scanning calorimetry*. Thermochemica Acta, 1980. **39**(1): p. 7-20.
19. Khelidj, N., et al., *Oxidation of polyethylene under irradiation at low temperature and low dose rate. Part I. The case of pure radiochemical initiation*. Polymer degradation and stability, 2006. **91**(7): p. 1593-1597.
20. Khelidj, N., et al., *Oxidation of polyethylene under irradiation at low temperature and low dose rate. Part II. Low temperature thermal oxidation*. Polymer degradation and stability, 2006. **91**(7): p. 1598-1605.

21. Colin, X., et al., *About a quasi-universal character of unstabilised polyethylene thermal oxidation kinetics*. Polymer degradation and stability, 2003. **80**(1): p. 67-74.
22. Sarrabi, S., X. Colin, and A. Tcharkhtchi, *Dégradation thermique du polypropylène au cours du rotomoulage*. Matériaux & Techniques, 2008. **96**(6): p. 281-294.
23. Calvert, J.G. and J.N. Pitts, *Photochemistry*. 1966: John Wiley & Sons.
24. Kelter, P., M. Mosher, and A. Scott, *Chemistry: the practical Science*. Vol. 10. 2008: Brooks/Cole Publishing Company.
25. Morrison, R.T. and R.N. Boyd, *Organic Chemistry*. 6th ed. 1992.
26. Bailey, H.C. and G.W. Godin, *The thermal decomposition of dibenzoyl and di- \hat{I} -cumyl peroxides in cumene*. Transactions of the Faraday Society, 1956. **52**: p. 68-73.
27. Khelidj, N., et al., *Oxidation of polyethylene under irradiation at low temperature and low dose rate. Part II. Low temperature thermal oxidation*. Polymer Degradation and Stability, 2005. **91**(7): p. 1598-1605.
28. Robbins, D., et al., *Experimental evaluation of nonisothermal, first-order reaction kinetics*. Macromolecules, 1995. **28**(26): p. 8729-8734.
29. Dixon, K., *II. Polymerization and Depolymerization-Decomposition Rates of Organic Free Radical Initiators in*. Polymer Handbook-4nd Edition (Ed. Brandrup, J., Immergut, EH, Grulke, EA, Pub. John Wiley & Sons, New York) Chap. II, 1999.
30. Antonovskii, V.L. and S.L. Khursan, *Thermolysis of organic peroxides in solution*. Russian chemical reviews, 2007. **72**(11): p. 939.
31. Wu, K., H. Hou, and C. Shu, *Thermal phenomena studies for dicumyl peroxide at various concentrations by DSC*. Journal of thermal analysis and calorimetry, 2006. **83**(1): p. 41-44.
32. Buback, M., M. Kling, and S. Schmatz, *Decomposition of tertiary alkoxy radicals*. Zeitschrift für Physikalische Chemie, 2005. **219**(9): p. 1205-1222.
33. Baignee, A., et al., *Absolute rate constants for reactions of cumyloxy in solution*. Journal of the American Chemical Society, 1983. **105**(19): p. 6120-6123.
34. Denisov, E.T. and I.B. Afanas' ev, *Oxidation and antioxidants in organic chemistry and biology*. 2005: CRC.
35. Colin, X., L. Audouin, and J. Verdu, *Kinetic modelling of the thermal oxidation of polyisoprene elastomers*. Polymer Degradation and Stability, 2007. **92**(5): p. 886-897.
36. Likozar, B. and M. Krajnc, *Simulation of chemical kinetics of elastomer crosslinking by organic peroxides*. Polymer Engineering & Science, 2009. **49**(1): p. 60-72.
37. Kelley, F.N. and F. Bueche, *Viscosity and glass temperature relations for polymer-diluent systems*. Journal of Polymer Science, 1961. **50**(154): p. 549-556.
38. Simha, R. and R.F. Boyer, *On a general relation involving the glass temperature and coefficients of expansion of polymers*. The Journal of Chemical Physics, 1962. **37**(5): p. 1003-1007.
39. G'Sell, C., et al., *Introduction à la mécanique des polymères*. 1995.
40. Fox, T.G. and P.J. Flory, *Second-order transition temperatures and related properties of polystyrene. I. Influence of molecular weight*. Journal of Applied Physics, 1950. **21**(6): p. 581-591.
41. Bicerano, J., *Prediction of polymer properties*. 2002: CRC.
42. Baldwin, F.P., P. Borzel, and H.S. Makowski, *The Correlation between Entanglement and Chemical Crosslinks in EPDM Vulcanizates*. Rubber Chemistry and Technology, 1969. **42**(4): p. 1167-1174.
43. Flory, P.J., *Principles of polymer chemistry*. 1953: Cornell University Press.
44. Verdu, J. and X. Colin, *Structures macromoléculaires tridimensionnelles*. 1993: Ed. Techniques Ingénieur.
45. Carman, C.J. and C.E. Wilkes, *Monomer sequence distribution in ethylene propylene elastomers. I. Measurement by carbon-13 nuclear magnetic resonance spectroscopy*. Rubber Chemistry and Technology, 1971. **44**(3): p. 781-804.
46. Ray, G.J., P.E. Johnson, and J.R. Knox, *Carbon-13 nuclear magnetic resonance determination of monomer composition and sequence distribution in ethylene-propylene copolymers prepared with a stereoregular catalyst system*. Macromolecules, 1977. **10**(4): p. 773-778.

47. Kakugo, M., et al., *Carbon-13 NMR determination of monomer sequence distribution in ethylene-propylene copolymers prepared with δ -titanium trichloride-diethylaluminum chloride*. *Macromolecules*, 1982. **15**(4): p. 1150-1152.
48. Davison, S. and G.L. Taylor, *Sequence length and crystallinity in alpha-olefin terpolymers*. *British Polymer Journal*, 1972. **4**(1): p. 65-82.
49. Alshuth, T., F. Abraham, and S. Jerrams, *Parameter dependence and prediction of fatigue properties of elastomer products*. *Rubber Chemistry and Technology*, 2002. **75**(4): p. 635-642.
50. Ha-Anh, T. and T. Vu-Khanh, *Prediction of mechanical properties of polychloroprene during thermo-oxidative aging*. *Polymer testing*, 2005. **24**(6): p. 775-780.
51. Kraus, G., *Swelling of filler • reinforced vulcanizates*. *Journal of Applied Polymer Science*, 1963. **7**(3): p. 861-871.
52. Smallwood, H.M., *Limiting law of the reinforcement of rubber*. *Journal of Applied Physics*, 1944. **15**(11): p. 758-766.
53. Einstein, A., *Eine neue Bestimmung der Moleküldimensionen*. *Annalen der Physik*, 1906. **324**(2): p. 289-306.
54. Guth, E., *Theory of filler reinforcement*. *Journal of Applied Physics*, 1945. **16**(1): p. 20-25.
55. Guth, E. and O. Gold, *On the hydrodynamical theory of the viscosity of suspensions*. *Phys. Rev*, 1938. **53**(322): p. 2.
56. Heinrich, G., M. Klüppel, and T.A. Vilgis, *Reinforcement of elastomers*. *Current opinion in solid state and materials science*, 2002. **6**(3): p. 195-203.
57. Simha, R., *A treatment of the viscosity of concentrated suspensions*. *Journal of Applied Physics*, 1952. **23**(9): p. 1020-1024.
58. Choi, S.S., *Filler-polymer interactions in both silica and carbon black-filled styrene-butadiene rubber compounds*. *Journal of Polymer Science Part B: Polymer Physics*, 2001. **39**(4): p. 439-445.
59. Mélé, P., et al., *Reinforcement effects in fractal-structure-filled rubber*. *Polymer*, 2002. **43**(20): p. 5577-5586.
60. Medalia, A.I., *Morphology of aggregates: VI. Effective volume of aggregates of carbon black from electron microscopy; Application to vehicle absorption and to die swell of filled rubber*. *Journal of Colloid and Interface Science*, 1970. **32**(1): p. 115-131.
61. Fukahori, Y., *New progress in the theory and model of carbon black reinforcement of elastomers*. *Journal of applied polymer science*, 2004. **95**(1): p. 60-67.
62. Berriot, J., et al., *Gradient of glass transition temperature in filled elastomers*. *EPL (Europhysics Letters)*, 2003. **64**(1): p. 50.

CHAPTER IV

4 Aging of EPDM & Composites **Molecular and Macromolecular Aspects**

Extended abstract (in French language)

Dans le chapitre précédent la réticulation de la matrice EPDM par le peroxyde de dicumyle a été étudiée, offrant une vision plus claire de l'état initial des échantillons avant leur exposition à un vieillissement accéléré. En outre, la présence de la charge ATH et son impact sur la structure et les propriétés mécaniques ont été étudiés. Ce chapitre est consacré à l'étude de la thermo- et radio-oxydation de la matrice EPDM pure et chargée aux échelles moléculaire et macromoléculaire. On rappelle brièvement que les échantillons sont soumis à des sollicitations thermiques à 90, 110 et 130°C, et radiochimiques à 0,1, 1 et 10 kGy.h⁻¹ dans l'air. Dans une première approche mécanistique, le vieillissement est étudié à l'échelle moléculaire au travers de la formation des produits d'oxydation. Par la suite, les conséquences de l'oxydation sur les propriétés macromoléculaires, ainsi que l'effet des charges ATH et de leur traitement de surface, sont étudiées.

Les résultats obtenus dans ce chapitre peuvent être résumés comme suit. Les paramètres cinétiques de la thermo-oxydation de l'EPDM pur ont été déterminés pour les trois matrices EPDM de l'étude. Ces données et, en particulier, les paramètres cinétiques de la consommation des doubles liaisons ENB, peuvent être maintenant utilisés pour compléter le modèle de vieillissement de thermo-radio-oxydation précédemment établi pour la famille des copolymères éthylène-propylène (EPR) au laboratoire PIMM. En outre, l'augmentation de la température provoque un contrôle de l'oxydation par la diffusion d'oxygène à partir de 110°C. Ce changement cinétique conduit à une hétérogénéité de l'oxydation, qui s'exprime par la création d'une couche superficielle oxydée (Figure III).

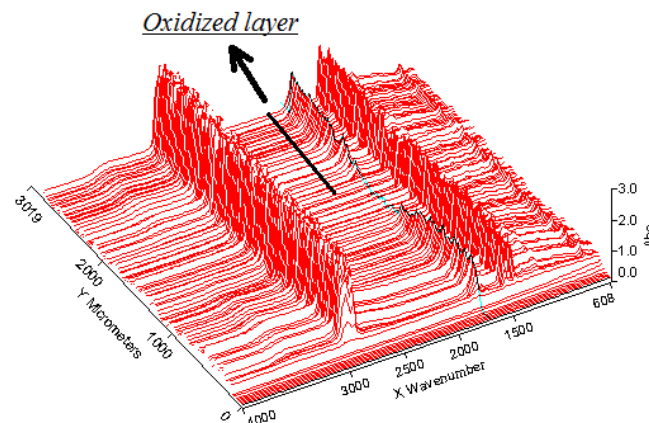
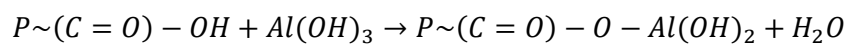


Figure III : Mise en évidence de la couche superficielle oxydée d'une plaque de matrice EPDM pure vieillie pendant 800 heures sous air à 110°C

De la même manière, en investiguant l'effet du débit de dose d'irradiation sur les échantillons, une zone de transition entre les régimes cinétiques dominés par un vieillissement radiochimique pur et un vieillissement radio-thermique a été observée pour des débits de dose d'irradiation compris entre 10 kGy.h⁻¹ et 0,1 kGy.h⁻¹.

L'analyse des courbes cinétiques de formation des hydroperoxydes révèle que la vitesse de formation des hydroperoxydes diminue avec l'augmentation du taux de charges ATH. En outre, la formation des hydroperoxydes est plus intense dans les matrices EPDM chargées par des ATH traitées en surface. D'autre part, les essais de gonflement montrent que la densité de réticulation augmente pendant l'oxydation, ce qui est attribué en partie au changement du paramètre d'interaction polymère/solvant. Toutefois, un examen plus précis du taux de gonflement révèle qu'un second phénomène se produit et diminue le taux de gonflement. Il est donc proposé qu'une réaction chimique entre les produits d'oxydation et les fonctions chimiques de la surface des charges, soit responsable de la densification du réseau de l'interphase charge/matrice. Le mécanisme proposé consiste en une condensation entre un acide carboxylique et une fonction hydroxyle de la surface des charges :



L'hypothèse d'une réaction chimique sur la surface de la charge peut convenablement expliquer les phénomènes observés dans ce chapitre. Cependant, cette approche soulève plusieurs questions qui constituent les perspectives futures de cette étude:

- Quel est le mécanisme chimique exact responsable des interactions charge/matrice?
- Comment la réaction chimique densifie-t-elle le réseau de l'interphase?
- Quel est le rôle du traitement de surface des charges? ...

Le prochain chapitre sera consacré à l'étude des conséquences des modifications macromoléculaires sur les propriétés mécaniques (propriétés élastiques et à la rupture) des matrices EPDM pures et chargées. Le module d'Young nous permettra de déterminer les variations de la concentration des chaînes élastiquement actives. Ces résultats seront ensuite comparés à ceux obtenus par la méthode de gonflement.

Introduction

In the previous chapter, the DCP crosslinking of EPDM was investigated, providing a clearer view of the initial state of the samples before exposure to accelerated aging. Furthermore, the presence of ATH fillers and their impact on structural and mechanical properties was introduced. This chapter is dedicated to thermal and radiochemical oxidation of neat EPDM matrix and its composites at molecular and macromolecular scales. We briefly remind that samples are exposed under thermal stress at 90, 110 and 130°C, and radiochemical aging under 0.1, 1 and 10 kGy.h⁻¹ in air. In a first mechanistic approach, the aging at molecular scale is surveyed by following the formation of oxidation products. Subsequently, the consequences of oxidation on macromolecular properties, as well as the effect of fillers and their surface treatment are discussed.

4.1 Molecular aspects of thermal aging of EPDM

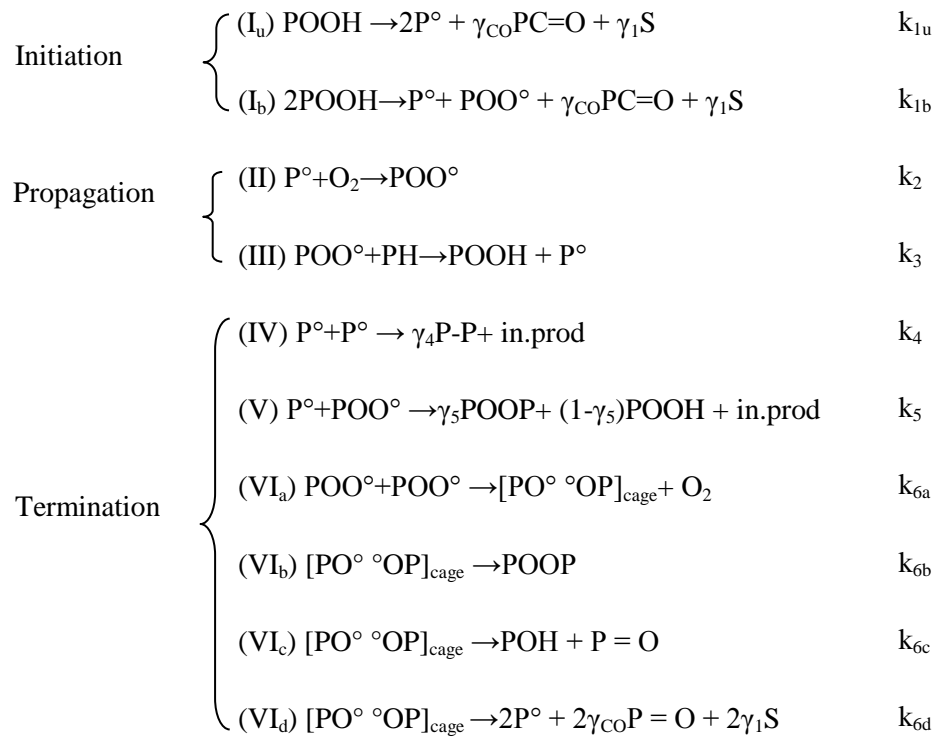
As a general rule, the oxidation is diffusion controlled. However, when the sample thickness becomes thin enough, oxygen diffusion into the sample's bulk can be considered as instantaneous, which induces a homogeneous oxidation all over the sample. In such a condition, the accurate mechanism of oxidation can be investigated and kinetic parameters can be determined through common laboratory analytical methods which, in this case, are thermogravimetric analysis and FTIR spectrophotometry.

4.1.1 Thermogravimetric analysis

In this section, the weight changes of EPDM samples exposed to accelerated aging at high temperatures in air have been studied.

4.1.1.1 Mass variations

According to the general mechanism presented in chapter I, the thermal oxidation reactions are regrouped into three distinct steps: initiation, propagation and termination. This oxidation mechanism is briefly recalled below:



In the course of aging, the weight of a sample changes in two ways:

- i. Sample gains weight by oxygen absorption according to equation II in propagation step (reaction II),
- ii. Sample loses weight by freeing an oxygen molecule (reaction VI_a) or other volatile products (reactions I_a, I_b and VI_d such as water, carbon monoxide and dioxide, etc.).

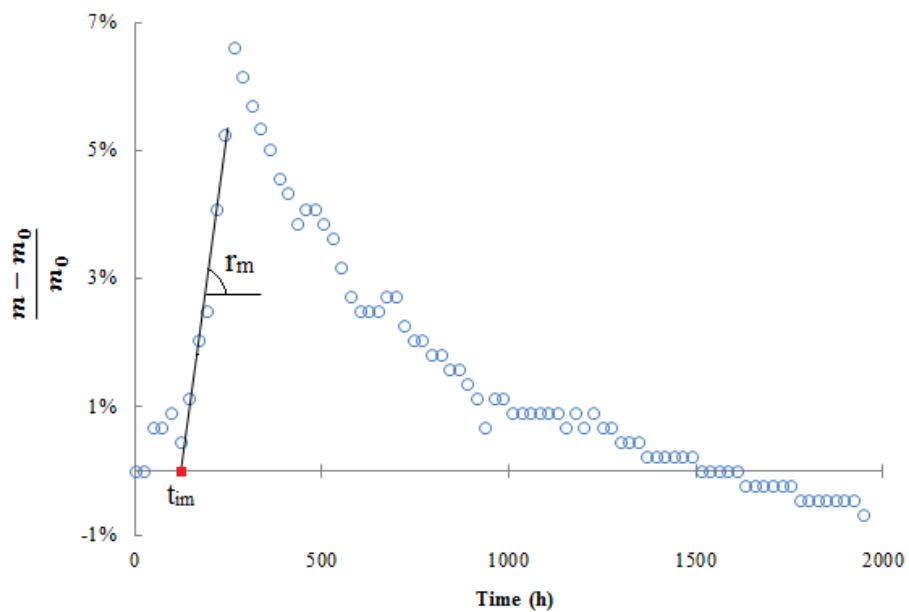


Figure 4-1: Weight changes of Nordel 4640 exposed at 90°C in air (sample thickness ~ 100µm)

After a short induction time t_{im} , the rate of oxygen absorption increases in an auto-accelerated way and reaches its highest value r_m , which is the maximum slope of the ascent (Figure 4-1). At this stage, the hydroperoxides concentration and their thermal decomposition rate, based on reactions I_u and I_b , are at their maximum (steady-state). This leads to the formation of more macroradicals and sharply accelerates the oxygen consumption and formation of volatile products. At the peak of thermogravimetric diagram, the rates of oxygen absorption and products formation becomes equal, resulting in r_m equal to zero. This balance does not last long and the weight of sample begins to decrease while formation of volatile products becomes predominant. As the aging progresses, the concentration of active sites decreases and leads to a progressive decline of the weight loss rate.

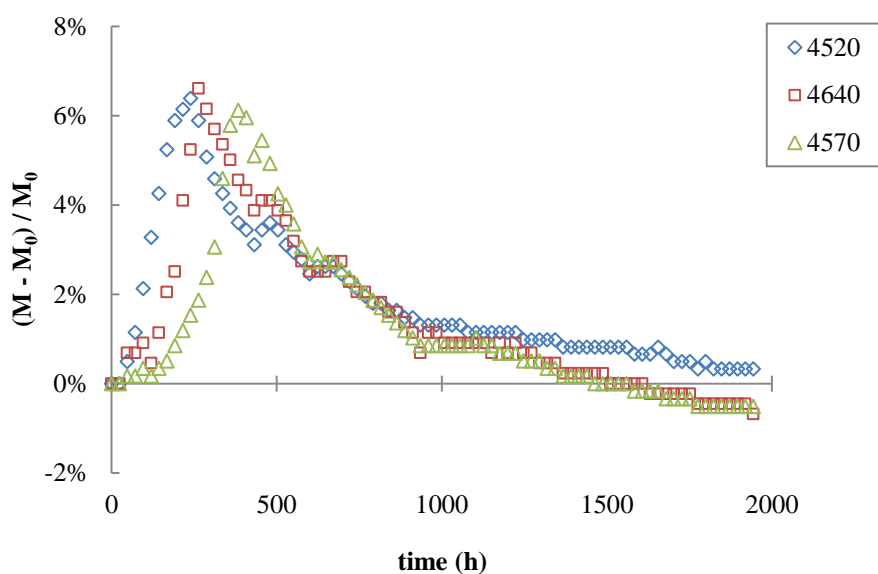


Figure 4-2: Weight changes for the three EPDM samples under study in air at 90°C (sample thickness ~ 100μm)

The same behavior is observed for the two other EPDM samples under study (Figure 4-2). The three EPDMs show a little difference in t_{im} , which is presumably due to the residual concentrations of antioxidants introduced into EPDMs by the polymer producer. Anyhow, r_m is approximately the same for the three EPDMs, which is related to the close chemical structure of samples (the calculated values of r_m are presented in next section).

4.1.1.2 Temperature effect

Similar to every chemical reaction, the global physico-chemical properties, such as oxygen absorption, are affected by variations in temperature. This effect is clearly noticeable in Figure 4-3.

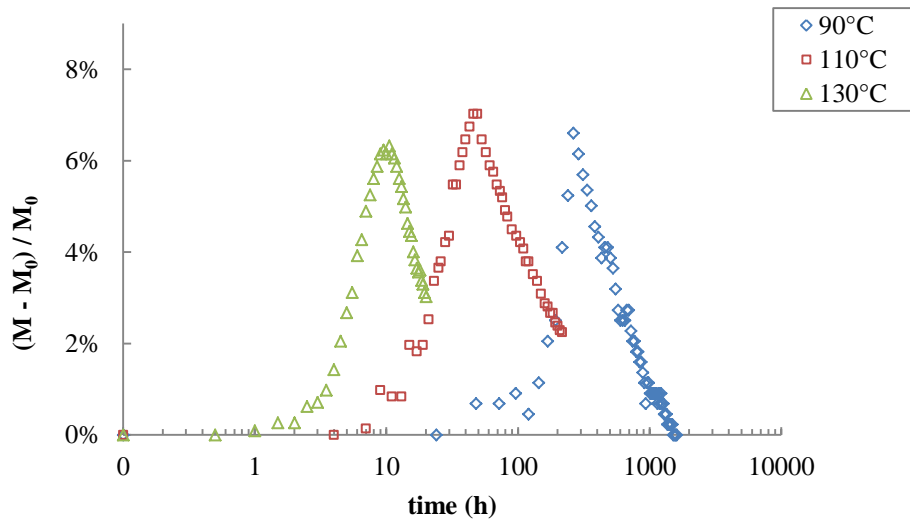


Figure 4-3: Temperature effect on thermogravimetric curves of Nordel 4640 in air (sample thickness $\sim 100\mu\text{m}$)

As the temperature rises, the hydroperoxidation and the radical formation are accelerated, leading to shorter induction times. Consequently, the thermogravimetric diagram reaches faster its maximum value, followed by a faster weight loss. As the weight changes are thermally activated, the values of t_{im} can be plotted in an Arrhenius diagram (Figure 4-4).

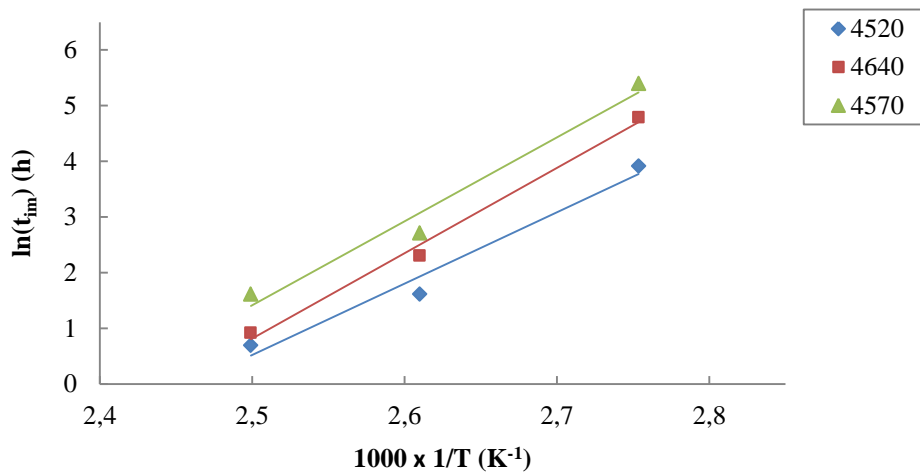


Figure 4-4: Arrhenius graph of t_{im} between 90 and 130°C for the three EPDMs under study

In the same manner as in Figure 4-1, r_m can be measured for other EPDMs under study. Between 90 and 130°C, the r_m obeys an Arrhenius law, and the corresponding diagrams show that the maximum rates of oxygen absorption are similar for the three EPDMs (Figure 4-5).

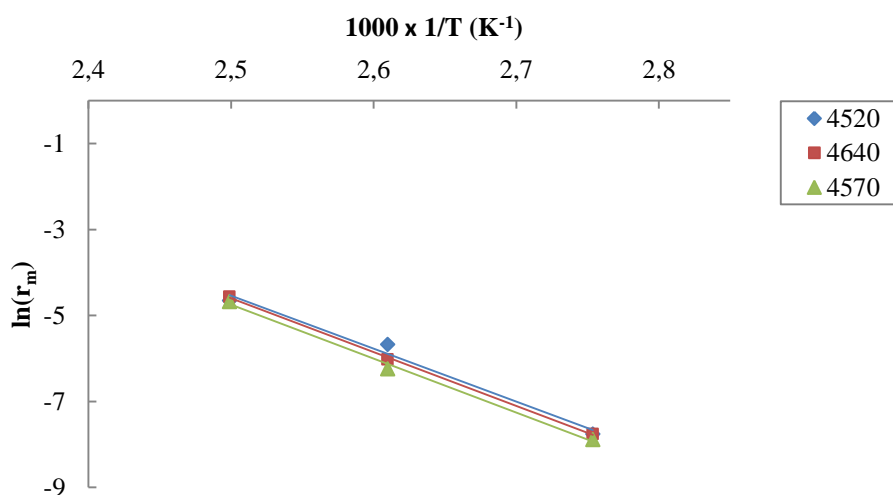


Figure 4-5: Arrhenius graph of r_m in air between 90 and 130°C for the three EPDMs under study

The linear regression of r_m values, allows calculating the parameters of the Arrhenius equation ($\ln r_m = \ln r_{m_0} - \frac{E_a}{RT}$) for the three samples (Table 4-1).

Nordel	(E_a) (kJ.mol ⁻¹)	($\ln r_{m_0}$)
4520	102	26.25
4640	104	26.75
4570	104	26.58

Table 4-1: Arrhenius parameters of r_m in air between 90 and 130°C for the three EPDMs under study

As explained in the previous chapter, methylenic C – H bonds and ENB double bonds are the most susceptible sites to be attacked by radicals. The next section will be devoted to the study of ENB double bonds consumption.

4.1.2 FTIR spectrophotometry

The FTIR spectrophotometry is a simple and reliable method to measure and follow the variations in concentration of chemical functions of the EPDMs under study. Thin (~100µm) films of crosslinked EPDM have been used to study the variations in the concentration of double bonds and the oxidation products. We recall that the samples used for this method are exactly the same as the ones used for thermogravimetric analysis, in order to have the best correlation between results.

4.1.2.1 Consumption of double bonds

It has been demonstrated in previous chapter that the ENB double bonds are far away from being totally consumed during peroxide crosslinking. The results of FTIR spectrophotometry have revealed

that the concentration of double bonds decreases throughout aging. In this section, it has been tried to explain the mechanism of double bonds consumption through a literature review. This explanation stands for both thermal and radiochemical exposure.

4.1.2.1.1 Mechanism of ENB double bonds consumption

Ethylidene norbornene double bonds, which are of vinylidene type, have an FTIR absorption band around 809 cm^{-1} assigned to the C – H groups of double bond. Exposure of samples to accelerated aging at high temperatures leads to a decrease in absorption intensity at the aforesaid wavelength (Figure 4-6).

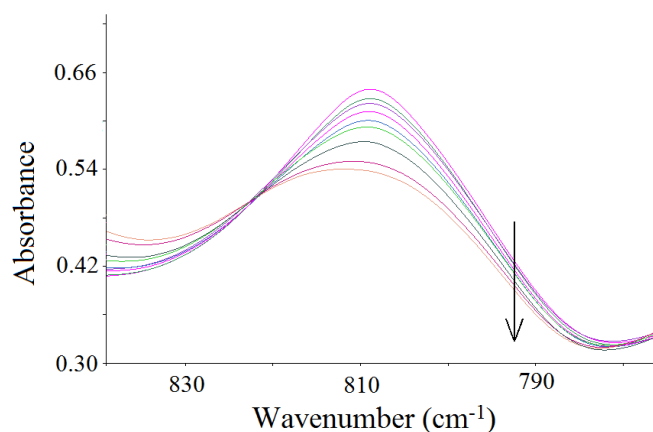
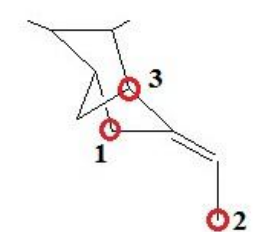


Figure 4-6: Decrease in the ENB double bond absorption at 809 cm^{-1} (Nordel 4640 ~ $100\mu\text{m}$, at 130°C , in air)

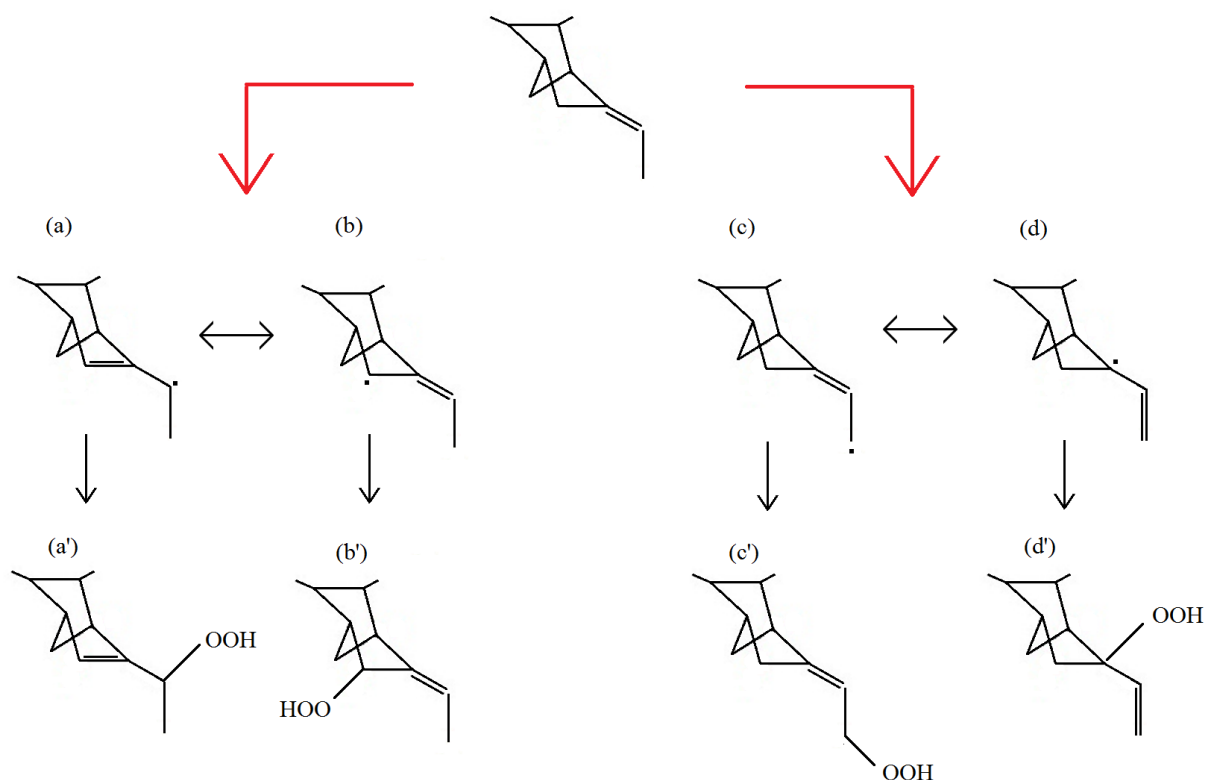
Confronting a radical attack on a hydrocarbon chain, the most labile hydrogens (allylic in this case) are the most susceptible to be abstracted by a peroxy radical to form macroradicals. The allylic hydrogens are at α -position from double bond, where the formed radical is stabilized due to resonance. ENB units possess three α -positions, schematized in Scheme 4-1.



Scheme 4-1: Reactive allylic radicals in an ENB unit

As previously explained (Chapter I, Section 3.4), the position 3 cannot take part in radical mechanism, which leaves the positions 1 and 2 as possible sites. Once the macroradical is formed, it reacts with a double oxygen molecule and, ultimately, forms a hydroperoxide.

FTIR studies by Coiffier et al. on photo-oxidation of EPDM-ENB showed the formation of isolated hydroperoxides at 3550 cm^{-1} and hydrogen bonded ones at 3380 cm^{-1} [1]. The authors attributed the band at 3550 cm^{-1} to tertiary hydroperoxides formed at position 3 of Scheme 4-1, and it was observed that this kind of hydroperoxide decomposes thermally at about 70°C . Ten years later, Scoponi et al. have reconsidered the same study and performed it for EPDMs containing 2-8 wt.-% of ENB [2]. It was also found that secondary and tertiary hydroperoxides are present, but another structure for tertiary ones was proposed (Scheme 4-2).



Scheme 4-2: Hydroperoxidation at allylic positions of ENB unit

In conformity with Bredt's rule, the hydrogen abstraction happens on positions 1 and 2, giving radicals b and c in Scheme 4-2, while both of these two radicals have a second resonance structure. The second structure of radical (b) is radical (a). However, the formation of radical (a) induces a change in hybridization of Norbornene cycle, which brings high stresses to the cycle and makes this mesomerism unfavorable [3]. Contrarily, the second structure of primary radical (c) is radical (d), which is more stable due to its tertiary nature. Subsequently, these radicals react with a di-oxygen and form a hydroperoxide as presented in Scheme 4-2. According to what explained above, radicals (b) and (d) are the most predisposed radicals to form hydroperoxide molecules.

On the other hand, as the FTIR absorption band of ENB at 809 cm^{-1} decreases, another band at 870 cm^{-1} appears, reaches to its maximum and declines afterwards (Figure 4-7). This phenomenon was

explained by the transformation of the vinylidene bond (absorbing at 809 cm^{-1}) into a vinyl bond (absorbing at 870 cm^{-1}) [4]. This latter corresponds to the structure (d) in Scheme 4-2.

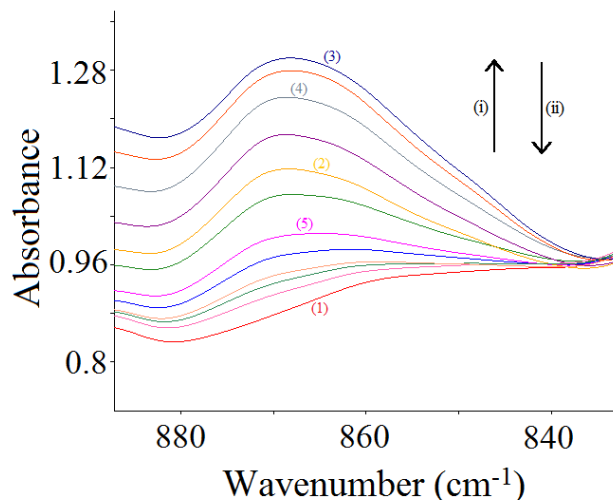
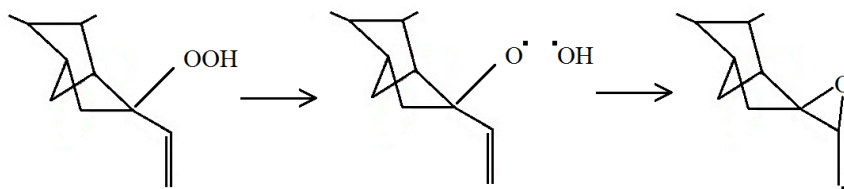


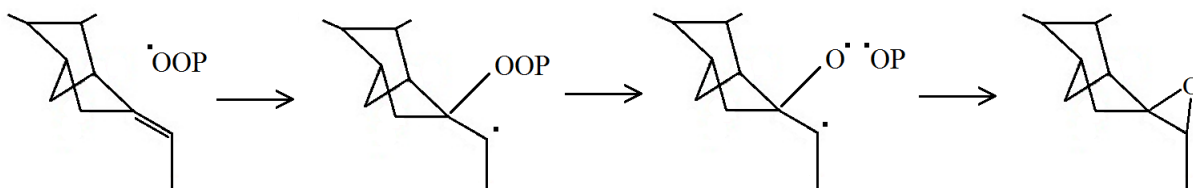
Figure 4-7: Built-up of epoxy ring at 870 cm^{-1} (Nordel 4640 ~ $100\mu\text{m}$, at 130°C , in air)

The band at 870 cm^{-1} has been attributed to epoxide ring as well [4, 5]. They would result from the intermolecular addition of alkoxy radicals (consequential to the decomposition of POOH) to ENB double bond, according to the Scheme 4-3 [6].



Scheme 4-3: Mechanism of peroxide ring formation according to Meyer^[6]. (Adapted for EPDM-ENB)

Mayo [7], on the other hand, proposed another mechanism of epoxide formation, which has been adopted by several researchers [5, 8-10]. In this mechanism, the double bond is attacked with a peroxy radical, who opens the double bond and forms a peroxide molecule. The peroxide decomposes subsequently to form an alkoxy, which in its turn can react with the free radical formed from bond opening and produces an epoxide ring (Scheme 4-4).



Scheme 4-4: Mechanism of epoxide ring formation according to Mayo^[7]. (Adapted for EPDM-ENB)

The epoxide ring, formed by any of the two mechanisms reported above, absorbs between 750 and 880 cm^{-1} [11]. A last possibility of IR absorption band attribution at 870 cm^{-1} is the stretching vibration of O – OH groups, which has been used by few authors [2, 12].

To summarize, three reactions are responsible for the decrease in the IR absorption band at 809 cm^{-1} :

- i. Transformation of vinylidene double bonds into vinyl double bonds (structure d') [13, 14];
- ii. Formation of epoxide rings;
- iii. Saturation of double bonds by a direct attack by peroxy radicals [2].

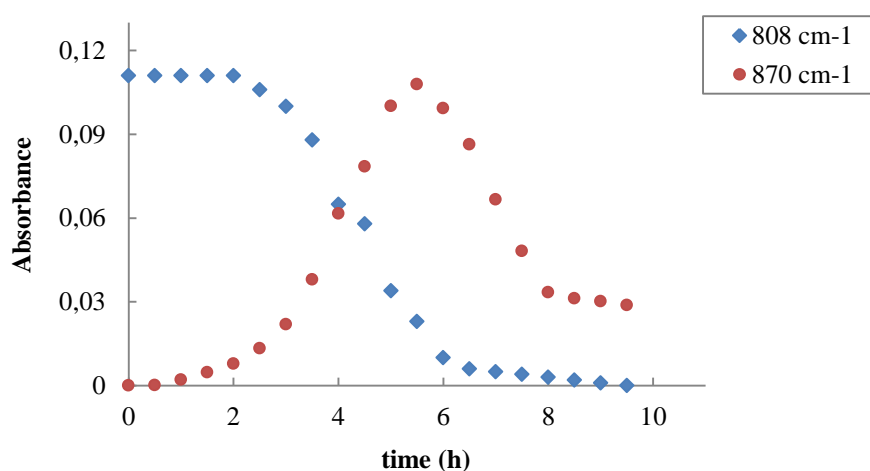


Figure 4-8: changes in the IR absorbance of the bands at 809 cm^{-1} and 870 cm^{-1} (Nordel 4640 ~ 100 μm , at 130°C, in air)

Opening of double bonds by radical attack results in consumption of double bonds. Transforming vinylidene double bonds into vinyl double bonds or epoxide rings results in formation of the absorption band at 870 cm^{-1} . This latter reaches its maximum absorbance when the ENB absorption band at 809 cm^{-1} disappears totally (Figure 4-8), confirming the succession of reactions as proposed. Anyhow, vinyl double bonds or epoxide rings eventually get involved in the overall mechanism and their concentration vanishes with time.

4.1.2.1.2 ENB consumption followed by FTIR spectrophotometry

Once exposed to thermal stress, the characteristic band at 809 cm^{-1} begins to decline after reaching an induction time (Figure 4-9). Whatever the mechanism, the disappearance of vinylidene double bonds illustrates the beginning of the degradation mechanism, for which the kinetic parameters can be calculated and employed subsequently to affine the model of EPDM oxidation. The three EPDM samples show slightly different oxidation induction times, which do agree in succession with induction times found through mass uptake measurements. The method to define the induction time for ENB t_{i-ENB} has been illustrated in Figure 4-9.

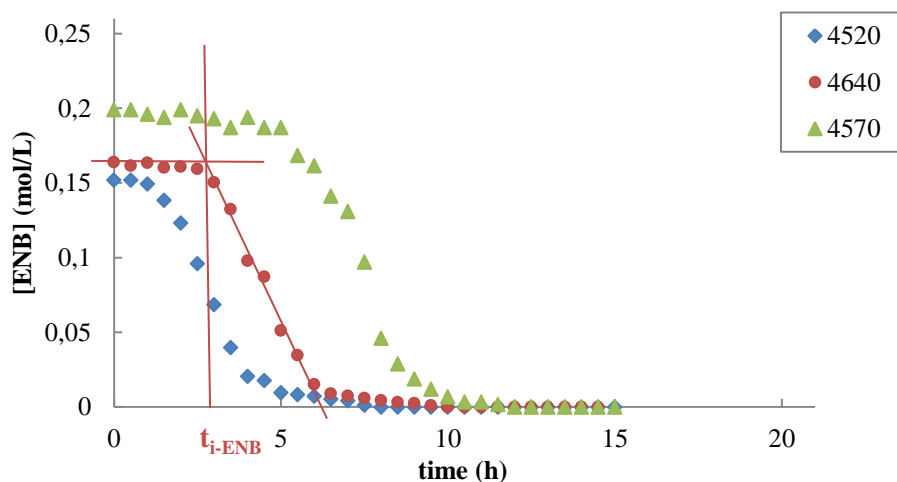


Figure 4-9: Kinetic curves of ENB double bonds consumption for the three EPDMs under study (at 130°C, in air)

Although the initial concentration of double bond is different from one sample to another, they show the same behavior, i.e. a decrease in concentration after surpassing the induction time with approximately the same rate. The quantitative values are calculated in the next section.

4.1.2.2 Effect of temperature

The changes in ENB double bonds concentrations have been followed by FTIR spectrophotometry for the three EPDMs under study. Results for Nordel 4640 are presented in Figure 4-10, where t_{i-ENB} decreases as the exposure temperature increases. The behavior for two other Nordels, i.e. 4520 and 4570 does not change.

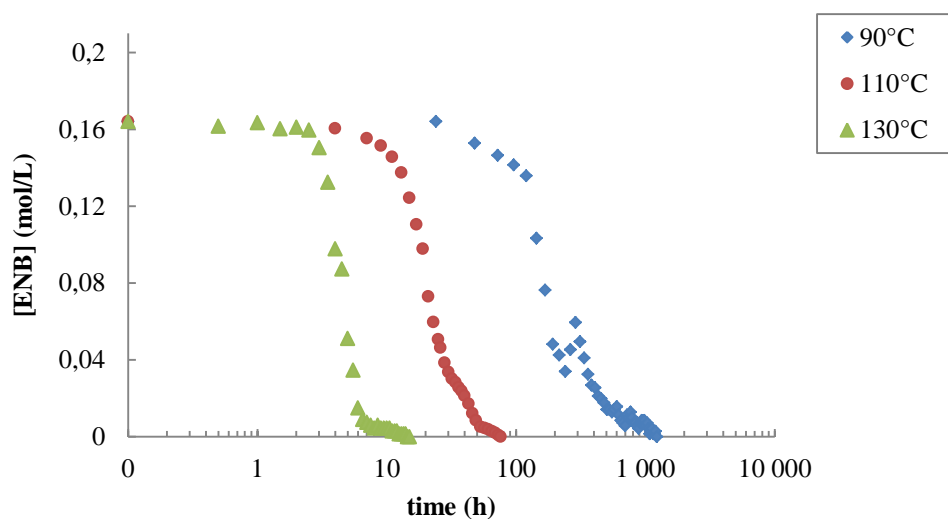


Figure 4-10: Effect of temperature on the consumption kinetics of ENB double bonds of Nordel 4640 in air

Measurement of t_{i-ENB} for all samples allows the plotting of the Arrhenius diagram of Figure 4-11. It is shown that the order of magnitude of t_{i-ENB} is the same for three samples under study.

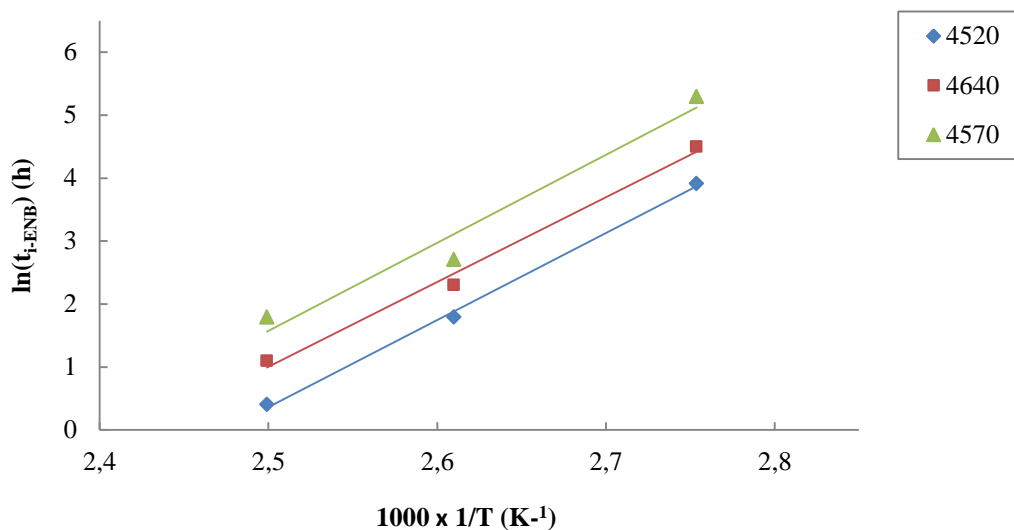


Figure 4-11: Arrhenius graph of t_{i-ENB} in air between 90 and 130°C for the three EPDMs under study

Furthermore, the maximum rate of ENB double bond consumption r_{ENB} at 809 cm^{-1} can be also calculated and plotted in an Arrhenius diagram (Figure 4-12). In view of having very similar molecular structure and concentrations for three EPDMs, one might expect very close outcomes for r_{ENB} . Indeed, Figure 4-12 divulges that the three samples show identical consumption rates.

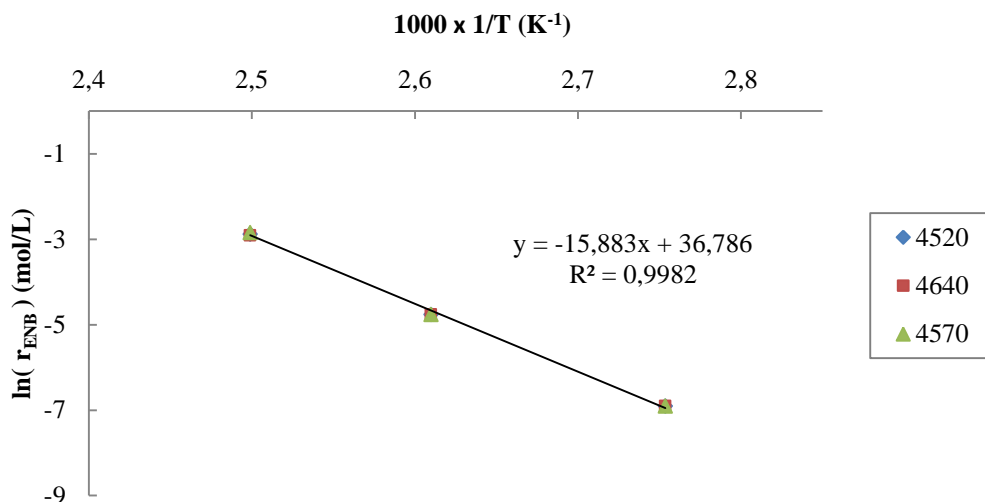


Figure 4-12: Arrhenius graph for r_{ENB} in air between 90 and 130°C for the three EPDMs under study

One can realize that although the three samples have different concentrations of double bonds and antioxidants, these small differences do not change the overall mechanism of double bond consumption during oxidation. In addition, between 90 and 130°C, r_{ENB} obeys an Arrhenius law. The

linear regression of r_{ENB} values gives an activation energy (Ea_{ENB}) equal to 132 kJ.mol⁻¹ and a pre-exponential factor ($\ln r_{0_{ENB}}$) equal to 36.79 mol.L⁻¹.s⁻¹. These values are the same for the three samples under study as their regression lines perfectly superpose.

4.1.2.3 Oxidation products

Oxidation products are divided into two main chemical species which are molecules containing hydroxyls (-OH) groups and molecules containing carbonyls (C=O) groups. In this section, the concentrations of these two species are measured by FTIR spectrophotometry over the entire exposure time, and the effect of temperature is studied.

4.1.2.3.1 Main oxidation products

Chemical reaction of a polymer with di-oxygen molecules creates new chemical oxygen bearing species known as oxidation products. Based on oxidation mechanism, the first step of oxidation is the production of hydroperoxides, which are known as primary products. Hydroperoxides are fairly reactive species that decompose to form more stable (inactive) products through rearrangement reactions (e.g. alcohols, ketones, carboxylic acids, aldehydes, etc.). Hydroxyl groups absorb between 3800 and 3000 cm⁻¹, which includes hydroperoxides, alcohols and hydroxylic acids. The most important hydroxyl bearing products and their absorption regions are listed in Table 4-2.

Chemical species	Absorption region (cm ⁻¹)
Isolated hydroperoxides	3430 – 3380
Hydrogen-bonded hydroperoxides	3557 – 3550
Isolated alcohols	3430
Hydrogen bonded alcohols	3620 – 3630
Carboxylic acids	3210

Table 4-2: FTIR absorption bands of main hydroxylic species ^[1, 11, 14, 15]

The accumulation of hydroxyl groups results in a major absorption band with a maximum around 3400 cm⁻¹ (Figure 4-13 a). The intensity of this band is used to calculate the concentration of (-OH) groups by employment of the Beer-Lambert law with an average molar absorptivity equal to 70 L.mol⁻¹.cm⁻¹ [16].

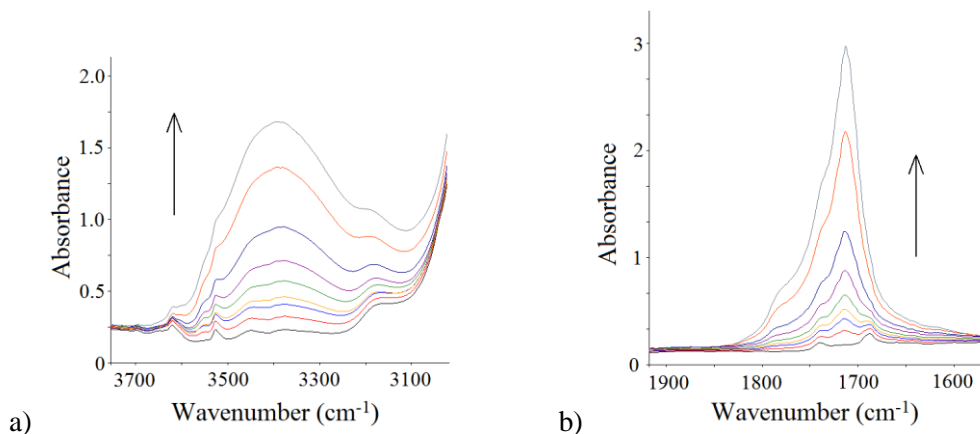


Figure 4-13: Build-up of oxidation products in thin EPDM films ($\sim 100 \mu\text{m}$) at 130°C in air
 a) Hydroxyls and b) Carbonyls

Carbonyl groups, absorbing within $1800 - 1600 \text{ cm}^{-1}$, are the other main oxidation products. Similarly to hydroxyls, the main carbonyl species and their corresponding absorption bands are listed in Table 4-3.

Chemical species	Absorption region (cm^{-1})
γ – lactones	1785
Saturated carboxylic acids	1760 – 1705
Esters	1740
Saturated ketones	1725 – 1718
Unsaturated carboxylic acids	1700
Unsaturated ketones	1685

Table 4-3: FTIR absorption bands of main carbonyl species ^[15, 17-19]

In conformity with other oxidation phenomena, formation of carbonyls and hydroxyls show induction times $t_{i\text{CO}}$ and $t_{i\text{OH}}$, correspondingly. These induction times are slightly longer than $t_{i\text{-ENB}}$. This difference in induction times can be explained by the succession of reactions involved in the oxidation mechanism.

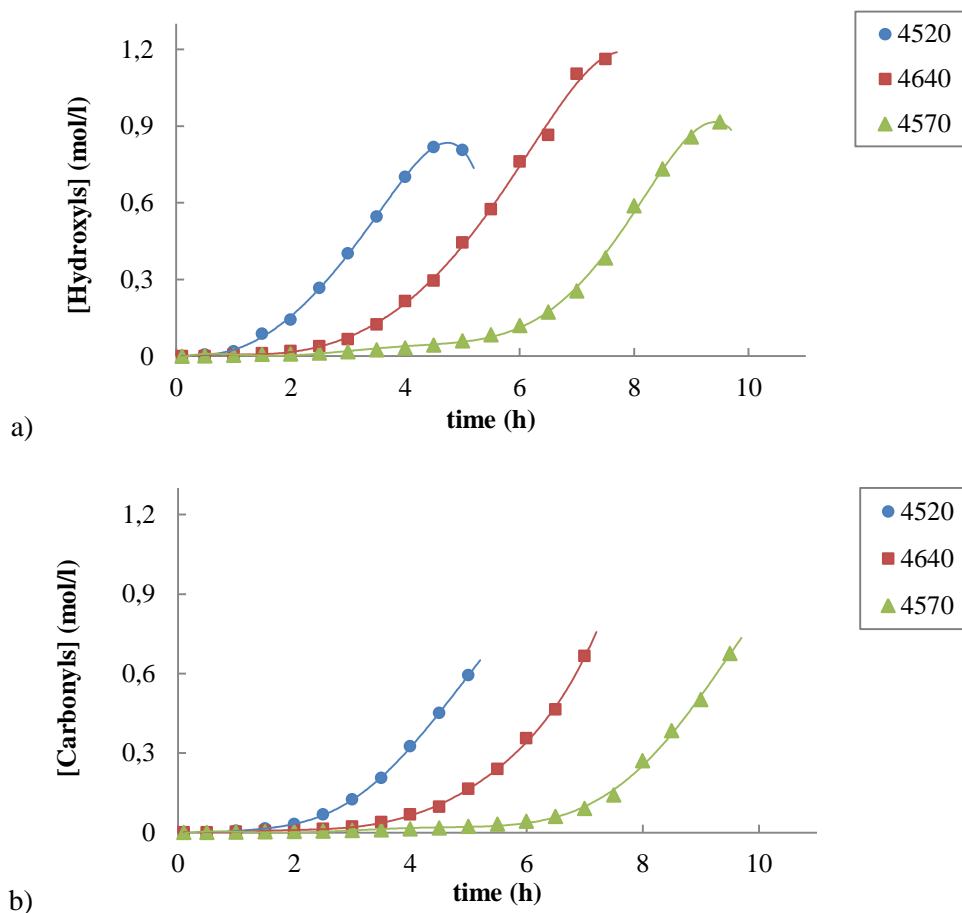


Figure 4-14: Kinetic curves of oxidation products build-up for the three EPDMs under study at 130°C
a) Hydroxyls and b) Carbonyls

Figure 4-14 presents the kinetic curves of hydroxyls and carbonyls. t_{iCO} and t_{iOH} take the same order of magnitude than t_{im} of the previous section. The induction time is slightly shorter for hydroperoxides than for carbonyls, which is explained by the primarily appearance of hydroperoxides.

Measurements by FTIR spectroscopy unveil that after the induction time, hydroperoxide formation rate r_{OH} reaches a maximum (steady-state). After this step, the r_{OH} decreases, the concentration of hydroperoxide reaches a maximum and declines afterward (substrate consumption). The decrease in hydroperoxides concentration is due to their consumption, and formation of volatile products which can leave the system. Evolution in carbonyls concentration could not be followed like hydroxyls due to the saturation of absorption band at 1714 cm^{-1} . This saturation is mostly because of high molar absorptivity of $C=O$ groups ($\sim 300\text{ L}\cdot\text{mol}^{-1}\cdot\text{cm}^{-1}$ [16]).

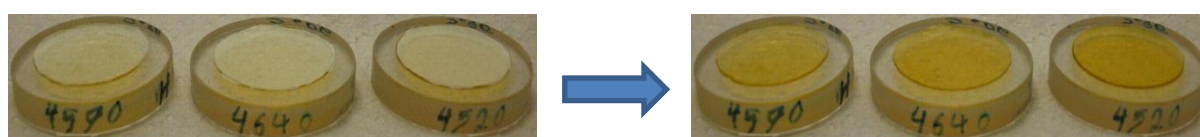


Figure 4-15: Yellowing of samples under the thermal oxidative aging in air at 130°C

The macroscopic state of samples changes as well with the exposure time. During the induction time, the samples keep their initial state and color. After induction time, the color of the samples begins to change and goes from colorless to pale yellow, and the surface of the samples becomes tacky. This color change is due to the formation of chromophore species, which can absorb in visible region (Figure 4-15). When hydroxyls concentration reaches its maximum value (Figure 4-14 a), the color of samples changes to bold yellow and the surface changes from tacky to sticky. At this state the material is completely degraded and, by continuing the thermal exposure, the material begins to flow and shapes a quasi-droplet.

4.1.2.3.2 Effect of temperature

Oxidation of the EPDM samples has been performed at three different temperatures, i.e. 90, 110, and 130°C, and the formation of oxidation products has been followed by FTIR spectroscopy. Similarly to the consumption of ENB double bonds, t_{iOC} and t_{iOH} decrease by increasing the temperature. As a case in point, the changes in hydroxyls and carbonyls concentration for Nordel 4640 are presented in Figure 4-16. In the same manner the maximum oxidation rates r_{CO} and r_{OH} are decreasing functions of temperature, as well.

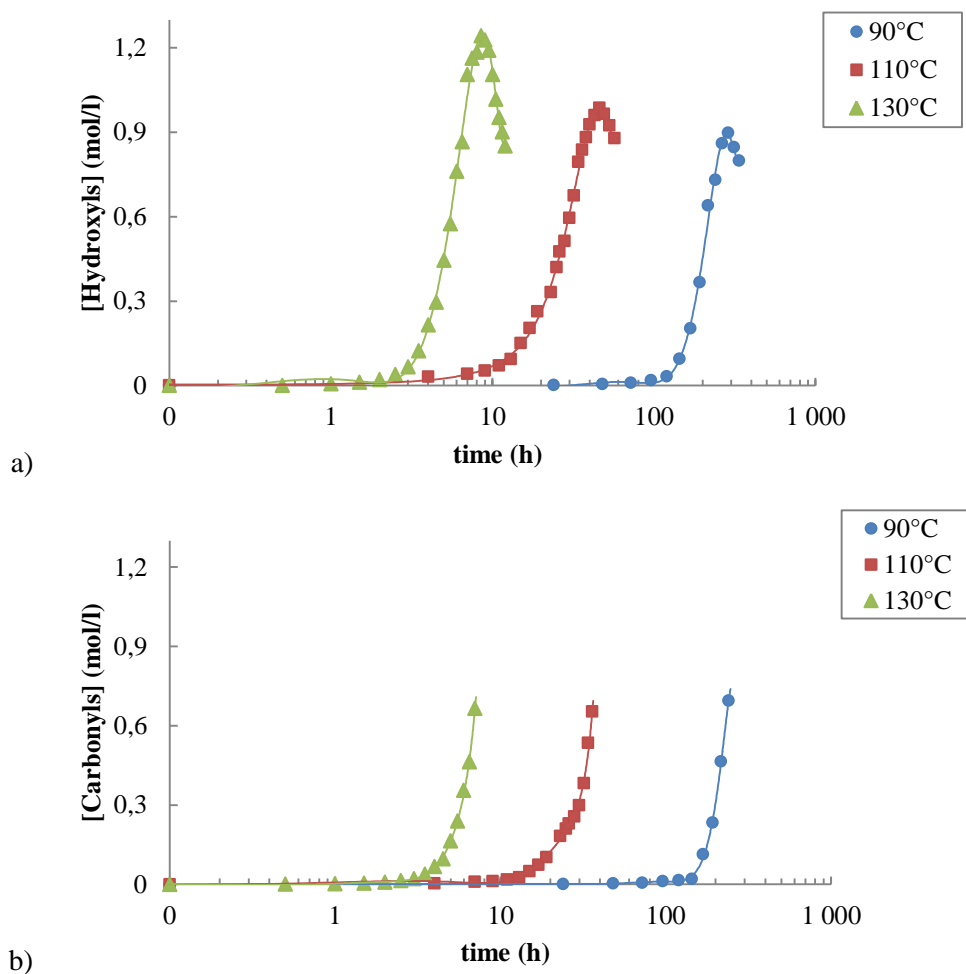


Figure 4-16: Temperature effect on the build-up kinetics of oxidation products for Nordel 4640 in air
a) Hydroxyls and b) Carbonyls

The kinetic curves of oxidation products build-up present a classic auto-accelerated character, from which the induction time (t_{iOH} and t_{iCO}) and oxidation rate (r_{OH} and r_{CO}) can be measured. As an example, the Arrhenius graphs of t_{iCO} and r_{CO} are presented in Figure 4-17. Subsequently, the Arrhenius parameters for carbonyls and hydroxyls in air between 90 and 130°C have been calculated and presented in Table 4-4.

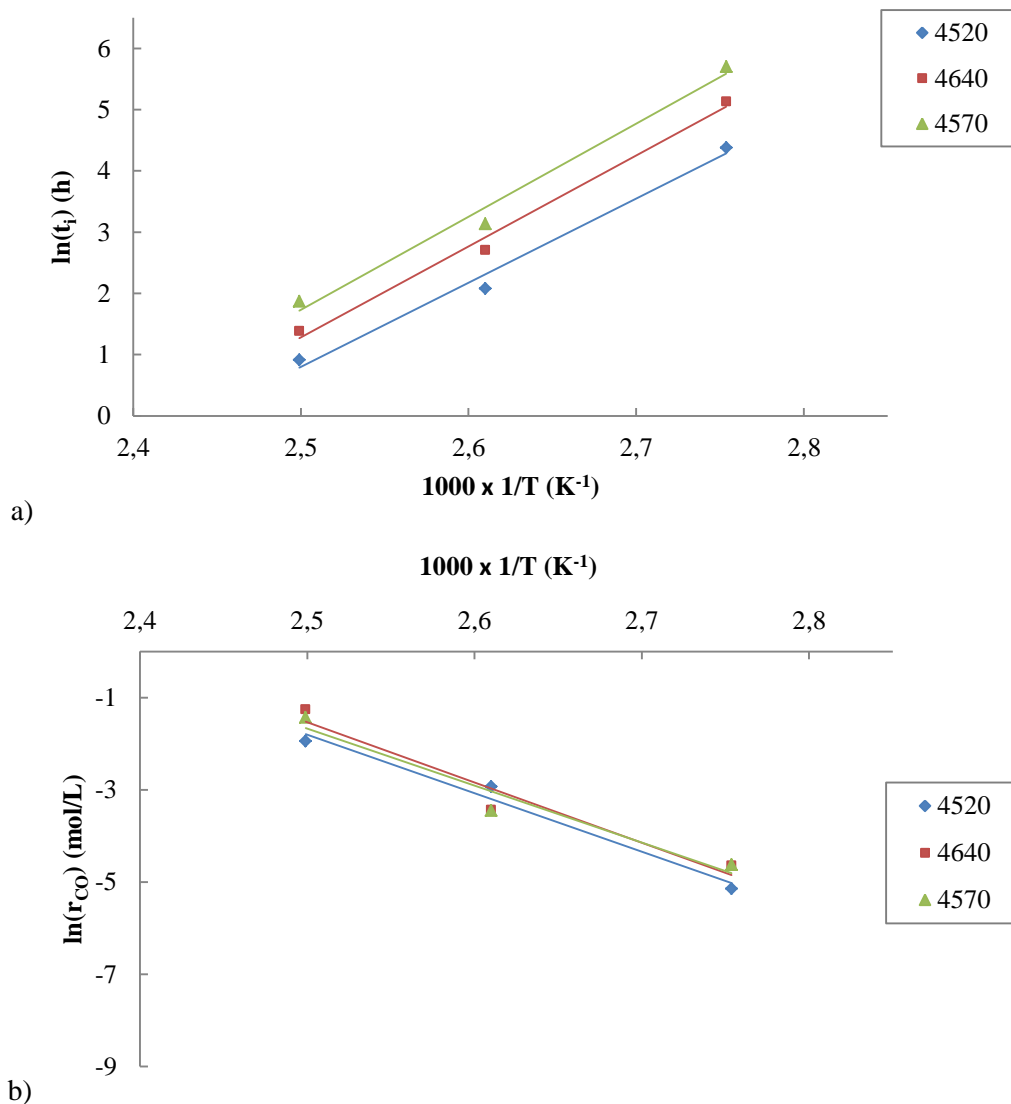


Figure 4-17: Arrhenius graph of carbonyls' a) t_{CO} and b) r_{CO} in air between 90 and 130°C for the three EPDMs under study

It has been tried to define the global, most important, kinetic parameters of thermal oxidation in natural atmosphere for the three EPDMs under study. Three main phenomena at molecular scale have been studied with the help of thermogravimetry and FTIR spectroscopy methods. The oxidation begins by ubiquitous formation and consumption of hydroperoxides, which implies the chemical interaction of the polymer and oxygen, leading to weight changes. Meanwhile, the residual double bonds are consumed in different ways. The oxidation process is then terminated by formation of stable products, which are quantified and their kinetic parameters are defined. A comparison of activation energies and pre-exponential factors of these three major phenomena reveals that the formation of hydroperoxides is the determining step of oxidation rate throughout the aging. Moreover, it was shown that the overall rate of oxidation is an increasing function of exposure temperature.

Nordel	Carbonyls		Hydroxyls	
	$(Ea_{C=O})$ (kJ.mol ⁻¹)	$(\ln r_{C=O_0})$	(Ea_{OH}) (kJ.mol ⁻¹)	$(\ln r_{OH_0})$
4520	106	29.93	110	31.73
4640	109	31.13	111	32.03
4570	103	29.19	111	32.04

Table 4-4: Arrhenius parameters of r_{CO} and r_{OH} for the three EPDMs under study in air between 90 and 130°C

The kinetic parameters found in this chapter can be used in future studies to verify the validity of the kinetic models of life-time prediction. For instance, the parameters found for ENB double bonds consumption can be integrated in the kinetic model developed by Colin et al. on aging of EPR, in order to extend this model to EPDM aging [20]. Further precision and advancement in this subject, although interesting, is beyond the scope of the present investigation.

4.1.3 Thermal oxidation of thick plates

Although the study of thermal oxidation on thin EPDM films provides valuable information at molecular scale and about kinetic aspect, the materials under real usage conditions are normally thicker than 2 mm. This is the reason why thick plates of about 2 – 3 mm have been aged thermally at the similar conditions as thin films in order to study their evolution at different structural scales. In addition, ATH fillers, with and without surface treatment, have been introduced only into the EPDM matrix Nordel 4640, and its effect on the oxidative aging kinetics has been carefully studied.

4.1.3.1 Thickness of oxidized layer

The concentration of oxidation products along the thickness of aged plates has been visualized and measured by FTIR imaging technique. An example of the FTIR cartography image obtained on a 3 mm thick sample aged in air for 800 hours at 110°C has been presented in Figure 4-18.

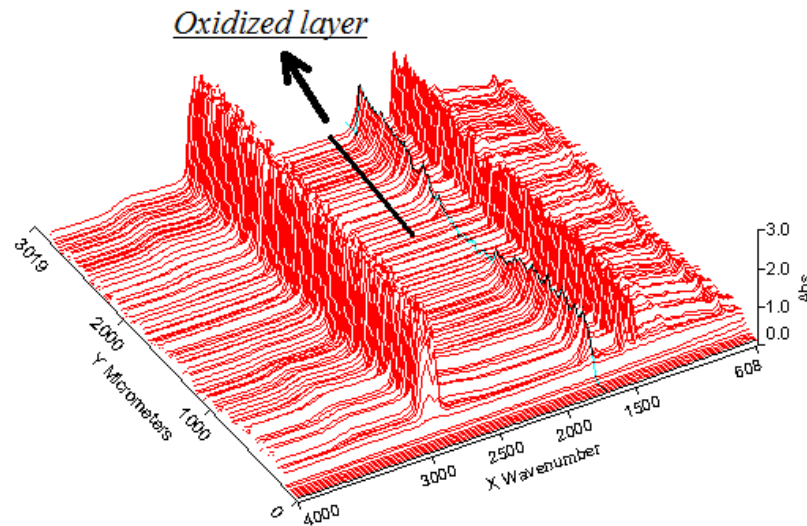


Figure 4-18: FTIR cartography along the thickness of 3 mm thick sample aged in air for 800 hours at 110°C – Monitoring the changes in the absorption band of carbonyls at 1714 cm⁻¹

Samples exposed at 90°C present a roughly homogeneous oxidation along the thickness of samples. However, as the exposure temperature increases the oxidation profile becomes more and more heterogeneous. It must be emphasized that after a limited time of oxidation the material becomes so degraded that procurement of thin samples (~30µm) by microtome is impossible, even at very low temperatures (-100°C).

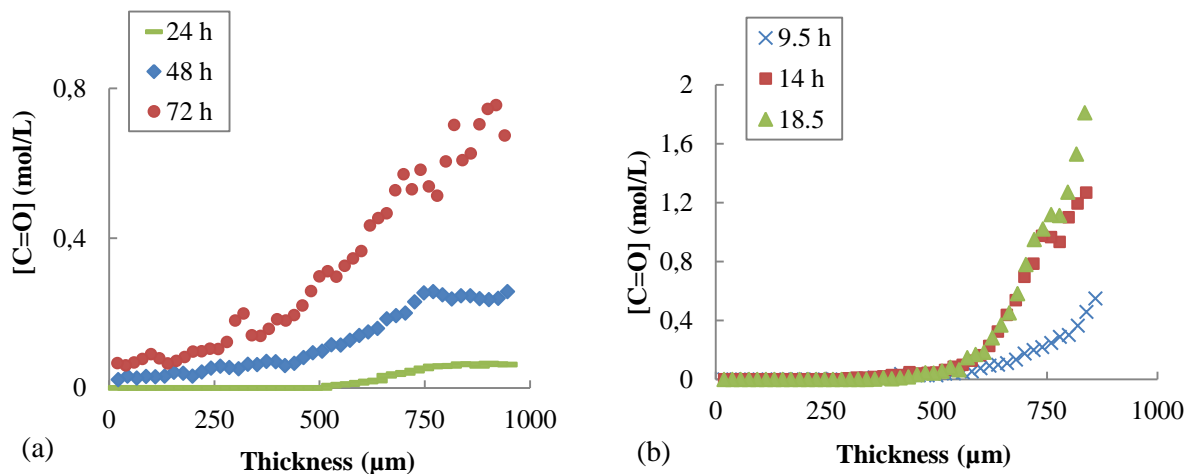


Figure 4-19: Changes in the carbonyls profiles along the thickness of EPDM 4640 samples in air at a) 110°C and b) 130°C

Figure 4-19 (a) shows the changes in oxidation profiles at 110°C in air. As the exposure time increases, the oxidized layer becomes thicker and, for longer exposure times, oxidation reaches the core of the sample. The evolution is different at 130°C, where the thickness of the oxidized layer remains almost constant while the concentration of oxidation products increases with time within the

oxidized layer (Figure 4-19 b). This heterogeneity of oxidation at high temperatures was previously shown for other polymers from the same family (in particular PE [21] and EPR [22]). As an example, the steady-state carbonyl profiles along the thickness of Nordel 4640 are presented in Figure 4-20

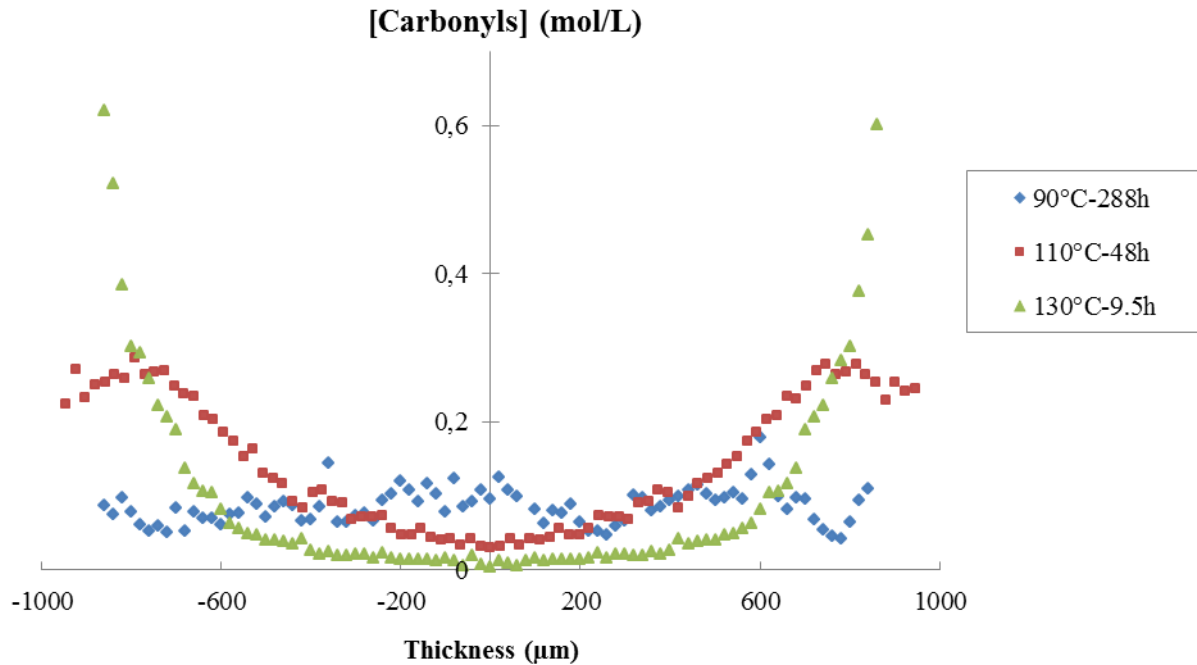


Figure 4-20: Effect of temperature on steady-state carbonyl profiles of Nordel 4640 in air

The presence of a superficial oxidized layer clearly indicates a heterogeneous oxidation of the EPDM plates, and imparts that the oxidation process is controlled by oxygen diffusion. This thickness (T_{OL}) depends on two parameters: the diffusion coefficient D of oxygen and its consumption rate throughout chemical reaction with polymer r_{O_2} [23]:

$$T_{OL} = \left(\frac{DC}{r_{O_2}}\right)^{0.5} \quad 4-1$$

with C the equilibrium concentration of oxygen in the EPDM samples.

The diffusion coefficient and the oxidation rate are both thermo-activated phenomena, which means they obey an Arrhenius law:

$$D = D_0 \exp\left(\frac{-E_D}{RT}\right) \quad 4-2$$

$$r_{O_2} = r_{O_2_0} \exp\left(\frac{-E_r}{RT}\right) \quad 4-3$$

Therefore, for thickness of oxidized layer we have:

$$T_{OL} = T_{OL_0} \exp \frac{-E_T}{RT}$$

4-4

with $T_{OL_0} = \left(\frac{D_0 c}{r_{O_2_0}}\right)^{0.5}$ and $E_T = \frac{1}{2}(E_D - E_r)$.

The quasi-homogeneous oxidation at 90°C prevents the determination of T_{OL} . However, from the values determined at 110 and 130°C, it can be tried to calculate the activation energy E_L .

4.1.3.2 Hydroperoxide titration by DSC

Hydroperoxides concentration for several exposure times provides important information for construction of the oxidation kinetic model. The concentration of hydroperoxides is conventionally measured through two experimental methods. The first method is iodometry, which can determine the concentration of hydroperoxides through chemical titration [24]. The second method consists in measuring the exothermic enthalpy of hydroperoxides decomposition through calorimetric methods. The validity of this second method has been verified by Richaud for PP [25], where a linear correlation has been found between these two methods.

The heat of hydroperoxide decomposition has been measured by modulated DSC (MDSC), which helps to acquire more precise results than conventional DSC method, by considering a correction on the phase lag due to the time dependency of the chemical reactions [26]. On a DCS thermogram, this phenomenon is visualized by an exotherm centered around 175°C. The area of this peak is plotted as a function of exposure time in Figure 4-21.

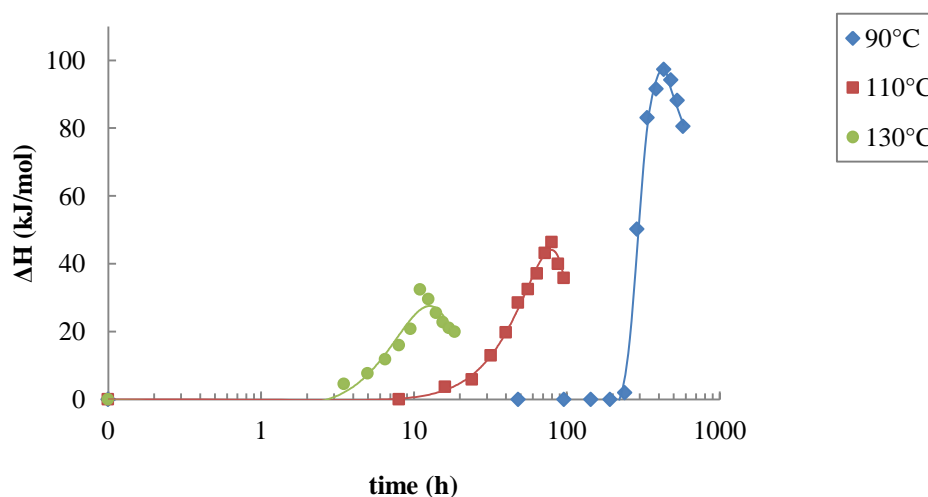


Figure 4-21: Kinetic curves of exothermic enthalpy of hydroperoxides decomposition for neat EPDM 4640 samples (2-3 mm thick) aged in nitrogen between 90 and 130°C

These results can be used to determine the changes in the concentration of hydroperoxides during the oxidation. It has been shown that the decomposition of hydroperoxides, in the temperature range under study, passes through bimolecular route [27, 28]. The simplified mechanistic scheme of hydroperoxides bimolecular decomposition is presented as follows:



The global enthalpy of hydroperoxide decomposition is the sum of the enthalpies for four elementary reactions above. The bond dissociation energies for each species are given in Table 4-5. Two simplifying hypotheses are to be considered:

- i. The alkoxy and peroxy radicals get involved only by hydrogen abstraction;
- ii. Only methylenic hydrogens are abstracted. From a simple kinetic analysis similar to that considered for EPDM crosslinking, it can be shown that the most probable site of the radical attack is the methylenic hydrogen.

Chemical bond	Dissociation energy (kJ.mol ⁻¹)
RO ₂ – H	376
RO – H	426
HO – H	498
RO – OH	150
> CH – H	393
P – P	343

Table 4-5: Bond dissociation energies of species involved in the bimolecular decomposition of hydroperoxides^[29, 30]

The total enthalpy of hydroperoxides bimolecular decomposition is calculated by Equation 4-5.

$$\Delta H_t = \Delta H_1 + \Delta H_2 + \Delta H_3 + \Delta H_4 \quad 4-5$$

The terms of Equation 4-5 are calculated separately based on the mechanistic scheme, and by using the data in Table 4-5. The results are grouped in Table 4-6.

ΔH_1 (kJ.mol ⁻¹)	ΔH_2 (kJ.mol ⁻¹)	ΔH_3 (kJ.mol ⁻¹)	ΔH_4 (kJ.mol ⁻¹)	ΔH_t (kJ.mol ⁻¹)
+28	-33	+17	-343	-331

Table 4-6: Enthalpy balance for elementary chemical acts of hydroperoxides bimolecular decomposition and total decomposition heat

However, one cannot simply divide the MDSC experimental enthalpies by the overall theoretical enthalpy to find the hydroperoxide concentration. As the formation of oxidation products is not homogeneous along the samples thickness, in order to calculate the concentration of hydroperoxides, we have to divide the thickness of the samples into two distinct regions: almost homogeneously oxidized superficial layers and an intact core (Figure 4-22).

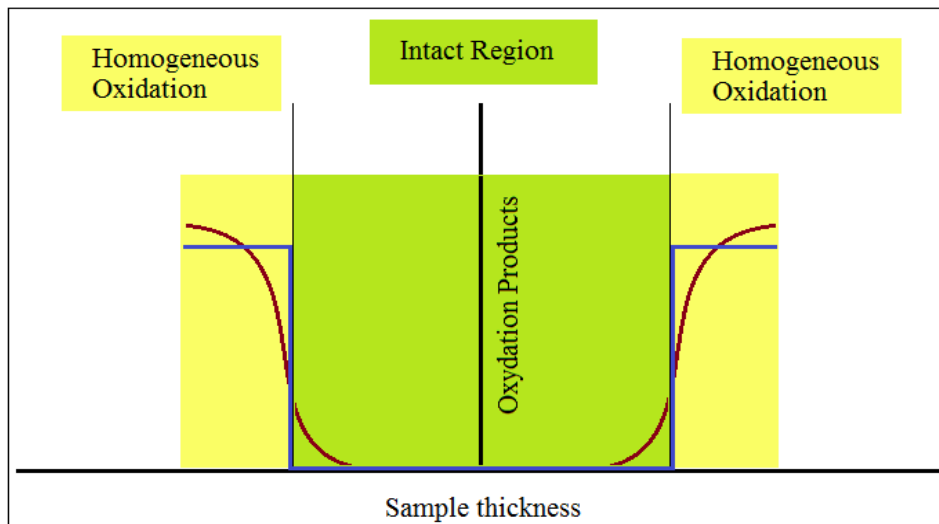


Figure 4-22: Partitioning the sample thickness into two homogeneously oxidized superficial layers plus one intact core

It is considered that the hydroperoxides are solely formed in the oxidized regions and, therefore, their concentration can be calculated by the following equation:

$$[POOH] = \frac{\Delta H_{ex}}{\Delta H_{th}} \cdot \frac{T_S}{2T_{OL}} \quad 4-6$$

where ΔH_{ex} and ΔH_{th} are enthalpies found experimentally by MDSC and theoretically by thermochemistry calculation, respectively, and T_S and T_{OL} are the thickness of sample and oxidized layer, correspondingly.

The application of Equation 4-6 to experimental results of Figure 4-21, by using the T_{OL} found in section 4.1.3.1 of this chapter, gives a more realistic hydroperoxide concentration. The results are plotted in

Figure 4-23.

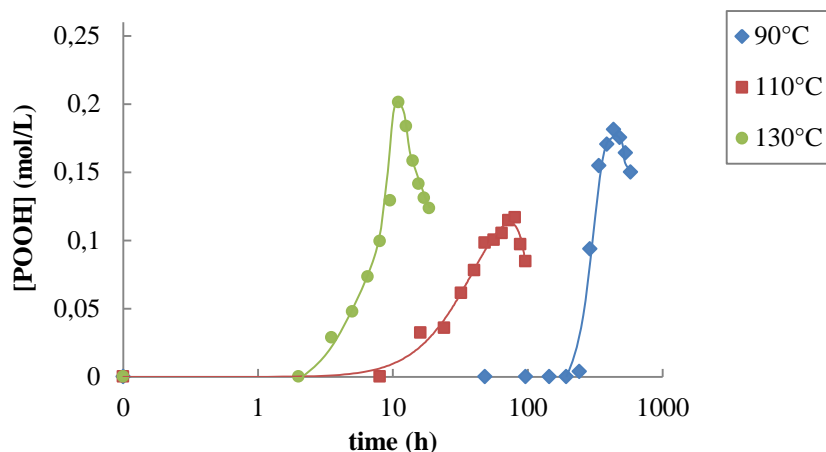


Figure 4-23: Kinetic curves of hydroperoxides accumulation for Neat plates of Nordel 4640 aged in air between 90 and 130°C

Contrarily to the samples of neat EPDM, which exhibit a distinct induction time and a subsequent increase in hydroperoxide concentration, the samples of filled EPDM do not behave in the same manner. At 90°C, none of the samples present a measurable exotherm corresponding to thermal decomposition of hydroperoxides, even for very long aging duration where the properties of samples have considerably changed (see the following sections). However, for higher temperatures (110 and 130°C) the exotherms are detected.

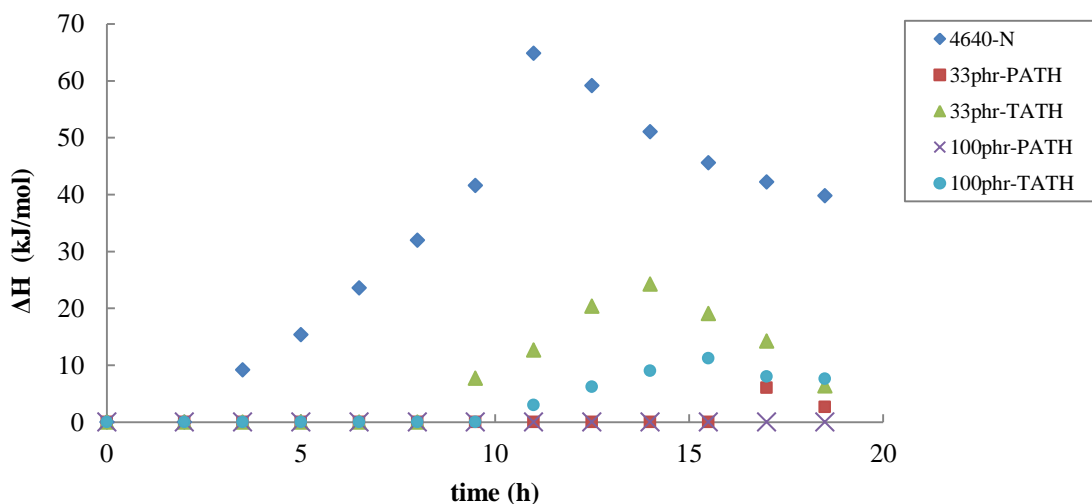


Figure 4-24: Kinetics of hydroperoxides decomposition enthalpy for Nordel 4640 aged at 130°C in air

Hydroperoxide formation at 110°C and 130°C follows roughly the same pattern. As a case in point, the evolutions in concentration of filled samples are shown in Figure 4-24 at 130°C. It should be pointed out that the precise concentrations of hydroperoxides could not be determined due to lack of an appropriate method to measure the oxidized layer in filled samples. Therefore, only the enthalpies brought to 100% of matrix has been presented.

The first point to realize is that the apparent induction time is fairly longer for filled samples, comparing to neat sample. Furthermore, the maximum hydroperoxides concentration in filled samples is considerably lower than neat sample. The comparison between samples with and without surface treatments provides interesting information as well. It can be observed that the samples containing surface treatment show shorter apparent induction times than the samples without surface treatment. On the other hand, the concentration of hydroperoxides is lower for samples without surface treatment.

These results clearly show that ATH fillers have an effect on the thermal oxidation of EPDM matrix. The chemical surface treatment of filler, which can react chemically with the matrix, also modifies this phenomenon.

In addition, the effect of filler content cannot be neglected either. One can see that, if the oxidized layer thickness remains constant, the concentration of hydroperoxides decreases with higher filler contents. This impact is clear for both PATH and TATH filled samples.

Herein, the effect of fillers, their concentration and their surface treatment is obvious. However, to understand how these parameters affect the thermal oxidation, further experimentations seems inevitable. The response to this question will be sought in the section devoted to the study of modifications at macromolecular and macroscopic scale.

4.2 EPDM network under irradiation

Samples of neat and filled Nordel 4640 have been γ -irradiated in dried air using ^{60}Co irradiation source. Radiochemical aging of EPDM has been only carried out on plates of 2 – 3 mm thick under dose rates of 0.1, 1 and 10 $\text{kGy}\cdot\text{h}^{-1}$, at $(40 \pm 5)^\circ\text{C}$. In this chapter, the radio-oxidation induced variations of properties at molecular scale are studied and the effect of dose rate, as well as the presence of fillers, has been investigated.

The main difference between thermal and radiochemical aging is expressed in the initiation step of the mechanistic scheme. While in the case of thermal aging, initiation consist in the thermo-activated phenomena of hydroperoxide decomposition, in the case of radiochemical aging, high energy rays are responsible for the direct radical creation from the rupture of lateral C – H bonds along the macromolecule as shown below:



The rest of mechanistic scheme, which are propagation and termination steps, remains practically the same. In fact, the energy of gamma rays of ^{60}Co source is around $120 \times 10^6 \text{ kJ.mol}^{-1}$, which is approximately 10^6 times higher than any C – H bond energy in the hydrocarbon macromolecule [31, 32]. However, as a general rule, the initiation due to irradiation does not happen in the backbone of the macromolecular chain because the lateral C – H bonds are much more reactive in comparison to C – C bonds [32].

4.2.1 Formation of oxidation products

In the case of radiochemical oxidation of 2 – 3 mm thick plates, the carbonyl profiles in the thickness of samples have been determined by FTIR spectrophotometry, as explained in the case of thermal aging.

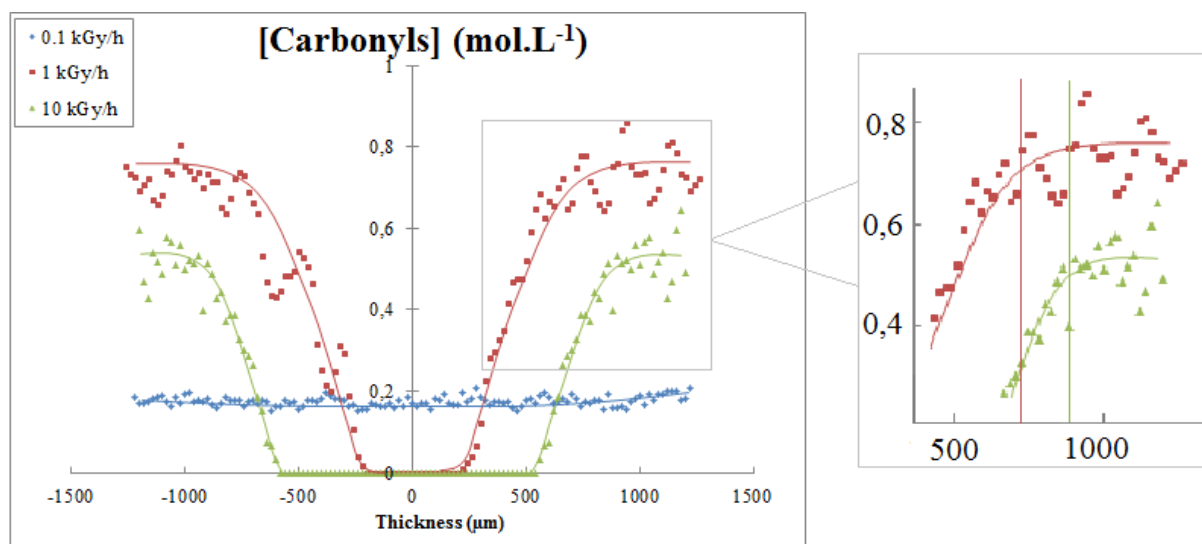


Figure 4-25 : Effect of dose rate on carbonyls profiles along the thickness of neat Nordel 4640 samples at 40°C in air: 0.1 kGy.h^{-1} -800h, 1 kGy.h^{-1} -800h, 10 kGy^{-1} -80h

Plotting the carbonyl profiles for the maximum received dose for each dose rate under study ($0.1 \text{ kGy.h}^{-1} - 800\text{h}$, $1 \text{ kGy.h}^{-1} - 800\text{h}$, $10 \text{ kGy}^{-1} - 80\text{h}$) shows a dependence of oxidation homogeneity on irradiation dose rate (Figure 4-25). Under 0.1 kGy.h^{-1} , the oxidation happens homogeneously in the entire sample's thickness, while under higher doses oxidation seems to be heterogeneous. This dependence is obvious for 1 and 10 kGy.h^{-1} dose rates, for which an almost homogeneously oxidized layer and an intact core can be defined.

In the same figure, it is possible to notice the effect of dose rate for a similar duration (800 hours) as well. One can see that, by increasing the dose rate from 0.1 to 1 kGy.h^{-1} , the oxidation profile becomes

more heterogeneous, while the concentration of carbonyls becomes more important in the superficial oxidized layer.

By neglecting the small differences in temperature between the different dose rates, such heterogeneity of oxidation can be explained by the diffusion controlled oxidation kinetics. The oxygen concentration at a defined depth in the sample thickness depends on both oxygen consumption rate at the sample superficial layer, and oxygen diffusion. This latter is generally described by the Fick's second law. The expression of the oxidation rate r_{O_2} is derived from the mechanistic scheme, and presented in Equation 4-7 [33]:

$$\frac{\partial O_2}{\partial t} = D \frac{\partial^2 O_2}{\partial z^2} - r_{O_2} \quad 4-7$$

where z is the axis of oxygen diffusion, D the oxygen diffusion coefficient, and O_2 the equilibrium concentration of oxygen.

The dose rate dependence of oxidation products concentration can as well be deduced from Figure 4-25. We can see that for the same received dose (800 kGy for 1 and 10 kGy.h⁻¹), this concentration decreases as the dose rate increases. In fact, for the same received dose, the exposure duration under 1kGy.h⁻¹ is 10 times longer than 10 kGy.h⁻¹. This provides more time for hydroperoxides to decompose and form oxidation products at lower dose rate.

T_{OL} increases rapidly at the beginning of exposure to finally reach an asymptotic value (steady-state) (Figure 4-26). This state happens when the local oxygen consumption (by chemical reaction with polymer) equals the oxygen supply by diffusion, i.e. when $\frac{\partial O_2}{\partial t} = 0$ or $D \frac{\partial^2 O_2}{\partial z^2} = r_{O_2}$.

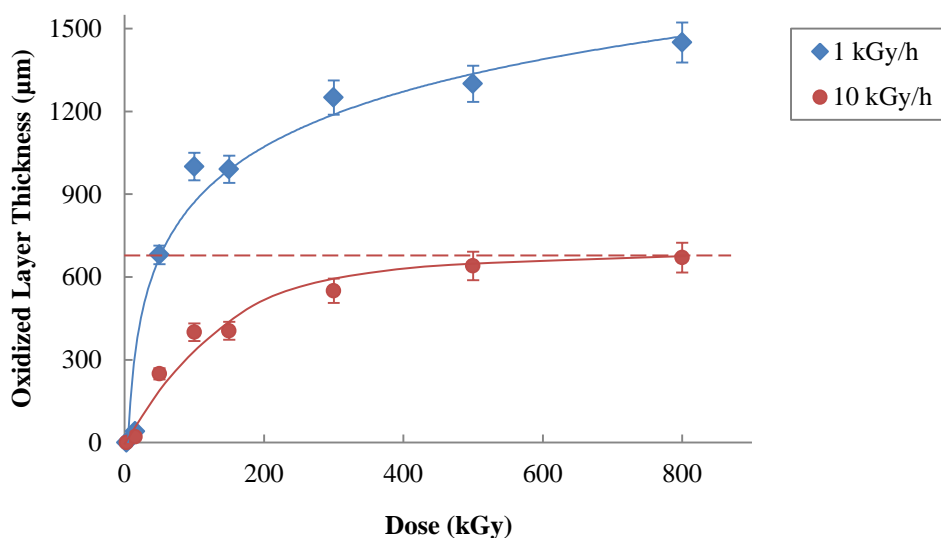


Figure 4-26 : Kinetic curves of T_{OL} for Nordel 4640 under 1 and 10 kGy.h⁻¹ in air at 40°C

Figure 4-26 reveals, as well, that by increasing the dose rate the stationary state is attained at lower received dose. Under $10 \text{ kGy}\cdot\text{h}^{-1}$, T_{OL} is approximately constant at about $700 \mu\text{m}$ after 500 kGy of received dose while under $1 \text{ kGy}\cdot\text{h}^{-1}$ up to maximum received dose, T_{OL} continues to increase.

4.2.2 Hydroperoxide titration by DSC

4.2.2.1 Neat EPDM

In the presented mechanism of radiochemical oxidation, hydroperoxides are mostly created in propagation step (III), and as well in termination (V). The concentration of these molecules is determined by measuring their heat of decomposition by DSC, as explained in section 1.4.2 of this chapter.

Kinetic curves of hydroperoxide accumulation with time of exposure under irradiation are different from those of thermal aging. The overall tendency in radiochemical oxidation is a continuous increase in the hydroperoxide concentration, leading to monotonous kinetic curves in Figure 4-27. One can observe that the rate of hydroperoxide accumulation r_{OOH} increases with irradiation intensity, and is at its maximum in the beginning of exposure. Subsequently, this rate decreases progressively with the exposure time. Under $1 \text{ kGy}\cdot\text{h}^{-1}$, r_{OOH} seems to tend toward an asymptotic value after 800 hours of exposure. This apparent equilibrium is presumably due to the decomposition of hydroperoxides for long periods of exposure under low dose rates (thermal decomposition activation).

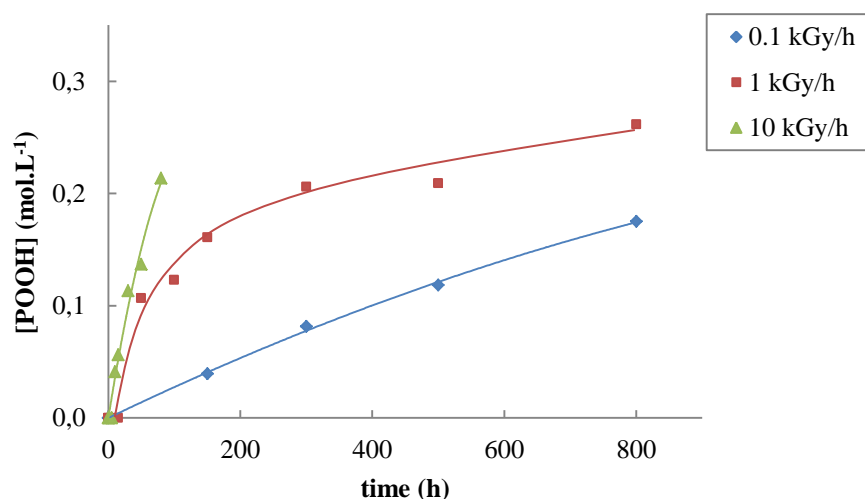


Figure 4-27 : Effect of dose rate on the kinetic curves of hydroperoxides accumulation for Nordel 4640 in air at 40°C

To better understand the kinetic curves of hydroperoxide formation, a rapid literature consulting can be helpful. In fact, for a polymeric samples under irradiation three different initiation mechanisms can be stated [32]:

- i. Purely thermal initiation: at low dose rates the irradiation induced initiation is negligible and the main act is the bi-molecular decomposition of hydroperoxides at relatively low temperatures.
- ii. Purely radiochemical irradiation: at high dose rates the consumption of hydroperoxides is negligible and the main act is polymer radiolysis. Therefore the hydroperoxides remain stable and accumulate in the system.
- iii. Combined radiochemical and thermal initiations: at the beginning, the accumulation of hydroperoxides is predominant. When the concentration of hydroperoxides attains a critical value $[POOH]_C$, the rate of hydroperoxide decomposition rate increases sharply due to their bimolecular decomposition.

These three domains have been illustrated by Khelidj et al. for unstabilized PE [34]. The authors have compiled the literature values of PE life-time and plotted them as a function of irradiation rate. The resulting master curve clearly defines the three aforementioned regions (Figure 4-27).

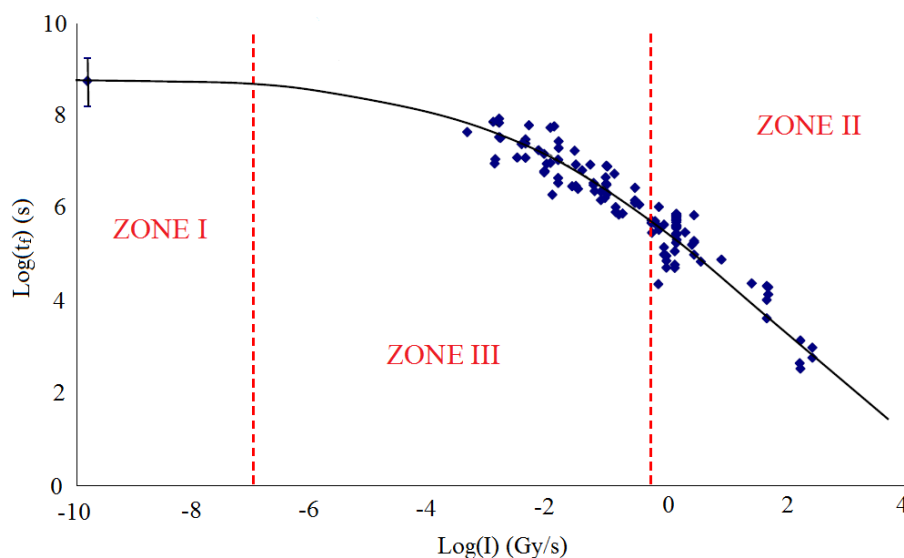


Figure 4-28 : Master curve of unstabilized PE life-time as a function of dose rate at room temperature^[34]. The three zones correspond to different oxidation kinetic regimes (See text)

The EPDMs under study contain more than 65 mol.-% of ethylene. In a first approximation, they can be considered equivalent to PE. Therefore, by positioning our EPDMs aging results on the diagram of Figure 4-28, we can have an idea on the oxidation mechanism. The irradiation dose rates used in this study are recalled in Table 4-7.

I (kGy/h)	0.1	1	10
I (Gy/s)	0,028	0,28	2,78
Log (I) (Gy/s)	-1,5563	-0,5563	0,443697

Table 4-7 : Dose rates of study and their corresponding values in logarithmic scale

Based on the information above, 0.1 kGy.h^{-1} is fully in the zone III and 10 kGy.h^{-1} in the zone II, while 1 kGy.h^{-1} is positioned at the frontier of zone II and III. Based on the zone explications and the kinetic curves of hydroperoxide accumulation (Figure 4-27), the predominant mechanism of EPDM radio-oxidation can be predicted by the diagram of Figure 4-28.

By zooming on the kinetic curves of hydroperoxides accumulation, one can distinguish two different regimes (Figure 4-29). In the first regime, where the built-up rate is higher, the material is mostly situated in propagation step. The hydroperoxides are created and their decomposition rate remains very low. In the second regime, the decomposition rate of hydroperoxides is no longer negligible. The critical hydroperoxide concentration delimitating both kinetic regimes is about $(1.0 - 1.5) \times 10^{-1} \text{ mol.L}^{-1}$. The rate of hydroperoxide built-up r_{OOH} can be measured by calculating the slope of regression lines which passes through the data of each region (Figure 4-29). The rate found for the first regime can be considered as the real rate of hydroperoxide formation as their consumption rate is negligible.

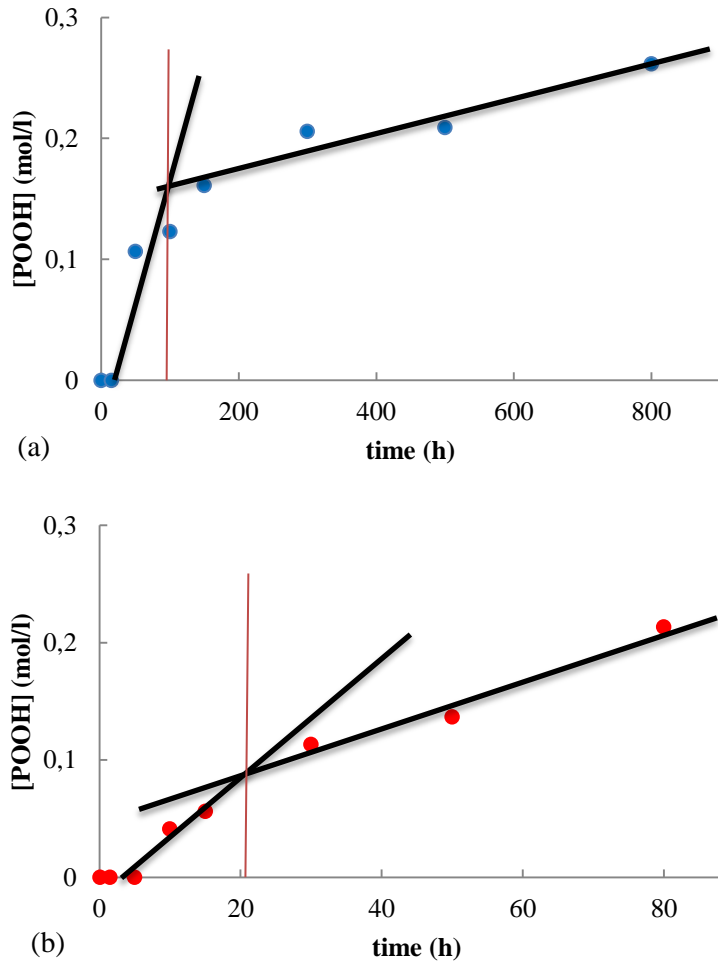


Figure 4-29 : Kinetic curves of hydroperoxide accumulation for neat EPDM aging in air at 40°C
a) 1kGy.h⁻¹ and b) 10 kGy.h⁻¹

The rate of hydroperoxide accumulation is proportional to the dose rate of irradiation I and the radiochemical yield G_{POOH} :

$$r_{POOH} = 10^{-7} G_{POOH} I \quad 4-8$$

Both values of measured hydroperoxide formation rate and calculated radiochemical yield are presented in Table 4-8. The definition of radiochemical yield implies that it depends only on the received dose. It is thus independent of the irradiation intensity. This definition is indeed respected by results of two different dose rates, which are satisfactorily close.

	1kGy.h ⁻¹	10 kGy.h ⁻¹
$r_{\text{POOH}} \times 10^{-3} \text{ (mol.L}^{-1}.\text{s}^{-1}\text{)}$	1.0	8.0
$G_{\text{POOH}} \times 10^{-3} \text{ (mol.L}^{-1}.\text{Gy}^{-1}\text{)}$	3.1	2.3

Table 4-8 : Hydroperoxide formation and radiochemical yield for Nordel 4640 in air at 40°C under 1 and 10 kGy.h⁻¹

It is noteworthy to point out that this measuring method cannot be applied to the second region. In fact, when the concentration of hydroperoxides attains the critical value $[\text{POOH}]_c$, the probability of finding two POOH molecule in mutual vicinity increases. The neighboring of two POOH facilitates their bi-molecular decomposition at the temperature of samples under irradiation. The bimolecular decomposition drives the oxidation in an auto-accelerated step. Therefore, the built-up rate measured in the second region is the outcome of several chemical reactions and cannot be directly related to the hydroperoxide formation.

4.2.2.2 Filled EPDM

The enthalpy of hydroperoxides decomposition has been also measured for filled samples, and brought to the volume unit of matrix in the samples. As an example, the evolution of hydroperoxides decomposition enthalpy as a function of exposure time under 1 kGy.h⁻¹ is plotted in Figure 4-30. The rate of hydroperoxide formation is of the same order of magnitude for filled and neat samples. Thus, it can be concluded that the presence of filler particles, pristine or treated, does not significantly change the hydroperoxide formation.

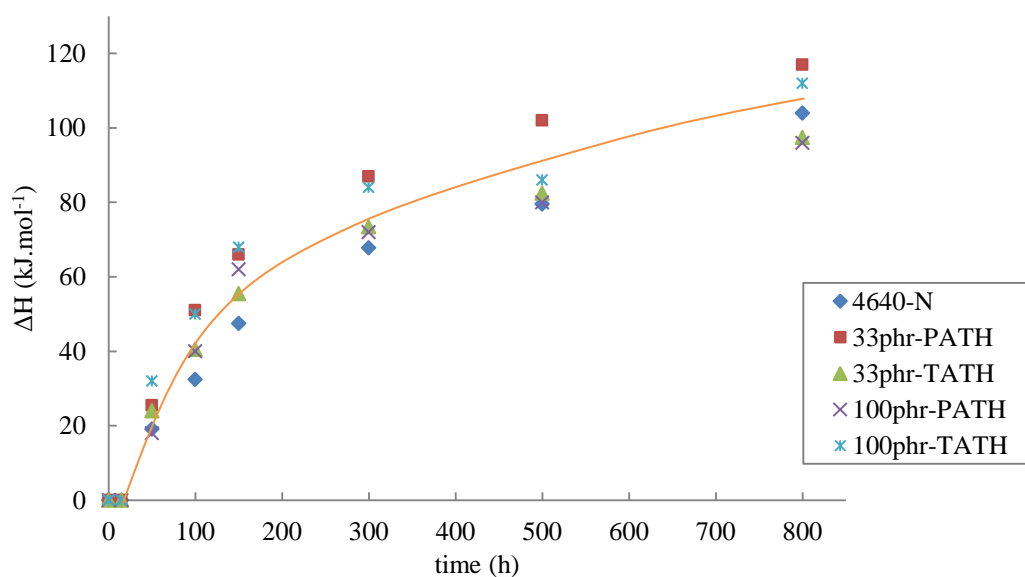


Figure 4-30 : Kinetic curves of hydroperoxides accumulation for neat and filled Nordel 4640 samples in air under 1 kGy.h⁻¹

The similarity of hydroperoxide formation rate between neat and filled samples exists as well for 0.1 and 10 kGy.h⁻¹.

4.3 Macromolecular structure evolution of EDPM network

4.3.1 EPDM network under thermal stress

The radical oxidation of EPDM can induce two main modifications in the macromolecular structure of the tridimensional network:

- i. Crosslinking due to bimolecular termination of macroradicals or addition of macroradicals to double bonds. This phenomenon increases the crosslink density of the network, i.e. the number of elastically active chains per volume unit.
- ii. Chain scission due to rearrangement of the macroradicals by β -scission. This phenomenon decreases the concentration of elastically active chains.

In this part, the macromolecular changes in the tridimensional network have been studied through measuring of swelling ratio and soluble fraction.

4.3.1.1 Swelling of neat EPDM

Aged samples have been swollen in cyclohexane according to the protocol previously explained in Chapter II. In this section, only the swelling behavior of samples aged at 130°C is shown, since they are consistent with the results obtained at the two other temperatures.

Throughout the swelling test, two characteristic entities are measured: swelling ratio and soluble fraction F_s . Swelling ratio is an index related to the tridimensional extensibility of the network due to penetration of solvent into elastomer network. F_s provides information about free molecular structures, which are physically trapped in the network and can leave it once the network is swelled.

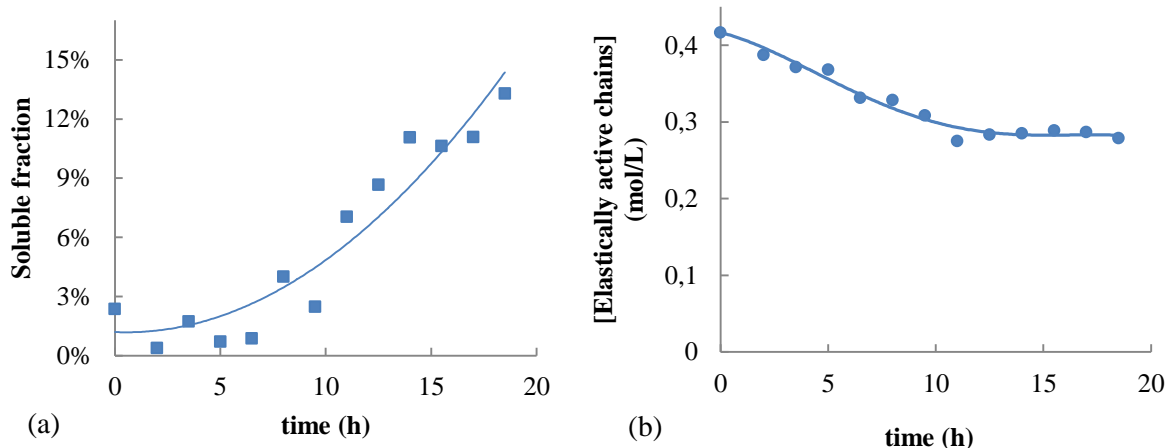


Figure 4-31: Kinetic curves for neat Nordel 4640 at 130°C in air: a) soluble fraction and b) concentration of elastically active chains

At the beginning of exposure, F_S of the network does not evolve considerably up to 7 hours, while the concentration of elastically active chains v decreases slowly (Figure 4-31), which means that although the elastically active chains undergo the chain scission, no soluble fraction is formed at this stage. The explanation of this behavior lies in the total number of chain scissions and the probability of having several of them in close vicinity. More explicitly, at the beginning of exposure, the number of chain scissions remains low comparing to the number of elastically active chains. So, the probability of having more than one chain scission per elastically active chain and forming free chains is very low, and the chain scissions result quasi-exclusively in creation of dangling chains. However, after an apparent induction time, which is around 7 hours at 130°C, the possibility of two chain scissions happening on one elastically active chain is no more negligible, and soluble fractures are formed.

The increase of F_S with the exposure time means that free chains are formed and extracted by the solvent. Disobediently, after 13 hours, v does not decrease anymore and remains quasi constant, while F_S continues to increase rapidly. This apparent discrepancy occurs at high conversion rates of oxidation process. To better understand the effect of higher oxidation products concentration on swelling capacity of the material, the fundamentals of solvent-polymer interaction must be re-viewed.

As discussed in Chapter II, the swelling capacity of a polymer network depends on Huggins solvent-polymer interaction parameter χ . The enthalpic part of this latter χ_H depends on chain/chain and chain/solvent interactions, which is expressed in form of solubility factor δ . Hansen has introduced a total solubility parameter δ_t , as bellow [35]:

$$\delta_t = \delta_d^2 + \delta_p^2 + \delta_h^2 \quad 4-9$$

where δ_d , δ_p , δ_h , are called dispersion, polar and hydrogen-bonding Hansen solubility factors, respectively.

Only dispersion solubility factors must be taken into account in the swelling of a virgin EPDM network for the reason that neither polar groups nor groups capable of hydrogen bonding are present in the system. However, in the course of oxidation, polar and hydrogen interactions are created by producing polar oxygenated species. In addition, the dispersion solubility factor depends as well on chemical groups present in the chain of polymer. This relation has been shown by Hoftyzer and Van Krevelen as below:

$$\delta_d = \frac{\sum C_{di}}{V} \quad 4-10$$

with C_{di} the contribution of species i to the dispersion solubility factor and V the molar volume.

Equation 4-10 implies that, by formation of oxidation products, δ_d does not remain constant. By considering the remarks above, it can be concluded that the values found by swelling test at high conversion rates of oxidation process cannot have a precise quantitative sense, and the values should be taken into account with caution. However, evolution of the calculated v can be served for visualizing the global evolution of the network, especially at the beginning of exposure where the concentrations of oxygenated products are still reasonably low. This approach is thus valid only for low conversion rates of oxidation process.

4.3.1.2 Swelling of filled EPDM

The previous discussion about quantitative invalidity of swelling test for aged materials is applicable to the case of filled samples too. Nonetheless, we have seen previously that the kinetic curves of hydroperoxide formation can be affected by the presence of filler particles. Since hydroperoxide decomposition is the main source of chain scissions, it is expected that the presence of filler particles affect the changes in the macromolecular characteristics of the EPDM network. So, the question here is: what are the potential influencing factors?

Values of F_S and swelling ratio of filled samples have been measured with the same method as for neat EPDM samples, and the final results have been expressed for 100% of matrix, i.e. the presence of filler has been virtually eliminated. Doing so, the results can be presented on a comparable basis (Figure 4-32).

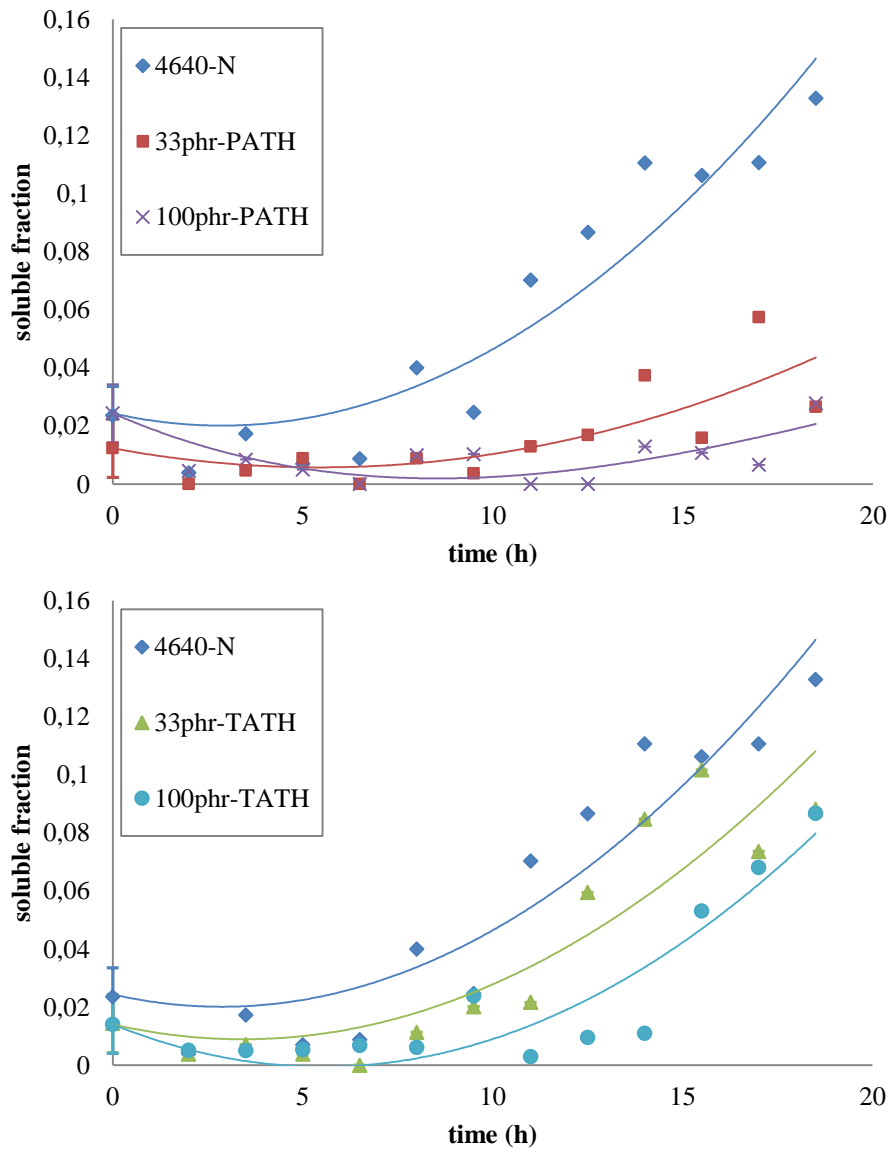


Figure 4-32: Kinetic curves of soluble fraction in air at 130°C for neat Nordel 4640 and its composites filled with: a) PATH and b) TATH

F_S has shown to be lower at higher filler contents, although its general evolution remains similar to neat EPDM in all cases. Comparing the outcomes, however, reveals a significant difference between pristine and treated ATH filled samples. It seems that PATH reduces the degradation rate, even though the apparent induction time of F_S remains practically unchanged for both types of filler.

In contrast, the kinetic curves of concentration of elastically active chains (from swelling test) show a diverged behavior of filled samples from that of neat EPDM. The introduction of fillers seems to slow down the changes in apparent ν for TATH, but to enhance them for PATH (Figure 4-33).

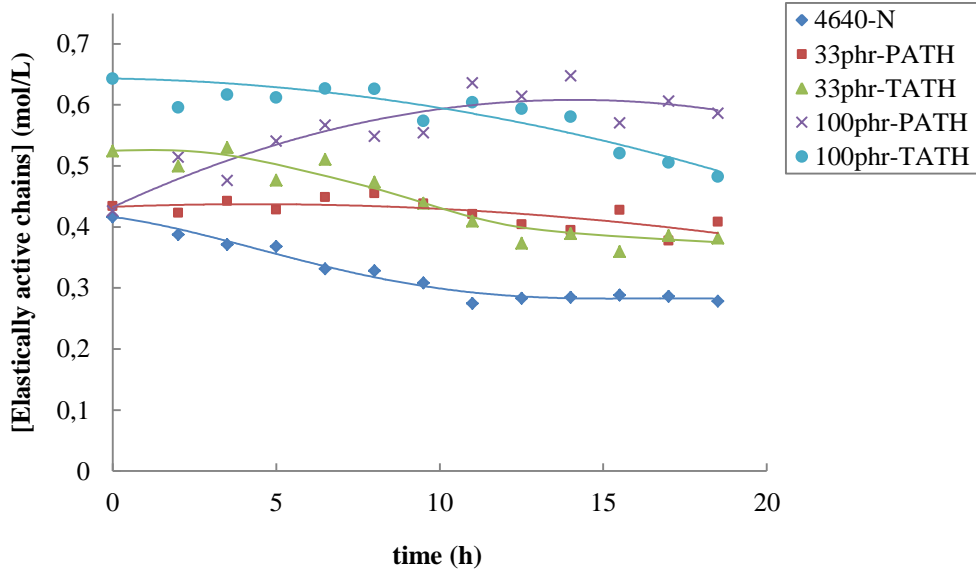


Figure 4-33: Kinetic curves of elastically active chains in air at 130°C for Nordel 4640 neat and filled samples (from swelling ratios)

More clarification can be obtained by comparing the variations in the concentration of elastically active chains (from swelling ratio) for different samples, in particular by comparing filled to neat samples. These values provide an enhanced comparing basis for a constructive discussion. Indeed, the variations in elastically active chains concentration Δv can be used in their domain of validity, i.e. up to 12 hours at 130°C, after which the error of method becomes important. The Δv is defined in Equation 3-3:

$$\Delta v = (v_t - v_m) - (v_{t0} - v_{m0}) \quad 4-11$$

with :

- v_t : concentration of elastically active chains of aged composite matrix,
- v_{t0} : initial concentration of elastically active chains of composite matrix,
- v_m : concentration of elastically active chains of aged neat EPDM matrix,
- v_{m0} : initial concentration of elastically active chains of neat EPDM matrix.

For a better understanding of what happens, the results for Δv are separated for identical filler contents, as shown in Figure 4-34. The increase in Δv is higher for PATH than TATH, but in both cases, is proportional to the filler content (Equation 4-12):

$$\left(\frac{\Delta v_{PATH}}{\Delta v_{TATH}}\right)_{33 \text{ phr}} \cong \left(\frac{\Delta v_{PATH}}{\Delta v_{TATH}}\right)_{100 \text{ phr}} \quad 4-12$$

This proportionality implies that this apparent densification of network is related to the filler specific surface available to polymer matrix.

In a first step, we assume that the matrix network in filled samples (see Section 3.3.2.3) degrades identically to unfilled samples. This assumption leads to the conclusion that the densification of the polymer phase in composite happens exclusively in the interphase network. In a first phenomenological approach, it was considered that this densification of interphase network happens while filled samples are exposed at high temperatures, and this phenomenon is related to the interactions between rubber and filler surface.

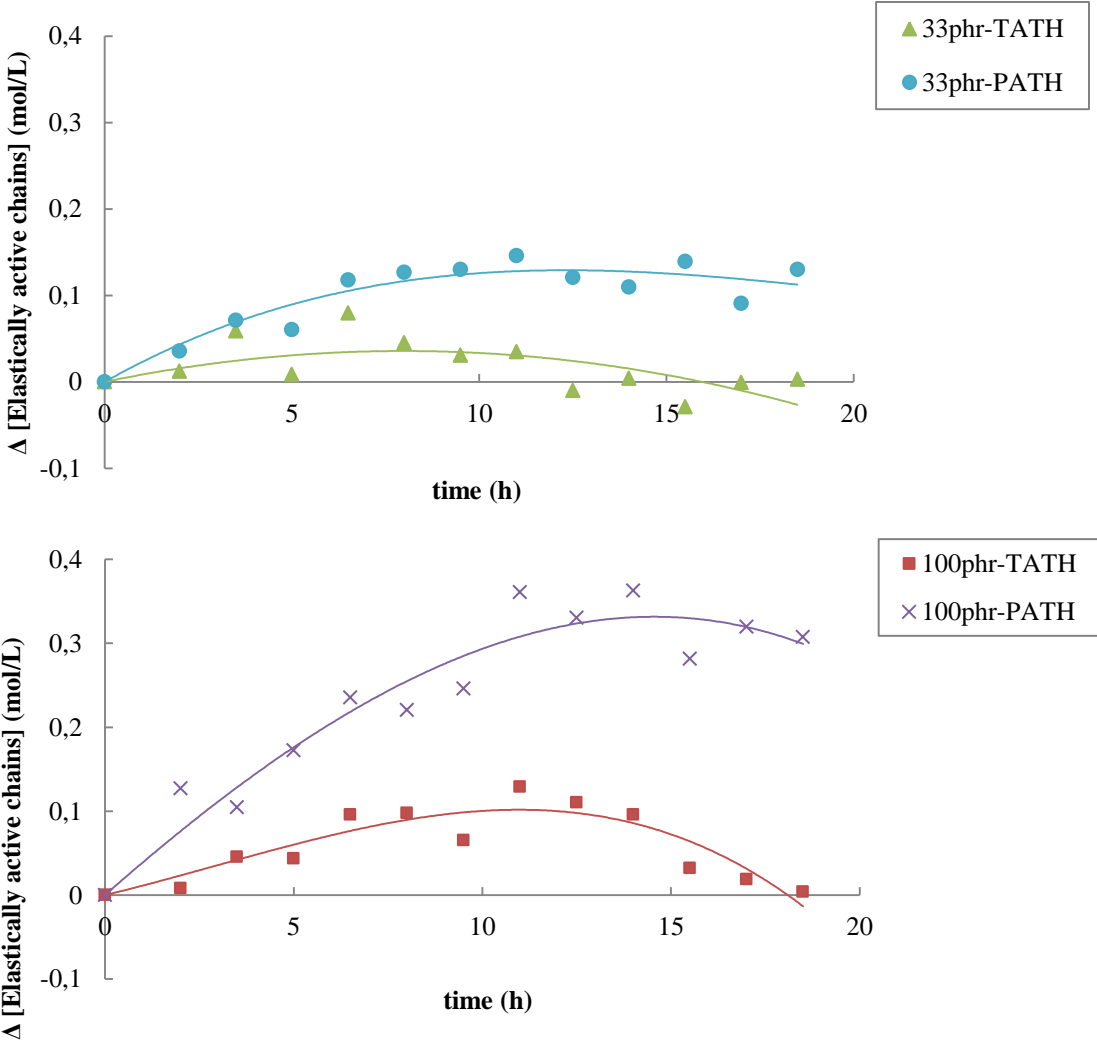


Figure 4-34: Kinetic curves of variations in concentration of elastically active chains in air at 130°C for filled Nordel EPDM samples

At this stage of study, the hypothesis of apparent interphase densification can explain the overall mechanism of filled EPDM behavior. However, we cannot conclude a definitive mechanism before the considering the results of radiochemical aging.

In next section, the evolution of neat and filled EPDM samples under irradiation is studied and by the end, the results will be compared with those obtained for thermal aging, and then the final conclusion will be presented.

4.3.2 EPDM network under irradiation

4.3.2.1 Swelling of Neat EPDM

Creation of oxidation products happens in different rhythms for thermal and radiochemical aging. Under thermal stress, hydroperoxides are decomposed and eventually transformed into secondary products, in particular alcohols, aldehydes carboxylic acids, etc. In contrast, under irradiation, hydroperoxides accumulate in early stages of exposure, so that the formation of secondary products is relatively delayed. However, the changes in samples polarity are independent of oxidation products succession, and depend on the global concentration of oxidation products (among the oxidation products, the highest polarity is attributed to hydroxyls and carboxylic acids [36]).

The kinetic curves of the soluble fraction F_S has been plotted in Figure 4-35 during exposure under 1 kGy.h^{-1} in air at 40°C . Two distinct kinetic regions can be detected. In the first region, from the beginning up to 150 hours (150 kGy received dose), F_S fluctuates around a constant value. In the second region, beyond 150 hours, F_S begins to increase and reaches relatively high values comparing to the initial state.

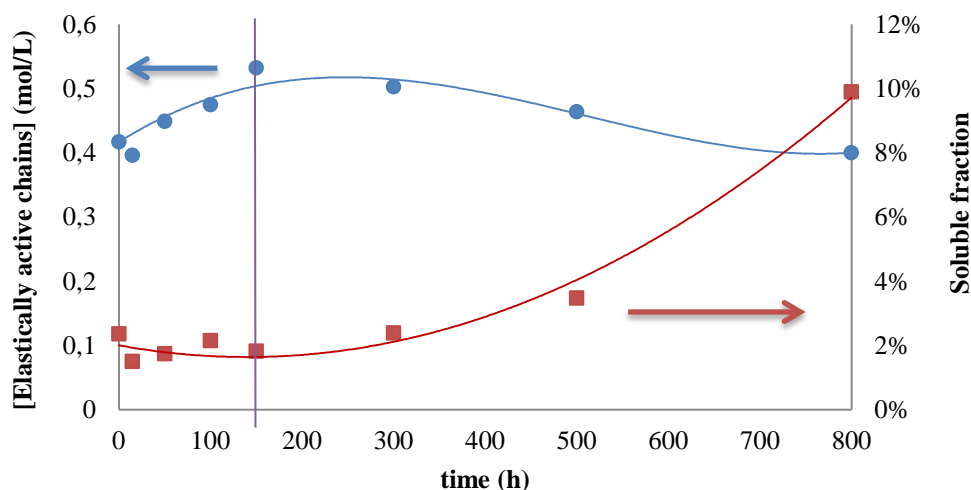


Figure 4-35 : Kinetic curves of soluble fraction and elastically active chains under 1 kGy.h^{-1} in air at 40°C for neat Nordel 4640

In the same figure, the changes in v for the same conditions are plotted, which shows two different regions as well, corresponding to those of F_S . The changes in v agree, to some extent, with those of F_S ,

i.e. in the first region, the increase in v caused by densification of the network decrease the swelling ratio. The oxidative crosslinking of EPDM matrix in the early period of irradiation is evident due to low concentrations of oxidation products. Such a behavior has been previously reported for an EPDM aged in the same conditions [37].

In the second region, the concentration of oxidation products, and consequently the number of chain scissions becomes significant. F_s rises radically, leading to a destruction of network and a decrease of apparent v . This transition region is validated by comparing the results of hydroperoxide formation (Figure 4-30) and Figure 4-35, where the line between two regions at $150 \text{ kGy}\cdot\text{h}^{-1}$ corresponds to the alteration region of hydroperoxide formation. This shows that, when the decomposition of hydroperoxides and, consequently, the formation of chain scissions are detected, the macromolecular network is deeply damaged resulting in the creation of a soluble fraction.

Based on what explained above, a dual mechanism for radiochemical aging of EPDM is considered:

- i. Region I ($0 < \text{received dose} < 150 \text{ kGy}$): Predominance of crosslinking.
- ii. Region II ($150 \text{ kGy} < \text{received dose} < 800 \text{ kGy}$): Predominance of chain scission.

By assuming that the aging is homogeneous along the oxidized layer, one can see that, above 300 kGy of received dose, the F_s increases in a much higher rate than v decreases. This difference clearly shows the loss of the capability of the solvent (cyclohexane) to swell the oxidized EPDM network.

The same behavior of network evolution has been observed at other dose rates, as shown in Figure 4-36. For all three dose rates, the network density increases at the beginning of exposure, reaches to a maximum and declines afterwards (unfortunately the exposure under $0.1 \text{ kGy}\cdot\text{h}^{-1}$ could not be prolonged more than 800 hours). Anyhow, the time for arriving to the maximal v is a decreasing function of dose rate, which gives the impression that chain scissions are favored when the dose rate increases. However, this latter cannot be totally approved because:

- a) Aging is time dependent and, for the same received dose the concentration of oxidation products under $0.1 \text{ kGy}\cdot\text{h}^{-1}$ can be higher than under $10 \text{ kGy}\cdot\text{h}^{-1}$, which leads to a decrease of swelling ratio and an increase in v .
- b) The swelling ratio is measured for cubic samples comprising the whole thickness of the sample's plate, which means that measured values do not consider only the thickness of oxidized layer. Therefore, the swelling behavior of homogeneously oxidized samples under $0.1 \text{ kGy}\cdot\text{h}^{-1}$ differs from that of highly heterogeneous oxidized samples under $10 \text{ kGy}\cdot\text{h}^{-1}$.

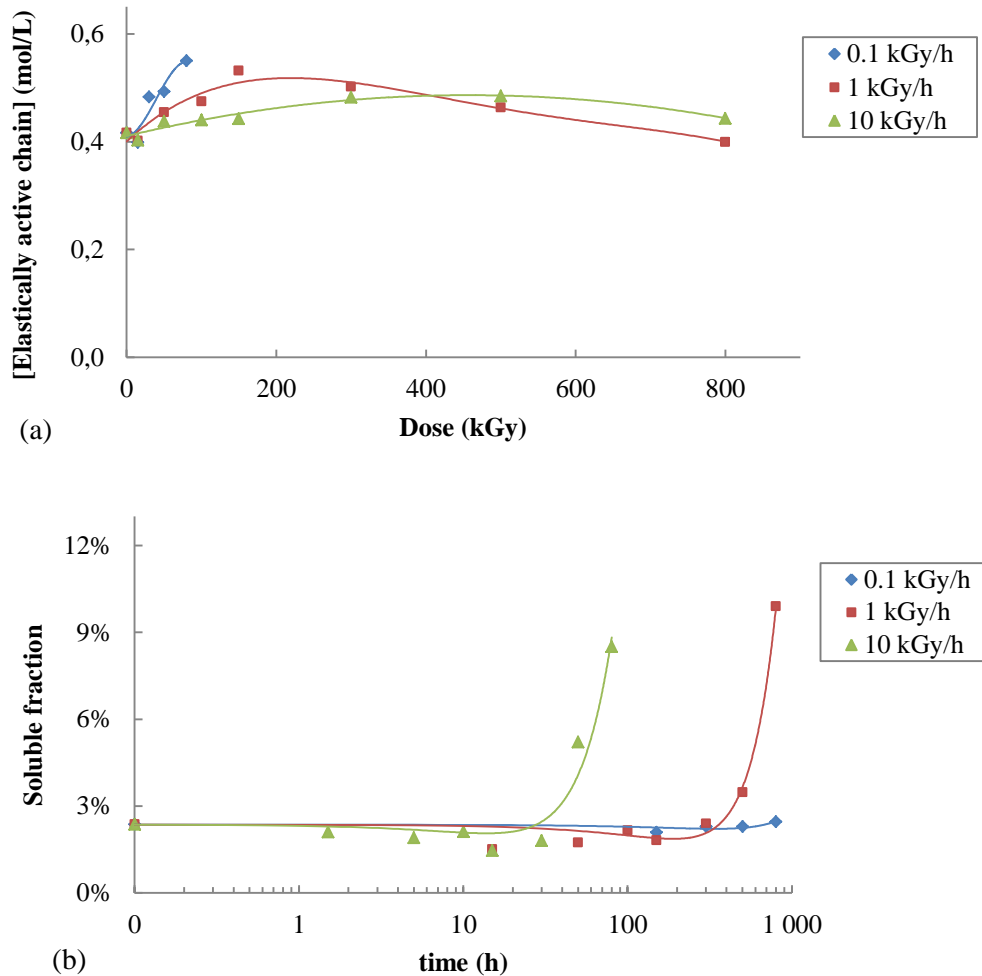


Figure 4-36: Effect of dose rate on the changes in (a) elastically active chains vs. received dose and (b) soluble fraction vs. time of exposure Neat Nordel 4640 in air at 40°C

The oxidation under 0.1 kGy.h⁻¹ showed to be homogeneous up to the maximum received dose, i.e. 80 kGy, but could not be continued any further. However, from what has been observed for two other dose rates, one may expect the same behavior about swelling characteristic of EPDM network for longer exposure times under 0.1 kGy.h⁻¹. This assumption however, remains to be established in future studies.

4.3.2.2 Swelling of filled EPDM

Changes in soluble fraction of filled samples expressed for volume unit of matrix has shown to be similar to neat rubber, with the alteration zone around 150 hours under 1 kGy/h⁻¹ (Figure 4-37). The quantitative values of F_S for all samples remain in the same order as well, except for the final received doses, where the samples are highly degraded, leading to higher amounts of experimental error. However, at this final step of exposure, a higher F_S can be reported for TATH filled samples.

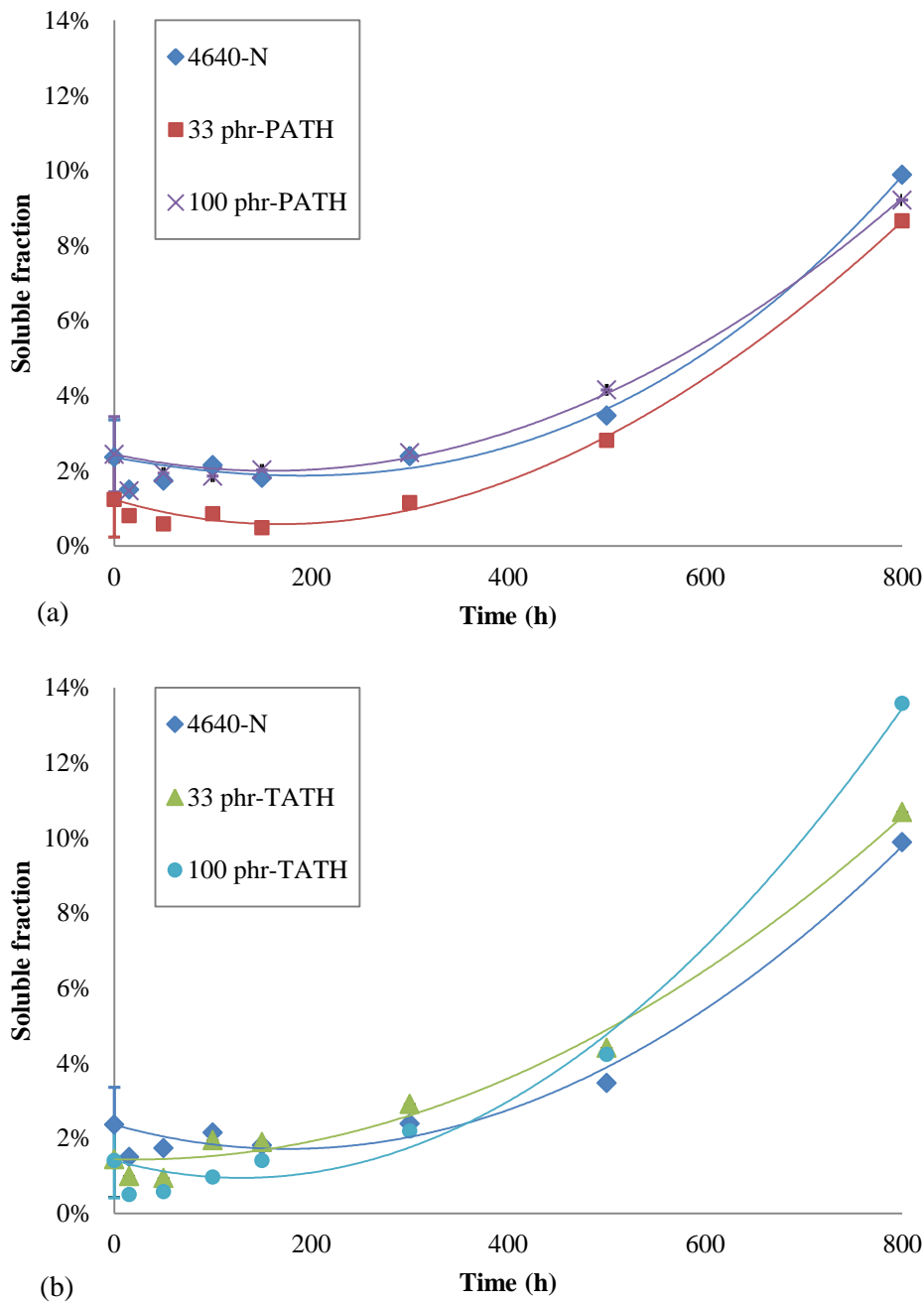


Figure 4-37: Kinetic curves of soluble fraction under $1 \text{ kGy}\cdot\text{h}^{-1}$ in air at 40°C for Nordel 4640 filled with: a) pristine ATH and b) surface treated ATH

One can recognize the similarity of F_S changes between thermal and chemical aging. In contrast, the changes of v under irradiation do not follow the same pattern as at high temperatures (Figure 4-38). Radiochemical oxidation seems to engender the same changes in v for neat and filled samples. The same succession of mechanism predominance observed for neat EPDM is evident for filled samples, although the amplitude of these variations differs slightly from one sample to another.

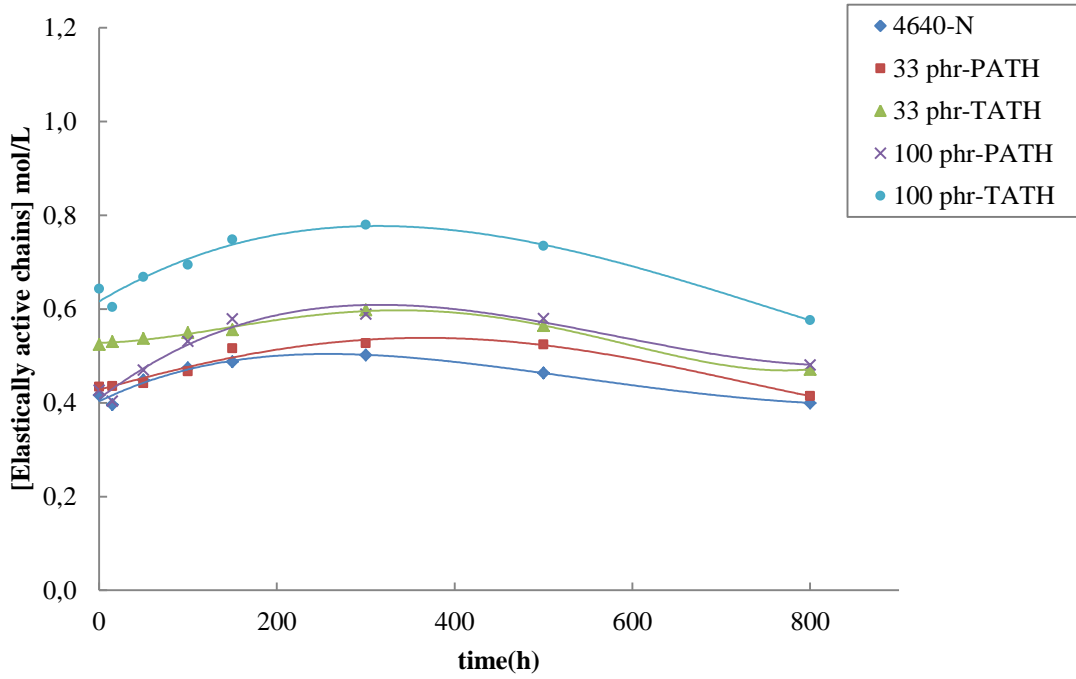


Figure 4-38: Kinetic curves of elastically active chains for neat and filled Nordel 4640 samples under $1 \text{ kGy}\cdot\text{h}^{-1}$ in air at 40°C

More clarifications about the extent of apparent densification due to filler type can be obtained by comparing the variations in concentration of elastically active chains Δv , as explained in Equation 4-11. Figure 4-39 clearly shows the densification phenomenon that increases with the filler content, as already seen in the case of thermal oxidation.

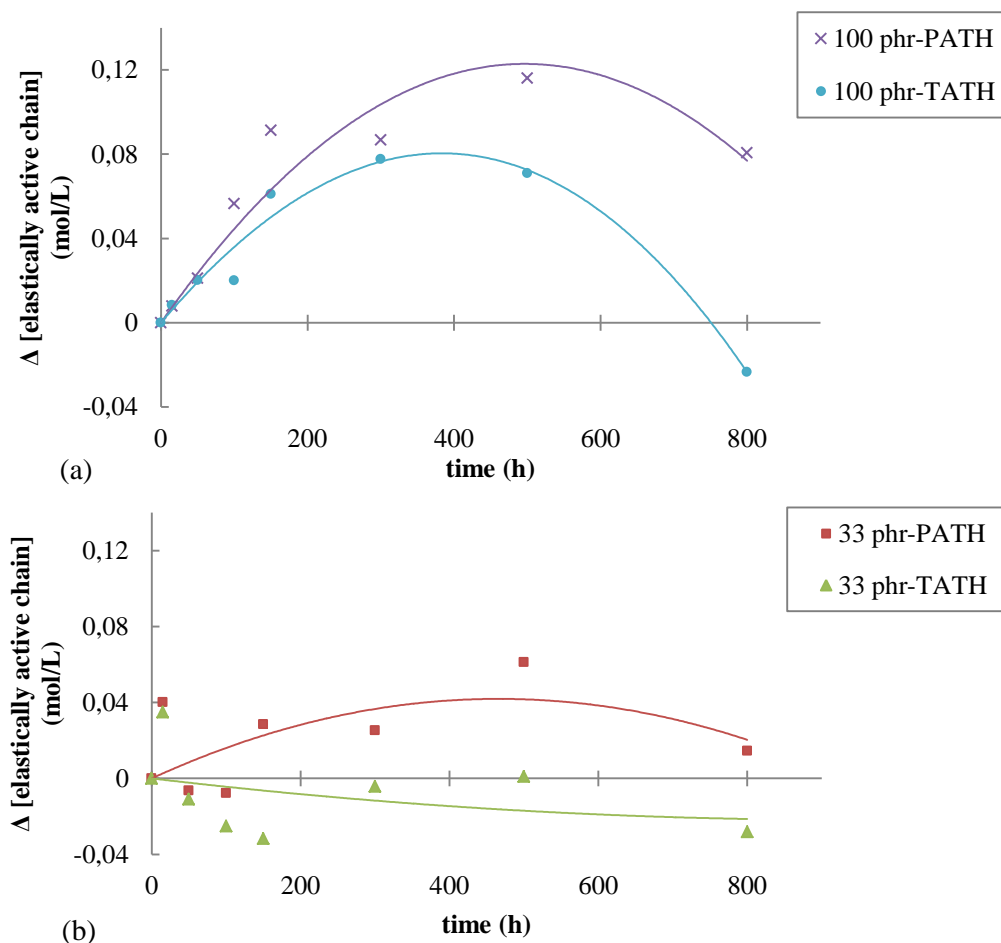


Figure 4-39: Kinetic curves of variations of elastically active chains of filled Nordel 4640 samples under 1 kGy.h^{-1} in air at 40°C

Globally, from what have been experienced here, one can say that although the predominant mechanism in the matrix network is different for thermal and radiochemical oxidation, it seems that in the vicinity of ATH particle, the interphase network goes through analogous changes. In the next section an explanation to this phenomenon will be provided.

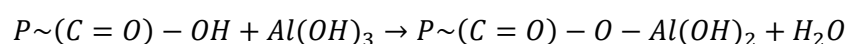
4.4 Discussion of swelling behavior throughout oxidative aging

The experimental results at macromolecular scale reveal that although the neat EPDM network structure undergoes dissimilar modifications under different source of stress, the introduction of ATH particles drives the filler/matrix interphase to similar alterations. The decrease in swelling ratio in the early stages of exposure is attributed to two possible phenomena:

1. Decrease in swelling ability of solvent due to formation of polar oxidation products and alteration of the Huggins polymer/solvent interaction,
2. Creation of strong bonds between the filler particles and the polymer chains throughout aging.

The second phenomenon cannot be refuted because, at the beginning of exposure where the concentration of oxidation products is still negligible comparing to total hydrocarbon species, v increases. This densification is influenced by the presence of a chemical treatment on the filler surface treatment as well, while the Huggins factor is assumed to change identically for the same volume fraction of polymer under the same aging conditions. Even though a very few studies have considered this aspect for ATH filled elastomers, such a densification has been reported in a considerable number of research works on aging of carbon black filled elastomers [38-40], despite the unexplained driving mechanism.

At unaged state, the interaction between filler particles and polymer chains is due to the weak Van der Waals forces induced by the polar surface of ATH particles. As highly polar oxidation products, such as hydroperoxides, alcohols or carboxylic acids, stronger dipole interactions can be established. This idea can be pushed even further by assuming the formation of chemical bonds between the reactive chemical groups at ATH surface and the oxidation products. For instance, a condensation reaction may take place between hydroxyl functions of the filler particles and carboxylic acids, based on following reaction:



The proposed mechanism can as well explain the effect of surface treatment on lower densification in the interphase network. Indeed, fillers with treated surface have lesser exposed hydroxyl groups reachable to oxidation products. Therefore, it is normal to observe lower densification for treated filled composites. There is no need to say that this densification is proportional to filler contents, as it was approved from experimental results.

The only issue remaining unexplained here is the difference between ultimate densifications in thermal and radiochemical oxidation. This comparison may be unnecessary because the aging mechanisms and conditions are different. However, the proposed mechanism can explain, to some extent, why the densification is higher in case of thermal oxidation. As it was explained in Chapter III, the interphase network formed around the filler particles show a lower mobility and is closer to glassy state than matrix network. Under irradiation the samples are exposed at a temperature slightly higher than room temperature while, under thermal exposure, the samples are exposed at temperatures much higher than the former. The higher temperature of aging implies that interphase network approaches rubbery state and its mobility increases, while diffusion of oxygen molecules is facilitated, as well. Therefore, a higher number of densification acts is probable at higher temperatures. Furthermore, the most probable products susceptible to participate in densification reactions seems to be carboxylic acids, which is a major product of EPDM thermal oxidation detected by FTIR spectrophotometry and, as it was previously mentioned, its formation yield is an increasing function of temperature.

Conclusion

The kinetic parameters of thermal oxidation of neat EPDM matrix have been determined for the three EPDM matrices under study. These data, and especially the kinetic parameters of ENB double bond consumption, can be now used to complete the model of thermo-radio-oxidation previously established for ethylene-propylene copolymer family (EPR) at PIMM laboratory. Furthermore, the increase in temperature induces a diffusion control of oxidation above 90°C. This kinetic change leads to a heterogeneous oxidation, i.e. to the formation of a superficial oxidized layer. Similarly, by investigating the effect of dose rate on samples, a transition zone from pure radiochemical aging to a radio-thermal aging dominated region has been observed from 10 kGy.h⁻¹ to 0.1 kGy.h⁻¹ of dose rate.

Analyzing the kinetic curves of hydroperoxide formation has revealed that the formation rate of hydroperoxides decreases with the filler content. Furthermore, the hydroperoxide formation is more intense in the case of samples filled with surface treated filler. On the other hand, the swelling tests have shown that the crosslink density increases during oxidation, which is attributed partially to changes in polymer/solvent interaction parameter. However, more precise examination of swelling ratio has revealed that another phenomenon happens to decrease the swelling ratio. It is proposed that a chemical reaction between oxidation products and chemical functions at the filler surface is responsible for densification of the network at filler/matrix interphase.

The hypothesis of chemical reaction at the filler surface can acceptably explain the phenomena observed in this chapter. However, this approach raises several questions which are placed in future perspectives of this study, such as:

- What is the exact chemical mechanism responsible of filler/matrix interactions?
- How exactly the chemical reaction densifies the interphase network?
- What is the role of the surface treatment of fillers? etc.

The next chapter will be devoted to analyze the consequences of macromolecular modifications on the mechanical properties (elastic and fracture properties) of neat and filled EPDM matrices. Young's modulus will allow us to determine more rigorously the changes in concentration of the elastically active chains. These results will consequently be compared with those found by the swelling method.

Reference

1. Coiffier, F., R. Arnaud, and J. Lemaire, *Hydroperoxydation primaire de terpolymères d'éthylène/propylène/éthylidene-5 norbornène-2*. Die Makromolekulare Chemie, 1984. **185**(6): p. 1095-1104.
2. Scoponi, M., et al., *Photodegradation of poly [ethylene - co - propene - co - (5-ethylidene-2-norbornene)] rubbers*. Macromolecular Chemistry and Physics, 1994. **195**(3): p. 985-997.
3. Hilborn, J. and B. Ranby, *Photocrosslinking of EPDM elastomers: reactions with model compounds studied by electron spin resonance*. Macromolecules, 1989. **22**(3): p. 1154-1159.
4. Delor, F., et al., *Ageing of EPDM—2. Role of hydroperoxides in photo- and thermo-oxidation*. Polymer Degradation and Stability, 1998. **60**(2-3): p. 321-331.
5. Adam, C., J. Lacoste, and J. Lemaire, *Photo-oxidation of elastomeric materials. Part I—Photo-oxidation of polybutadienes*. Polymer degradation and stability, 1989. **24**(3): p. 185-200.
6. Meyer, W. and G. Spiteller, *Epoxidierung von Kohlenstoff-Kohlenstoff-Doppelbindungen in Terpenen durch Linolsaurehydroperoxide*. Liebigs Annalen der Chemie, 2006. **1993**(12): p. 1253-1256.
7. Mayo, F.R., *The Oxidation of Unsaturated Compounds. V. The Effect of Oxygen Pressure on the Oxidation of Styrene* 1, 2. Journal of the American Chemical Society, 1958. **80**(10): p. 2465-2480.
8. Gemmer, R.V., M.A. Golub, and E.G. Brame Jr, *Applications of Polymer Spectroscopy*. Academic Press, New York, 1978: p. 79.
9. Shelton, J.R., *Oxidation and stabilization of rubbers*. Rubber Chemistry and Technology, 1983. **56**(3): p. 71-86.
10. Coquillat, M., et al., *Thermal oxidation of polybutadiene. Part 2: Mechanistic and kinetic schemes for additive-free non-crosslinked polybutadiene*. Polymer Degradation and Stability, 2007. **92**(7): p. 1334-1342.
11. Lin, V.D., et al., *The handbook of infrared and raman characteristic frequencies of organic molecules*. 1991, Academic Press, New York. p. 68.
12. Colthup, N.B., L.H. Daly, and S.E. Wiberley, *Introduction to infrared and raman spectroscopy POD*. 1990.
13. Arnaud, R., J.Y. Moisan, and J. Lemaire, *Primary hydroperoxidation in low-density polyethylene*. Macromolecules, 1984. **17**(3): p. 332-336.
14. Avram, M., G.D. Mateescu, and A.M. Glatz, *Spectroscopie infrarouge: applications en chimie organique*. 1970: Dunod.
15. Lacoste, J. and D.J. Carlsson, *Gamma-, photo-, and thermally-initiated oxidation of linear low density polyethylene: A quantitative comparison of oxidation products*. Journal of Polymer Science Part A: Polymer Chemistry, 1992. **30**(3): p. 493-500.
16. Audouin, L., et al., *Effect of temperature on the photooxidation of polypropylene films*. Polymer degradation and stability, 1998. **60**(1): p. 137-143.
17. Cambon, S., *Etude du mécanisme de dégradation radiochimique d'un élastomère de type EPDM*. 2001, Thèse de Doctorat.
18. Gugumus, F., *Effect of temperature on the lifetime of stabilized and unstabilized PP films*. Polymer degradation and stability. Polymer Degradation and Stability, 1999. **63**(1): p. 41-52.
19. Gugumus, F., *Physico-chemical aspects of polyethylene processing in open mixers I: Review of published work*. Polymer degradation and stability, 1999. **66**(2): p. 161-172.
20. Colin, X., et al., *Kinetic modelling of radiochemical ageing of ethylene-propylene copolymers*. Radiation Physics and chemistry, 2010. **79**(3): p. 365-370.
21. Langlois, V., *Vieillissement Thermique du Polyéthylène Reticulé*, PhD Thesis.
22. Gueguen, V., *Vieillissement d'élastomères utilisés comme isolant électriques en ambiance nucléaire*. 1992.
23. Colin, X., G. Teyssedre, and M. Fois, *Ageing and degradation of multiphase polymer systems*, in *Handbook of Multiphase Polymer Systems*. 2011, Wiley.

24. Mallécol, J., et al., *Thermal (DSC) and chemical (iodometric titration) methods for peroxides measurements in order to monitor drying extent of alkyd resins*. Progress in Organic Coatings, 2001. **41**(1-3): p. 171-176.
25. Richaud, E., *Durabilité des géotextiles en polypropylène*. 2006, Arts et Métiers ParisTech.
26. Simon, S.L., *Temperature-modulated differential scanning calorimetry: theory and application*. Thermochimica Acta, 2001. **374**(1): p. 55-71.
27. Rincon-Rubio, L.M., et al., *A general solution of the closed-loop kinetic scheme for the thermal oxidation of polypropylene*. Polymer degradation and stability, 2001. **74**(1): p. 177-188.
28. Colin, X., L. Audouin, and J. Verdu., *Determination of thermal oxidation rate constants by an inverse method. application to polyethylene*. Polymer Degradation and Stability, 2004. **86**(2): p. 309–321.
29. Calvert, J.G. and J.N. Pitts, *Photochemistry*. 1966: John Wiley & Sons.
30. Blanksby, S.J. and G.B. Ellison, *Bond dissociation energies of organic molecules*. Accounts of chemical research, 2003. **36**(4): p. 255-263.
31. Ridgefield, A. and J. Tittmaa, *GAMMA RAY ENERGY*. 1972, Google Patents.
32. Fayolle, B., et al., *Polymères en ambiance nucléaire: Comportement à long terme*. 2012: Lavoisier.
33. Colin, X., G. Teyssedre, and M. Fois, *Ageing and Degradation of Multiphase Polymer Systems*. Handbook of Multiphase Polymer Systems: p. 797-841.
34. Khelidj, N., et al., *A simplified approach for the lifetime prediction of PE in nuclear environments*. Nuclear Instruments and Methods in Physics Research Section B: Beam Interactions with Materials and Atoms, 2005. **236**(1): p. 88-94.
35. Hansen, C.M., *I. Solvents, plasticizers, polymers, and resins-the three dimensional solubility parameter-key to paint component affinities*. Journal of paint technology, 1967. **39**(505): p. 104-117.
36. Van Krevelen, D.W. and K. Te Nijenhuis, *Properties of polymers: their correlation with chemical structure; their numerical estimation and prediction from additive group contributions*. 2009: Elsevier Science.
37. Planes, E., et al., *Evolution of EPDM networks aged by gamma irradiation – Consequences on the mechanical properties*. Polymer, 2009. **50**(16): p. 4028–4038.
38. Fröhlich, J., W. Niedermeier, and H.-D. Luginsland, *The effect of filler–filler and filler–elastomer interaction on rubber reinforcement*. Composites Part A: Applied Science and Manufacturing, 2005. **36**(4): p. 449-460.
39. Sosson, F., et al., *Highlight of a compensation effect between filler morphology and loading on dynamic properties of filled rubbers*. Journal of applied polymer science, 2010. **117**(5): p. 2715-2723.
40. O'brien, J., et al., *An NMR investigation of the interaction between carbon black and cis-polybutadiene*. Macromolecules, 1976. **9**(4): p. 653-660.

CHAPTER V

5 Mechanical Aspects

Extended abstract (in French language)

Dans le chapitre précédent, les mécanismes d'oxydation thermique et radiochimique et leurs conséquences à l'échelle moléculaire et macromoléculaire ont été étudiés. Néanmoins, d'autres méthodes expérimentales complémentaires sont nécessaires pour identifier clairement les effets aux échelles macromoléculaire et macroscopique. Dans ce chapitre, l'essai de traction, complémentaire de la méthode de gonflement, est utilisé pour déterminer les modifications exactes du réseau EPDM pendant le vieillissement. Le module d'Young est utilisé pour préciser les modifications à l'échelle macromoléculaire. Par la suite, les conséquences de ces modifications sur les propriétés à la rupture, et en particulier l'allongement à la rupture, sont étudiées.

Les résultats obtenus dans ce chapitre peuvent être résumés comme suit.

La détermination des variations du module d'Young est une méthode classique pour déterminer les modifications macromoléculaires du réseau EPDM tridimensionnel. Comme mentionné dans le chapitre IV, la validité de la méthode de gonflement est limitée par la concentration des produits d'oxydation. La concentration des chaînes élastiquement actives mesurée par des essais de traction montre clairement ces limites, et permet de définir un domaine de validité pour l'essai de gonflement. Ce domaine de validité est mis en évidence par la Figure IV pour la matrice EPDM pure à 110°C dans l'air. A environ 50 heures, la densité des chaînes élastiquement actives mesurées par gonflement commence à se stabiliser, alors que la densité des chaînes élastiquement actives déterminée par l'essai de traction continue à diminuer.

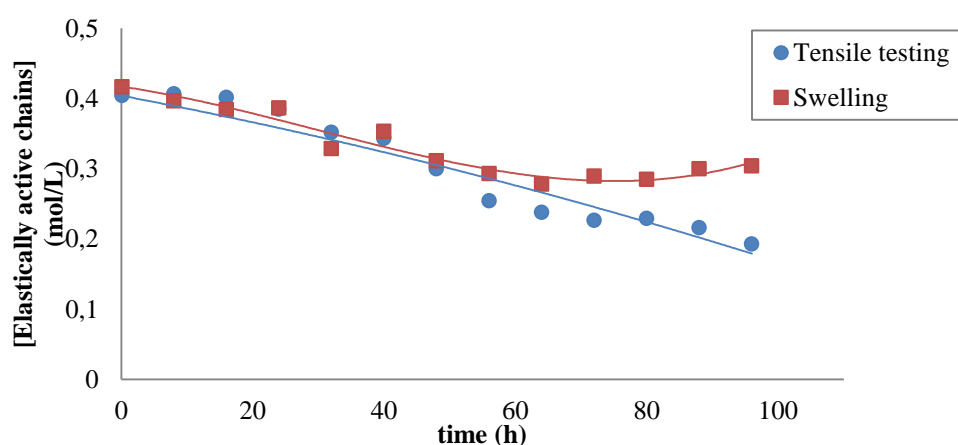


Figure IV : Comparaison entre les courbes cinétiques de densité des chaînes élastiquement actives déterminées par les essais de gonflement et de traction

L'essai de traction met également en évidence un changement de phénomène prédominant dans les matrices chargées. La densification du réseau observée au début de l'exposition oxydative, est suivie par la destruction du réseau EPDM à plus long terme. A partir d'un modèle d'interphase à deux phases,

il est montré que la densification se produit exclusivement dans l'interphase (Figure V), entraînant une augmentation du module d'Young dans cette interphase, tandis que ce module diminue dans la matrice EPDM. Ce phénomène se traduit par une augmentation de la concentration des chaînes élastiquement actives dans l'interphase, et la diminution de la concentration des chaînes élastiquement actives dans la matrice EPDM.

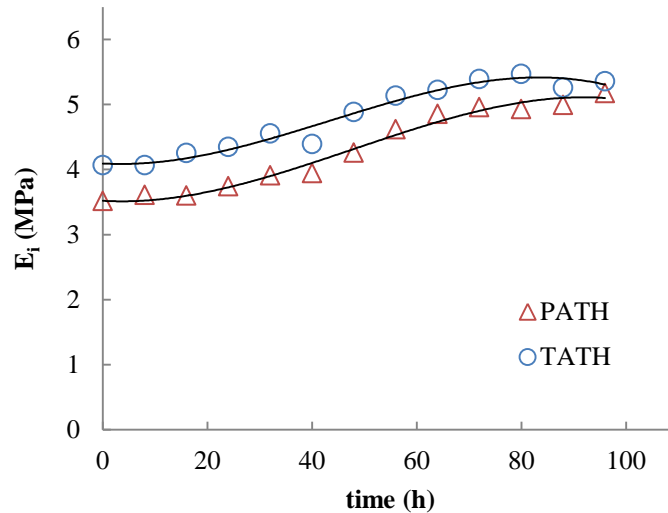


Figure V : Augmentation du module d'Young de l'interphase dans l'air à 110°C pour la matrice EPDM chargée par des ATH vierge (PATH) et traité en surface (TATH)

Une méthode empirique a été proposée pour calculer l'épaisseur de l'interphase. Cette méthode repose sur un réseau de l'interphase en parallèle avec le réseau de la matrice EPDM. A partir de cette méthode, le module d'Young du réseau de l'interphase a été calculé à partir du module d'Young global connu de la phase polymère dans le composite.

L'analyse des courbes cinétiques de module d'Young de l'interphase pendant les vieillissements thermique et radiochimique a montré que le mécanisme de densification du réseau diffère pour ces deux types de vieillissement. Les interactions entre la matrice EPDM et la surface des charges ATH vierges sont responsables de densification à haute température, alors que les molécules de traitement de surface sont responsables de la densification de l'interphase sous irradiation.

L'allure des courbes cinétique d'allongement à la rupture semble être similaire pour la thermo- et la radio-oxydation, i.e. une hausse initiale suivie d'une dégradation. Cependant, les mécanismes responsables de ces modifications se révèlent être complètement différents. Dans le cas de la thermo-oxydation, la transformation des nœuds de réseaux nœuds tétrafonctionnels en trifonctionnels conduit à une augmentation de l'allongement à la rupture, tandis que le module d'Young diminue constamment (Figure VI).

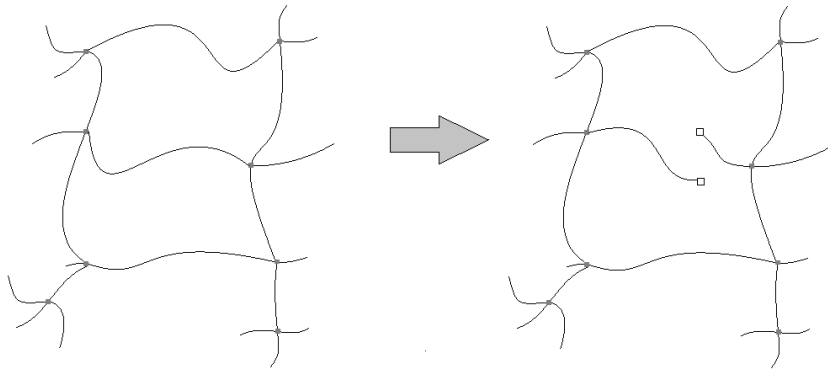


Figure VI : Schématisation de la transformation de nœuds tétrafonctionnels en nœuds trifonctionnels

Sous irradiation, la réticulation est responsable de l'augmentation initiale simultanée de l'allongement à la rupture et du module d'Young de la matrice chargée. En fait, sous irradiation à basse température, l'évolution de la matrice EPDM chargée est identique à celle de la matrice EPDM pure, sauf que les molécules de traitement de surface amplifient les effets de la réticulation. Au contraire, à haute température, l'interaction entre les produits d'oxydation et la surface des charges ATH vierges entraîne une amplification des effets de la réticulation de la matrice EPDM chargée. Le deuxième mécanisme rencontré est complexe, et nécessite des études complémentaires pour le clarifier.

Introduction

In the previous chapter, the mechanisms of thermal and radiochemical oxidation, and their consequences at molecular and macromolecular scale have been studied. However, additional experimental methods seemed to be necessary to clarify the effects at the macromolecular and macroscopic scales. In this chapter, tensile testing, complementary to swelling method, is employed to determine the exact modification of EPDM network throughout aging. The Young's modulus will be used to clarify the modifications at macromolecular scale. Subsequently, the effect of these modifications on the ultimate properties, and in particular the elongation at break, will be studied

5.1 Effect of thermal aging on mechanical properties

5.1.1 Changes in Young's modulus

Creation of elastically active chains increases Young's modulus, while chain scissions decrease this mechanical property. Consequently, the evolution of the network throughout aging can be demonstrated by measuring the changes in Young's modulus through tensile testing. In what follows, the changes in Young's modulus of neat and filled EPDM samples are presented and discussed.

5.1.1.1 Neat EPDM

The equation of Flory establishes a linear relationship between Young's modulus and crosslink density of a tridimensional elastomer network [1]. The advantage of this method, comparing to swelling method, is that the creation of oxidation products does not affect the values determined for ν .

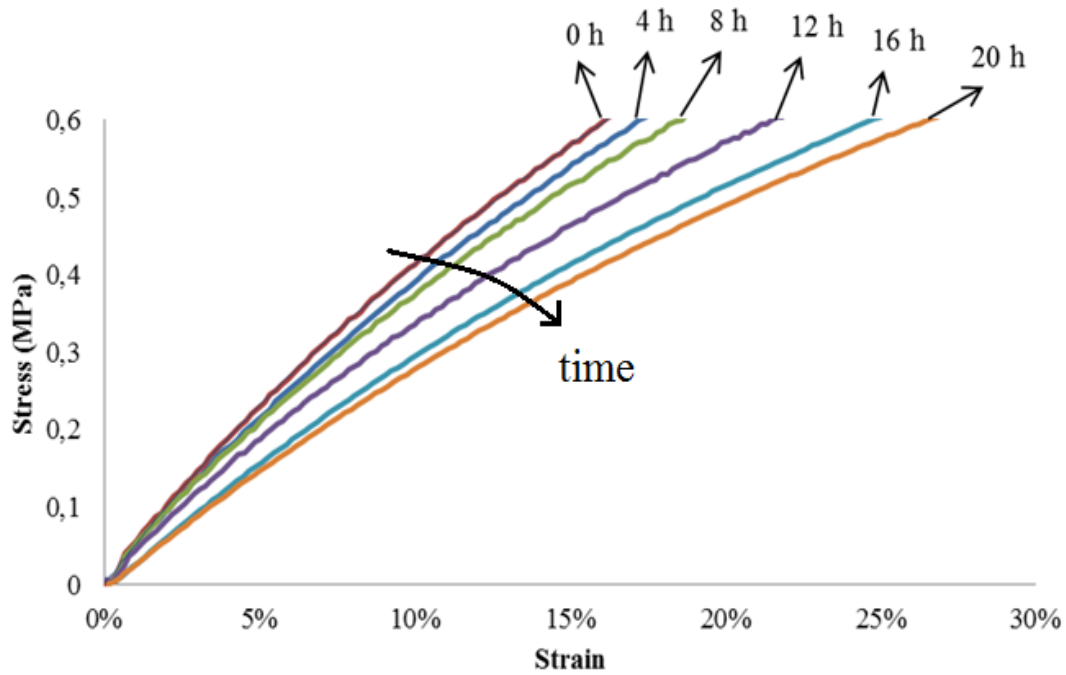


Figure 5-1: Changes in Young's modulus of neat Nordel 4640 at 130°C in air monitored by tensile testing – The arrow indicates the sense of variations with aging time (For more clarity, the stress-strain curves are not presented up to their ultimate elongation)

Figure 5-1 shows the evolution of the initial part of stress-strain curves of neat EPDM samples at 130°C in air. It can be seen that the Young's modulus decreases with the time of exposure. The general behavior is similar for other temperatures except for 90°C where, similar to the swelling results, a minor crosslinking step is observable in the early periods of exposure (Figure 5-2).

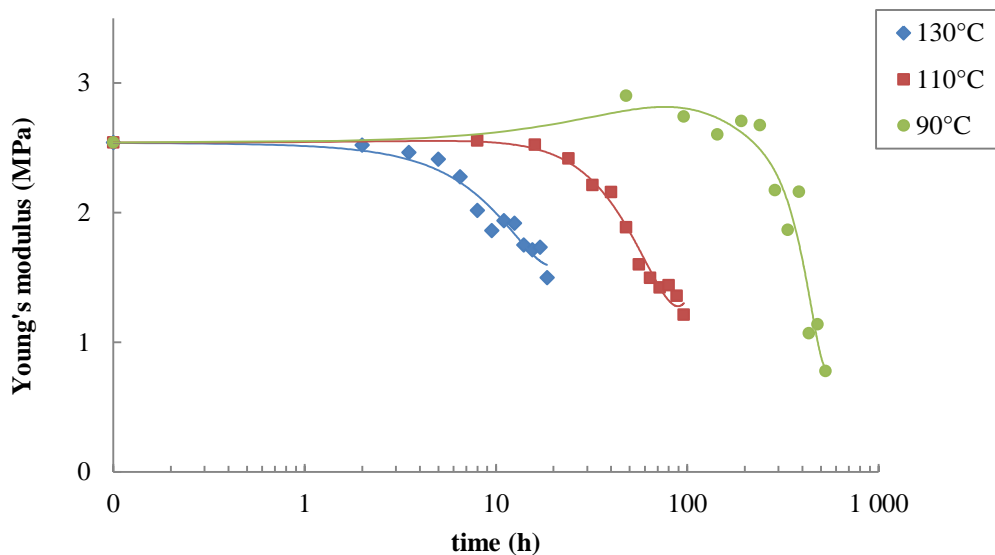


Figure 5-2: Effect of temperature on the kinetic curves of Young's modulus of neat Nordel 4640 in air

It should be pointed out that, for each aging temperature under study, the exposure has been carried on as longest as possible. After a specific time, the EPDM samples become so degraded and sticky at their surface that any type of characterization experiment becomes e.

5.1.1.2 Filled EPDM

At 90°C, the modulus of neat EPDM sample does not change before 150 hours and decreases afterwards (Figure 5-3). This time coincides with the time at which the carbonyls increases sharply and approaches its maximal rate (steady-state). By introducing 33phr of ATH (pristine or surface treated), the moduli remain roughly constant all along the exposure time. Meanwhile, the samples containing 100 phr show a complete different behavior. Both samples, i.e. containing 100 phr of PATH and TATH, show an initial increase, up to 150 – 300 hours and then remain stable. The increase in Young’s modulus is higher for PATH containing samples. Therefore, it can be seen that the presence of filler particles induces a stress hardening in tensile curves during oxidation, and that the introduction of surface treatment decreases this effect. This behavior is in complete conformity with the results of swelling method presented in the previous chapter.

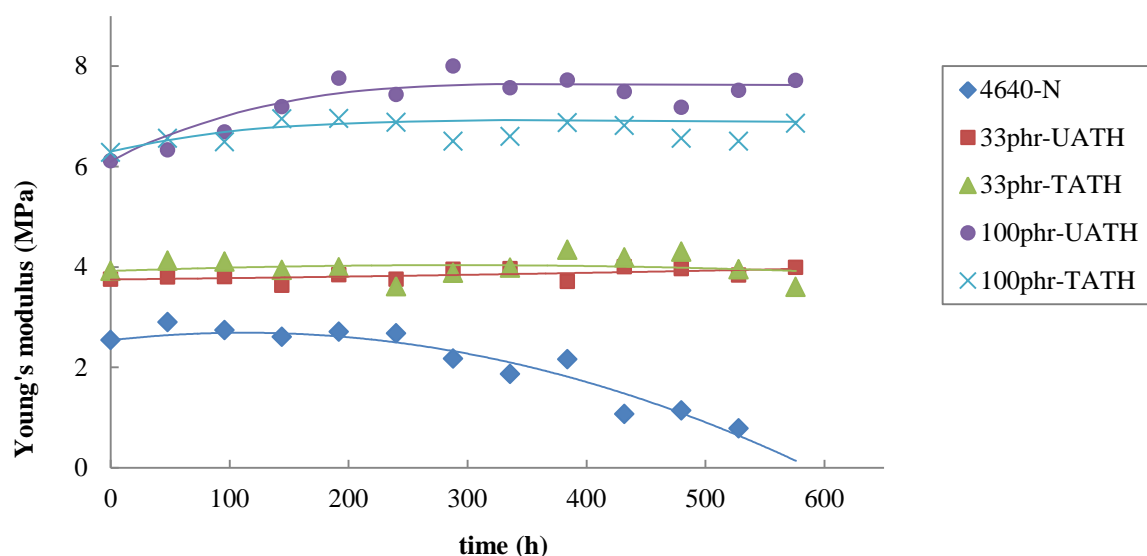


Figure 5-3: Kinetic curves of Young’s modulus at 90°C in air for neat and filled Nordel 4640 samples

Comparison of samples behavior at 90°C with other exposure temperatures seems irrational due to different time scales. But, the rise in temperature decreases the apparent stress hardening effect, as it can be seen for samples aged in air at 130°C in Figure 5-4. Results of exposure at 110°C are not presented, but they follow the same rule.

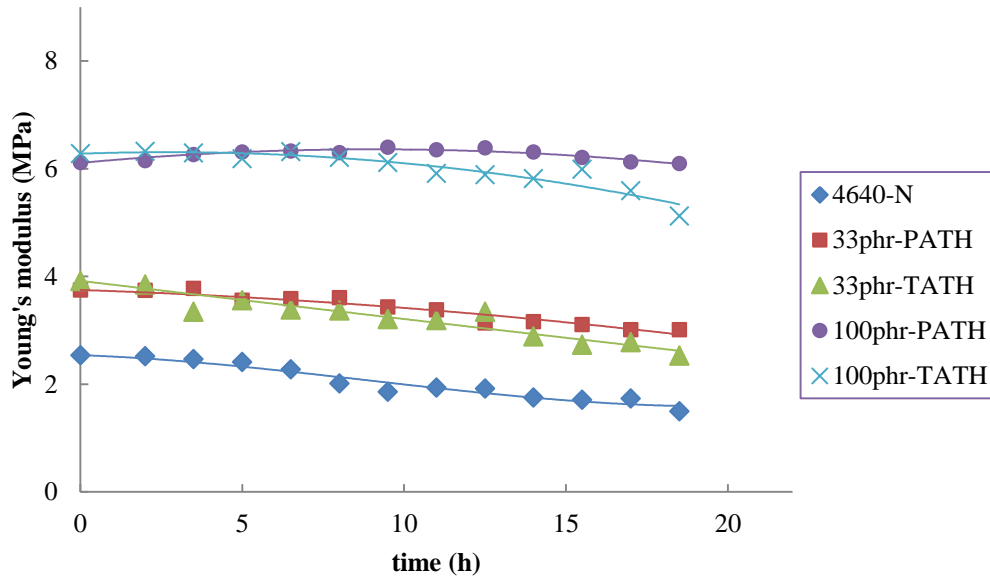


Figure 5-4: Kinetic curves of Young's modulus at 130°C in air for neat and filled Nordel 4640 samples

The results above show that the temperature and the filler content, as well as the surface treatment, can affect the kinetic curves of modulus throughout thermal oxidation. These effects can be regrouped as follow:

- I. Creation of strong filler/matrix interactions: Neat EPDM behavior shows that chain scission is the predominant phenomenon in the matrix network, while the introduction of filler particles into polymer matrix changes this predominance. The presence of 33 phr of ATH nullifies the effect of chain scissions, and the presence of 100 phr of ATH counterbalances this predominance and replaces it by a toughening.
- II. As the temperature increases, although the behavior of neat sample remains the same, the toughening phenomenon appeases. Indeed, this latter is hardly observable at the highest filler content at 130°C.
- III. Surface treatment of filler particles decreases the amplitude of the toughening phenomenon. This effect is better observable for fillers with 100 phr content.

The results found by tensile testing validate the hypothesis that was proposed in Chapter III, stating the formation of strong filler/matrix interactions throughout thermal exposure. After this confirmation we will quantify macromolecular changes in the tridimensional network in both neat and filled samples.

5.1.2 Discussion

5.1.2.1 Neat EPDM

In the previous chapter, we have mentioned that the swelling test has a validity time interval and becomes erroneous when the concentration of oxidation products increases sharply (high conversion ratios of oxidation process). To better visualize this phenomenon, the evolution of v calculated by both experimental methods have been plotted in Figure 5-5 for neat Nordel 4640 samples at 110°C in air.

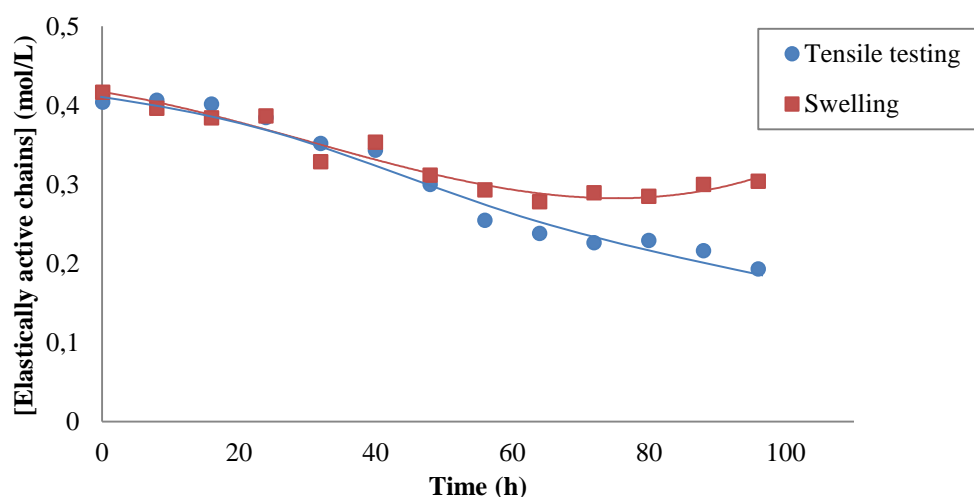


Figure 5-5: Comparison of the kinetic curves of elastically active chains determined by tensile testing and swelling for neat Nordel 4640 at 110°C in air

At the beginning of exposure, the results obtained with the two methods correspond perfectly to each other. Then, at about 50 hours of thermal exposure, the two plots begin to deviate. Indeed, the tensile results show a constant decrease, while the swelling results tend to stabilize, or even to slightly increase. This behavior is related to the changes in polymer/solvent interaction factor, which leads to an over-estimation of v . The physical sense of this discrepancy is the modification of the swellability of a polymer by changing its non-polar with highly polar chemical groups. This phenomenon abnormally decreases the swelling ratio of the network, which is equivalent to an abnormal increase in v . Evidently, the deviation increases for longer exposure times. On the other hand, before 50h at 110°C, the results found by the two methods are practically identical and change in the same manner. This deviation is observable at other temperatures of study and happens after 300 hours at 90°C and 15 hours at 130°C.

5.1.2.2 Filled EPDM

PATH is mainly considered as a neutral filler. That is the reason why the chemical surface treatment is in general used for increasing the mechanical properties of the composites. However, we have seen that this neutrality becomes invalid during thermal and radiochemical oxidation. Recalling from the results obtained from Chapter III Section 3.2.3, the polymer in composites forms two interpenetrating networks, known as matrix and sticky interphase. In order to differentiate the changes in mechanical properties of these two networks, it is assumed in a first approach that composite matrix behaves as the neat EPDM. Thus, E and ν would change identically in the composite's matrix network and neat EPDM. As the properties of matrix network and polymer phase in composite are known, the properties of interphase network can be deduced.

From equation 3-37 and 3-39 of Chapter III we have:

$$\psi = \frac{\delta_i}{D} (E_i - E_M) \quad 5-1$$

where, ψ was the slope of the regression straight line passing through the results of polymer modulus versus filler volume fraction. It was shown that this regression line is linear for unaged samples for both types of filler. The linearity confirms that networks can be connected in parallel to calculate the overall Young's modulus. Since it is assumed that the degradation of the matrix network, as well as the interphase network, is independent of the filler contents, the regression lines for aged samples should be linear as well. Indeed, the preservation of this linearity during thermal aging is evidenced (Figure 5-6).

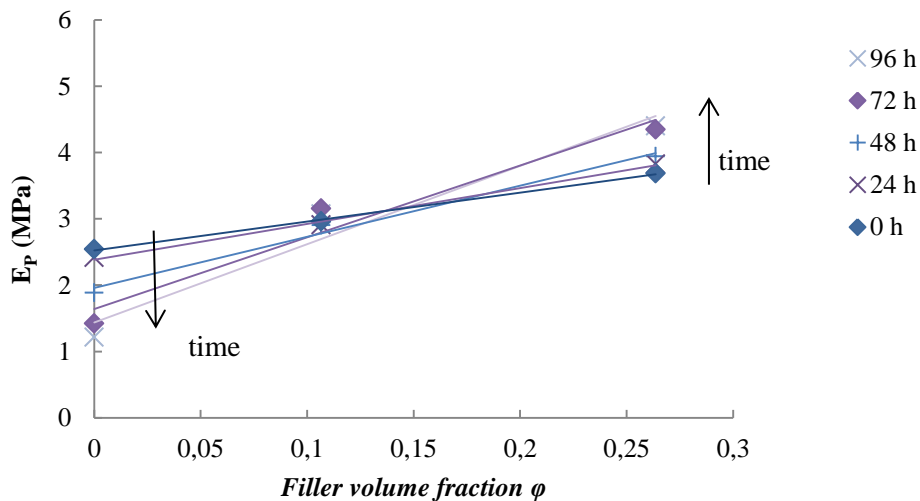


Figure 5-6: Young's modulus of polymer phase E_p versus volume fraction of filler ϕ in Nordel 4640 TATH filled composites at 110°C in air – The arrow indicates the sense of variations with aging time

The value of ψ for the aged samples increases with the exposure time and, although this behavior is only presented for aging at 110°C (Figure 5-7), the same behavior has been observed for the two other temperatures (90 and 130°C). The minimum correlation coefficient is 94%, which reveals that the regression curves of Figure 5-6 are roughly linear.

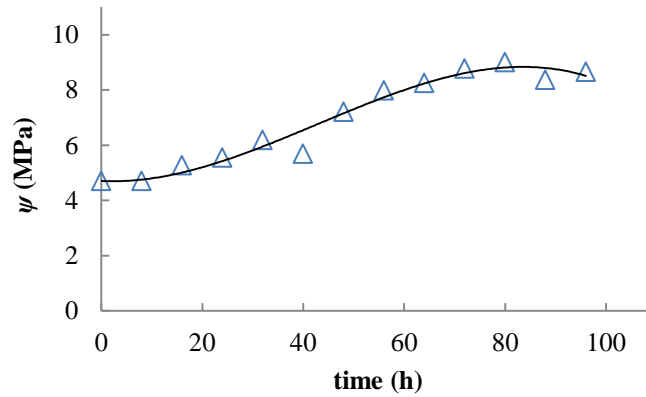


Figure 5-7: Changes in the regression slope ψ at 110°C in air for Nordel 4640 filled with TATH

The unknown parameters of Equation 5-1 are E_M and E_i , which will define the value of ψ . Consequently, changes in the slope can be determined by knowing the changes in matrix and interphase moduli. The derivative of Equation 5-1 with respect to E_M , is:

$$\frac{d\psi}{dE_M} = \frac{6i}{D} \left(\frac{dE_i}{dE_M} - 1 \right) \quad 5-2$$

The interphase network evolves differently from that of the matrix network due to the presence of filler particles in its vicinity. Thus, it is reasonable to consider that E_i and E_M are independent ($\frac{dE_i}{dE_M} = 0$). Finally, Equation 5-2 becomes:

$$\frac{d\psi}{dE_M} = -\frac{6i}{D} \quad 5-3$$

Equation 5-3 suggests that the thickness of the sticky interphase can be calculated, knowing the derivative of ψ with respect to E_M and the diameter of filler particles. For this latter, the average value is equal to 1.3 μm . In contrast, the derivative term needs to be determined. To do so, the changes of ψ versus E_M have been plotted in Figure 5-8 for different temperatures of exposure, and the slope of the regression straight lines $\frac{d\psi}{dE_M}$ has been determined.

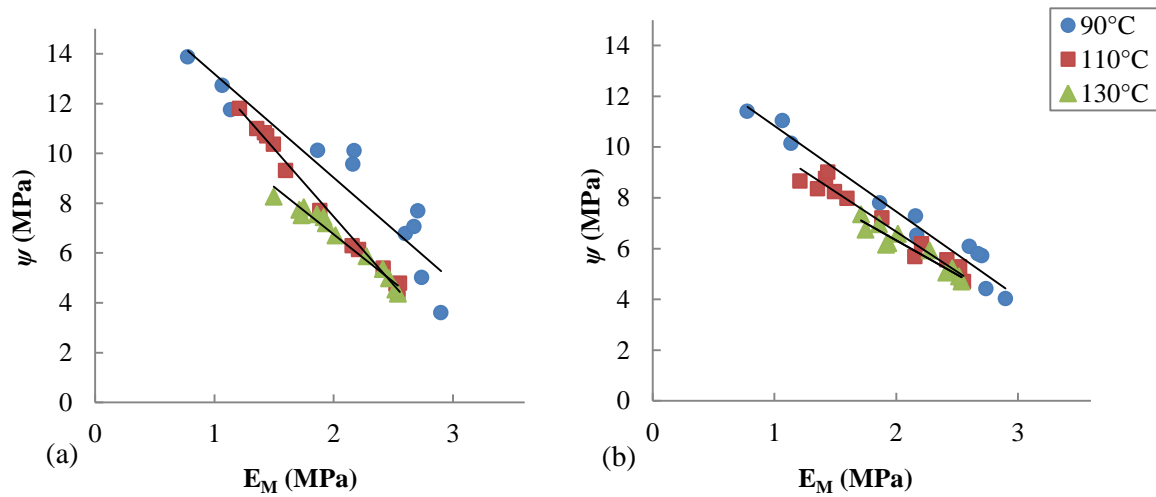


Figure 5-8: ψ versus E_M for: a) PATH and b) THAT in Nordel 4640 at 90, 110 and 130°C in air

Considering Equation 5-3, and constant parameters i and D , $\frac{d\psi}{dE_M}$ should be constant, which is so to a good extent for both types of filler. As a result, the thickness of sticky interphase can be calculated for samples filled with either type of filler (Table 5-1).

Filler type	Thickness of sticky interphase i (μm)
PATH	0.97 ± 0.19
TATH	0.67 ± 0.08

Table 5-1: Values calculated for the sticky interphase thickness i with Equation 5-3

Now that the thickness of interphase is estimated, and E_M and E_P have been previously determined, the modulus of the interphase E_i can be determined for each step of oxidation by using the following equation from chapter III:

$$E_P = \frac{6i}{D}(E_i - E_M)\varphi + E_M \quad 5-4$$

By using the equation above, the changes of E_i during exposure at different temperatures has been plotted in Figure 5-9. The general trend seems to be an immediate increase in E_i to reach an asymptotic value. This sounds licit based on the proposed mechanism. One can observe that the increase of E_i happens more slowly but more intensely at lower temperatures; one can see that the plot of 90°C does not reach its maximum value by the end of exposure, while E_i is already higher than two other temperatures. This behavior can be conveniently explained by considering the oxidation kinetics at the vicinity of filler surface. The simple basis of interphase densification theory is the creation of strong interactions between the filler surface and oxidation products. The two essential parameters are

the formation rate of oxidation products and the available specific surface of ATH. By increasing the exposure temperature, the oxidation rate increases while the available specific ATH surface remains constant. The interphase goes through densification with filler surface. This densification of interphase is a decreasing function of temperature.

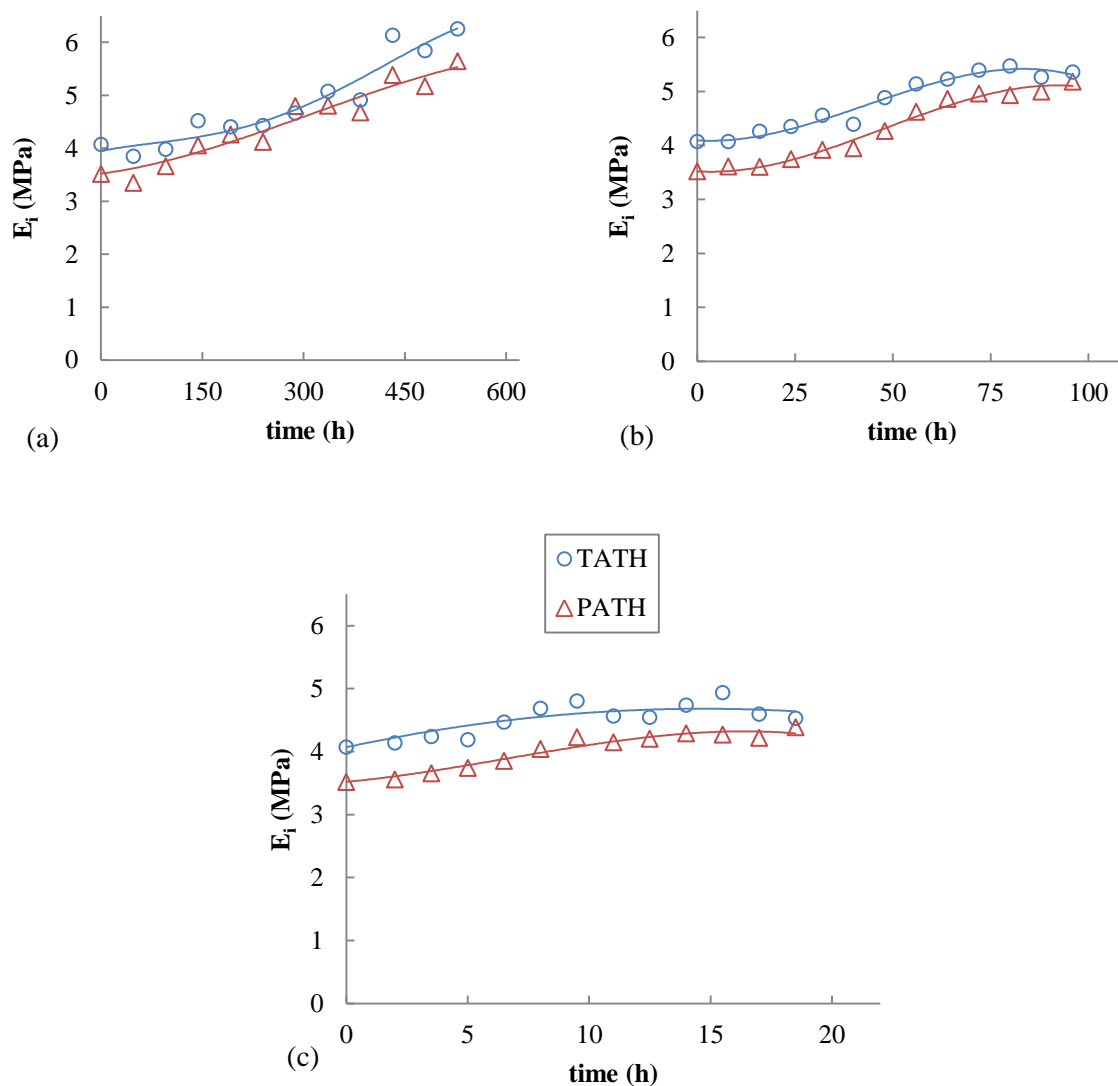
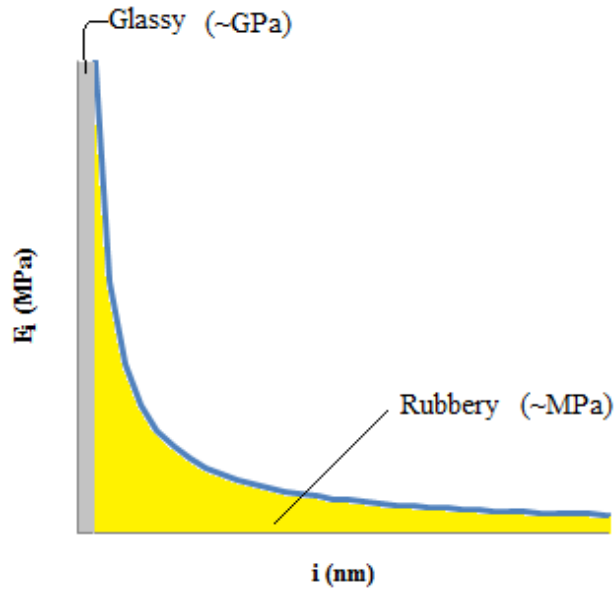


Figure 5-9: Kinetic curves of interphase modulus for Nordel 4640 composites in air at a) 90°C, b) 110°C and c) 130°C

This method provides an approximation of the sticky interphase Young's modulus, which indeed should be verified in the future by more precise experimental methods (e.g. nano-indentation, ATM, etc.). These results, however, are expressed as average values along the sticky interphase thickness. In reality, the interphase network should display a steep modulus gradient. Values should range between high glassy values (~GPa) at the close vicinity of the filler surface and low rubbery values (~MPa) in the matrix, as demonstrated in Scheme 5-1.



Scheme 5-1: Schematizing the modulus gradient in the interphase region

The densification of interphase network is an indicator of higher concentration of elastically active chains, which can be calculated by the Flory's equation. The results of average Young's moduli and concentration of elastically active chains in the interphase for un-aged EPDM composites are grouped in Table 5-2.

	E_i (MPa)	v_i (mol.L⁻¹)
PATH filled EPDM	3.52	0.55
TATH filled EPDM	4.07	0.64
Neat EPDM	2.54	0.40

Table 5-2: Initial values of average moduli and concentration of elastically active chains in interphase region

Each interphase above, contributes to the global polymer modulus in the composite, according to the following common mixture law:

$$E_p = E_M \varphi_M + E_i \varphi_i \quad 5-5$$

On the other hand, in Chapter III Section 3.2.3, it has been shown that the volume fraction of interphases φ_i can be determined by:

$$\varphi_i = \varphi \frac{6i}{D} \quad 5-6$$

where φ is the volumic fraction of filler in the EPDM composite.

Based on Equation 5-6 and knowing its different parameters, the volume fraction of interphases φ_i has been calculated for both types of ATH and different filler content (Table 5-3).

	Filler content (phr)	φ_i (%)
PATH	33	49
	100	100
TATH	33	34
	100	80

Table 5-3: Volume fraction of interphases in different ATH filled Nordel 4640 samples

5.1.3 Ultimate properties

The ultimate (or fracture) behavior of elastomers has been an important subject in the literature with complex explanations and equations. Based on the theory of rubber elasticity, an elastomer network is made up of elastically active chains, which contains N_e deformable bonds of the length l . These chains of average mass M_e , with a tortuosity factor of C_∞ , has an end to end distance equal to d_0 at rest which is equal to [2]:

$$d_0 = (C_\infty N_e l^2)^{0.5} \quad 5-7$$

The same chain at the maximum stretched state has an end to end length of d_r , equal to:

$$d_r = \alpha N_e \quad 5-8$$

where α is related to the geometric factor of chemical structure of monomers. Therefore, the deformation at break Λ_r , which is the ratio between the stretched and at rest states, can be written as:

$$\Lambda_r = \frac{d_r}{d_0} = A N_e^{0.5} \quad 5-9$$

with A a structural factor of the material.

The mass of elastically active chains M_e is the sum of its N_e composing monomers of molar mass M_m ($M_e = N_e \cdot M_m$). By replacing this latter in Equation 5-9, we have:

$$\Lambda_r = \frac{d_r}{d_0} = B M_e^{0.5} \quad 5-10$$

where B is another structural factor of the material.

Thus, in an ideal network the deformation at break is proportional to $M_e^{0.5}$ (i.e. to $\nu^{-0.5}$). Obviously, deviation from ideality will change this proportionality.

After this brief introduction, the results of ultimate properties will be presented and discussed.

5.1.3.1 Neat EPDM

The changes in ultimate deformation Λ_r throughout oxidation at 110°C in air have been plotted in Figure 5-10. In the same figure, the changes in the concentration of elastically active chains deduced from Young's modulus have been plotted as a comparative basis. As it was explained in previous section, the ultimate deformation is proportional (or inversely proportional) to the square root of M_e (ν). However, one can observe that this relationship is not respected. Indeed, ν decreases constantly while, Λ_r shows a slight increase, reaches a maximum value, and decreases slowly afterward. The same behavior has been observed for the two other temperatures under study.

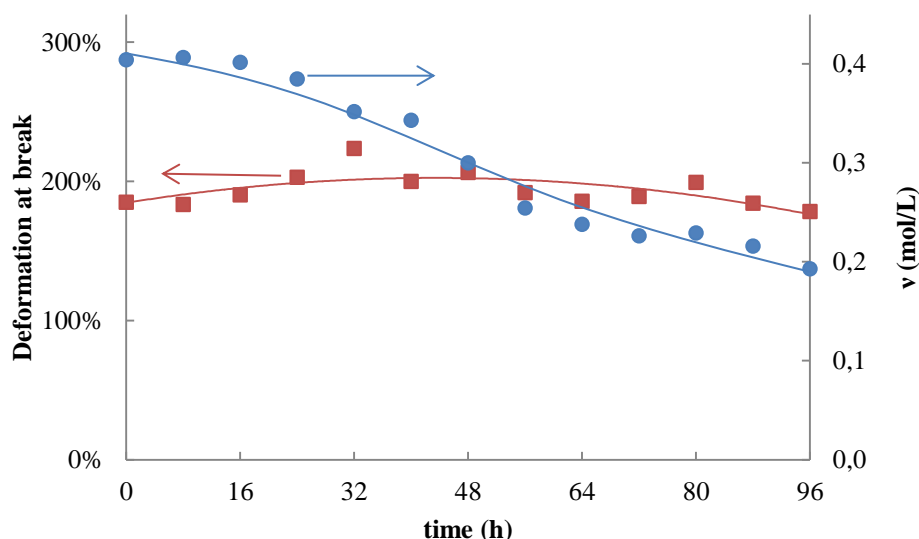


Figure 5-10: Comparison of the kinetic curves of deformation at break and concentration of elastically active chains for neat Nordel 4640 in air at 110°C

To establish a better correlation between the ultimate deformation and the concentration of elastically active chains, the former has been plotted versus the latter in Figure 5-11. Two distinct regions are evidenced by bolded regression straight lines. In the first region ($-0.5 < \log(\nu) < -0.3$), Λ_r increases and the slope of the straight regression line is close to -0.5, which is in a good agreement with the theory of rubber elasticity. It should be mentioned that this result is valid for all temperatures, as seen in Figure 5-11. Subsequently, although in this region the predominant phenomenon is the chain scission that should lead to a deviation from ideal network by creating dangling chains, the ultimate behavior reveals the existence of a quasi-ideal network. Anyhow, one can distinguish that the

maximum Λ_r corresponds to a transition point where the proportionality between Λ_r and v is no longer respected.

The changes in correlation between Λ_r and v in the second region ($\log(v) < -0.5$), turn out to be dependent of temperature. At this stage both Λ_r and v decrease with time of exposure, but for the same Λ_r , the v is bigger at higher temperature. This behavior is probably due to the presence of a superficial oxidized layer, whose thickness is temperature-dependent.

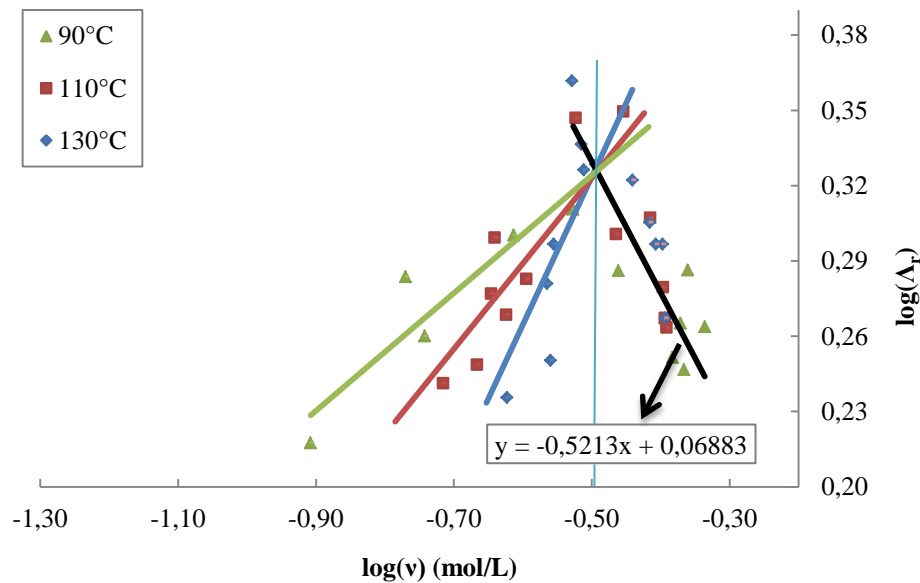


Figure 5-11: Ultimate deformation versus concentration of elastically active chains at 90, 110 and 130°C for neat Nordel 4640 in air

The oxidative scissions of elastically active chains lead to the formation of dangling chains which are not considered in definition of an ideal network. The scission of one elastically active chain leads to formation of two dangling chains ($2b$), which is added to the initial number of dangling chains ($2/M_n$). Doing so, the changes in the concentration of dangling chains during the thermal exposure is plotted in Figure 5-12, where the changes in v are presented as well. At the intersection of these two entities (the circled area), b becomes equal to v . At longer exposure times, b becomes superior to v . Interestingly, this intersection coincides with the transition region seen in Figure 5-11, i.e. the deviation from ideal network.

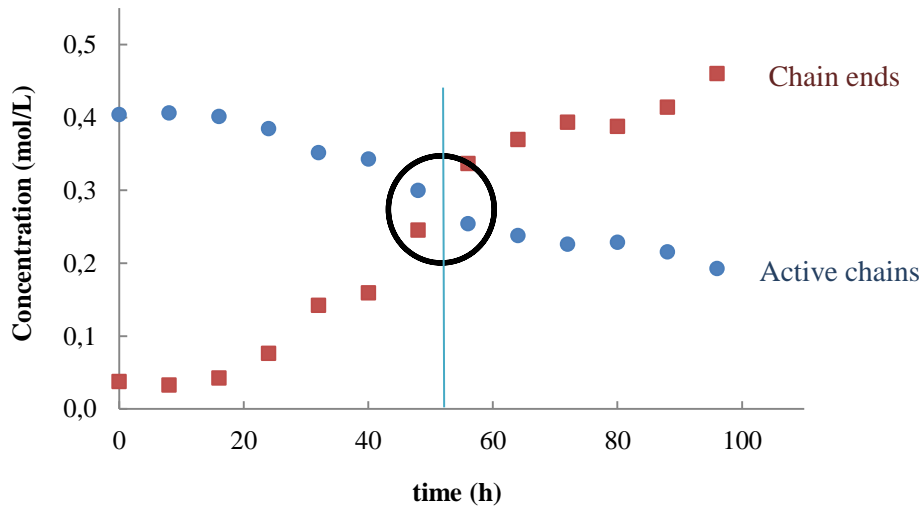


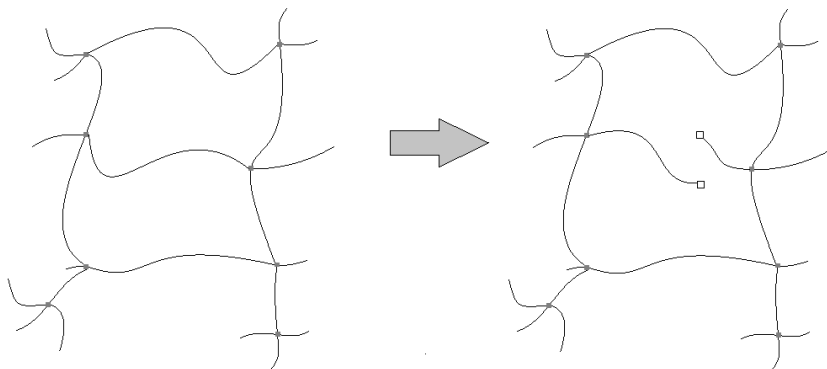
Figure 5-12: Comparison of the kinetic curves of concentration of elastically active chains and dangling chains for neat Nordel 4640 in air at 110°C

What is obvious here is that the ultimate deformation depends on b , v and their ratio.

“How do these factors affect the ultimate behavior of the network?” is the subject of next section.

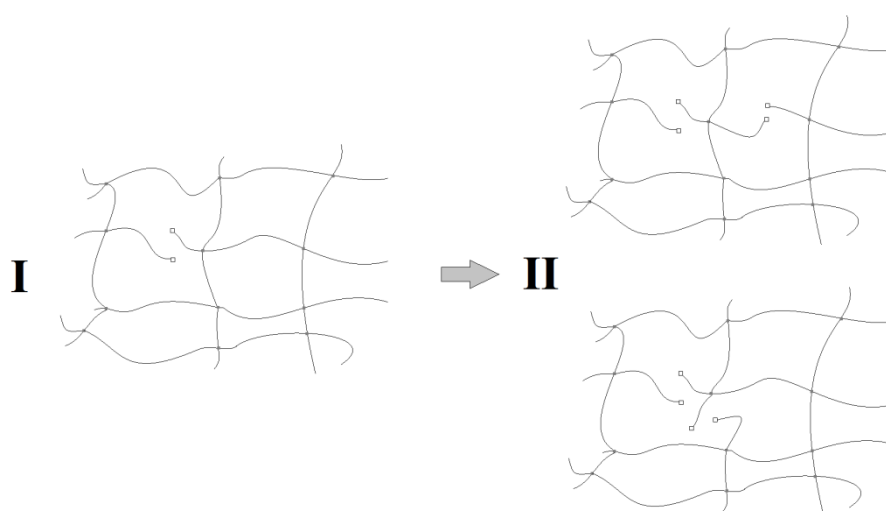
5.1.3.2 Discussion

To better understand the succession of chemical events during oxidation, the tetrafunctional structure of EPDM network has been considered in Scheme 5-2. One scission on an elastically active chain produces two dangling chains. In spite of losing one elastically active chain, the molar mass between the remaining elastically active chains remains still equal to initial value M_{e0} . This chain scission does not change the number of crosslinks either, but changes their functionality from four to three. In fact, one scission transforms 2 tetrafunctional crosslink to 2 trifunctional crosslinks.



Scheme 5-2: Schematizing of one scission on one elastically active chain and formation of two dangling chains in an initial tetrafunctional network

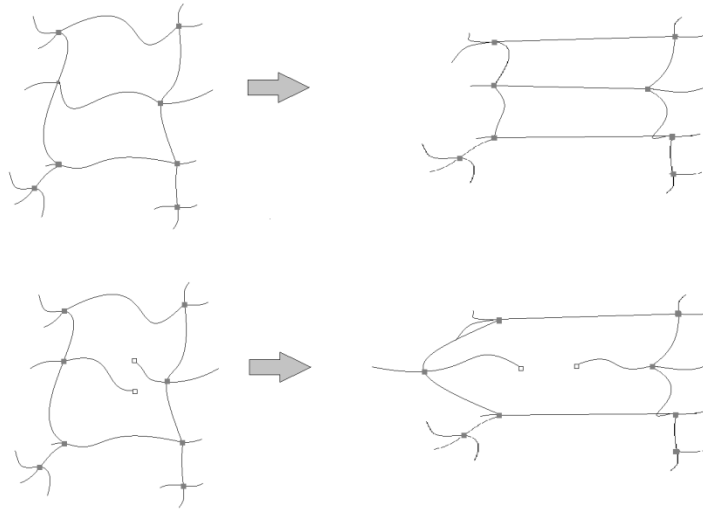
At the beginning of oxidation, the number of chain scissions is much lower than v_0 and, therefore, the possibility of having two scissions in close vicinity remains very low. Thus, chain scissions lead to the formation of trifunctional crosslinks all over the oxidized network. However, as thermal aging progresses, the number of chain scissions increases, and so is the probability of two scissions occurring in close vicinity. The suppression of two elastically active chains connected to the same junction results in the destruction of this latter (Scheme 5-3). The resulting elastically active chain present a molar mass of $M_e = 2M_{e0}$. The number of elastically active chains drops from 4 to 1, and the number of dangling chains increases from 0 to 4.



Scheme 5-3: Schematizing the accumulation of chain scissions in an initial tetrafunctional network

When an ideal network is at its ultimate deformation, all the elastically active chains are totally stretched, and the next step will be the cascade rupture of elastically active chains. Therefore, the maximum deformation of an ideal network is only dependent on stretching capability of the elastically active chains.

Concerning a network with few number of chain scissions (Scheme 5-3 I), the elastically active chains are at their maximum extension and the ultimate deformation will be only dependent of the extensibility. However, as shown in Scheme 5-4, the sporadic broken chains all over the network, let this latter to extend to higher deformation. In fact, in the case of an ideal network, some elastically active chains act as limiting factor of deformation. It can be concluded that at this stage of aging, where number of chain scissions remains fairly inferior to the number of elastically active chains, the network can still be considered as ideal, and therefore, its ultimate deformation may increase. The presentation in Scheme 5-4 is of course an exaggerated illustration of what happens in tetrafunctional network at high strains.



Scheme 5-4: Schematization of an ideal network and a slightly damaged network at their maximum deformation

The increasing number of chain scissions leads to the formation of longer elastically active chains (Scheme 5-3 II). Once this network is at its maximum extension, the elastically active chains having a mass equal to M_{e0} are at their maximum extension rate, while the elastically active chains having a mass equal to $2M_{e0}$ are not totally extended. Therefore, the ultimate deformation depends no more on extensibility of chains, but on the number of elastically active chains completely extended.

Finally, it can be concluded that the two distinct regions observed in Figure 5-11, represent the dependence of the ultimate deformation on two factors:

- I. In the first region, ν decreases but Λ_r increases, where this latter depends on the extensibility of chains. Few chain scissions give more liberty of deformation to the network, while the Young's modulus decreases. In this region, the concentration of dangling chains is inferior to the concentration of elastically active chains, so that the network can be considered as quasi-ideal
- II. In the second region, ν and Λ_r decrease simultaneously. Chain scissions destroy the network. This phenomenon happens when the concentration of chain scissions is fairly high to increase the molar mass of elastically active chains between crosslinks. In this region, the ultimate deformation becomes dependent of the number of elastically active chains and not their extensibility.

5.1.3.3 Filled EPDM

It has been previously shown that the interactions between the fillers and the EPDM matrix changes throughout the thermal exposure, which means that the arguments used to explain the ultimate

deformation for neat samples, are too simplistic in the case of filled samples. In fact, several other parameters should be considered, which are:

- The creation of strong filler/matrix interactions during thermal aging which can have a double effect: an increase in ϵ_r like in the case of surface treated ATH at high loadings, or a decrease in ϵ_r by preventing void formation due to filler/matrix interphase decohesion [3].
- The different in volume fraction of interphases between composites of different filler contents.
- The differences in interphase degradation between PATH and TATH filled samples.

The lack of experimental facilities and explanatory arguments for these issues prevents us to look deeply into the changes of ϵ_r during both thermal and radiochemical exposures. Consequently, in the following part, we will just present and discuss the global behavior of ultimate elongation.

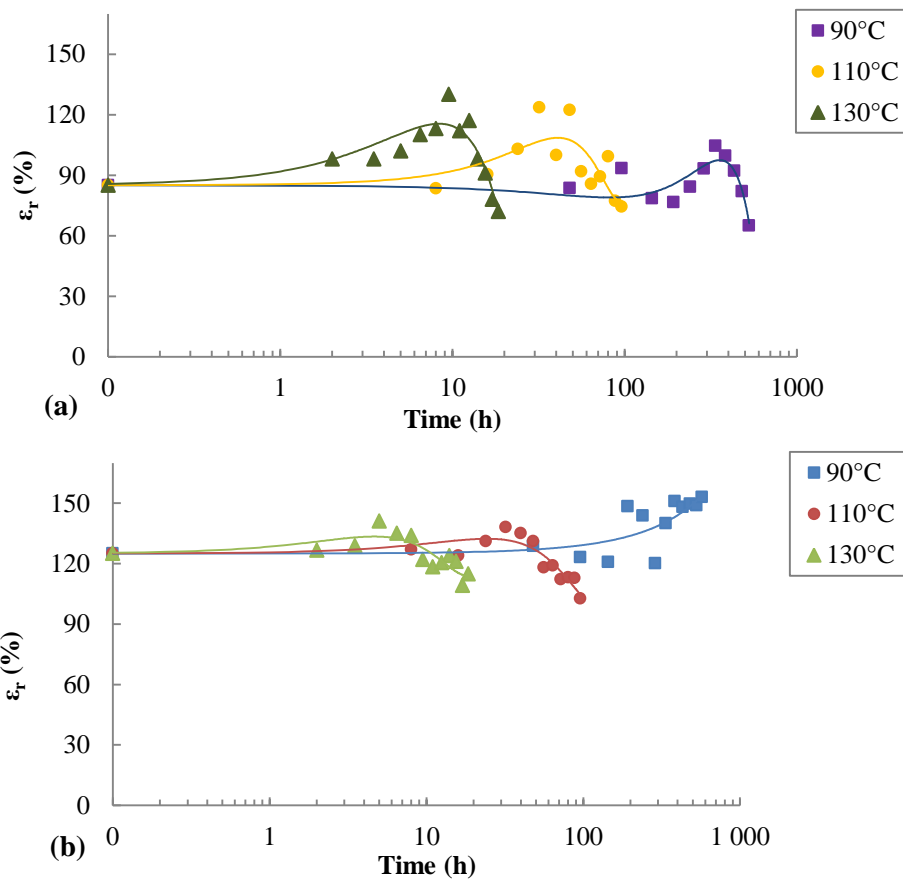


Figure 5-13: Kinetic curves of the ultimate deformation at 90, 110 and 130°C in air for a) neat and b) 33 phr PATH filled Nordel 4640

The changes in ultimate elongation of 33 phr PATH filled samples at the different temperatures under study are presented in Figure 5-13 b, as an indicator for all other samples due to their similar changes.

Similar to neat samples (Figure 5-13 a), ϵ_r of filled samples first increases and then declines when the material is highly degraded.

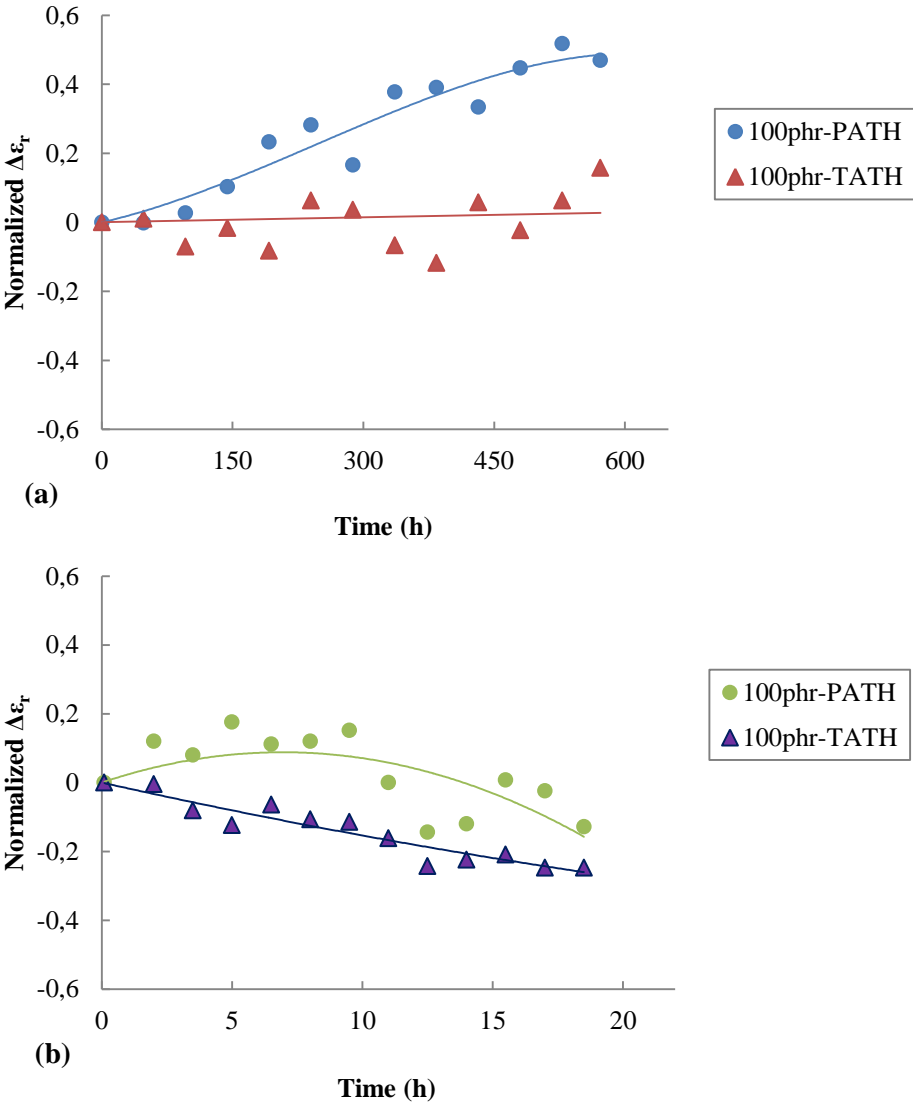


Figure 5-14: Effect of filler surface treatment on the changes of ultimate properties for 100 phr filled Nordel 4640 at a) 90°C and b) 130°C in air

Despite the fact that the general behavior is similar for all samples, the intensity of these variations is dependent on existence of filler surface treatment. This effect is evidenced in Figure 5-14 by normalizing the values of ϵ_r ($\Delta\epsilon_r = \frac{\epsilon_r - \epsilon_{r0}}{\epsilon_{r0}}$) for 100 phr filled samples, for which the differences are more distinct. The initial increase for PATH filled samples seems to be more intense in all cases and all exposure temperatures. At 90°C, while the PATH filled samples show a neat increase, the TATH filled samples keep constant $\Delta\epsilon_r$. A temperature rise, obviously, attenuates the initial increase for pristine samples, and induces a direct fall for treated samples. This behavior is similar to that reported in section 1.1.2 of this chapter for the Young's modulus of these samples.

5.2 Effect of radiochemical aging on mechanical properties

5.2.1 Neat EPDM Young's modulus

In order to verify the conformity between the results found by swelling method and tensile testing, the changes in Young's modulus with time of exposure at 40°C under dose rate of 1 kGy.h⁻¹ have been plotted in Figure 5-15.

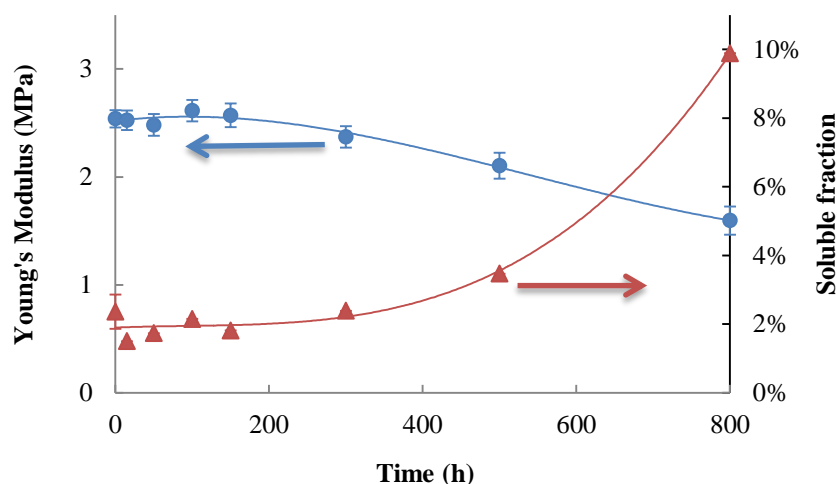


Figure 5-15 : Kinetic curves of Young's modulus and soluble fraction of neat Nordel 4640 samples under 1 kGy .h⁻¹ in air at 40°C

Two distinct regions are detectable for Young's modulus variations. At first, from beginning of the exposure up to approximately 150 hours (150 kGy), the modulus fluctuates toward slightly higher values. Secondly, from 150 hours until the end of exposure period, the modulus falls consistently. This behavior agrees with the changes in S_F , as shown in Figure 5-15. The results are in a good harmony with the general behavior at the macromolecular scale, described in previous chapter. The same behavior can be observed for the two other dose rates under study, as shown in Figure 5-16. Under 0.1 kGy.h⁻¹, the too short duration of exposure does not allow to observe more than modulus increase. However, this latter evidences the existence of an oxidative crosslinking phenomenon under low dose rates. The crosslinking phenomenon is more evident at low dose rates because the oxidation is slower and more homogeneous.

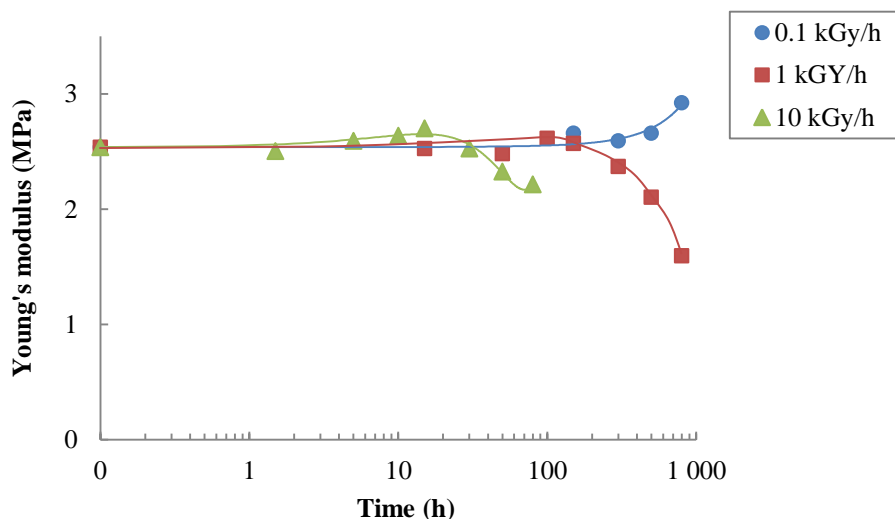


Figure 5-16 : Effect of dose rate on the changes in Young's modulus at 40°C in air for neat Nordel 4640

The changes in Young's modulus express the fact that the number of elastically active chains is changing throughout the radiochemical exposure. We recall that the relationship between shear modulus G' and concentration of elastically active chains ν has been established by Flory [1], and introduced in Chapter II. Neat EPDM network, like other elastomers, is considered incompressible and therefore, having a Poisson ratio equal to 0.5 that allows deducing the shear modulus from Young's modulus. This procedure will allow calculating the values of ν from the Young's modulus in next section.

5.2.2 Macromolecular changes

Experimental results propose that the chain scission governs the overall behavior of an EPDM network exposed to γ -irradiation. Nevertheless, at the beginning of exposure, no significant chain scission takes place but, on the contrary, a very slight increase in ν is detectable. The predominance of chain scissions becomes evident under 1 and 10 kGy.h⁻¹ dose rates at around 150 kGy of received dose, which corresponds to 150 and 15 hours of exposure, respectively. This predominance transition takes place where the rate of hydroperoxide accumulation reduces. Indeed, when the chain scission begins with decomposition of hydroperoxides, the number of elastically active chains begins to decline, as shown for samples aged under 1 kGy.h⁻¹ (Figure 5-17). This behavior reveals that in the first region, the mechanism of aging is pure radio-oxidation.

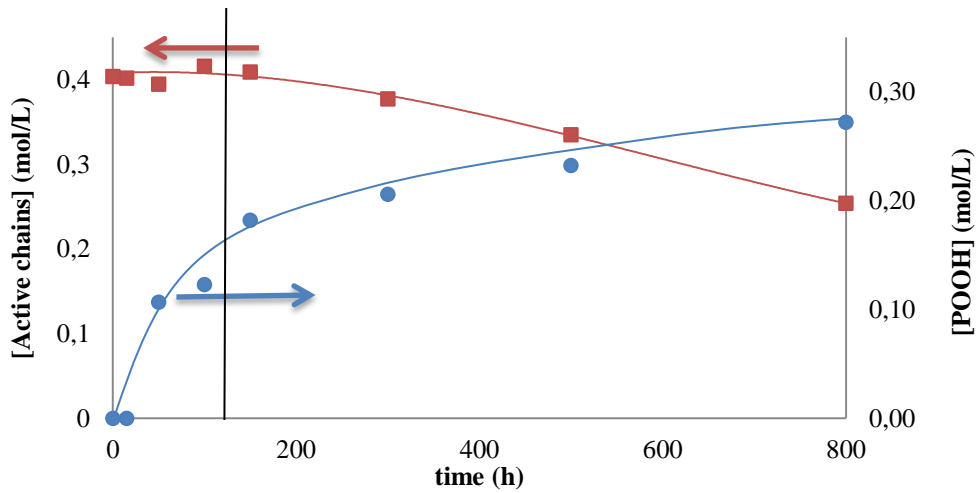


Figure 5-17 : Comparison of the kinetic curves for elastically active chains v and hydroperoxides for neat Nordel 4640 under $1\text{kGy}\cdot\text{h}^{-1}$ at 40°C in air

	Scission of elastically active chains	$dl = 0$ $db = 2dS$ $dv = -dS$
	Scission of dangling chains	$dl = dS$ $db = 0$ $dv = 0$
	Scission of free chains	$dl = ds$ $db = 0$ $dv = 0$

Table 5-4 : Chain scission possibilities in an initial tetrafunctional polymer network

In a tridimensional network, the scission can happen on elastically active (v), dangling (v) or free (l) chains, as schematized in Table 5-4. If the scission happens on an elastically active chain v , two

dangling chains and no free chain are created. The same action on a dangling chain creates one free chain, but the concentration of elastically active and dangling chains remain constant. Finally, a scission on a free chain creates one new free chain and leaves all other chains intact. Since free chains cannot be easily measured, they will be neglected in a first approach.

All these macromolecular changes lead to the following system of differential equations:

$$\left\{ \begin{array}{l} dl = \frac{b}{v+b+l} dS \\ db = \frac{2v}{v+b+l} dS \\ dv = \frac{-v}{v+b+l} dS \end{array} \right. \quad 5-11$$

The numerical resolution of this system will give access to the concentration of free chains from which the soluble fraction will be deduced. (The further advancement in this field belongs to the future prospects to this study)

5.2.3 Fillers effect

The macromolecular changes in filled EPDM samples have been studied by using the swelling method in chapter IV. Similar to what has been observed for neat samples, the v of filled samples increases in the beginning and decreases subsequently. Figure 5-18 reveals the evolution of Young's modulus for the samples under study, whose behavior does not deviate from what expected. The most notable aspect, here, is the amplification of changes in modulus for 100 phr TATH filled samples.

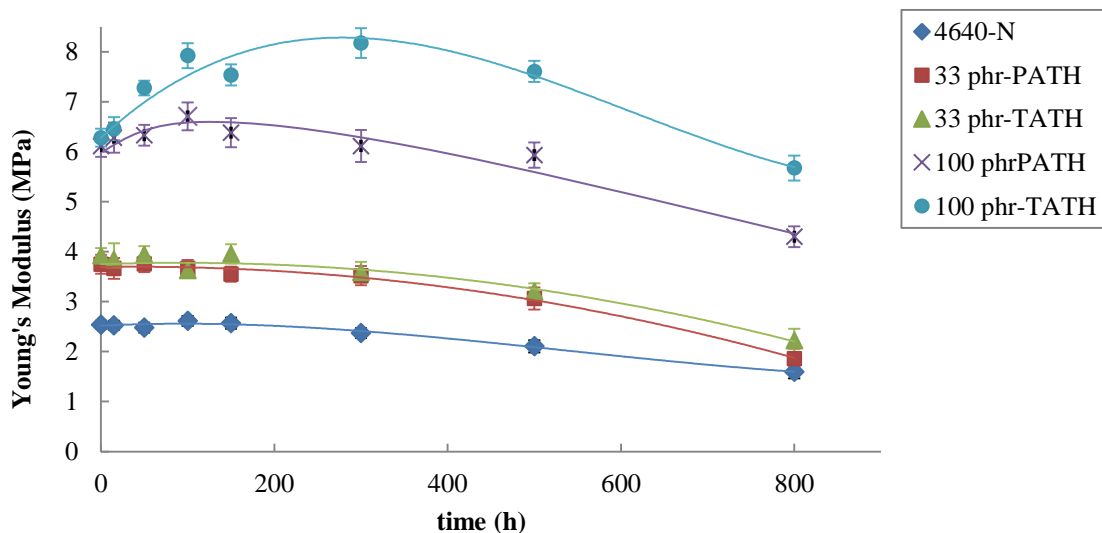


Figure 5-18 : Kinetic curves of Young's modulus for neat and ATH filled Nordel 4640 in air at 40°C under 1 kGy.h⁻¹

For further advance in this part, we simply make reference to what has been discussed in the case of thermal aging, and take advantage from some data determined previously. In the same manner, the changes in the interphase modulus E_i has been determined and plotted for 1 and 10 $\text{kGy}\cdot\text{h}^{-1}$ in Figure 5-19.

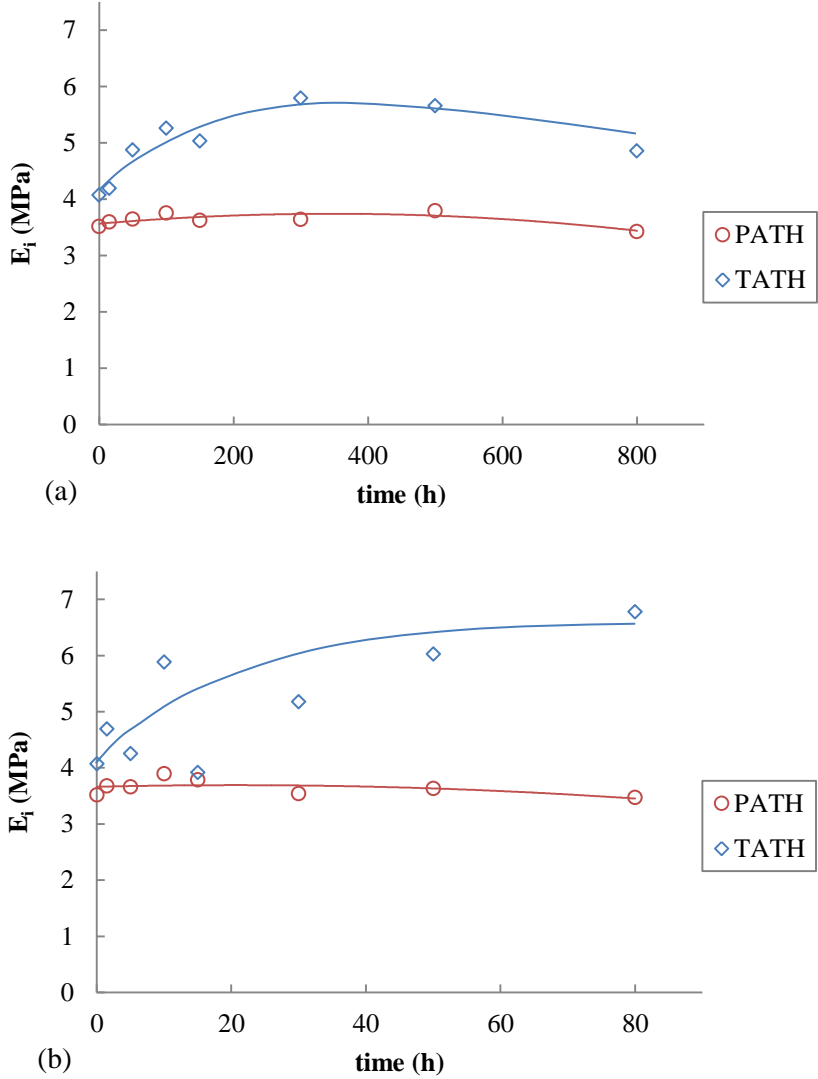


Figure 5-19: Kinetic curves of interphase modulus for ATH filled Nordel 4640 in air at 40°C under a) $1 \text{ kGy}\cdot\text{h}^{-1}$ and b) $10 \text{ kGy}\cdot\text{h}^{-1}$

These curves show an important interphase densification in the case of TATH filled samples. In contrast, in the case of PATH this densification is very low. The only difference between these two fillers, to whom this different behavior can be attributed, is the presence of organo-silane surface treatment molecules. Therefore, a crosslinking step seems to take place in the interphase, which implies the existence of active organo-silanes residual after sample processing.

The crosslink density found by swelling test in Chapter III has shown a higher ν for the TATH filled samples, while no difference was detected for PATH filled samples (Table 5-5). The Flory-Rehner equation (or its version modified by Kraus for filled polymers) is based on an affine tetrafunctional network model. Although the EPDM matrix network is considered as tetrafunctional, the functionality of the interphase network getting chemically attached to the surface of filler particles remains unknown. Furthermore, for the time being, it is not clear that how many crosslinks are formed because of one organo-silane molecule. This is the reason why the concentration of elastically active chains was not calculated from the E_i (Figure 5-19). Of course, this will be an interesting subject of research and discussion in future studies.

Filler	0 phr	33 phr	100 phr
PATH	0.42	0.43	0.43
TATH	0.42	0.52	0.64

Table 5-5: Concentration of elastically active chains ν (mol.L⁻¹) determined by swelling method for initial ATH filled Nordel 4640

Stiffening of filled samples under thermal exposure has been related to an amplification of the chemical interactions between the filler surface and oxidation products. This effect was more pronounced for PATH filled samples. On the other hand, Figure 5-19 clearly shows that the stiffening effect is more important for TATH filled samples. Therefore, it can be concluded that the stiffening mechanism differs between irradiation and thermal oxidation. This difference can be explained as follows:

- i. Under thermal exposure at the temperatures under study, the interphase is mostly in rubbery state, which facilitates the penetration of oxygen molecules. This leads to higher concentrations of oxidation products and their easy access to the surface of the ATH particles. Therefore the densification of interphase is controlled by temperature and the kinetic parameters of aforesaid condensation mechanism.
- ii. Under irradiation, the samples are at lower temperature comparing to thermal exposure, and the interphase is closer to the glassy state. Therefore the previously mentioned mechanism of condensation becomes less probable. Macroradicals formed under ionizing irradiation (P°) cannot have a chemical reaction with filler surface, but they can easily react with the residual surface treatment molecules on the surface of TATH particles. This can explain the higher interphase densification of TATH filled EPDM samples.

Hereby, one may conclude that the stiffening under irradiation is due to creation of chemical links between the filler and the polymer chains, via the vinyl-silane molecules of surface treatment. As

mentioned in Chapter III, these molecules contain a vinyl function. This latter can contribute in extra crosslinks in two ways:

- Addition of macroradicals formed in the matrix on vinyl double bond,
- Coupling of macroradicals formed in the matrix with allylic radicals.

5.3 Macroscopic scale

5.3.1 Ultimate properties of Neat EPDM network

Consistent with other presented results, the changes in ultimate properties for neat EPDM at $(40\pm 5)^\circ\text{C}$ in air under $1\text{ kGy}\cdot\text{h}^{-1}$ are presented in Figure 5-20, where the maximum and minimum limits are shown. As previously seen for young's modulus, a slight crosslinking is evidenced at the beginning of exposure, which leads to an increase in both stress and strain at break. Anyhow, after 100 hours under $1\text{ kGy}\cdot\text{h}^{-1}$ and 5 hours under $10\text{ kGy}\cdot\text{h}^{-1}$, the predominant mechanism, i.e. chain scissions, becomes obvious (Figure 5-20).

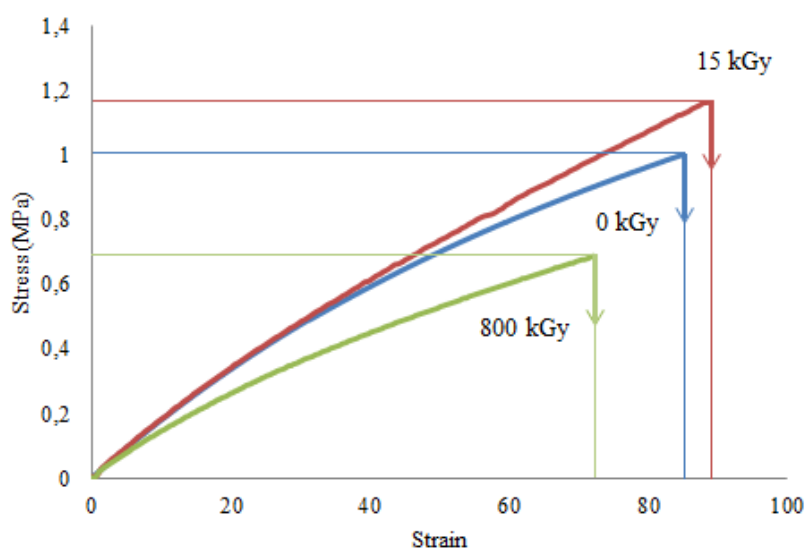


Figure 5-20 : Changes in the ultimate properties of neat Nordel 4640 network under $1\text{ kGy}\cdot\text{h}^{-1}$ in air at 40°C , monitored by tensile testing

The kinetic curves of ultimate elongation under $1\text{ kGy}\cdot\text{h}^{-1}$ and $10\text{ kGy}\cdot\text{h}^{-1}$ (Figure 5-21) show an undisputable resemblance. The changes for $1\text{ kGy}\cdot\text{h}^{-1}$ show the same pattern but, due to few numbers of data acquisitions and a high dispersion of results, they have not been presented here. These results are the average values of at least seven tensile tests, for which the deviations are presented by error bars. The general behavior is an initial increase of ultimate elongation followed by a small sharp fall,

then a very slow decrease until the end of exposure. This type of behavior has been previously reported for other elastomers [4-6].

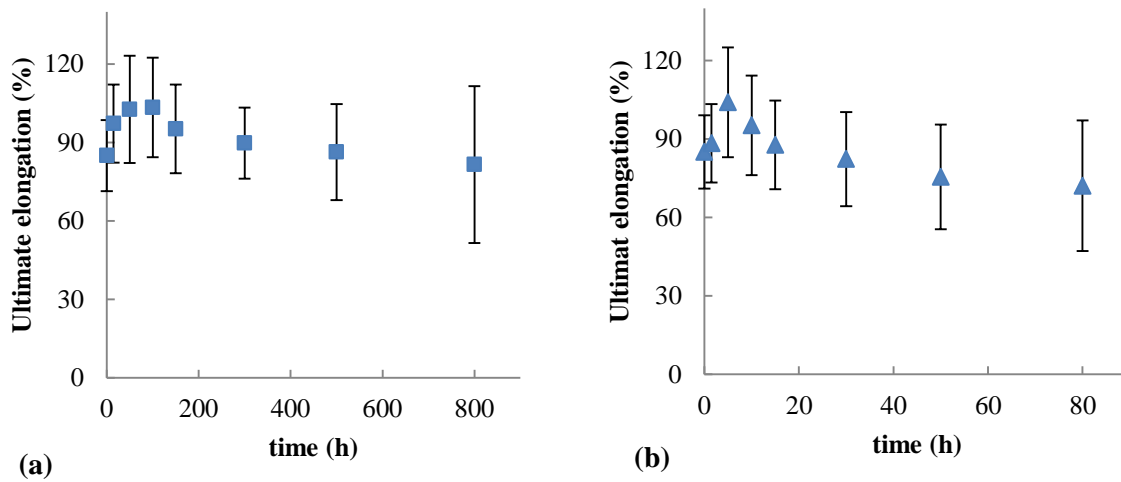


Figure 5-21 : Kinetic curves of ultimate properties of neat Nordel 4640 network under a) 1 kGy.h⁻¹ and b) 10 kGy.h⁻¹ in air at 40°C, monitored by tensile testing

As it has been previously shown for the rupture envelope of elastomers [7], the initial crosslinking leads to small increase in the ultimate elongation [8]. This behavior is in complete agreement with experimental results previously found, and is the outcome of the competition between crosslinking and chain scission. In the early stages of exposure, while hydroperoxides are being accumulated and chain scissions are fairly low, the effect of crosslinking becomes evident. After this step, when hydroperoxides decompose, the chain scissions take over and the ultimate elongation decreases. However, after a specific time, the changes seem to stabilize, showing a quasi-equilibrium between crosslinking and chain scission.

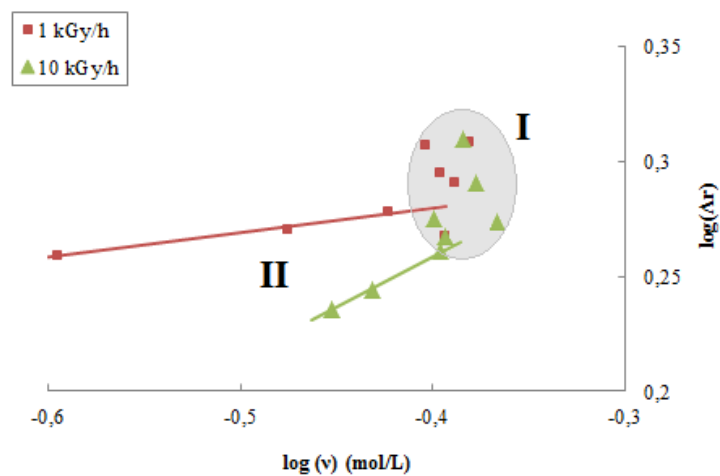


Figure 5-22: Ultimate deformation versus the concentration of elastically active chains for neat Nordel 4640 in air at 40°C under 1 and 10 kGy.h⁻¹

For a better visualization of the dependence of ultimate elongation on crosslink density of the network, the former has been plotted as a function of the latter in Figure 5-22. Two distinct regions are thus evidenced. In region I (the circled area) v increases, while Λ_r increases and then decreases in the same region. In the second region both v and Λ_r decrease, and the material degradation is principally dominated by chain scissions.

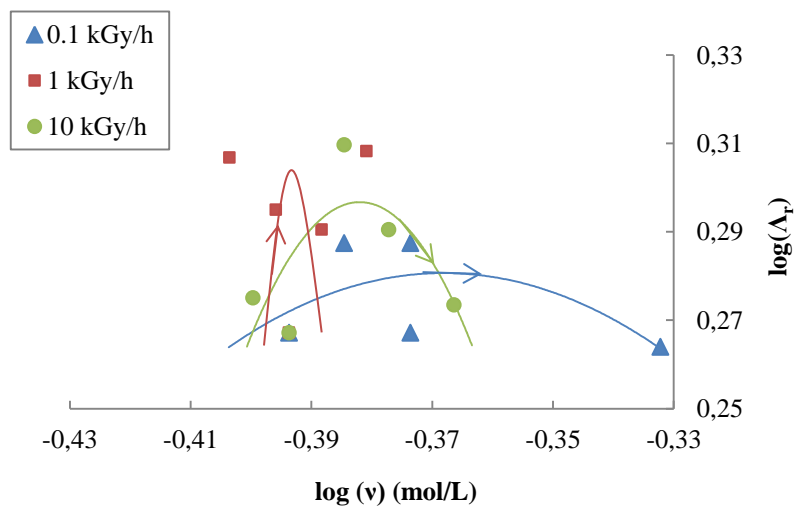


Figure 5-23: Ultimate deformation versus concentration of elastically active chains for neat Nordel 4640 in region I only

Although the evolution in the second region is clear enough, the first region needs to be more detailed. For this purpose a zoom is made on this region (Figure 5-23), and the results of 0.1 kGy.h⁻¹, which are positioned strictly in this region, are added. The diagram shows that by decreasing irradiation dose rate the crosslink density reaches higher values, while the maximum values of ultimate deformation decreases. The dual mechanism of radio-thermal degradation, along with time dependence of aging, can explain the complex behavior in this first region. The increase in irradiation dose increases the number of radiochemical initiation acts in a fixed time range, which means a higher concentration of macroradicals that can react whether with each other to form a crosslink or react with oxygen to subsequently form a hydroperoxide. At higher dose rate, the concentration of macroradicals is higher so the crosslink and hydroperoxide formation happen in higher rates. However, we know that the decomposition mechanism of hydroperoxides is bimolecular in the temperature range under study and the chain scissions happen after attaining a critical hydroperoxide concentration. Therefore, the chain scissions begin with a delay regarding the crosslink formation, providing the time to attain sufficient hydroperoxide concentration. Consequently, it seems licit that dose rate increase, tighten the width of the peaks in Figure 5-23. Decreasing of dose rate, seems to be in favor of hydroperoxide formation, and therefor reduces the amplitude of variations of ultimate deformation.

5.3.2 Fillers effect

The reinforcement effect of fillers has been well established at their initial state in Chapter III. It has been noticed that the presence of surface treatment does not have an effect on Young's modulus, while at large strains, their effect appears for high filler contents (100 phr). The ultimate elongation of filled samples show similar variations in all cases, which do not differ from what have been seen for neat samples (Figure 5-24).

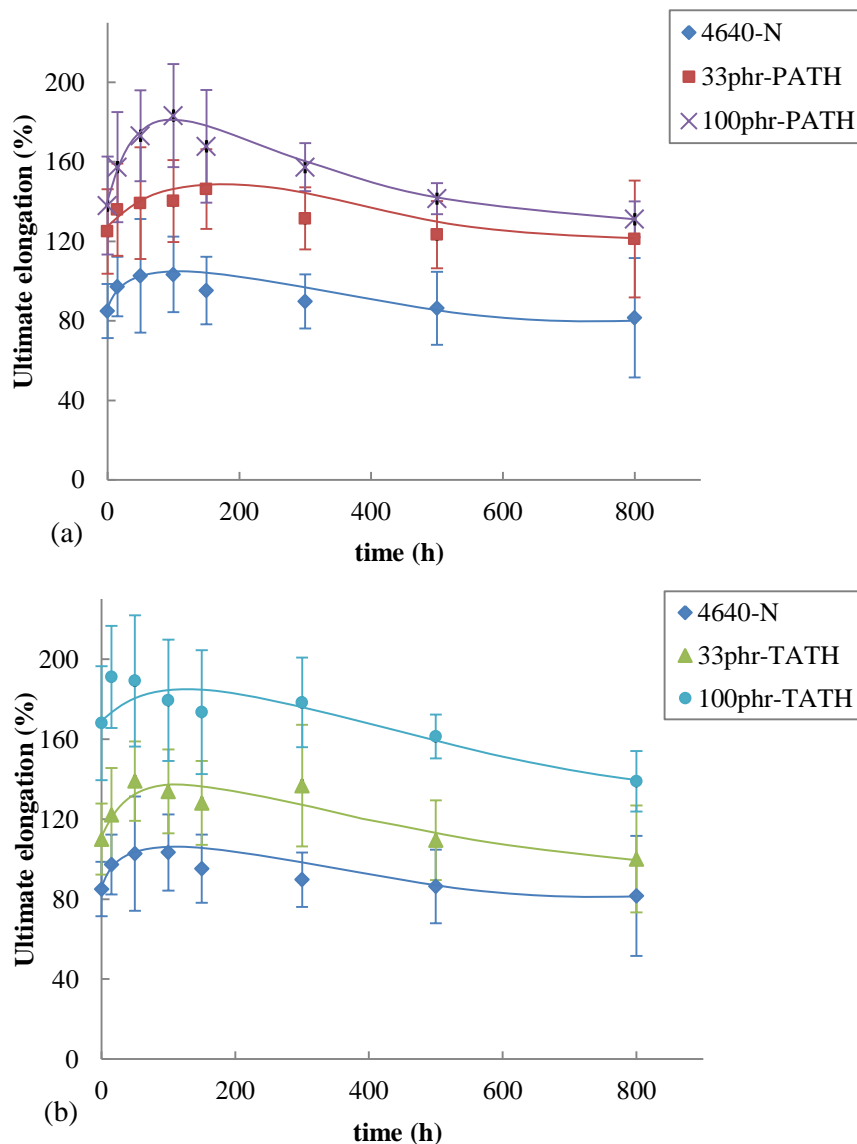


Figure 5-24 : Kinetic curves of ultimate elongation in air at 40°C of Nordel 4640 under 1 kGy.h⁻¹ filled with: a) PATH and b) TATH

The dependence of ultimate elongation on macromolecular structure of the network, explained in Section 1-3 of this chapter, becomes much more complicated when filler particles are introduced. The

presence of particles, along with reinforcement effects and creation of interphase network, introduces flaws in structure of composites that leads to perplexing behavior of material and high error margins. The trend lines in Figure 5-24 show the similar behavior for all samples. In addition, we have previously seen that both Young's moduli of interphase and matrix networks evolve in the same manner, which indeed reminds of ultimate elongation variations. As a consequence, it seems impossible to differentiate the contribution of each network to the changes in ultimate elongation. However, it may be concluded that the resemblance between degradation of interphase and matrix network leads to similar fracture behavior for filled as neat EPDM. Anyhow, the ultimate elongation for the final exposure time does not go below 80% of its initial value, which highly satisfies the industrial endlife criterion (50% of elongation at break).

Conclusion

The determination of the changes in Young's modulus is a reliable method to determine the macromolecular modifications of EPDM tridimensional network. As mentioned in Chapter IV, the validity of swelling method is limited by the concentration of oxidation products. The concentration of elastically active chains measured by tensile testing clearly shows these limitations, and allows defining a domain of validity for swelling test. Anyhow, the tensile test has also illustrated a transition domain for the predominant phenomenon in filled matrices. The densification observed in the beginning of exposure is followed by the destruction of the polymer network at longer times. Based on a two-phased interphase model, it was shown that the initial densification happens exclusively in the interphase. An empirical method has been proposed to calculate the thickness of the interphase, which consist in connecting the networks of interphase an EPDM matrix in series. As the consequence, it was possible to calculate the Young's modulus of the interphase network by knowing the global modulus of polymer phase in the composite.

An assessment of the kinetic curves of the interphase modulus for both thermal and radiochemical aging has shown that the mechanism of network densification differs from one to another. It was observed that the interactions between the polymer matrix and the surface of pristine ATH is responsible for densification at high temperature, while the molecules of surface treatment are responsible for the densification of the interphase under irradiation.

The shape of ultimate elongation kinetic curves seems to be similar for both thermal and radiochemical oxidation, i.e. an initial increase followed by a decline. However, the mechanisms of these modifications turn out to be completely different. Under thermal oxidation, the transformation of the tetrafunctional to trifunctional crosslinks results in a rise of the ultimate elongation, while the Young's modulus decreases constantly. Under irradiation, crosslinking is responsible for the simultaneous initial increase in ultimate elongation and Young's modulus. In fact, under irradiation at

low temperature, the filled matrix behaves like the neat matrix, except that the presence of surface treatment molecules amplifies the crosslinking effect. On the contrary, at high temperatures, the interaction between oxidation products and PATH filler surface leads to higher intensifications in the case of PATH filled samples. Anyhow, the second mechanism is more complicated and needs further studies for more clarifications.

Reference

1. Flory, P.J., *Principles of polymer chemistry*. 1953: Cornell University.
2. Fayolle, B., et al., *Polymères en ambiance nucléaire: Comportement à long terme*. 2012: Lavoisier.
3. Planes, E., *Influence des charges sur l'évolution des propriétés mécaniques des EPDM chargés lors de leur vieillissement par irradiation*. 2008.
4. Gueguen, V., *Vieillessement d'elastomeres utilises comme isolant electriques en ambiance nucleaire*. 1992.
5. Makhlis, F.A., *Radiation physics and chemistry of polymers*. 1972: John Wiley and Sons.
6. Planes, E., et al., *Evolution of EPDM networks aged by gamma irradiation – Consequences on the mechanical properties*. *Polymer*, 2009. **50**(16): p. 4028–4038.
7. Gueguen, V., et al., *Radiochemical oxidation of an ethylene-propylene-hexadiene terpolymer*. *Radiation Physics and Chemistry*, 1994. **44**(6): p. 557–565.
8. Verdu, J., *Effect of aging on the mechanical properties of polymeric materials*. *Macromolecular Science*, 1994. **31**(10): p. 1383-1398.

Conclusions and Prospects

The main objective of this study was to establish a better understanding about the modifications brought to EPDM terpolymers and its fire retardant composites at different structural scales throughout oxidative aging. This study can be considered as a beginning spot for developing a non-empirical approach to predict the life-time of EPDM based cable materials under radiochemical and thermal stresses. This method helps to relate the modifications in properties at macromolecular and macroscopic scale to elementary chemical acts of oxidation at molecular scale. Furthermore, the relationship between the industrial and the structural endlife criteria can be established.

The crosslinking of EPDM by dicumyl peroxide (crosslinking agent) has been the starting point of this study. The complete investigation on peroxide crosslinking has helped, from one part, to understand the formation and the structure of EPDM tridimensional network, which represent the initial state of the material destined to be aged. For the second part, this investigation considerably helped the phenomenological approach to analyze the aging phenomena.

It was shown that the complete cure time of EPDM by peroxide is independent of initial concentration of crosslinking agent. The main species to create crosslinks has shown to be ethylene units, which presents the highest concentration among the others (propylene and ENB). The concentration of residual ENB double bonds after crosslinking is more than 50%, despite the fact that the concentration of crosslinking agent was high enough to create sufficient radicals for total consumption of insaturations.

Based on experimental data at molecular scale, a crosslinking mechanistic scheme has been proposed, and the subsequent system of differential equation of the kinetic scheme has been derived. The kinetic parameters for this scheme have been found in the literature and the kinetic scheme has been solved numerically. The results of the simulation have shown an acceptable coherence with experimental data.

Introduction of different concentrations of peroxide into EPDM matrices provided interesting data regarding the effect of macromolecular chains entanglements in linear EPDMs. At low concentration of crosslinking agent, it has been observed that the plasticizing effect, induced by small molecules of peroxide before cure, and the crosslink density of network after cure are influenced by a relatively high initial concentration of entanglements. It was deduced that, as the chemical crosslinks get formed through bimolecular coupling of macroradicals, the concentration of entanglements decreases subsequently. The average structure of the tridimensional network has been determined by measuring the crosslink density through different analytical methods at macromolecular scale. The outcomes of these methods were all in a good agreement. Furthermore, the crosslink density calculated numerically through kinetic model has shown to be acceptable with respect to the experimental data.

Incorporation of pristine ATH into EPDM gum does not change the crosslinking mechanism, and the crosslink densities of filled matrices are equal to that of neat EPDM matrix. However, the mechanical properties are increased due to the hydrodynamic effect of filler particles. On the other hand, EPDM matrices containing surface treated ATH show higher crosslink densities, which evidence the creation of chemical bonds between macromolecular chains and filler surface. No significant difference has been observed between the mechanical properties of the EPDM matrices filled with pristine and surfaces treated ATH, except at large strains. The presence of chemical bonds between the polymer chains and filler surface significantly increased the ultimate properties at high filler content.

The filler/matrix interphase was divided into two different phases: Firstly, the glassy hard phase, which is in contact with filler surface. Secondly, the sticky hard phase, linked to the EPDM matrix. The thickness of glassy hard phase is assumed to be negligible comparing to the thickness of sticky hard phase. This latter builds up an interpenetration network in a parallel system with the matrix network, which is unaffected by filler particles. This two-phased system convincingly models the reinforcement effect of fillers.

Neat EPDM matrices undergoing thermal aging, show a short oxidation induction time, and as the oxidation takes off, the crosslink density of the network as well as the Young's modulus begins to fall. By increasing the temperature of exposure, the control of oxidation by oxygen diffusion increases, leading to a more heterogeneous oxidation. The creation of oxidation products changes the swelling properties of the network and therefore the crosslink density of the network is overestimated through this method. However, the crosslink density values found by tensile testing are not influenced by creation of oxidation products. Furthermore, a simple comparison between the results obtained by these two methods reveals the validity domain of the swelling method.

The kinetic curves of ultimate elongation of the neat EPDM matrices under thermal oxidative aging show an initial increase, while the Young's modulus decreases. This phenomenon was explained by a change in the functionality of crosslinks. It was shown that the crosslinks of the EPDM tridimensional network are initially tetrafunctional. At the beginning of thermal exposure, as the chain scissions happen due to oxidative aging, the concentration of elastically active chains, and consequently the Young's modulus, decreases. Meanwhile, the functionality of crosslinks drops from four to three, but the number of junctions remains constant. This alteration of functionality provides the network with higher elongations at break. However, when the number of chain scissions becomes important, the junctions disappear and the ultimate elongation decreases. In other words, at early stages of exposure, when the number of chain scission is fairly low, the ultimate elongation is governed by the functionality of crosslinks. As the number of chain scissions increases, the ultimate elongation is governed by the number of crosslinks.

It was observed that, although the predominant phenomenon during thermal aging is chains scission, the Young's modulus of filled matrices increases after the oxidation induction time, which is in contrast with the neat EPDM matrix behavior. This densification is attributed to the formation of strong interactions between the filler surface and oxidation products. As this effect is more pronounced for EPDM matrices filled with pristine ATH, it is concluded that the interactions must be related to the chemical functions at the filler surface, i.e. hydroxyl functions. Moreover, these interactions do not disappear when the samples are swelled, which is an indicator of their chemical nature. Consequently, the proposed mechanism of the reinforcement of composites under thermal oxidative aging is a condensation between the hydroxyl functions of pristine ATH surface and the oxidation products.

Under ionizing irradiation, the neat EPDM matrix goes through a slight initial crosslinking, while the main chemical reaction is the formation and accumulation of hydroperoxides. After a specific received dose, the hydroperoxides begin to decompose and the chain scissions become predominant. The thickness of oxidized layer has shown to be an inverse function of dose rate, which leads to a more pronounced oxidation heterogeneity at higher intensity.

The elastic and ultimate properties under irradiation follow the same evolution as the network crosslink density, i.e. an initial increase followed by a decrease, which is valid for both neat and filled EPDM matrices. However, the initial densification is more important for filled EPDM matrices, which means that in addition to the matrix network, the interphase network goes through a densification as well.

The densification of the interphase has been observed in both thermal and radiochemical oxidative agings. However, the comparison of these two types of aging has revealed that, in the case of thermal oxidation, the densification is more intense for EPDM matrices filled with pristine ATH, while under irradiation, the densification is more important for EPDM matrices filled with surface treated ATH. These results uncover the difference between the densification mechanisms under thermal and radiochemical agings. Under thermal aging, the densification goes through a condensation between the chemical functions of filler surface and oxidation products. Under radiochemical aging, the densification is dominated by creation of extra crosslinks between polymer chains and molecules of surface treatment.

The crosslinking mechanism of EPDM by peroxide has been the subject of several researches for more than 50 years, and fairly well defined. The accuracy and the coherence between the results of numerical simulation and experimental data have validated the proposed kinetic model for further use. However, the real-time evolution of mechanical properties throughout crosslinking of the elastomer can be further developed. For instance, a real-time study on evolution of Young's modulus as a

function of double bond consumption can be envisaged by coupling nano-indentation test with Raman spectrophotometry.

The effect of chemical surface treatment of ATH has been observed throughout this study. It was shown that these sizing molecules get involved in the crosslinking of the network, which results in a higher crosslink density in the interphase. In addition, a significant densification effect has been detected, due to the presence of these molecules under radiochemical oxidative aging. Although we have proposed an approach to calculate the concentration of surface treatment molecules, their exact structure and distribution pattern on filler surface are still unknown. The further study on this subject may bring more clarifications about the functionality of junctions at the filler surface, and define the exact mechanism of interphase reinforcement under irradiation.

In the case of EPDM matrices filled with pristine ATH, a different mechanism of interphase reinforcement, which is a condensation between the oxidation products and chemical functions on the filler surface, has been proposed. However, no further approval was brought to this proposition, in this study. The determination of the exact mechanism and the influencing kinetic parameters seems an interesting field for further researches.

The aging of an EPDM with low concentration of insaturations can be considered as equivalent to that of an EPR. However, as the concentration of double bond increases, their effect may not be neglected. Investigation on the kinetics of EPDM thermal oxidation has provided kinetic parameters on ENB double bonds consumption throughout exposure. These data can be now introduced in the non-empirical model for EPR endlife prediction, previously developed at PIMM.

The reinforcement effect of filler particles in ATH/EPDM composites could be well explained by considering a two-phased interphase. Base on this model, a new approach has been proposed to measure the structural modifications at macromolecular scale and, furthermore, to calculate the thickness of the sticky hard interphase and its Young's modulus. However, this phenomenological approach remains an indirect method. It is of quite interest to determine the thickness and Young's modulus of the interphase through a direct measurement technique (AFM, nano-indentation) in order to validate the proposed method.

Conclusions et Perspectives

(in French language)

L'objectif principal de cette étude était de mieux comprendre les modifications induites par le vieillissement oxydant dans les terpolymères EPDM et ses composites ignifugés à différentes échelles structurales. Cette étude peut être considérée comme le point de départ d'une approche non-empirique de prédiction de la durée de vie des matériaux de câbles électriques à base d'EPDM soumis à des sollicitations thermiques et radiochimiques. Cette méthode permet de relier les modifications des propriétés aux échelles macromoléculaire et macroscopique aux actes chimiques élémentaires d'oxydation qui se produisent à l'échelle moléculaire. En outre, la relation entre les critères de fin de vie structuraux et industriels a été établie.

La réticulation de l'EPDM par le peroxyde de dicumyle (agent de réticulation) a été le point de départ de cette étude. L'investigation de la réticulation par le peroxyde a permis, d'une part, de comprendre la formation et la structure du réseau EPDM tridimensionnel, qui représente l'état initial du matériau destiné à être vieilli. Elle a également contribué dans l'approche phénoménologique d'analyse des phénomènes de vieillissement.

Il a été montré que le temps de cuisson complète de l'EPDM par le peroxyde est indépendant de la concentration initiale d'agent de réticulation. Les principales espèces à l'origine des nœuds de réticulation sont les unités éthylène, qui représentent la plus forte concentration parmi les autres unités monomères (propylène et ENB). La concentration des doubles liaisons ENB résiduelles après réticulation est supérieure à 50 mol.%, bien que la concentration initiale de l'agent de réticulation était suffisamment élevée pour créer suffisamment de radicaux et permettre la consommation totale des insaturations.

Sur la base de ces données expérimentales à l'échelle moléculaire, un schéma mécanistique de réticulation a été proposé, à partir duquel un système d'équations différentielles a été dérivé. Les valeurs des paramètres cinétiques ont été trouvées dans la littérature et le schéma cinétique a été résolu numériquement. Les résultats de la simulation sont en bon accord avec les données expérimentales.

L'introduction de différentes concentrations de peroxyde dans des matrices EPDM a fourni d'appréhender l'effet de l'enchevêtrement des chaînes dans les EPDMs linéaires. A faible concentration d'agent de réticulation, on a vu que l'effet plastifiant, induit par les petites molécules de peroxyde avant cuisson, et la densité de réticulation du réseau EPDM après réticulation sont influencés par la concentration initiale relativement élevée des enchevêtrements. Il a été déduit que, comme les nœuds chimiques de réticulation se forment par couplage bimoléculaire des macroradicaux, la concentration des enchevêtrements diminue. La structure moyenne du réseau tridimensionnel a été déterminée à partir de la densité de réticulation mesurée par différentes méthodes analytiques à l'échelle macromoléculaire. Les résultats de ces méthodes sont en bon accord. De plus, la densité de réticulation, calculée numériquement grâce au modèle cinétique, est en bon accord avec les données expérimentales.

L'incorporation de particules d'ATH vierges dans la gomme EPDM ne modifie pas le mécanisme de réticulation, et les densités de réticulation des matrices EPDM chargées sont égales à celle de la matrice EPDM pure. Toutefois, les propriétés mécaniques sont améliorées en raison de l'effet hydrodynamique des particules de charge. D'autre part, les matrices EPDM contenant des particules ATH traitées en surface présentent des densités de réticulation plus élevées, ce qui indique la création de liaisons chimiques entre les chaînes de polymère et la surface des charges. Aucune différence significative n'a été observée entre les propriétés mécaniques des matrices EPDM chargées par des ATH vierges et traitées en surface dans le domaine des petites déformations, mais la différence est notable aux grandes déformations. La présence de liaisons chimiques entre les chaînes de polymère et les molécules de traitement de surface des charges augmente significativement les propriétés à rupture pour les forts taux de charges.

L'interphase charge/matrice a été divisée en deux phases différentes: d'abord, une phase rigide, qui est en contact direct avec la surface de la charge, et qui est considérée comme une phase vitreuse et la seconde, une phase dure et collante, liée avec la matrice EPDM. L'épaisseur de la phase vitreuse est supposée être négligeable en comparaison de l'épaisseur de l'interphase collante. Cette dernière constitue un réseau d'interpénétration, connecté en parallèle avec le réseau matriciel, i.e. non affecté par les particules de charge. Ce système à deux phases modélise de manière convaincante l'effet de renforcement des charges.

Les matrices EPDM pures subissant un vieillissement thermique présentent un temps d'induction de l'oxydation court, et quand l'oxydation s'auto-accélère, la densité de réticulation du réseau, ainsi que le module de Young, commencent à chuter. En augmentant la température d'exposition, la dépendance de l'oxydation contrôlée par la diffusion d'oxygène augmente, ce qui conduit à une oxydation plus hétérogène. La création des produits d'oxydation modifie les propriétés de gonflement du réseau et donc la densité de réticulation du réseau est surestimée par cette méthode. Toutefois, les valeurs de densité de réticulation trouvées par l'essai de traction ne sont pas influencées par la création des produits d'oxydation. La comparaison entre les résultats obtenus par ces deux méthodes révèle le domaine de validité de l'essai de gonflement.

Les courbes cinétiques d'allongement à la rupture des matrices EPDM pures soumises au vieillissement thermo-oxydant augmentent initialement, tandis que le module d'Young diminue. Ce phénomène a été expliqué par un changement de la fonctionnalité des nœuds de réticulation. Il est montré que les nœuds de réticulation du réseau tridimensionnel EPDM sont initialement tétrafonctionnels. Au début de l'exposition thermique, comme les coupures de chaînes se produisent au cours du vieillissement oxydant, la concentration des chaînes élastiquement actives, et par conséquent, le module d'Young, baisse. Pendant ce temps, la fonctionnalité des nœuds de réticulation passe de quatre à trois, mais le nombre de jonctions reste constant. Cette modification de la fonctionnalité

confère au réseau une capacité d'allongements à la rupture plus grande. Au fur et à mesure que l'oxydation du matériau avance, le nombre de coupures de chaînes devient plus important, les jonctions disparaissent et l'allongement à la rupture diminue. En d'autres termes, dans les premières étapes de l'exposition, lorsque le nombre de coupures de chaîne est assez faible, l'allongement à la rupture est régi par la fonctionnalité de nœuds de réticulation. Quand l'augmentation du nombre de coupures de chaîne augmente, l'allongement à la rupture est régi par le nombre de nœuds.

Bien que le phénomène prédominant au cours du vieillissement thermique soit la coupure des chaînes il a été observé que le module d'Young des matrices EPDM chargées augmente après le temps d'induction de l'oxydation, ce qui contraste avec le comportement de la matrice EPDM pure. Cette densification est attribuée à la formation de fortes interactions entre la surface des charges et les produits d'oxydation. Comme cet effet est plus prononcé pour les matrices EPDM chargées d'ATH vierges, il a été conclu que ces interactions semblent être liées à la présence de fonctions chimiques à la surface des charges i.e. les fonctions hydroxyles. Ces interactions ne disparaissent pas lorsque les échantillons sont gonflés, ce qui confirme leur nature chimique. Par conséquent, le mécanisme proposé pour décrire le renforcement des composites soumis au vieillissement thermo-oxydant est une condensation entre les fonctions hydroxyles de la surface des ATH vierges et les produits d'oxydation.

Sous irradiation ionisante, la matrice EPDM pure subit initialement une faible réticulation, alors que la principale réaction chimique est la formation et l'accumulation des hydroperoxydes. Pour une dose spécifique, les hydroperoxydes commencent à se décomposer et les coupures de chaîne deviennent prédominantes. L'épaisseur de la couche oxydée est une fonction décroissante du débit de dose, conduisant à une hétérogénéité de l'oxydation qui est plus marquée aux fortes intensités d'irradiation.

Pour les matrices EPDM pures et chargées, les propriétés élastiques et à la rupture suivent la même évolution que la densité de réticulation du réseau, i.e. une augmentation initiale suivie d'une diminution. Cependant, la densification initiale est plus importante pour les matrices EPDM chargées, indiquant une densification du réseau de l'interphase.

La densification de l'interphase a été observée à la fois pendant les vieillissements thermo- et radio-oxydant. La comparaison de ces deux types de vieillissement a révélé que, dans le cas du vieillissement thermique, la densification est plus intense pour les matrices chargées d'ATH vierges, alors que sous irradiation, la densification est plus importante pour les matrices chargées d'ATH traitées en surface. Ces résultats mettent clairement en lumière une différence entre les mécanismes de densification au cours des vieillissements thermiques et radiochimique. Au cours du vieillissement thermique, la densification résulte d'une condensation entre la fonction chimique de la surface de la charge et les produits d'oxydation. Au cours du vieillissement radiochimique, la densification est dominée par l'addition des macroradicaux sur les doubles liaisons résiduelles des molécules de traitement de surface.

Le mécanisme de réticulation de l'EPDM par le peroxyde a fait l'objet de nombreuses recherches depuis plus de 50 ans, et est assez bien défini. La précision et la cohérence des résultats de la simulation numérique avec les données expérimentales ont permis de valider le modèle cinétique proposé. La simulation de l'évolution en temps réel des propriétés mécaniques tout au long de la réticulation de l'élastomère peut être optimisée. Par exemple, une étude en temps réel de l'évolution du module d'Young en fonction de la consommation des doubles liaisons pourrait être réalisée en couplant des essais de nano-indentation avec des analyses par spectrophotométrie Raman.

L'effet du traitement chimique de surface des ATH a été observé tout au long de cette étude. Il a été montré que les molécules de traitement de surface participent à la réticulation du réseau, ce qui se traduit par une densité de réticulation plus élevée à l'interphase. En outre, un effet significatif sur la densification a été détecté, dû à la présence de ces molécules sous vieillissement radio-oxydant. Bien que nous ayons proposé une approche expérimentale pour calculer la concentration des molécules de traitement de surface, leur structure exacte et leur distribution sur la surface des charges sont encore méconnus. Une étude plus approfondie sur ce sujet pourrait apporter davantage de précisions sur la fonctionnalité des jonctions sur la surface des charges, et définir le mécanisme exact de renforcement de l'interphase sous irradiation.

Dans le cas des matrices EPDM chargées d'ATH vierges, un mécanisme différent de renforcement de l'interphase, qui est une condensation entre les produits d'oxydation et des fonctions chimiques sur la surface des charges, a été proposé. Cependant, la validité de cette proposition n'a pas été vérifiée dans cette étude. La détermination du mécanisme exact et des paramètres cinétiques associés semble un domaine intéressant de recherches ultérieures.

Le vieillissement de l'EPDM avec une faible concentration d'insaturations peut être considéré comme équivalent à celui d'un EPR. Cependant, lorsque la concentration des doubles liaisons est importante, leur effet ne peut plus être négligé. L'investigation de la cinétique de thermo-oxydation de l'EPDM a fourni des paramètres cinétiques sur la consommation des doubles liaisons ENB au cours de l'exposition. Ces données pourront être utilisées dans le modèle non-empirique de prédiction de la durée de vie de l'EPR établi dans des études précédentes au PIMM, une fois que la présence des insaturations aura été introduite dans le schéma mécanistique d'oxydation correspondant.

L'effet de renforcement des particules de charge dans les composites ATH/EPDM pourrait être expliqué en considérant une interphase en deux phases. Sur la base de ce modèle, une nouvelle approche a été proposée pour déterminer les modifications de la structure à l'échelle macromoléculaire et, pour calculer l'épaisseur et le module d'Young de l'interphase collante. Cette approche phénoménologique reste une méthode indirecte, et il est d'un grand intérêt de déterminer l'épaisseur et le module de l'interphase à l'aide d'une technique de mesure directe (AFM, nano-indentation) afin de valider la méthode proposée.

Vieillessement thermique et radiochimique de matrices EPDM pures et chargées d'ATH: Mise au point de relations structure/propriétés

RESUME : La prédiction de la durée de vie des isolants en EPDM des câbles de faible à moyenne tension dans les centrales nucléaires nécessite une connaissance précise des relations structure/propriétés mécaniques, et les critères de fragilisation structuraux pertinents. Pour tenter de combler cette lacune, trois matrices EPDM chargées par 0, 33 et 100 phr de particules d'ATH vierges ou ensimées ont été réticulées par le peroxyde de dicumyle à 170°C, avant de subir un vieillissement thermique à 90, 110 et 130°C, ou radiochimique à 40°C sous 0,1, 1 et 10 kGy.h⁻¹ dans l'air. Une approche multi-échelles a été mise en place pour déterminer l'oxydation des matrices EPDM à l'échelle moléculaire et ses conséquences aux échelles macromoléculaire et macroscopique, à l'aide de plusieurs techniques de caractérisation complémentaires : spectrophotométrie IRTF, calorimétrie différentielle, rhéométrie à l'état fondu, gonflement dans un solvant, traction uniaxiale, etc. Les relations structure-propriétés établies dans cette étude permettent d'expliquer, en outre, la dégradation des propriétés élastiques et à la rupture des matrices EPDM par coupures de chaînes, et le renforcement des interphases charge/matrice sous l'action de mécanismes physico-chimiques spécifiques des conditions d'oxydation.

Mots clés : EPDM, ATH, thermo-oxydation, radio-oxydation, réticulation, coupures de chaînes, taux de gonflement, module d'Young, allongement à la rupture.

Thermal and radiochemical aging of neat and ATH filled EPDM: Establishment of structure/property relationships

ABSTRACT : EPDM elastomer is widely used as the insulation of low to medium voltage electrical cables used in power plants, for which the life-time prediction has been hampered by the lack of knowledge on structure/mechanical properties, and the nonexistence of pertinent criteria of structural failure. In an attempt to fill this gap, three EPDM matrices filled with 0, 33 and 100 phr of pristine and surface treated ATH were crosslinked by dicumyl peroxide at 170°C and, subsequently, aged thermally at 90, 110 and 130°C, and radiochemically under 0.1, 1 and 10 kGy.h⁻¹, in air. A multi-scale approach was employed to analyze the oxidation of EPDM at molecular scale, and to determine its consequences at macromolecular and macroscopic scales by using several complementary characterization techniques: FTIR spectrophotometry, differential calorimetry, rheometry in melt state, swelling test, uniaxial tensile testing, etc. The structure/property relationships established in this study are capable to explain, in particular, the alteration of elastic and fracture properties of the EPDM matrices due to chain scissions, and the reinforcement of the filler/matrix interphases, induced by the specific conditions of oxidation.

Keywords : EPDM, ATH, thermal oxidation, radiochemical oxidation, crosslinking, chain scissions, swelling ratio, Young's modulus, ultimate elongation.

